U.PORTO

FEUP FACULDADE DE ENGENHARIA
UNIVERSIDADE DO PORTO

PERFORMANCE-BASED DESIGN OF SCC TO ENSURE DURABILITY OF CONCRETE STRUCTURES

Helena Isabel Maia Figueiras

A thesis submitted for the degree of Doctor of Philosophy in Civil Engineering
at the Faculty of Engineering of the University of Porto

Supervisor

Professora Doutora Maria Joana Álvares Ribeiro de Sousa Coutinho

Co-Supervisors

Professora Doutora María del Carmen Andrade Perdix

Professora Doutora Sandra da Conceição Barbosa Nunes

December 2013

To my husband Mario and my little Carolina…

To my lovely family…

Abstract

Durability of concrete structures is currently viewed with great concern, representing a true challenge for the development of sustainable construction. Prevention of concrete degradation and steel corrosion has to be taken into account since the design stage, being especially important the development of concrete design approaches that ensure durability performance and contribute to extend service life of concrete structures. In this sense, present research work aims at contributing to an integrated view of durability, from the design phase, over the in-situ appraisal, towards a more realistic prediction of service life of the structure.

This thesis provides a systematic methodology for a performance-based design of SCC exposed to severe marine environment, supported by numerical modelling and statistic design tools. In a first phase, a probabilistic durability modelling approach is performed to define concrete durability requirements and, in a second phase, a statistical experimental design is used to optimize concrete mix-proportions given the specified requirements. The statistical experimental design makes use of experimental techniques and statistical tools, such as factorial plans and analysis of variance (ANOVA), to mathematically model the relevant properties of concrete (fresh and hardened properties) and simplify optimization of concrete composition. This performance-based design methodology was applied to the particular case of a cruise terminal building demanding special requirements in terms of architecture (colour), fresh state (self-compactability) and hardened state (compressive strength and high durability).

A multi-level approach has, undoubtedly, great advantages in performance-based design of concrete mixtures. In this sense, new developments and contributions to a multi-level concrete design are presented, particularly, linking fresh and durability properties of paste, mortar and concrete. A procedure, based on statistical experimental design was used to establish the link between fresh properties of paste and SCC mortar, for a set of materials. The derived numerical models were used to define an area, labelled by self-compacting zone at paste level (SCZ), where rheological properties of the paste enable the design of SCC mortar. In hardened state, the capacity of effective medium theories (EMT) to predict the influence of the aggregate on electrical resistivity and chloride ion diffusion properties of SCC was explored. Experimental results were

compared with the predictions provided by different models derived from the differential effective medium theories (D-EMT). A good approximation was also found with the predictions provided by the Hashin-Shtrikman lower bound.

The durability performance-based design of SCC mixtures was articulated with the implementation, on site, of a durability monitoring system based on automatic data acquisition and embedded sensors (galvanic current sensors, reference electrodes and temperature sensors). The working principle and the methodologies of analysis and interpretation of the acquired data are discussed. Laboratory tests were conducted to establish the sensors measuring protocol, assess its behaviour towards temperature and humidity variations and appraise its performance to detect corrosion activity. This durability monitoring system was installed in two structures, the Lezíria Bridge and a yachting harbour structure. Data obtained from field monitoring, data collected in the continuous monitoring system and during periodic inspections, were used to update and validate the service life prediction of the yachting harbour structure performed during the design phase.

Resumo

A durabilidade das estruturas de betão armado é actualmente encarada com grande preocupação, constituindo um verdadeiro desafio para o desenvolvimento de uma construção sustentável. A prevenção da degradação do betão e corrosão das armaduras deve ser tida em consideração desde a fase de dimensionamento das composições. Torna-se por isso particularmente importante que sejam desenvolvidas abordagens de dimensionamento que garantam o desempenho de durabilidade do betão e contribuam para aumentar o tempo de vida útil das estruturas. Neste sentido, o presente trabalho de investigação pretende dar um contributo para uma visão integrada da durabilidade das estruturas de betão, desde a fase de dimensionamento da composição passando pela avaliação em obra, com vista a uma previsão mais realista da vida útil das estruturas.

A presente dissertação visa implementar uma metodologia sistemática de dimensionamento de composições de betão auto-compactável (BAC) expostas a ambiente marítimo, baseado no seu desempenho. A metodologia apresentada apoia-se em modelos numéricos e ferramentas estatísticas. Numa primeira fase, é realizada uma análise probabilística dos modelos degradação do betão para definir os requisitos de durabilidade da composição e, numa segunda fase, é usado um dimensionamento experimental estatístico para optimizar as composições de betão com base nos requisitos de desempenho definidos. O dimensionamento estatístico recorre a técnicas de experimentação e ferramentas estatísticas, como é o caso dos planos factoriais e a análise de variância (ANOVA), para modelar matematicamente as propriedades relevantes do betão (propriedades do estado fresco e endurecido), e desta forma facilitar o processo de dimensionamento da composição. Esta metodologia de dimensionamento de composições baseada em requisitos de desempenho foi aplicada ao caso particular de um edifício num terminal de cruzeiros com requisitos bastante exigentes em termos arquitectónicos (cor branca), propriedades do estado fresco (auto-compactabilidade) e propriedades do estado endurecido (resistência à compressão e durabilidade).

Uma abordagem multinível tem sem dúvida grandes vantagens no dimensionamento de composições de betão com base no seu desempenho. Neste âmbito, foram realizados alguns desenvolvimentos e dadas algumas contribuições para o dimensionamento de

composições de betão segundo uma abordagem em multinível, em particular, na forma de estabelecer a ligação entre pastas, argamassas e betões, ao nível das propriedades do estado fresco e de durabilidade. Para estabelecer a ligação entre as propriedades do estado fresco da pasta e uma argamassa com propriedades auto-compactáveis foi usado um procedimento baseado no dimensionamento experimental estatístico. Os modelos numéricos ajustados permitiram definir uma zona de auto-compactabilidade ao nível da pasta, onde as propriedades reológicas da pasta conduzem a argamassas adequadas para produzir um BAC. No estado endurecido, foi explorada a capacidade das teorias do meio efectivo para prever a influência do agregado nas propriedades do BAC, nomeadamente, resistividade elétrica e coeficiente de difusão aos cloretos. Os resultados de um estudo experimental realizado ao nível da pasta, argamassa e betão, foram comparados com as previsões fornecidas por diferentes modelos obtidos a partir da teoria diferencial do meio efectivo e com os limites inferior e superior da análise variacional de Hashin-Shtrikman.

O dimensionamento de composições de BAC baseado no seu desempenho de durabilidade foi articulado com a implementação, em obra, de um sistema de monitorização da durabilidade com aquisição automática de dados e sensores de embeber no betão (sensores de corrente galvânica, eléctrodos de referência e sensores de temperatura). Neste trabalho são discutidos os princípios de funcionamento e as metodologias de análise e interpretação dos dados fornecidos pelos sensores. A nível laboratorial foi realizada uma campanha de ensaios com o intuito de estabelecer o protocolo de medição dos sensores, avaliar o seu comportamento face a variações de temperatura e humidade e a avaliar o seu desempenho na detecção do início da corrosão. Este sistema de monitorização de durabilidade foi instalado em duas estruturas, na Ponte da Lezíria e numa estrutura de suporte a barcos de recreio. Neste último caso, os dados obtidos pelo sistema de monitorização contínuo e por uma inspecção realizada à estrutura, foram utilizados para actualizar e validar a previsão do tempo de vida útil realizada durante a fase de dimensionamento.

Acknowledgments

This research work was carried out at the Laboratory of Concrete Technology and Structural Behaviour (LABEST) of Faculty of Engineering of the University of Porto under the supervision of Professor Joana Sousa Coutinho. I wish to express my gratitude for her support, guidance and enthusiastic following of the work. To Professor Sandra Nunes, one of the co-supervisors of this thesis, I want to express my deep gratitude for her support, for the fruitful discussions and valuable comments.

I would also like to thank Doctor Carmen Andrade, co-supervisor of this thesis, for having welcomed me during three month stay at the Instituto de Ciencias de la Construcción Eduardo Torroja, as well as for the fruitful discussions and continuous advices. As a result I gained a new and valuable insight steel corrosion process and corrosion monitoring.

The support given by the Portuguese Foundation for Science and Technology (FCT) through the PhD grant SFRH/BD/25552/2005 is also gratefully acknowledged.

I would like to show my deepest appreciation to my friends and co-workers Lino Maia, Bruno Costa, Diogo Ribeiro, Filipe Cavadas, Remy Faria, Miguel Azenha, Américo Dimande, Leonel Ramos and Hélder Silva. Additionally, I would like to acknowledge the precious collaboration of the technical staff of LABEST/FEUP, Alberto Monteiro, Cláudio Ferraz, Cláudia Correia, Marta Poínhas and Cecília Barbosa, and in addition I would like to particularly thank to Paula Silva for her friendship, patience and help.

I also would like to express my profound gratitude for the unconditional love and support from my family, my parents Emília and Joaquim and my sister Luísa, and more recently from Alice, José Mário, Ana and Miguel. A very special thanks to my grandmother Maria and my late friend and grandfather Alberto. Finally, I am deeply thankful to my beloved husband Mário and my daughter Carolina for their encouragement and love.

Contents

List of figures

List of Tables

Symbols and abbreviations

Small Roman letters

c	concrete cover thickness
c_{nom}	nominal concrete cover
i_{gal}	galvanic current density
k_{cl}	factor that considers the influence of the external chloride ionic concentration
$k_{D,c}$	factor that considers the influence of curing conditions on the chloride diffusion coefficient
$k_{D,RH}$	factor that considers the influence of relative humidity on the chloride diffusion coefficient
$k_{D,T}$	factor that considers the influence of temperature on the chloride diffusion coefficient
k_{hor}	coefficients related to environmental exposure considering the concrete location with reference to its distance to sea coast
k_{temp}	coefficient that accounts for concrete temperature
k_{vert}	coefficients related to environmental exposure considering the concrete location with reference to sea level
$k_{\rho,c}$	factor that considers the influence of curing on the electrical resistivity
$k_{\rho,RH}$	factor that considers the influence of humidity on the electrical resistivity
$k_{\rho,T}$	factor that considers the influence of temperature on the electrical resistivity
mtk/c	metakaolin to cement weight ratio
n	factor that considers the influence of ageing effect of concrete on the chloride diffusion coefficient
p_f	probability of failure
p_{target}	target probability of failure
q	factor that considers the influence of ageing effect of concrete on the electrical resistivity
r_{cl}	reaction or chloride binding factor
t_d	service life value
t_i	initiation period

t_g	target service life
t_L	design service life
t_{hydr}	period of time the ageing factor should be applied on the electrical resistivity
t_0	reference age
w/c	water to cement weight ratio
w/b	water to binder weight ratio
w_c	cement content in mass
w_f	limestone filler content in mass
$\mathrm{w_{free}}$	free water content obtain from centrifuge test in mass
w_{gd}	coarse aggregate content in mass
w_{mtk}	metakaolin content in mass
w_{sdi}	sand i content in mass
w_{sp}	superplasticizer content in mass
w_w	water content in mass
w_{wc}	corrected water content in mass

Capital Roman letters

C_b	surface chloride content in percentage
C_c	cement content in the concrete mixture
C_m	cement content in the mortar mixture
C_r	chloride threshold level necessary to depassivate reinforcing steel
C_s	chloride content on the concrete surface in percentage of cement by weight
C_o	initial chloride content in percentage of cement by weight
D_{center}	distance to the center of the modelled region
D_{flow}	spread flow diameter
E_{corr}	corrosion potential
H	final concrete height of concrete in the U-Box test
$H2/H1$	ratio of the concrete heights in the front and back parts of the box in the L-box test
I	electrical current
I_{gal}	galvanic current
R	electrical resistance
R_a	anode polarization resistance
R_c	cathode polarization resistance

R_{el}	electrolyte resistance
Rs	surface hardness
Sp	superplasticizer
Sp/p	liquid superplasticizer to powder ratio
Sr	concrete segregation resistance
T_{funnel}	time necessary for mortar/concrete to flow out a V-funnel
T_{50}	time necessary for concrete to reach a 50 cm diameter in the slump-flow test
V	voltage
Va	concrete air content in volume
Vg	coarse aggregate content in a reference volume
Vgd	coarse aggregate content in volume
Vg,lim	dry rodded coarse aggregate content in volume
Vm	mortar content in volume
Vp	powders content in volume
V_{paste}	paste content in volume
Vs	fine aggregate content in volume
Vw	water content in volume

Small Greek letters

$\alpha_{f,j}^{a}$	depolarization factor along j axis
$\dot{\gamma}$	shear strain rate
γ_l	lifetime safety factor
Δx	the depth of the capillary suction zone
ε_{ef}	effective dielectric constant
$\varepsilon_{ef,j}$	effective dielectric constant along j axis
ε_m	matrix dielectric constant
ε_p	particles dielectric constant
ρ	electrical resistivity
ρ_c	specific gravity of cement
ρ_f	specific gravity of limestone filler
ρ_{gd}	specific gravity of coarse aggregate
ρ_{mtk}	specific gravity of metakaolin
ρ_{sdi}	specific gravity of sand i
$\rho_{Spearman}$	Spearman's correlation coefficient

ρ_w	specific gravity of water
σ	electrical conductivity
τ	shear stress
τ_0	yield stress
η_{pl}	plastic viscosity
φ_p	volumetric content of particles

Acronyms

ANOVA	analysis of variance
CC	conventional vibrated concrete
CED	concrete experimental design
CCD	central composite design
CPF	controlled permeability formwork
CKS	corrosion kit-sensor
D-EMT	differential effective medium theory
EMT	effective medium theory
FEUP	Faculty of Civil Engineering, Porto University, Portugal
RH	relative humidity of the environment
ITZ	interfacial transition zone
LABEST	Laboratory for the Concrete Technology and Structural Behaviour
LNEC	Portuguese National Laboratory for Civil Engineering
MED	mortar experimental design
PED	Paste experimental design
SCC	self-compacting concrete

Chapter 1

Introduction

1.1. Scope and motivation of the research

Concrete industry has witnessed a huge growth in the last century. The world cement production stood around 3.6 billion tons in 2012 (CEMBUREAU, 2012) and this amount gets converted into around 30 billion tons of concrete. Within Europe it has been estimated that concrete structures represent approximately 50 % of the national wealth of most countries (Long *et al.*, 2001). Civil engineering infrastructure is generally the most costly to create and develop, and thus an invaluable national asset for any country. While this remarkable growth has been occurring in concrete production, there is extensive evidence to show that concrete structures all over the world are deteriorating at an alarming and unacceptable rate (Swamy, 2007).

In the more developed European countries approximately 50 % of the expenditures in the construction industry are devoted to repair and maintenance of existing structures (Bakhoum *et al.*, 2010). The problem of unsatisfactory durability of structures causes not only economic impact, but also environmental and social problems, due to decrease of reliability and safety. In addition, we are also faced with an urgent need to ensure sustainable development and achieve an economic progress without damaging our environmental resources. Therefore it becomes clear that not only costs of a new building, but most of all integral costs, including maintenance, adaptation and demolition have to be considered (Walraven, 2009). In most cases, indirect costs due to traffic delays or loss of productivity, which can be higher than the direct costs of maintenance and repair, should also be allocated (Breugel, 2006).

Durability, and especially prevention of steel corrosion, has become a critical issue in management of reinforced concrete structures. Concrete structures designers are now aware that prevention of concrete degradation and steel corrosion has to be taken into account since the design stage. Worldwide efforts are being made to develop durability design approaches, that ensure the production of new concrete structures with improved and more controlled durability and long-term performance (Gjørv, 2010). In this sense, a performance-based approach seems particularly relevant for durability issues. This approach would allow a holistic durability design philosophy, in which performance requirements could integrate all aspects of concrete production, construction technology and maintenance. Indeed, performance-based approach is a response to an overall change in our society (AFGC, 2007), in particular, the use of new types of concrete such as high-performance concrete or self-compacting concrete, demanding the use of non-traditional constituents such as superplasticizers or mineral additions, and the growing concern for increasing performance at the least cost, while at the same time protecting the environment. Moreover, a performance-based design corresponds to the expectations of concrete industry, which already in many cases, "thinks" in terms of performance requirements, such as fresh and hardened concrete properties, concrete appearance or required service life.

One of the most revolutionary steps of the last decades in terms of concrete technology, with decisive influence on the quality and durability of concrete structures, was self-compacting concrete (SCC). SCC, initially developed in Japan (Okamura *et al.*, 2000), corresponds to an advanced special concrete type as it leads to technological, economic and environmental benefits. The main advantage of this sustainable technology lies in the unneeded compaction during placing, leading to a homogeneous and more durable material. The selection of constituent materials and the design of mix-proportions are key factors to achieve adequate fresh properties of self-compacting concrete. However, the concrete mix-design process has become very complex due to a considerable increase in the variety of constituent materials available to produce concrete and of performance requirements that the composition must meet. Hence, the mix-design process involves a large number of variables, with individual and interaction effects on concrete properties, which makes mixture optimization much more difficult. The typical mixture optimization approach based on trial and error or "one factor at a time" approach needs to be replaced by a more systematic and scientifically supported

mix-design method that dealing with specific properties of constituent materials reaches an optimized concrete mixture for the defined performance requirements. Accomplishing this aim can be carried out through the use of factorial experimental design to mathematically model the influence of mixture parameters on relevant properties of paste, mortar and/or concrete (Khayat *et al.*, 2000; Nehdi and Summer, 2002; Sonebi, 2004; Nunes *et al.*, 2006a; Nunes *et al.*, 2009b).

Unlike normal vibrated concrete, where fresh concrete behaviour is dominated by grain to grain contacts, SCC behaves like a suspension of aggregates in a paste (Flatt *et al.*, 2006). Paste plays a major role in concrete workability and therefore it is reasonable to expect that there is a direct relationship between paste and concrete flow behaviour (Hidalgo *et al.*, 2008). Besides controlling concrete workability, paste composition also has a large influence on early-age and long term properties, including durability. The prediction of concrete behaviour based on properties of paste and aggregate facilitates design of a SCC with defined requirements, inasmuch as reduces the volume of material required for testing and takes advantage of the greater accuracy of paste testing results. This multi-level approach applied to concrete mix-design requires, however, that the link between paste and concrete has already been established.

Durability of concrete structures is essentially controlled by the thickness and quality of concrete cover and cracking. The quality of concrete cover is determined not only by mix-design and material properties, but also by construction issues namely, execution and curing conditions. Upon completion of new concrete structures, the achieved construction quality always shows high scatter and variability. Since, much of the durability problems may be related with glitches occurred during construction and poor quality control, the issue of construction quality and variability must also be considered in the prediction models, in order to achieve a better control over durability (Gjørv, 2010). In fact, some of the input data that are assumed in prediction models could be very different from reality and lead to inaccurate predictions, as some parameters are uncertain and can also vary widely in space and time (Cusson *et al.*, 2011). In this sense, service life predictions, using probabilistic models updated with monitored field data can provide more reliable assessment of the probability of concrete structures degradation.

1.2. Research objectives

Current challenges facing the construction sector refer to durability, sustainability and design for service life. In this sense, one of the main objectives of the current research work is to contribute to ensure durability of concrete structures through a performance-based design of SCC mixtures. On one hand, it is crucial to develop durability design approaches that leveraging the current state of knowledge on materials science and production technologies, lead to better controlled and enhanced durability of concrete structures. Therefore, an approach based on performance criteria seems to be particularly appropriate for durability design. On the other hand, SCC technology promotes not only incorporation of powdered materials (including industrial by-products), but also has minimal dependence on available workmanship on site. Both truly contribute to improve concrete sustainability and quality and extend structure service life.

To accomplish this objective, a systematic methodology for performance-based design of SCC mixtures considering environmental exposure was pursued. A method based on a probabilistic durability modelling approach to define concrete durability requirements and on a statistical experimental design methodology to optimize concrete mix-proportions given the specified requirements was adopted. Probabilistic methods applied to the concrete degradation models enables to take into consideration the variations of material properties, environmental action and the effect of the quality of the construction. The statistical design approach, conducted through a factorial experimental design, offers a valid basis for developing empirical models that express the relationship between the response (fresh and hardened concrete properties) and the design factors (mixture parameters). Empirical models can be manipulated mathematically for various proposes, including mixture optimization. These statistical experimental approaches, generally used to model concrete fresh properties (Nunes, 2008), are now extended to durability properties. The capacity to mathematically model the influence of mixture parameters on durability variables was investigated.

The prediction of concrete properties from cement paste behaviour has great advantages to design performance-based concrete mixtures. However it is required that the link between paste and concrete properties has been previously established, in fresh and hardened states. In fresh state, although mortar requirements that lead to SCC have

already been sufficiently well defined during the early development of SCC (Okamura *et al.*, 2000), paste properties have not been fully determined. Bearing this in mind, another objective of this work is to define a self-compacting zone at paste level (SCZ), establishing the link between paste and mortar mixtures that exhibit adequate fresh properties (deformability and viscosity) to produce SCC. In hardened state, the presence of aggregate in a cement paste matrix has two opposite effects on the transport properties: firstly, the dilution and tortuosity effects that reduce the permeability; secondly, the presence of a porous interfacial transition zone (ITZ) between paste and aggregate that facilitates the movement of ions. In order to establish this link it is necessary to know how to predict the influence of the aggregate (aggregate content and aggregate skeleton) in the mixture properties. Taking advantage of effective medium theories (EMT), applied in several scientific areas to predict physical properties of heterogeneous media, it was intended to explore the use of these theories to predict the influence of the aggregate on some durability properties (electrical resistivity and chloride ion diffusion). Electrical resistivity, although still rarely considered in current standards, has arisen as a very promising durability indicator, and therefore was deeply worked throughout this research work.

Implementation of durability monitoring systems can also be a useful tool to continuously assess and ensure durability performance of concrete and predict service life of structures more accurately. However, there still is a long way to go with regard to the reliability of the results, data interpretation and effective decision-making in terms of timely rehabilitation action. In this sense, the present research work included the implementation of a durability monitoring system based on automatic data acquisition and embedded sensors, namely, temperature, galvanic current and reference electrodes. It is intended, on one side, to discuss the working principle and the methodologies of analysis and interpretation of the data collected by the sensors, and, on the other side, to demonstrate the effective use of data obtained from field monitoring to update and validate the service life of concrete structures predicted during the design phase.

In summary, this research work aims at contributing to an integrated view of durability, from the design phase, over the in-situ appraisal, towards a more realistic prediction of structures service life. In this sense, the following main goals were proposed:

- Implementing a systematic methodology for durability performance-based design of SCC mixtures exposed to severe marine environment;
- Linking fresh properties of paste to SCC mortar;
- Linking durability properties of paste to mortar and SCC;
- Implementing a durability monitoring system to improve service life predictions.

1.3. Research work program and outline of the thesis

Emerging from the experience acquired during research project BACPOR (Figueiras, 2006) (Nunes *et al.*, 2005a; Nunes *et al.*, 2005c), the present work began with the preparation and holding of a full-scale test in a precast factory. BACPOR was a research project funded by Adi-Agência de Inovação and in co-operation with national industry, namely, Grupo Mota-Engil, Sika and Maprel, to develop a robust technology for the production, transport and placement of SCC (Nunes *et al.*, 2005b). The main goal of this full-scale test was to assess the efficiency and synergetic effect of two technologies that confer additional protection to concrete structures against the ingress of aggressive agents, Controlled Permeability Formwork (CPF) and Self-Compacting Concrete (SCC). Therefore, the research program of the full-scale test was designed to compare the performance of two CPF systems and to assess the combined effect of using CPF on SCC compared to conventional vibrated concrete. There was an additional intention to identify the most critical issues concerning implementation of these technologies under actual conditions at the precast factory. Despite the good performance exhibited by both technologies, this full-scale test highlighted some critical issues that became, to some extent, the main goals of the present PhD research work. The methodology used for SCC mix-design, a trial and error method based on the Japanese SCC-designing method, proved to be inappropriate for concrete with specific requirements (fresh and hardened requirements). For this particular application, SCC should exhibit the same strength class as conventional concrete in production at the precast factory, using the same constituent materials. This full-scale test also alerted to poor quality and high variability of concrete of the full size precast elements, when

compared with laboratory results or even with results obtained in specimens cast in-situ. On the other hand, analysis of results obtained during this experimental campaign showed the great potential of electrical resistivity as a durability indicator. Main results of this full-scale test are presented in Chapter 2.

The structure of the present thesis is shown in Figure 1.1. This research work was carried out at paste, mortar and concrete level and included laboratory tests, as well as full-scale applications. Each chapter, from 2 to 6, was written as an independent research work, corresponding to papers already published or submitted to scientific journals. Hence, the beginning of each chapter holds an introduction and the state of art on research topic and, at the end, a section with the most relevant conclusions is provided. Therefore in each chapter all the necessary information for clear comprehension of research work carried out is provided, thus some repetitions arise.

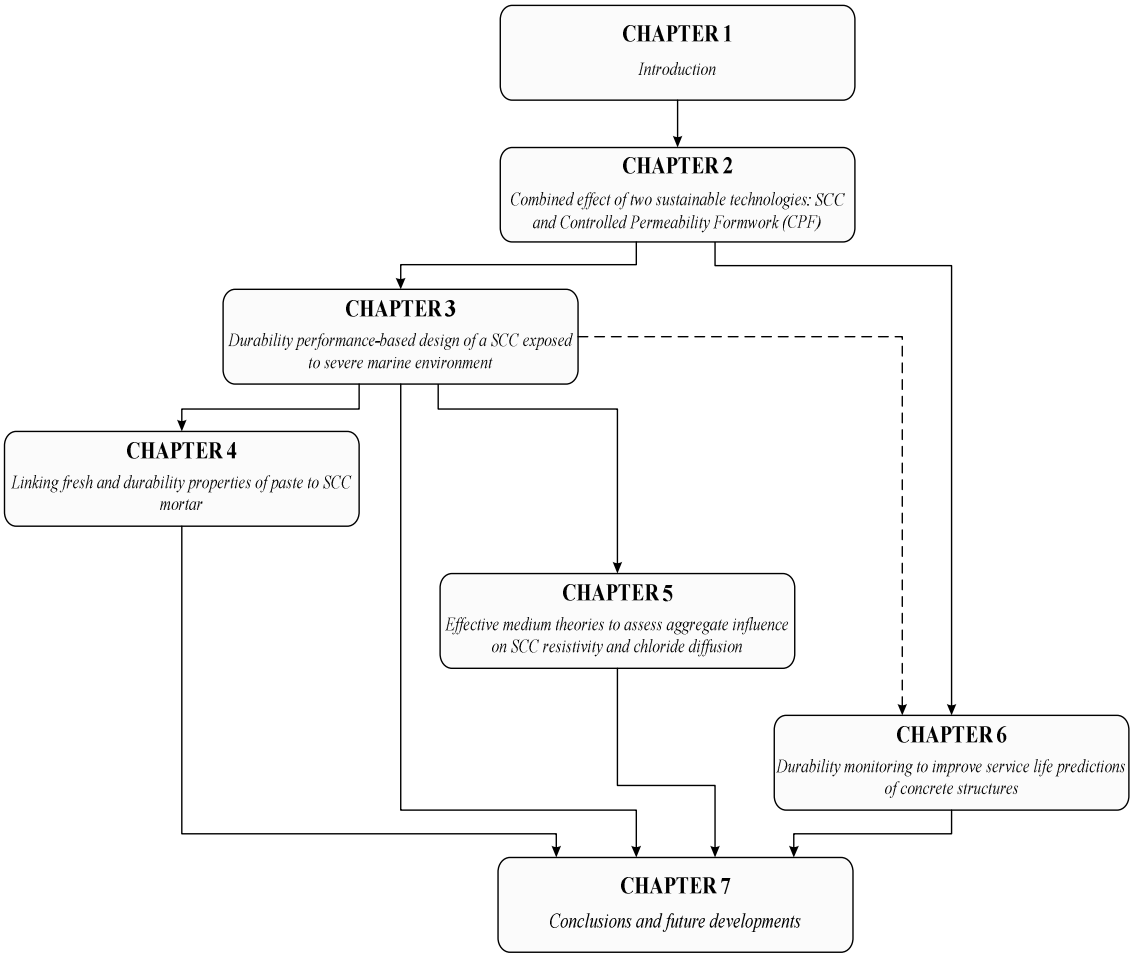

Figure 1.1 – Structure of the thesis.

Chapter 3 presents a systematic methodology to design performance-based SCC exposed to severe marine environment. This methodology is based on a probabilistic durability modelling to define concrete durability requirements and uses a statistical experimental design approach to optimize concrete mix-proportions given the specified requirements. Limit values of the durability indicators are specified through a probabilistic calculation of the limit state functions, established on the basis of target service life, limit state criterion and degradation mathematical models. The statistical experimental design used to optimize concrete mixtures holds three phases: firstly, an experimental phase conducted according to a central composite design; second, a statistical analysis and model fitting of data collected during the experimental phase and; third, a numerical optimization of mixture parameters using the derived models. In order to simplify SCC design, the study was developed in a mortar and in a concrete level. This performance-based design methodology was applied to the particular case of a cruise terminal building demanding special requirements in terms of architecture, fresh state (self-compactability) and hardened state (compressive strength and high durability). The mix design for the cruise terminal building was further applied in-situ, in a yachting harbour structure, with assessment of durability performance (see Chapter 6).

In Chapter 4 and Chapter 5 new developments and contributions to the concrete performance-based design approach are presented, particularly in establishing the link between paste, mortar and concrete, in fresh and hardened state. In Chapter 4 two statistical experimental designs were carried out, one at paste level and the other at mortar level, to mathematically model the influence of mixture parameters on fresh and durability properties (electrical resistivity). The derived numerical models were used to define an area, labelled self-compacting zone at paste level (SCZ), where fresh properties of the paste (rheological and empirical) enable the design of SCC mortar, for a specific set of materials. Furthermore, in order to extend this link to durability properties, the effect of including aggregate in cement paste was evaluated by means of the electrical resistivity test.

In Chapter 5 an experimental programme was conducted to assess the capacity of effective medium theories to predict the influence of the aggregate (aggregate content, aggregate skeleton and shape of aggregate particles) on the electrical resistivity and chloride ion diffusion properties of SCC. Different models derived from the differential

effective medium theories (D-EMT) were explored and predictions provided by the Hashin-Shtrikman bounds were assessed.

Chapter 6 presents the implementation of a durability monitoring system based on automatic data acquisition and embedded sensors. The working principle and the methodologies of analysis and interpretation of the acquired data are discussed. Laboratory tests were conducted to establish the corrosion kit-sensor measuring protocol, assess its behaviour towards temperature and humidity variations and appraise its performance to detect corrosion activity. This durability monitoring system was installed in two structures, the Lezíria Bridge and a yachting harbour structure. Data obtained from field monitoring, collected in the continuous monitoring system and during periodic inspections, was used to update and validate the service life prediction of the yachting harbour structure performed during the design phase.

Finally, Chapter 7 presents the global conclusions of the research work and some recommendations for extending its scope in the future are pointed out.

The chapters of this thesis are based on the following journal papers:

Chapter 2: Figueiras, H; Nunes, S; Sousa Coutinho, J.; Figueiras, J.; Combined effect of two sustainable technologies: Self-compacting concrete (SCC) and controlled permeability formwork (CPF); Construction and Building Materials Vol 23 (7): pp 2518-2526; 2009.

Chapter 3: Figueiras, H; Nunes, S; Sousa Coutinho, J. ; Andrade, C.; Durability performance-based design of a SCC exposed to severe marine environment using a statistical design approach; (submitted for publication).

Chapter 4: Figueiras, H; Nunes, S; Sousa Coutinho, J.; Andrade, C.; Linking fresh and durability properties of paste to SCC mortar; Cement and Concrete Composites Vol 45: pp 209-226; 2014.

Chapter 5: Figueiras, H; Nunes, S; Sousa Coutinho, J.; Andrade, C.; Effective medium theories to assess aggregate influence on SCC properties: electrical resistivity and chloride diffusion; (submitted for publication).

Chapter 6: Figueiras, H; Nunes, S; Sousa Coutinho, J.; Andrade, C.; Figueiras, J.; Durability monitoring to improve service life predictions of concrete structures; (submitted for publication).

Chapter 2

Combined effect of two sustainable technologies: SCC and Controlled Permeability Formwork (CPF)

2.1. Scope of the research

The work presented in this chapter aims at contributing to sustainable construction through enhancement of durability of concrete structures. Full size precast elements were cast with both Self-Compacting Concrete (SCC) and conventional vibrated concrete (CC) using Controlled Permeability Formwork (CPF). SCC is known to impart a more homogeneous and finer microstructure, compared to conventional concrete, therefore leading to more durable reinforced and pre-stressed concrete structures. CPF enables, in fresh concrete, drainage of excess water and air besides retaining binder particles at the concrete surface, leading to a blow-hole free surface and enhanced quality of the outer layers. The research program developed was designed to compare performance of two different CPF systems and to assess the combined effect of using CPF on SCC compared to CC.

2.2. Introduction

It is needless to say that concrete has played an extremely important role in the construction of various structures for the improvement of our living environment. An enormous amount of concrete has been used as a construction material. There is no

doubt that its use as a major construction material will continue in the future (Sakai *et al.*, 1999). Concrete for the future will have to be more durable, easier to apply, more predictable and greener. At the same time it will have to be more cost competitive (Shah *et al.*, 1999). In fact there is extensive evidence to show that concrete materials and concrete structures all over the world are deteriorating at a rapid rate, and that it has not been possible to ensure their long-term durable service life performance. A durable, efficient and effective infrastructure system is fundamental for economic prosperity, social justice, political stability and the quality of human life. However, sustainability in construction cannot be achieved if used materials and built structures cannot give durable service life. In fact, material degradation and structural damage in service shows that the progress of damage involves many interactive and interdependent parameters, several of which are beyond the control of engineers, and indeed, not anticipated or fully appreciated at the design stage. The complex, highly unpredictable and extremely variable interactive effects of load, ageing, cracking, exposure conditions and climatic changes emphasize the limitations of what is understood of the performance of materials and structures in real life exposure conditions. Therefore to achieve durable service life performance, a holistic durability design philosophy must be used, this is, an integrated material and structural design strategy of strength through durability rather than of durability through strength, where materials are manufactured for durability rather than for strength, and structures are designed for ductility and structural integrity. Holistic design envisages a global approach to all aspects of concrete and construction technology from material selection, design, construction, and maintenance to service life, integrating material characteristics with in-situ performance (Swamy, 2007).

In particular, durability of concrete structures depends primarily on permeability of the outer concrete cover which, generally, is a result of the production standard, casting conditions, compaction in heavily reinforced areas and curing conditions. The growing need to achieve durable service life performance may require considering additional protective measures which hinder corrosion and concrete degradation. In fact, using Controlled Permeability Formwork (CPF) or Self-Compacting Concrete (SCC) enhances quality of the concrete cover and therefore resistance to ingress of aggressive agents.

SCC, initially developed in Japan (Okamura *et al.*, 2000), consists of a social, economic and environmental sustainable technology. SCC probably corresponds to the most revolutionary advance of the last decades, in terms of concrete technology. It involves a new production and casting process in where compaction is banned. This leads to reduction in casting costs, increased productivity and a more homogeneous product (Okamura *et al.*, 2000; Skarendahl and Petersson, 2001). In fact, SCC compared to conventional concrete (CC) is free of local variation due to man-dependent poker vibration. Also, as SCC uses more powder materials than CC, imposed by fresh-state properties, this potentially leads to better durability performance. However, it is still uncertain whether the significant differences in the mix-proportions and in placing and compaction processes of the SCC and CC have a considerable effect on the transport properties and their relationships with the microstructural characteristics (RILEM-Report 38, 2007). The refined pore structure and more uniform and denser interfacial transition zone (ITZ) in the SCC mixes are believed to be among the main contributors to enhanced resistance to fluid transport (RILEM-Report 38, 2007) and, therefore, SCC enables postponing and hindering deterioration.

Controlled Permeability Formwork is one of the few techniques for directly improving the concrete surface zone. This technique reduces the near surface water/binder ratio and reduces the sensitivity of the concrete to poor site curing. CPF consists in the application of a textile liner on the usual formwork, allowing air bubbles and surplus water to drain out but retaining binder particles and so enabling the water-binder ratio of the outer layer to become very low and the concrete to hydrate to a very dense surface skin as the filter provides enough water available at the right time to activate optimum hydration. So CPF enhances durability by providing an outer concrete layer which is richer in binder particles, with a lower water/binder ratio, less porous and so much less permeable than when ordinary formwork is used (Sousa Coutinho, 2003). Although CPF has proved to improve the quality of concrete cover, it does not prevent CC problems resulting from poor compaction or aggregate nesting induced by lack of paste.

Considering the advantages and limitations of both additional protective measures, SCC and CPF, it is possible that they will reveal a synergetic effect, thus further enhancing durability performance of concrete structures. Therefore the aim of this work is to assess the efficiency of two CPF systems on SCC and on conventional concrete (CC)

and compare the effect of each of the systems used. Two box-culverts, one with SCC and the other with CC, were cast using two different CPF systems. Mechanical and durability-related properties were compared for the CPF systems and for the box-culverts made of the different types of concrete thus enabling considerations on homogeneity of concrete throughout each element. In the particular case of assessing resistance of concrete to chloride penetration, two different tests were used, the CTH Rapid Method and the ASTM C1202 method. Therefore an analysis comparing test results of both methods is presented.

2.3. Experimental program

2.3.1. Materials characterization

Concrete was produced using Portland cement (CEM I 52.5 R) and a mineral addition (limestone filler), of specific gravity 3.12 and 2.70, respectively. The specific surface (Blaine) and the mean particle size of limestone filler were 5150 cm^2/g and 4.52 μm, respectively. A polycarboxylate type superplasticizer of specific gravity of 1.05 and 18.5 % solid content was used. Crushed calcareous aggregate, siliceous natural fine sand (sand 1) with a fineness modulus of 2.52 and a natural coarse sand (sand 2) with a fineness modulus of 3.27 were used, see Table 2.1. The specific gravity of the coarse aggregate, sand 1 and sand 2 were 2.61, 2.60 and 2.62, and absorption values 1.29%, 0.68% and 0.51%, respectively, according to EN 1097-6 (IPQ, 2003a).

Table 2.1 – Grading of aggregates.

Sieve size (mm)	0.074	0.150	0.297	0.590	1.180	2.380	4.750	6.300	9.500	12.500
Sand 1	1.00	6.70	19.40	44.90	78.00	99.00	100.00	100.00	100.00	100.00
Sand 2	0.70	3.30	10.10	27.70	53.00	79.50	99.70	100.00	100.00	100.00
Coarse aggregate	0.00	0.11	0.30	0.30	0.30	0.40	6.20	32.40	84.20	100.00

2.3.2. Self-compacting concrete mix-design

A key phase when producing SCC lies on the design of mix-proportions so as to obtain adequate properties of fresh concrete. SCC in the fresh state must show filling ability,

resistance to segregation and passing ability (EFNARC, 2005). Several mix-design techniques have been proposed and some general recommendations can be taken into account for SCC proportioning (EFNARC, 2005), which mainly consist of limiting the coarse aggregate volume and maximum aggregate size, using low water to powder ratio and a superplasticizer. The "excess paste" should be the minimal quantity to create a "lubricating" layer around the aggregate particles and reduce the inter-particle friction necessary to achieve self-compactability (Walraven, 2005). Based on the Japanese SCC-designing method, the mix-design method used in this work consisted on a two level (mortar and concrete) optimization method and is described more in detail in (Nunes *et al.*, 2005a). At mortar level, mortar flow and funnel tests were carried out to study the relation between both sands (fine aggregate was a combination of two sands) along with paste volume and volumetric water/powder ratio. Mortar properties adequate for SCC are sufficiently well defined at this level (Nunes *et al.*, 2005a) and if target values are achieved, in the next stage, tests on concrete, although essential, are reduced to a minimum. Final trials at concrete level were necessary to quantify the amount of coarse aggregate, to adjust superplasticizer dosage (if necessary) and to confirm self-compactability of the designed concrete (Nunes *et al.*, 2005a). Slump-flow, V-funnel and U-box tests were used to characterize SCC in the fresh state. The slump-flow test is used to evaluate deformation capacity, viscosity and also resistance to segregation of SCC by visual observation. This test enabled recording final slump flow diameter (D_{flow}) and time necessary for concrete to reach a 50 cm diameter (T_{50}). The V-funnel test is used to assess viscosity and passing ability of SCC and this test enabled recording flow time (T_{funnel}). With the U-box test it is possible to assess ability of concrete to pass through tight openings between reinforcing bars and filling ability. This test enabled recording filling height (H). Details of the equipment used for testing fresh concrete and test procedures used can be found in EFNARC (2005).

Mix-proportions for both SCC and similar conventional concrete are presented in Table 2.2. The CC mix corresponded to the one being used at the prefabrication plant at the time and the SCC composition was designed to have similar strength to the CC composition, at 28 days. Full scale testing was carried out in winter, at a precast factory under normal working conditions. The paddle-mixer and the mixing procedure used for the SCC was the same as for conventional concrete, except for increased mixing time, about two times longer. Results concerning fresh SCC testing were D_{flow}=565 mm,

T_{50}=5.6 s, T_{funnel}=14.9 s and H=340 mm. The mixture exhibited good filling ability, high segregation resistance and enough deformability for this type of application. SCC filled up the entire mould, completely enclosing the reinforcement. After stripping the formwork a few blowholes were visible only on the horizontal parts.

Table 2.2 – Mix-proportions of SCC and CC produced during full-scale tests.

Constituent materials	SCC (kg/m³)	CC (kg/m³)
Cement	387	350
limestone filler	197	85
sand 1	618	407
sand 2	202	413
coarse aggregate	829	938
Water	138	171
superplasticizer (liquid)	12.45	3.70*
water/cement (w/c)**	0.38	0.49
water/binder (w/b)	0.25	0.40

* different superplasticizer was used for conventional concrete
** including water in superplasticizer

The main differences between mix-proportions of the SCC and the CC, as can be observed in Table 2.2, concern in less coarse aggregate and more powder materials and superplasticizer. These differences led to higher cost of materials for SCC, about 18% higher. According to Juvas (2003), although materials for SCC are 15 % to 25 % more expensive than those of normal concrete of the same strength grade, the total costs will be 5 % to 15 % lower when all savings in work are included. The difference in costs of materials referred to, will be smaller, the higher the strength class.

The motor vehicle, shown in Figure 2.1, used to transport concrete from the mixer to the casting area, includes an endless screw which drives concrete upwards from the tank and then discharges it into the formwork. This system presented several limitations such as the discharge height permitted, smaller than the elevation required for larger box-culvert moulds also handled in this factory. Conversely, if the mould is smaller, concrete drops from a high distance and air is entrapped during the fall. Another relevant limitation concerns the capacity of the tank which is smaller than the maximum capacity of the mixer. In fact this can delay SCC production since no waiting

period for vibration is required as when using conventional concrete. One of the main advantages of SCC is increased productivity. However, the construction site layout has to be optimized to achieve a more competitive production and reduce costs, in particular costs related to materials, to increased mixing time and to quality control (Nunes *et al.*, 2006b). Production capacity and casting capacity on site should be balanced off so as to ensure that SCC is placed without breaks in supply and within flowability retention time. Discontinued SCC production will affect filling ability and may result in unwanted lift lines on vertical surfaces as well as possible bonding problems between layers. As mentioned before, full-scale tests carried out at this precast factory demonstrated that for SCC to be placed in one continuous pour, installations and equipment set for conventional concrete have to be adjusted.

Figure 2.1 – Motor-vehicle used to transport and cast concrete.

Conventional concrete elements were externally vibrated and as vibration is eliminated for SCC, for production of these elements work on site was far lighter and noise reduced. Environment on site was improved considerably with the use of SCC leading to a very positive attitude among workers and engineers. It is recommended that workers involved should be specially trained.

As both concrete types are clearly different, both in terms of mix-proportions and in terms of casting procedures, it is important to analyse and compare hardened properties for each one (Klug and Holschemacher, 2003). Results concerning comparison and evaluation of hardened concrete properties of both, self-compacting concrete and

conventional concrete, obtained in moulded specimens, were presented in Figueiras (2006) and Nunes *et al.* (2009a).

2.3.3. Controlled permeability formwork systems

Controlled Permeability Formwork (CPF) consists in the application of a textile liner on the usual formwork, allowing air bubbles and surplus water to drain out but retaining binder particles at the surface of concrete, thus reducing permeability of the outer layer, see Figure 2.2. CPF also enables the concrete surface to hydrate to a very dense surface skin as the filter makes enough water available at the right time to activate optimum hydration. Besides a blow-hole free surface and an enhanced quality cover concrete, that is durability, due to controlled reduction of the water/binder ratio, CPF reduces pressure on the formwork (Sousa Coutinho, 2005). An increased volume of a more impermeable and denser paste together with a reduction of the water/binder ratio at the concrete surface may lead to further reduced carbonation and chloride ion ingress as well as a higher resistance to freeze-thaw attack.

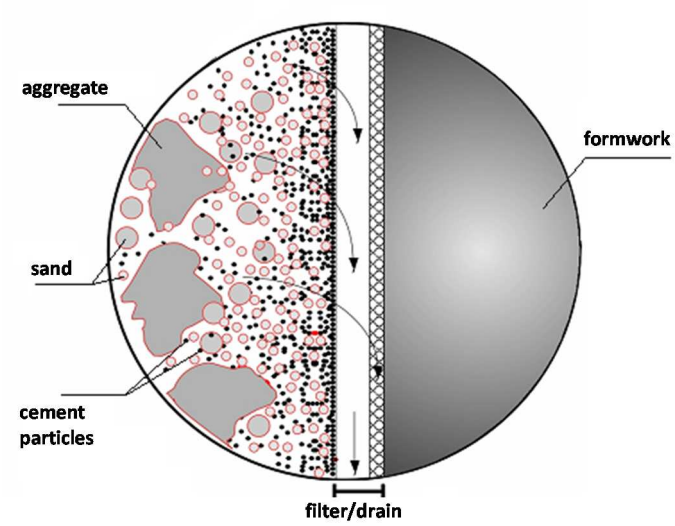

Figure 2.2 – CPF – Schematic representation (Sousa Coutinho, 2005).

One of the aims of this experimental program is to compare the performance of two CPF systems, from this point on named CPF-A and CPF-B. These systems were used on two elements, one cast with conventional concrete and the other with self-compacting concrete. CPF-A, classified as a Type II system according to the CIRIA Report (Price, 2000), consists of a single-layer fabric system that is placed over a

structural support and tensioned in situ. These systems are usually single-use products. As the fabric is not stiff, tensioning over the mould must be carried out during application to ensure no creases will form, leading to unsightly defects of the concrete surface. CPF-B is a Type III system consisting of a two-layer system combining a filter fabric bonded to a backing grid. This type does not need tensioning. The filter fabric is pre-tensioned in the manufacturing process and tension is maintained by the backing grid. This type may be used more than once. Properties of both CPF systems are shown in Table 2.3 and Figure 2.3 shows application at the site.

Table 2.3 – Properties of CPF-A and CPF-B filter-drains.

Properties	CPF-A	CPF-B
Composition	100% polypropylene	100% polypropylene
Thickness	1.2mm	2.0mm (±10%)
Pore size	<30μm	<35μm
Air permeability	0.1-0.5 m^3/m^2.sec	< 3 m^3/m^2.sec

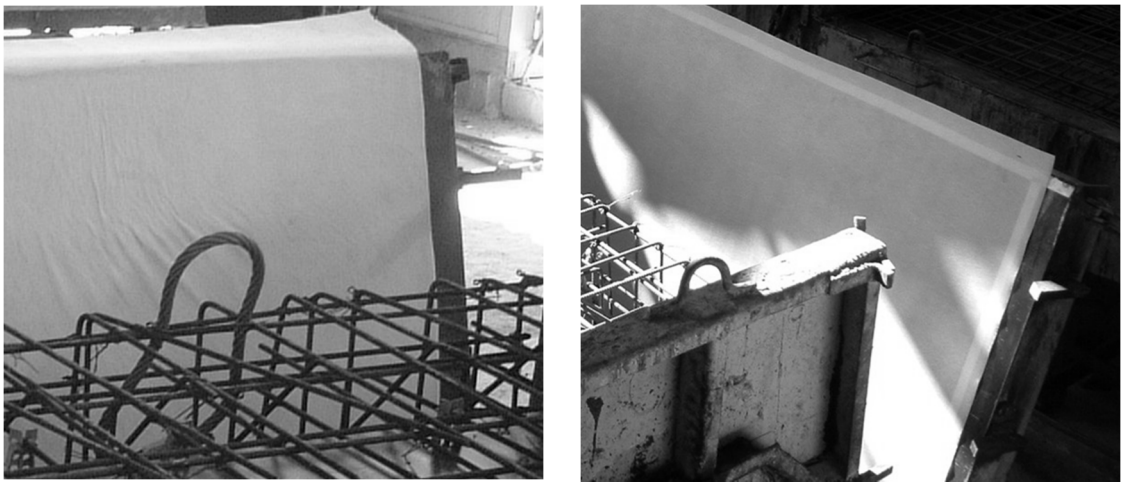

(a) (b)

Figure 2.3 – Application of the filter-drain on the formwork of the box-culverts outer side-walls A and B: (a) filter-drain A (CPF-A); (b) filter-drain B (CPF-B).

Current cost for CPF-A filter drain is about 5.00 €/m^2 and 10.00 €/m^2 for CPF-B. The CPF-B filter/drain may be reused once or twice, therefore reducing overall cost. The application cost depends, not only on the system used, but also on the shape of the element. Anyway, the final application cost corresponds to the cost of the filter/drain plus the application cost. Nevertheless two costs must be deduced: the cost related to

the usual concrete surface repairs after stripping common formwork and the cost concerning releasing agent which must not be used with CPF.

2.3.4. Selected elements

The precast concrete elements considered for this research were two identical shaped box-culverts (length=2.5 m; height=1.15 m; width=2.32 m; slab thickness=0.15 m; wall thickness=0.14-0.16 m). The box-culverts were cast, as mentioned before, one with SCC and the other with conventional concrete. Each side-wall of both box-culverts, SCC and CC, was cast with two different CPF systems. On the exterior side of the side-wall A, CPF-A was used and on the exterior side of the side-wall B, CPF-B was used. To enable drilling cores from the box-culvert for further testing, three zones with no reinforcement were planned, one in the centre of each side wall and the third on the slab, as shown in Figure 2.4. These cores enabled assessment of concrete properties including the effect of both CPF systems considered.

Figure 2.4 – Box-culvert element: reinforcement and location of test cores in side-wall A.

2.4. Final Product

Both box-culverts presented dense and blowhole free concrete on CPF faces, standing out against the traditionally cast faces, with the usual blow-holes and imperfections which result from air and water retained at the formwork surface during production. Faces showing these blemishes corresponded to the inner facades of both box-culverts. Nevertheless, they were more profuse in the CC box-culvert, compared to the SCC one, Figure 2.5. The CPF faces, though, had an inconsistent appearance with lighter coloured areas (Figure 2.6) which may have been due to a non-uniform concentration

of limestone filler throughout the CPF cast surface. This did not occur at the traditionally cast surfaces.

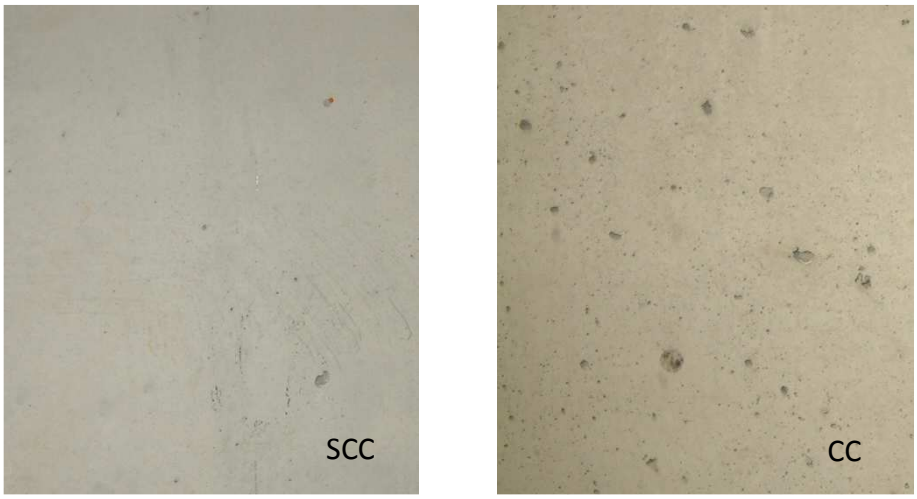

Figure 2.5 – Detail of concrete surfaces resulting from SCC and CC.

Figure 2.6 – Concrete surfaces resulting from application of CPF-A on CC box-culvert and from application of CPF-B on CC box-culvert.

2.5. Hardened properties

2.5.1. Mechanical properties

2.5.1.1. Specific gravity and compressive strength

Compressive strength of concrete was determined at 60 days on cores drilled from the top slab and side-walls of each box-culvert (wall A and wall B), see Figure 2.4. Cores drilled from the sides were loaded perpendicular to the casting direction whereas slab cores were loaded parallel to casting direction. The diameter of these cores was 94 mm and the height/diameter ratio varied between 1.58 and 1.72. Core strength was converted to the strength of corresponding standard cylinders (ϕ=150 mm; h=300 mm) using the relations established by Mansur *et al.* (2002), dependent on the level of strength ranging from 20 to 100 MPa. Converted values from the mean compressive strength as well as the specific gravity results for both SCC and CC box-culvert elements are presented in Table 2.4.

Table 2.4 – Specific gravity and converted compressive strength of cores. Average results and variation coefficient, in brackets.

Concrete property	Location	Nº of cores	SCC	CC
Specific gravity (kg/m³)	Wall A	6	2339 (1.3%)	2380 (2.0%)
	Wall B	6	2329 (1.2%)	2345 (2.8%)
	Slab	6	2305 (0.8%)	2289 (0.6%)
Compressive strength (MPa)	Wall A	6	67.9 (3.1%)	67.5 (2.2%)
	Wall B	6	69.7 (3.0%)	66.3 (6.0%)
	Slab	6	70.7 (7%)	58.1 (8.0%)

In spite of the lower coarse aggregate content, SCC exhibited a slightly improved compressive strength due to the lower water/cement ratio. Compressive strength and specific gravity results were consistent throughout the SCC box-culvert whereas for the conventional concrete box-culvert, compressive strength and specific gravity decreased considerably in the slab, due to lack of efficient compaction in the upper part of the mould. Therefore SCC led to a more homogeneous and isotropic material along the box-culvert. It should be notice that the mean compressive strength obtained for SCC

and CC cores (60 days) was lower compared to moulded specimens (28 days cylinders, (Nunes *et al.*, 2009a)).

2.5.1.2. Surface hardness

The most used non-destructive test to estimate concrete strength is the hardness test using a portable Schmidt Hammer. This test assesses the uniformity of the concrete surface layers and also determines hardness which can be correlated to concrete strength. Schmidt Hammer tests following the procedure in EN 12504-2 (IPQ, 2003b) were carried out on 3 areas (0.15 m×0.15 m), at mid-level of the 8 faces of the side-walls of the two box-culverts (SCC and CC), at 7, 14 and 28 days. Thus, assessment of the surface hardness was performed on each box-culvert for each side-wall: on side-wall A, on the outside face corresponding to the CPF-A surface and on the inside face corresponding to the control face, this is, the traditionally cast face, and on side-wall B, on the outside face corresponding to the CPF-B surface and on the inside face corresponding to the non-CPF face. Results for the SCC and CC box-culvert are shown in Table 2.5.

Table 2.5 – Surface hardness of SCC and CC box-culvert walls. Median, average results and variation coefficient, in brackets.

Reference	Age of concrete	SCC		CC	
		$R_{s,median}$ (MPa)	$R_{s,average}$ (MPa)	$R_{s,median}$ (MPa)	$R_{s,average}$ (MPa)
Wall A, CPF-A face	7 days	36.0	36.0 (4.2%)	34.0	34.7 (6.3%)
	14 days	38.0	37.9 (4.5%)	37.0	37.3 (6.1%)
	28 days	47.5	47.6 (8.2%)	42.0	42.1 (7.8%)
Wall A, non-CPF face	7 days	33.0	32.8 (4.6%)	32.0	32.0 (5.0%)
	14 days	35.0	35.1 (5.9%)	34.0	34.2 (5.4%)
	28 days	42.0	41.7 (5.6%)	38.0	37.7 (5.8%)
Wall B, CPF-B face	7 days	36.0	35.4 (6.4%)	36.0	36.4 (4.1%)
	14 days	37.0	37.2 (4.8%)	38.0	37.6 (5.0%)
	28 days	42.0	42.1 (8.4%)	44.0	44.7 (11.0%)
Wall B, non-CPF face	7 days	33.5	33.4 (6.9%)	32.0	32.5 (5.2%)
	14 days	37.0	36.2 (6.2%)	34.0	34.5 (5.8%)
	28 days	40.0	41.1 (8.9%)	38.0	38.0 (5.1%)

The graph presented in Figure 2.7 shows efficiency of SCC technology and CPF against conventional concrete in accordance with equation (2.1):

$$\text{Efficiency (\%)} = \frac{\Delta_T - \Delta_{CC}}{\Delta_{cc}} \times 100 \tag{2.1}$$

where Δ_T is the average surface hardness at 28 days when one or two technologies were used, this is, SCC, CPF or SCC combined with CPF, and Δ_{CC} is the average surface hardness at 28 days for CC (reference). Results lead to the conclusion that surface hardness of CPF cast concrete is higher than for the same concrete cast traditionally. Comparing results from both box-culverts, surface hardness for SCC is higher than for CC and SCC combined with CPF is 18.4% more efficient than using only CC. CPF-A is more efficient with SCC than with CC and CPF-B is more efficient with CC compared to SCC.

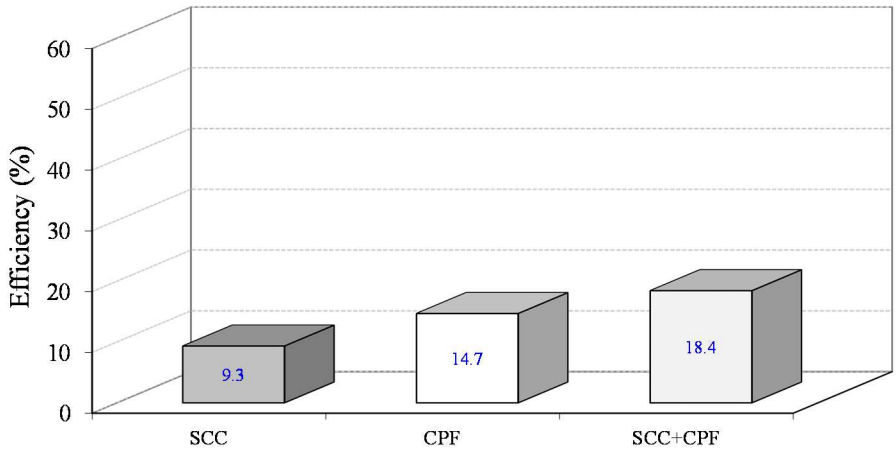

Figure 2.7 – Efficiency of SCC, CPF and SCC with CPF systems on surface hardness.

2.5.2. Durability properties

Transport properties of the near-surface concrete, which play a major role in durability of reinforced concrete, are controlled by three mechanisms, namely, capillary absorption, permeability and diffusion (Neville, 1998). Usually, the more resistant concrete is to the ingress of aggressive agents (pure water or carrying ions, oxygen and carbon dioxide) the more durable it will be (Neville, 1998). When testing concrete for durability each mechanism is considered separately, but naturally, in real structures these mechanisms act together and in certain periods one or another may play a

dominant role. In the present study water absorption by capillarity and two chloride migration tests were carried out to assess concrete durability.

2.5.2.1. Water absorption by capillarity

Water absorption by capillarity was assessed following the procedure described in RILEM TC 116-PCD (1999) slightly altered by suggestions in Sonebi *et al.* (2000). Cores with 75 mm diameter were extracted from each side-wall A and B of both box-culverts, from the CPF face right through to the non-CPF (control) face, and 50 mm thick slices were sawn off from each end. These test-specimens were then put to dry in a ventilated heater at 40 ºC until the difference between two consecutive weights was less than 0.5 % of the original weight (constant mass). After cooling, the specimens were prepared and tested according to the RILEM recommendation. The uptake of water by capillary absorption was measured through the weight gain of each specimen at time intervals up to 24 hours from the start of the test (Sonebi *et al.*, 2000). The absorption of water into concrete under capillary action is dependent on the square-root of time and may be modelled by the following equation (Sousa Coutinho, 2003):

$$A = a_0 + St^{0.5} \tag{2.2}$$

where A (g/m²) is the water absorption by unit area of concrete surface since the moment the core is dipped in water, S is the "Sorptivity" of the material, t is the elapsed time and a_0 (g/m²) is the water absorbed initially by pores in contact with water. Sorptivity is a measure of the capillary forces exerted by the pore structure, it measures the unsaturated flow of fluids into concrete (Stanish *et al.*, 1997).

Water absorption data collected during the test led to the linear relations presented in Figure 2.8. Sorptivity results (g/(m²×min$^{1/2}$)) are presented in Table 2.6 for core samples taken from the SCC box-culvert and CC box-culvert. Results of core specimens show that the rate of capillary absorption, indicated by the sorptivity parameter, is slightly lower for SCC, compared to CC, and is lower in cores from the CPF faces. Comparing sorptivity of core specimens from CPF faces, results indicate that cores taken from CPF-A face have a higher rate of capillary absorption than cores taken from CPF-B face.

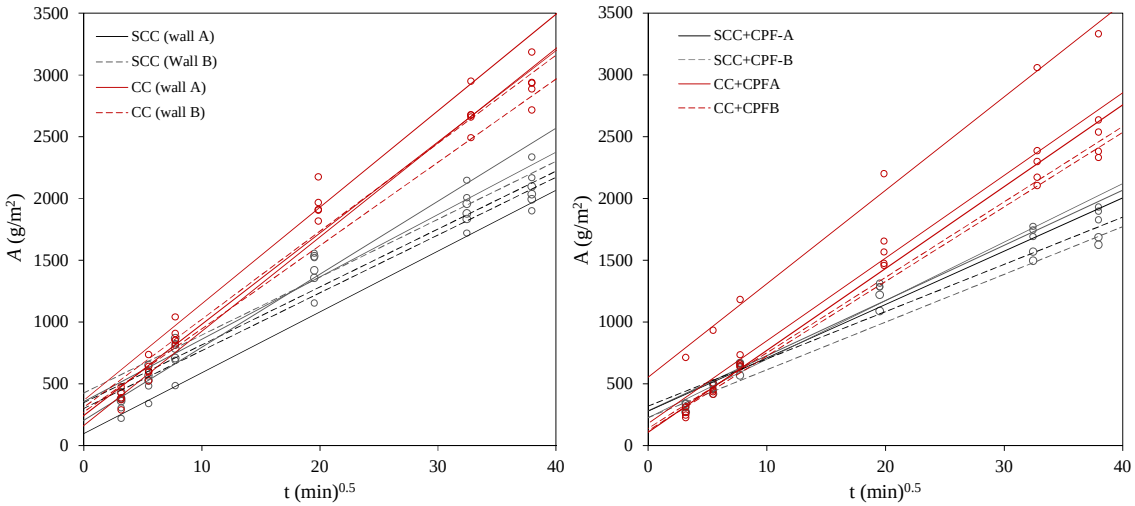

Figure 2.8 – Water absorption (by capillarity) results of cores.

Table 2.6 – Sorptivity (g/(m²×min$^{1/2}$) of cores from SCC and CC box-culvert walls, average results and variation coefficient, in brackets.

	Location	N° of cores	Average (v.c.)
SCC box-culvert	Wall A, CPF-A face	3	45.07 (4.8%)
	Wall A, non-CPF face	3	52.94 (10.2%)
	Wall B, CPF-B face	2	38.44 (--)
	Wall B, non-CPF face	3	46.84 (0.1%)
CC box-culvert	Wall A, CPF-A face	3	69.60 (7.5%)
	Wall A, non-CPF face	3	76.04 (2.8%)
	Wall B, CPF-B face	2	60.73 (--)
	Wall B, non-CPF face	3	69.30 (--)

Comparing sorpitivity of cube specimens, presented in Nunes *et al.* (2009a) and of cores taken from the box-culvert elements results indicate that the rate of capillary absorption is between 2 and 3 times higher for cores of SCC and conventional concrete. Furthermore, a larger variation of results was found with cores. This might be explained by the different curing conditions and/or any surface defects induced by the drilling machine.

2.5.2.2. Resistance to chloride ion penetration

Resistance to chloride ion penetration was assessed following ASTM C1202 (ASTM, 1997), more popular in America, and the CTH Rapid method described in

NT BUILD 492 (NORDTEST, 1999). This last method was adopted in Portugal through a LNEC specification, E 463 (LNEC, 2004). Cores of approximately 100 mm diameter were drilled out from each side-wall of both box-culverts; the top 50 mm discs (moulded faces) were used. The conditioning of the concrete disc specimens for both test procedures consisted of: 1 hour air drying; 3 hours vacuum (pressure <600 mm Hg); 1 hour of additional vacuum with specimens under deaerated water, followed by 18 hours of soaking in water for the ASTM test and soaking in saturated calcium hydroxide solution for the CTH Rapid Method.

ASTM C1202 method

The method described in the ASTM C1202 (ASTM, 1997) consists of monitoring the amount of electric current passed through concrete specimen, when a potential difference of 60 V is maintained across the specimen for a period of six hours. Chloride ions are forced to migrate out of a NaCl solution subjected to a negative charge, through the concrete into a NaOH solution maintained at a positive potential. The total charge passed, in coulombs, is used as an indicator of the resistance of the concrete to the ingress of chloride ions, the lower it is, the more resistant is the concrete to chloride penetration.

CTH Rapid Method

The CTH Rapid Method is a non-steady state migration method based on a theoretical relationship between diffusion and migration, which enables the calculation of the apparent chloride diffusion coefficient from an accelerated test, equations (2.3) to (2.5). It is based on measuring the depth of colour change of a silver nitrate solution sprayed on specimens previously submitted to a migration test.

$$\mathrm{Dcl_{ns}} = \frac{RT}{zFE} \cdot \frac{x_d - \alpha\sqrt{x_d}}{t} \tag{2.3}$$

where,

$$E = \frac{U - 2}{L} \tag{2.4}$$

$$\alpha = 2\sqrt{\frac{RT}{zFE}} \cdot erf^{-1}\left(1 - \frac{2C_d}{C_0}\right) \quad (2.5)$$

where Dcl_{ns} is the apparent diffusion coefficient obtained in a non-steady-state migration test (m^2/s); R is the gas constant (R=8.314 J/(mol.K)); T is the average value of the initial and final temperatures in the anolyte solution (K); L is the thickness of the specimen (m); z is the absolute value of ion valence, for chloride (z=1); F is the Faraday constant (F=9.648×10^4 J/(V.mol)), U is the absolute value of the applied voltage (V); x_d is the average depth of chloride penetration measured by using a colorimetric method (m); t is the test duration (s); C_d is the concentration of free chloride at which the colour changes when using the colorimetric method to measure the chloride penetration depth (C_d ≈0.07 N) and C_0 is the concentration of free chloride in the catholyte solution (C_0 ≈2 N).

Disc specimens were submitted to an electric current corresponding to a potential difference of 30 V, during 24 hours. After switching off the electrical field, the specimens were split in two halves and the depth of chloride penetration was measured using a colorimetric technique in which a silver nitrate solution is used as a colorimetric indicator. When a silver nitrate solution is sprayed on a concrete containing chloride ions, a chemical reaction occurs. The chlorides bind with the silver to produce silver chloride, a whitish substance. In the absence of chlorides, the silver instead bonds with the hydroxides present in the concrete, creating a brownish colour (Stanish *et al.*, 1997).

Results

Results of ASTM C1202 test and CTH Rapid Method are presented in Table 2.7 and Table 2.8 for the core samples taken from the SCC box-culvert and CC box-culvert. Both tests results show that conventional concrete is less resistant to chloride ingress. Based on ASTM C1202 (ASTM, 1997), the SCC mixture can be classified as having moderate chloride ion penetrability while conventional concrete mixture presented high chloride ion penetrability. The lower water/cement ratio can be responsible for the improved behaviour of SCC. Besides, due to increased content and variety of fine materials (cement and limestone filler) and dispersing effect of superplasticizer, as well as, the absence of vibration, an improved microstructure can be obtained, related to higher packing density of paste and reduced size and porosity of the interfacial

transition zone (ITZ) (Klug and Holschemacher, 2003). According to the results the application of CPF systems on the formwork improves the resistance to chloride ion penetration. It should be noticed that in the case of resistance to chloride penetration tests, insignificant differences were found between core samples and cube specimen results, presented in (Nunes *et al.*, 2009a).

Table 2.7 – Resistance to chloride (ASTM C1202) in electrical charge (coulombs) of cores from SCC and CC box-culvert walls, average results and variation coefficient, in brackets.

	Location	Nº of cores	Average (v.c.)
SCC box-culvert	Wall A, CPF-A face	4	2534 (4.6%)
	Wall A, non-CPF face	4	3068 (5.9%)
	Wall B, CPF-B face	4	2648 (3.3%)
	Wall B, non-CPF face	4	3191 (6.6%)
CC box-culvert	Wall A, CPF-A face	3	3915 (6.4%)
	Wall A, non-CPF face	3	4218 (5.0%)
	Wall B, CPF-B face	4	3868 (8.8%)
	Wall B, non-CPF face	4	4384 (11.6%)

Table 2.8 – Resistance to chloride (CTH test) in apparent diffusion coefficient (cm^2/s) of cores from SCC and CC box-culvert walls, average results and variation coefficient, in brackets.

	Location	Nº of cores	Average (v.c.)
SCC box-culvert	Wall A, CPF-A face	4	$9.6x10^{-8}$ (6.9%)
	Wall A, non-CPF face	4	$10.0x10^{-8}$ (23.0%)
	Wall B, CPF-B face	4	$9.6x10^{-8}$ (8.8%)
	Wall B, non-CPF face	4	$11.4x10^{-8}$ (9.9%)
CC box-culvert	Wall A, CPF-A face	4	$15.0x10^{-8}$ (4.3%)
	Wall A, non-CPF face	3	$16.0\ x10^{-8}$ (20%)
	Wall B, CPF-B face	3	$13.6x10^{-8}$ (5.4%)
	Wall B, non-CPF face	4	$15.6x10^{-8}$ (4.7%)

Data provided by both tests, ASTM C1202 test and CTH Rapid Method, also enabled determining electrical conductivity in saturated conditions, as the specimens must be fully saturated prior to testing. Therefore, when current is imposed during the test, conductivity, inverse of resistivity, gives an indication on how easily electric current

flows through the saturated pore system. Conductivity can be determined according to equation (2.6):

$$\sigma = \frac{1}{\rho} = \frac{1}{R} \cdot \frac{L}{A} = \frac{IL}{VA} \tag{2.6}$$

where σ is the conductivity (S.m^{-1}); ρ is the electrical resistivity (Ω.m); R, electrical resistance, (Ω); I, current (A); V, voltage (V); L, length (m), and A (m^2), the area of the cross section of test specimens.

Mean conductivity and initial conductivity were determined and, in the case of initial conductivity determination, current I was taken after 15 minutes of the beginning of the CTH Rapid Test and after 5 minutes of the beginning of the ASTM C1202 test. Mean conductivity was determined using the electrical charged data collected during the tests. In fact, the current (I), measured in amperes (A), is defined as the amount of electric charge (Q), measured in coulombs (C), flowing through the cross section of the test specimen, over time (t), see equation (2.7). Therefore, the total charge passed through a specimen, in coulombs, according to equation (2.6) and (2.7), enables determination of the mean conductivity of the specimen throughout the test.

$$I = \frac{Q}{t} \tag{2.7}$$

Graphs presented in Figure 2.9 and Figure 2.10 illustrate correlation between initial conductivity, determined from initial electric current, and mean conductivity calculated from the total charge passed throughout the test. This analysis made it possible to conclude that initial and mean conductivity are well correlated, concerning both tests, with R^2 of 0.94 and 0.96 for the CTH Rapid Test and the ASTM C1202 test, respectively. It was also possible to observe that for the CTH Rapid Test initial and mean conductivity values are practically the same (y=1.0326x) but for the ASTM C1202 test mean conductivity calculated from the total charge passed, is about 15% higher than initial conductivity (y=0.8586x).

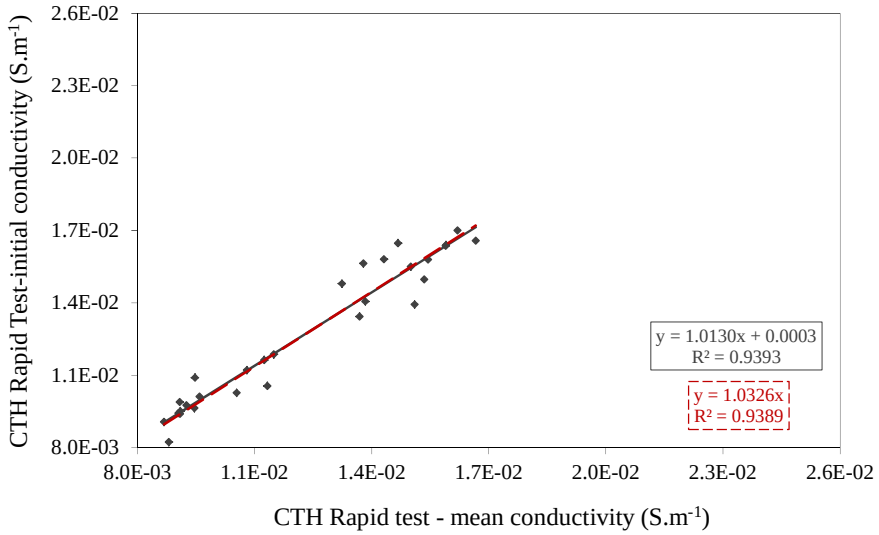

Figure 2.9 – Correlation between initial and mean conductivity, established using CTH Rapid Test results.

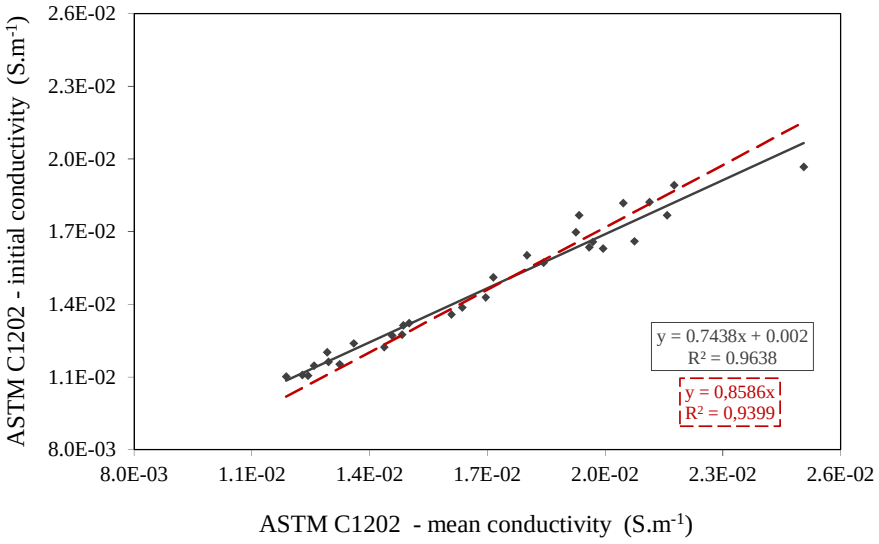

Figure 2.10 – Correlation between initial and mean conductivity, established using ASTM C1202 test results.

Indeed, considering ASTM C1202 test results, conductivity calculated from final electric current is approximately 20% higher than initial conductivity (y=0.8042x), see Figure 2.11. Some doubts have been expressed with regard to this test. The main criticisms of this technique are: (i) the current passed is related to all ions in the pore solution not just chloride ions, (ii) the measurements are performed before steady-state migration is achieved and (iii) the high voltage applied leads to an increase temperature,

especially for low quality concretes (Stanish *et al.*, 1997). According to Feldman *et al.* (1999) the severe measurement conditions of this test may cause both physical and chemical change in the specimen, resulting in unrealistic values. However the ASTM C1202 test is versatile and rapid to conduct and provides results that are easy to interpret.

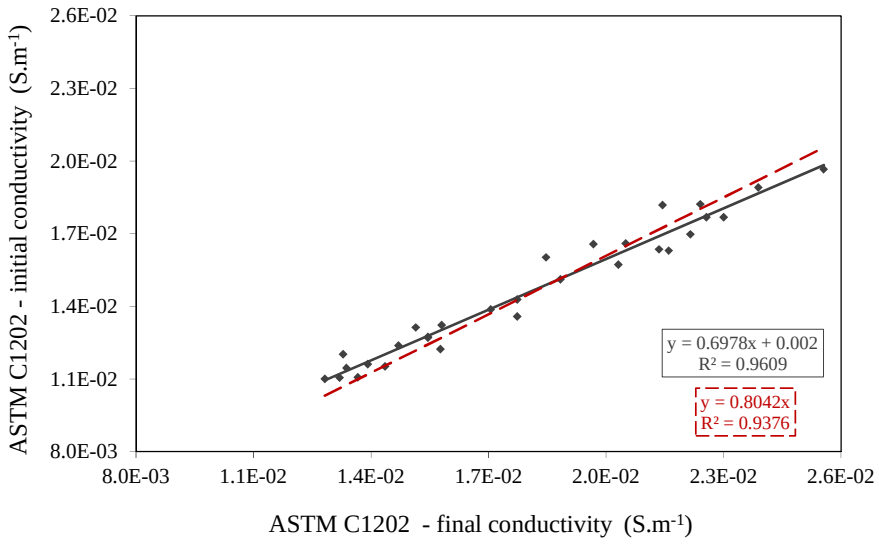

Figure 2.11 – Correlation between initial and final conductivity, established using ASTM C1202 test results.

Regarding CTH Rapid Test results, also good correlation was found between mean conductivity and apparent diffusion coefficient (R^2=0.95), see Figure 2.12. According to the Nernst-Einstein equation (equation (2.8)), for a given concrete with a given moisture condition, there is a general relationship between chloride diffusivity and electrical resistivity or conductivity (Gjørv, 2003).

$$D_i = \frac{RT\sigma t_i}{z_i^2 F^2 C_i} \tag{2.8}$$

Where D_i is the diffusivity of species i, R is the universal gas constant, T is the absolute temperature, σ is the conductivity of concrete, z is the ion valence of species i, F is Faraday constant, C_i is the concentration of species i and t_i is the transference number of species i, which is defined as the proportion of current carried by this ion in relation to the current carried by the rest of the ions (Andrade, 1993; Lu, 1997).

In fact, when the transference number of an ion is known, in this case the chloride ion, the diffusivity of this ion in concrete can be obtained by measuring the total conductivity of the concrete. However, the calculation of the diffusion coefficient of the chloride ion, using conductivity measurements, doesn´t take into account the reaction of chlorides with cement phases and therefore, the values obtained correspond to the effective diffusion coefficient (Dcl_{eff}) and not to the apparent diffusion coefficient (Dcl_{app}) (Andrade, 1993; Andrade *et al.*, 2007). On the other hand the transference number of chloride ions is difficult to measure because is complex to quantitatively describe the ionic components of the pore solution that participate in the migration process (Gjørv and Zhang, 1998). If these difficulties could be solved, in routine testing, the resistance against chloride penetration could more easily be monitored by testing the conductivity or electrical resistivity.

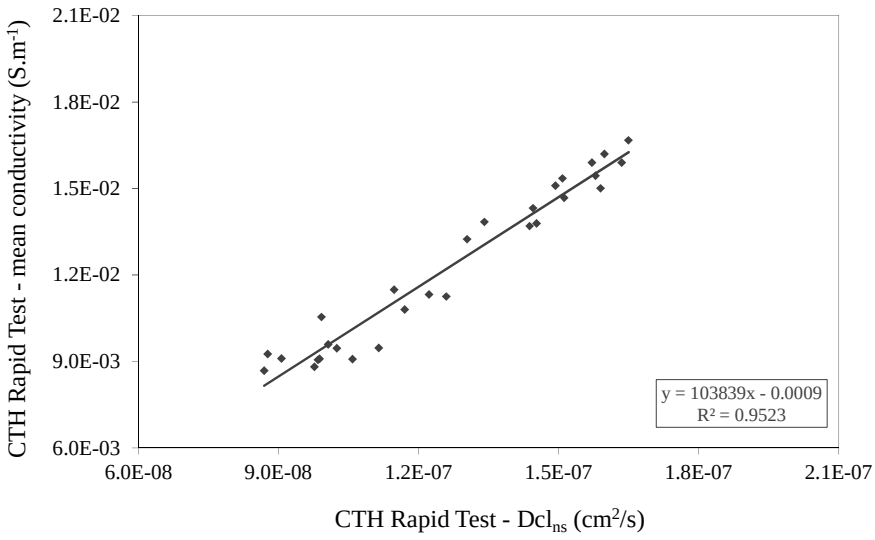

Figure 2.12 – Correlation between mean conductivity and Dcl_{ns}, established using CTH Rapid Test results.

2.5.2.3. Resistance to carbonation

Resistance to carbonation was assessed in accordance with the procedure described in LNEC specification E 391 (LNEC, 1993) where specimens were exposed to 5 %±0.1 % carbon dioxide, relative humidity of 60 %±5 % and temperature of 23 ±3 ºC, in an accelerated carbonation chamber. Specimens used were sawn off at the ends of 94mm diameter cores extracted from the side-walls of the box-culverts. Results of this test are presented in Table 2.9 for SCC and CC core samples. In the case of

CPF-A with conventional concrete no results were obtained because specimens were damaged. According to the results, the application of CPF seems to have a clear beneficial effect in concrete resistance to carbonation.

Table 2.9 – Resistance to carbonation in depth of carbonation (mm) of cores from SCC and CC box-culvert walls, average results and variation coefficient, in brackets.

	Location	Nº of cores	Average (v.c.)
SCC box-culvert	Wall A, CPF-A face	3	4.0 (8.5%)
	Wall A, non-CPF face	3	6.8 (10.2%)
	Wall B, CPF-B face	2	5.0 (--)
	Wall B, non-CPF face	2	8.8 (--)
CC box-culvert	Wall A, CPF-A face	--	--
	Wall A, non-CPF face	3	8.6 (7.5%)
	Wall B, CPF-B face	2	4.5 (--)
	Wall B, non-CPF face	2	10.0 (--)

2.5.3. Discussion

Considering hardened SCC and conventional vibrated concrete of similar strength, it can be assumed that properties are comparable and any differences lie in the scattering range for conventional concrete. As it was shown in this study, it is possible to compensate for the lower aggregate content (or higher paste content) in the SCC mixtures with a denser paste to get similar or improved concrete properties. SCC is often produced with low water/cement ratio to get high segregation resistance. This provides potential for high early strength, earlier formwork stripping and quicker mould turnaround, which may be of high interest in precast industry. A positive effect of high segregation resistance of SCC is enhanced homogeneity. Indeed, in this study it was found that concrete strength measured at different locations of the box-culvert element disperses less than in a similar element with conventional concrete. Compaction resulting from external vibration is uneven depending on the vibration sources. SCC provides potential for a superior level of homogeneity for the structure.

Results of the durability related properties considered, shown in Table 2.6 to Table 2.9, may be presented in terms of efficiency comparing effect of one or two technologies (SCC and CPF) with the effect on CC, Figure 2.13. Analysing these results makes it

possible to, on one hand, compare performance of SCC, CPF-A and CPF-B versus CC in terms of durability and on the other hand, evaluate the efficiency of each CPF system, CPF-A and CPF-B on SCC comparing it with CC.

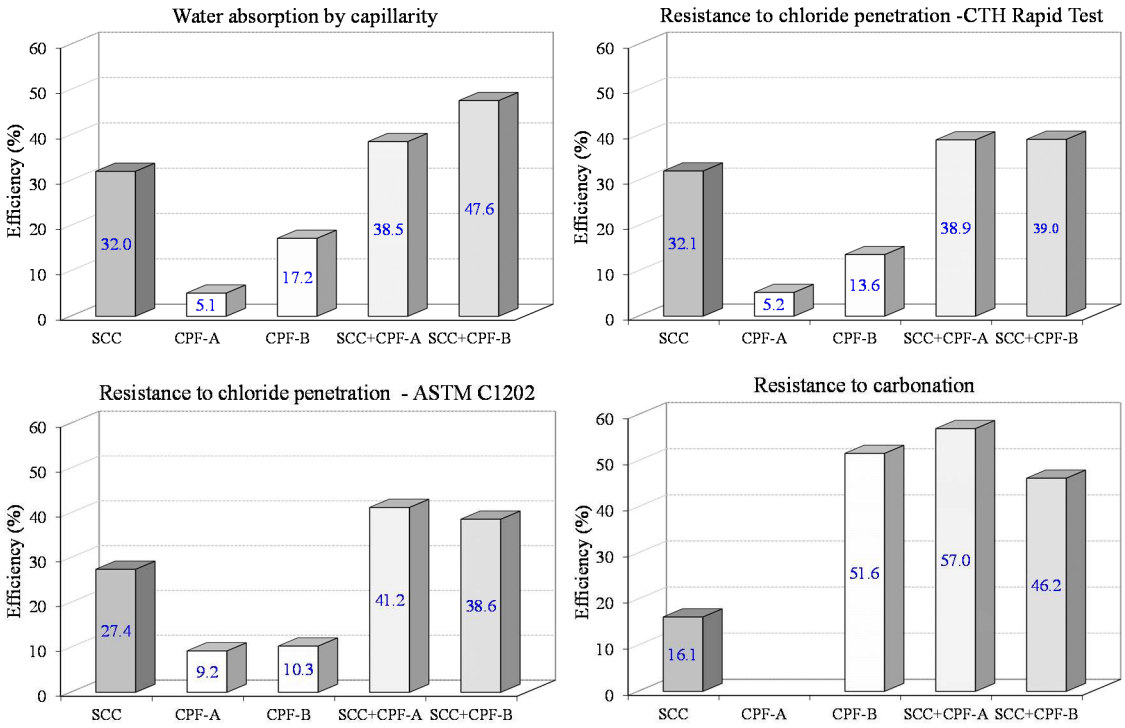

Figure 2.13 – Efficiency of SCC, CPF-A, CPF-B, SCC with CPF-A and SCC with CPF-B systems on durability properties.

Concrete in the SCC box-culvert presented lower sorptivity, this is, absorption by capillarity, higher resistance to chlorides and to carbonation. Considering the first two parameters, SCC technology leads to a 30% enhancement whilst for carbonation resistance efficiency is around 16%. In theory, the factors controlling durability-related properties depend on the amount of paste, the pore structure and the interfacial aggregate/paste zone. The transport properties of concrete depend primarily on the paste volume, pore structure of the paste and ITZ between paste and aggregate particles Zhu *et al.* (2001). Although SCC has higher paste volume, the pore structure of the bulk paste and the ITZ are often improved due to the low water-cementitious materials ratios and the use of additions, but not all additions have the same effect. Zhu et al. (2001) found that chloride diffusivity was very much dependent on the type of addition used in concrete. Fresh SCC compared to CC is more stable and the extra powdered material used, together with the absence of vibration, leads to a more

homogeneous microstructure with denser interfacial zones. A very comprehensive and complete state-of-art concerning all relevant durability issues of SCC was prepared by the RILEM Technical Committee TC 205-DSC: Durability of Self-Compacting Concrete and is presented in RILEM-Report 38 (2007).

Regarding CPF performance, all tests carried out confirmed that durability related parameters are improved with either CPF system. CPF-B, with a stiffer filter-drain compared to CPF-A, led to higher quality concrete cover in terms of absorption by capillarity (17.2%) and chloride ingress (approximately 12%). SCC technology seems more efficient for absorption by capillarity and resistance to chloride ingress whereas CPF reveals better performance in terms of resistance to carbonation. Using SCC together with controlled permeability formwork leads to 40-50% enhancement of properties in the concrete cover. Concerning absorption by capillarity and chloride ion results, CPF on SCC presents similar efficiency to CPF on CC. However, in some cases, CPF on SCC proved to be more effective than on CC, probably due to the higher powdered materials content in SCC composition, which in the concrete cover, as a result of CPF, are drawn and retained at concrete surface.

It should be mentioned that the comparison of durability parameters was based on tests performed in specimens extracted only from the box-culvert side-walls. The slab, wherein the concrete compaction was less efficient in case of CC box-culvert (see 2.5.1.1), was not considered in the analysis, otherwise, the beneficial effect of SCC and CPF would be expected to be greater.

2.6. Conclusions

Results obtained throughout the present research program carried out in actual on-site conditions, led to the following conclusions:

- Innovative technologies such as SCC and CPF seem to be technically and economically viable when used on-site.
- Precast concrete factories are especially suited for the use of self-compacting concrete but some adjustments in installations and equipment might be

necessary in order to optimize casting procedures and maximize benefit from this technology.

- The differences between mix-proportions of the SCC and CC lead to 18 % increase of materials cost for SCC, but final cost will be reduced due to energy and work savings related to absence of compaction as well as savings related to enhanced durability. Full-scale tests carried out at this precast factory demonstrated that the installations and equipment set of for CC has to be adjusted to achieve a more competitive production of SCC.

- In terms of CPF, costs may be reduced by suppression of releasing agents and of surface repairing. Overall costs will also be mitigated by reuse of certain CPF systems as well as enhanced durability.

- In spite of the lower coarse aggregate content of SCC, when compared with CC, with a reduction in water/cement and water/fines ratios, better mechanical properties and resistance to ingress of aggressive agents were obtained. In generally, improved properties were found in moulded specimens than in cores drilled from different parts of the box-curverts, which may be explained by different curing conditions and in the case of CC, also, by different compaction efficiencies.

- Properly proportioned, produced and placed SCC is generally more compact and homogeneous than equivalent vibrated concrete, thus leading to enhanced durability performance of concrete structures when made with SCC.

- Concrete surfaces resulting from CPF application were blow-hole free with no blemishes and, on the contrary, the non-CPF faces, corresponding to the inner sides of the box-culverts side-walls, presented the usual blow-holes which were more prolific in the CC compared to SCC.

- SCC and CPF enhance quality of the concrete cover, however efficiency of CPF technology depends on the system used. Using both technologies

together, controlled permeability formwork on SCC, durability-related parameters analysed improved 40-50%.

- Efficiency of CPF on SCC is similar to efficiency on CC, however, in some cases, CPF on SCC promotes a synergetic effect in terms of quality of the concrete cover thus contributing to sustainable construction.

- A more detailed analysis of the results collected from CTH Rapid Test and ASTM C1202 test led to the conclusion that measuring initial electrical conductivity or electrical resistivity may be a more rapid and economic way to predict resistance of concrete to chloride ion ingress, being, however necessary to know the reaction factor of chlorides with cement phases and the transference number of chloride ions in concrete.

Chapter 3

Durability performance-based design of a SCC exposed to severe marine environment

3.1. Synopsis

The aim of this chapter is to present a systematic methodology to design performance-based self-compacting concrete (SCC) exposed to severe marine environment using a statistical experimental approach. This methodology was applied to the particular case of a cruise terminal building demanding special requirements in terms of architecture, fresh state (self-compactability) and hardened state (compressive strength and high durability). A performance-based design methodology, based on a probabilistic safety format, is presented and applied to define concrete durability requirements. A central composite design was carried out to identify the best mixture, given a set of constituent materials and performance requirements.

3.2. Introduction

Durability, and especially prevention of steel corrosion, has become a critical issue in the management of reinforced concrete structures. Insufficient attention on the durability of concrete structures has led to expensive repair and even demolition and replacement, with great impact on resources, environment and human safety (Walraven, 2009; Gjørv, 2010). Indeed, durability of concrete structures is important from a technical and economical point of view, but also represents a challenge to achieve sustainable development in construction. Designers of reinforced concrete structures

are now aware that prevention of concrete degradation and steel corrosion has to be taken into account since the design stage. In the most recent regulations, the design for durability has attained the same significance as design for safety and serviceability. In particular, in the new *fib*-Model Code (CEB-FIP, 2012) service life design follows the same principle and framework as structural design. Using a performance-based approach, the structure is designed to perform as required during its life cycle. Generally, the performance requirements have to be defined and described in terms of three criteria: definition of the relevant limit state; duration of the relevant period and level of reliability for not passing the limit state during this period (Walraven and Bigaj-van Vliet, 2008). Traditionally, durability design verification provided in standards is simply based on one of two approaches: avoidance of reaction approach or deemed-to-satisfy approach. An avoidance of reaction approach implies that the design excludes the detrimental reaction, which can be achieved for instance by applying membranes or coatings or using non-reactive aggregate (Walraven and Bigaj-van Vliet, 2008). The deemed-to-satisfy approach, also designated by prescriptive approach, is mostly based on empirical requirements which are focused on material properties, material proportions and execution procedures. The design requirement is not explicitly formulated as a predicted service life. This approach has however shown its limitations, in particular with the increasing use of complex mixtures incorporating several types of additions and various organic and mineral admixtures (Baroghel-Bouny, 2002). In fact, when "new" materials are used, when a longer service life is required or under special conditions of aggressiveness, a specific design procedure is required. More recently, performance-based design methodologies based on a probabilistic safety format have been developed (DuraCrete, 2000; CEB-FIP, 2012). In this approach the environmental load is compared with the resistance of the structure, taking into account the influence of time and the probabilistic nature of the environmental aggressiveness, the degradation process and the material properties involved. A full probabilistic design is well suited to design structures with large relevance or to assess existing structures from which relevant data might be derived from (Walraven and Bigaj-van Vliet, 2008). For current structures a semi-probabilistic approach, also called partial safety factor approach, is sufficient.

In fact, nowadays the concrete mix-design process has become very complex due to a considerable increase in the number of constituent materials used in the composition

and performance criteria that the composition must meet (e.g. self-compactability, compressive strength, chloride resistance and cost). Therefore, the typical mixture optimization based on trial and error or "one factor at a time" approaches are inefficient, costly and may not provide the best combination of materials at minimum cost. A statistical experimental design is a more scientific and efficient approach for establishing an optimized mixture for a given set of constraints, while minimizing the number of experimental data tests (Nehdi and Summer, 2002). The derived statistical models, established on the basis of a factorial design, enable a multi-parametric optimization with the user controlling the goal of the optimization and the significance of each experimental parameter. This mix-design approach was followed in the present work.

The aim of this chapter is to present a systematic methodology to design a performance-based SCC exposed to severe marine environment using a statistical experimental design approach. The methodology will be applied to the particular case of a cruise terminal building demanding special requirements in terms of architecture (white concrete with a good quality surface finishing), fresh state (self-compactability) and hardened state (compressive strength and high durability). A performance-based design approach, based on a probabilistic safety format, is presented and applied to define concrete durability requirements. Limit values of the selected durability indicators (apparent chloride diffusion coefficient and electrical resistivity) were specified given the target service life, reliability level and limit state criterion established for the structure. Once the set of concrete requirements (fresh and hardened properties) was defined, mixture optimization was derived from numerical models established on the basis of a factorial central composite design. In order to simplify SCC design, the study was developed in two phases: first at mortar level and then at concrete level.

3.3. Probabilistic performance-based durability design

According to Tuutti's model (Tuutti, 1982) for the deterioration process of structures, the service life of reinforced concrete structures depends on the length of two time periods: the initiation period and the propagation period. The initiation period is the

time required for the aggressive substance to reach the reinforcement and induce depassivation, while the propagation period is related to the evolution of different forms of deterioration after corrosion has been initiated (e.g. cracking or spalling of the concrete cover). Figure 3.1 presents a schematic representation of the service life and limit states considered for a reinforced concrete structure affected by corrosion, according to Tuutti's model.

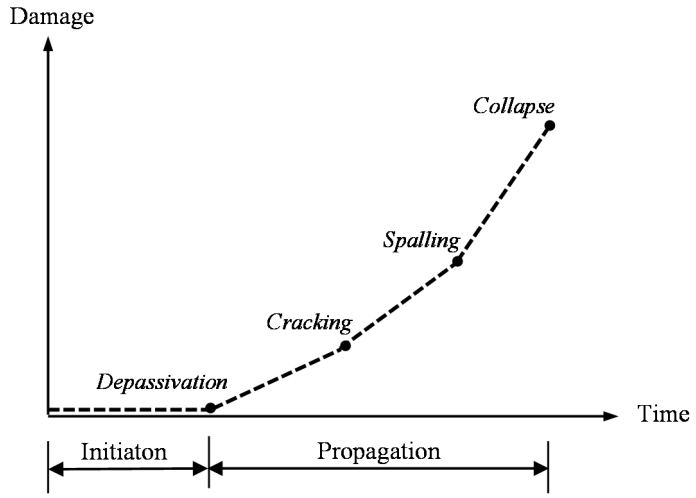

Figure 3.1 – Service life and limit states with respect to reinforced concrete structures affected by corrosion according to Tuutti's model (Tuutti, 1982).

The performance-based design of a structure is generally based on the safety concept, expressed in terms of the limit state function (Z). The limit state function defines safety as the requirement that resistance, R, is greater than or equal to the total action-effect, S, as translated by equation (3.1):

$$Z = R - S \geq 0 \tag{3.1}$$

As for the structural safety, in the performance-based durability design, R and S functions have input parameters that are time-dependent and stochastic variables. Structure behaviour has uncertainties associated with the structural layout, material characteristics, execution conditions and environmental input. Hence, a probabilistic approach as opposed to a deterministic one is recommended to generate reliable predictions of the limit state function. In a probabilistic approach, the probability of exceeding the limit state, denoted probability of failure (p_f), is compared with the target probability of failure (p_{target}), according to equation (3.2). Once the limit state function

has been established, and the variables have been characterized, it is possible to determine the probability of failure by means of several reliability techniques such as First Order Reliability Methods (FORM), Second Order Reliability Methods (SORM) or simulation techniques (e.g. Monte Carlo method).

$$p_f(t) = P\big(R(t) \leq S(t)\big) = P(R(t) - S(t) \leq 0) = P(Z(t) \leq 0) < p_{target} \tag{3.2}$$

In fact, durability design of a structure can be presented in two different formats: the service period design format (expressed in equation (3.2)) and the lifetime design format (DuraCrete, 1999). In the lifetime design format the reliability of the structure is related to the probability that the design service life (t_L) will be exceeded when compared with the target service life (t_g), see equation (3.3). The service life is ended at the moment the limit state is reach. Although they have different formats, service period design and lifetime design use the same basic theoretical concepts and deliver exactly the same result (DuraCrete, 1999). A schematic representation of the problem is shown in Figure 3.2, for the service period design format and lifetime design format.

$$p_f(t) = P\big(t_L \leq t_g\big) < p_{target} \tag{3.3}$$

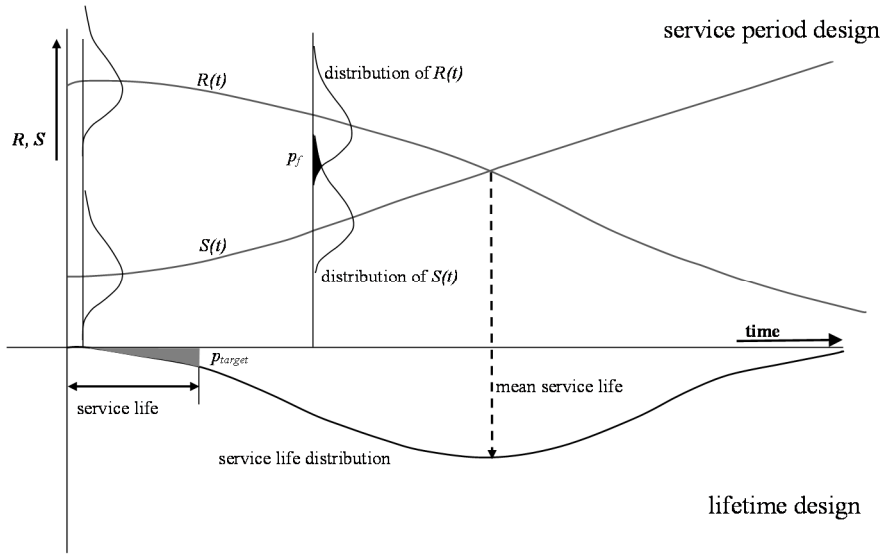

Figure 3.2 – Durability design of a structure by two different formats: service period design and lifetime design (illustrative presentation) (DuraCrete, 1999).

In contrast to a deterministic approach, a sufficient amount of statistical information on each model parameter should be available to characterize the parameters by probability

density distributions, mean value and standard deviation. The absence of reliable databases and the lack of knowledge to adequately characterize the condition and performance of a steel reinforced concrete structure, prevents the correct application of this level of calculation (Ferreira, 2007; Gulikers, 2007; Marques *et al.*, 2012). Therefore, with the durability becoming a functional requirement in the same way as mechanical stability, some recommendations and normative documents have been proposing a modified formalization of the calculation rules able to allow the concept of durability and its associated uncertainty to be presented in the form of partial safety factor method (DuraCrete, 2000; LNEC, 2007; CEB-FIP, 2012). The method directs to a deterministic computation, using safety factors in order to introduce the probabilistic nature of the problem (semi-probabilistic approach), see equation (3.4), where t_d is the service life value, γ_l is the lifetime safety factor and t_g is the target service life.

$$t_d = \gamma_l \cdot t_g \tag{3.4}$$

A probabilistic performance-based service life design should be implemented in several steps: (i) defining the desired/required performance of the structure in terms of target service life, limit state criterion and reliability level (Section 3.4.1.1); (ii) identifying failure mechanism and corresponding degradation processes, selecting relevant durability indicators (Section 3.4.1.2); (iii) defining constituent materials, concreting practices and curing conditions (Section 3.4.1.3); (iv) establishing time dependant mathematical models for the selected durability indicators describing the degradation processes, and based on target service life, limit state criterion and established mathematical models, a limit state function is defined (Section 3.4.1.4); and (v) performing the probabilistic calculation of the limit state function to quantify limit values for the durability indicators (Section 3.4.1.5).

3.4. Case study: concrete requirements

A new cruise terminal building exhibiting a special architecture was designed to serve the north region of Portugal (see Figure 3.3). The external part of the structure consists of a spiral laminar element of white concrete (architectural requirement), which envelops the entire building. Besides its complex geometry this laminar element includes a significant density of reinforcement (prestressing and ordinary reinforcing

steel) and requires good quality of surface finishing, therefore SCC was considered for this specific application. Given these constraints, the SCC for the cruise terminal building should exhibit a slump flow diameter ($D_{flow,concrete}$) between 750.0 and 850.0 mm, a flow time ($T_{funnel,concrete}$) between 10.0 and 15.0 s, a relative filling height (H_2/H_1) higher than 0.90 and a segregation (Sr) lower than 15.0%. In addition to the requirements of self-compactability, the colour (white) and the good quality of surface finishing, performance requirements included compressive strength exceeding 70 MPa and high durability, due to the building location in a very aggressive environment. Durability requirements are specified in Section 3.4.1.

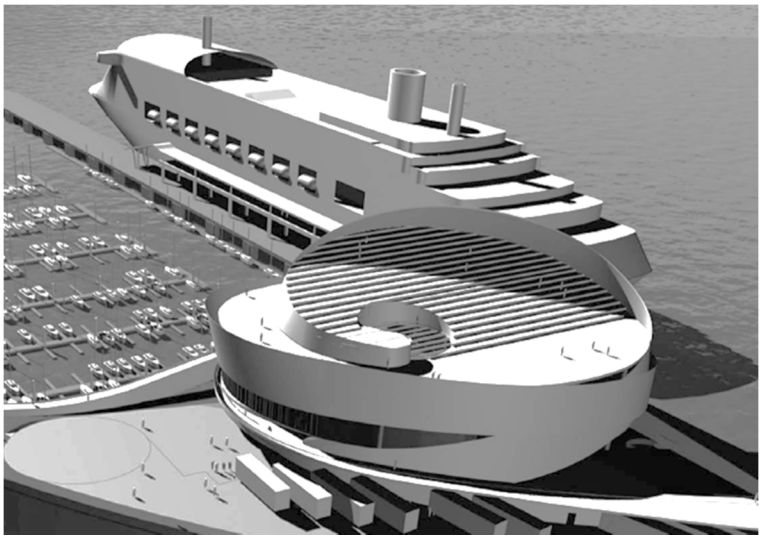

Figure 3.3 – Three-dimensional representation of the cruise terminal building (APDL, 2012).

3.4.1. Durability performance-based specifications

3.4.1.1. Limit state criterion, target service life and reliability level

In some practical cases there is an implied agreement that the end of service life is achieved at the moment that the initially passive condition of the embedded reinforcing steel is lost due to the presence of an excessive amount of chlorides or the arrival of the carbonation front (Gulikers, 2007). In tidal or even splash zones of marine structures, as it is the case of the structure under analysis, the penetration of chloride ions (initiation period) is relatively slow, but as soon as the dissolution of the reinforcement passive layer occurs, corrosion can develop with considerable intensity because there is sufficient amount of moisture and oxygen (propagation period) (Andrade *et al.*, 1993).

Therefore, in the present study, a serviceability limit state of depassivation (structure service life is equal to the initiation period) was considered for the durability requirements specification.

According to the European standard NP EN 1990 (IPQ, 2009), the new cruise terminal building fits into the RC3 reliability class, concerning the high importance of the structure in terms of consequences after failure. Given the reliability class of the structure, the probability of failure for serviceability limit state should not exceed 2.3×10^{-2}, according to E 465 (LNEC, 2007), and the structure service life was established at 75 years (target service life), corresponding to the structural class S5 (NP EN 1992-1-1 (IPQ, 2010b)).

3.4.1.2. Degradation mechanisms and corresponding durability indicators

Concrete structures in marine environment are exposed to the action of many physical and chemical deterioration processes, which may act simultaneously with mutual interdependence and synergistic effects (Liu, 1991; Mehta, 2003). The schematic diagram presented in Figure 3.4 illustrates how different degradation mechanisms can act on concrete structures in a marine environment depending on the exposure zone conditions, namely, the submerged zone, the tidal zone, which includes the splash zone, and the atmospheric zone.

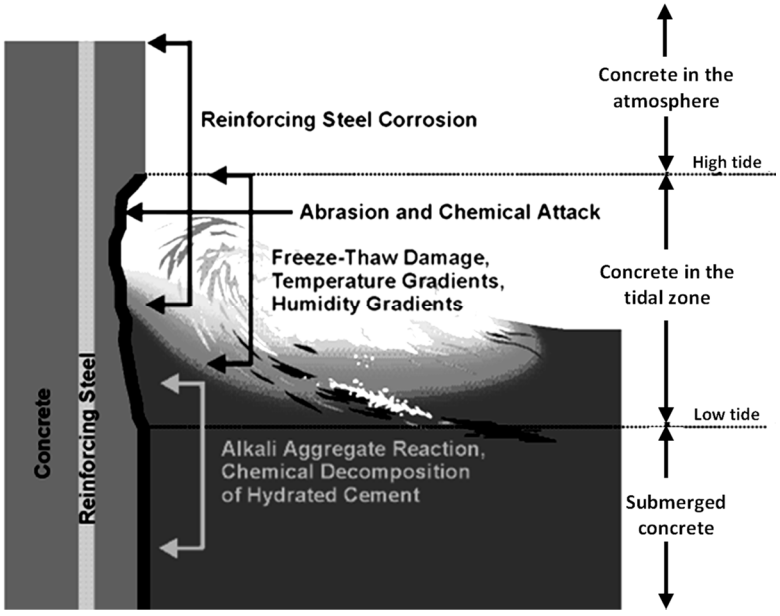

Figure 3.4 – Degradation mechanisms responsible for deterioration of a concrete structure exposed to sea water (Mehta, 2003).

The concrete mixture of the new cruise terminal was designed for the tidal and splash zone, exposure class XS3 according to NP EN 206-1 (IPQ, 2007), since this is the zone with more severe environmental conditions for reinforced concrete.

The physical-chemical processes of sea water attack lead to disintegration of concrete or corrosion of steel. Disintegration of concrete in marine environments is mostly caused by chemical deterioration such as sulphate attack, magnesium attack, alkali-aggregate reaction or leaching. Physical deterioration from crystallisation of soluble hydrated salts in pores of concrete, freezing and thawing, erosion and abrasion also promote further concrete disintegration. Although most of these deteriorating processes may represent potential durability problems, corrosion of embedded steel has been acknowledged as the most critical threat to durability and long-term performance of concrete structures in severe marine environments (Mehta, 2003; Gjørv, 2009). In general, experience has shown that most of these deterioration processes could be controlled or avoided by taking the necessary precautions in selecting material composition (Gjørv, 2009). Nevertheless, preventive measures should take into account the type of environment that the structure is exposed to, since their potential benefit depends on the combined action of the various existing degradation mechanisms.

Since reinforcement corrosion due to chloride penetration is the main cause of concrete degradation in marine environment, concrete permeability, chloride content, availability of oxygen and moisture at the steel surface are the important factors controlling the phenomenon. Therefore, given the main degradation mechanism and the selected limit state (limit state of depassivation) corresponding to the period of chloride penetration, the design of the new cruise terminal building was based on the following durability indicators: apparent chloride diffusion coefficient measured by the migration test ($Dcl_{concrete}$) and electrical resistivity of water saturated test specimens ($\rho_{concrete}$). In fact, for the initiation period the electrical resistivity of concrete in saturated conditions can be correlated with the apparent chloride diffusion coefficient, as shown later. Nevertheless, these two durability indicators were considered as independent variables.

Although not discussed in this work, shrinkage cracking is also a major problem in view of the durability of concrete structures, since if cracking occurs aggressive ions get open access to penetrate into concrete. Properties such as heat of hydration, autogenous shrinkage or early-age deformations, should in some cases be included as durability

indicators in the concrete performance specifications. Also, given the presence of large amounts of sulphates in seawater, sulphate attack would be expected. However, the formation of ettringite in a chloride rich environment is not accompanied by swelling of ettringite through water adsorption, rather than in an alkaline environment (Mehta, 2003).

3.4.1.3. Materials selection

The selection of constituent materials, the design of mix-proportion and the appropriate concreting practices are essential factors to achieve the specified performance-based requirements, both at fresh and hardened states. The design of durable structures should focus on one hand, on the possibility of using additional protective measures, like the use of CPF (controlled permeability formwork) or/and SCC (Figueiras *et al.*, 2009), that could delay the corrosion process and the deterioration of concrete, and on the other hand, the composition design should be appropriate for the exposure class. Sustainable design of highly durable concrete requires an adequate selection and combination of constituent materials, exploiting synergies between different cements and additions (Figueiras *et al.*, 2011). Given all the specified requirements for the concrete of the new cruise terminal building (architectural, hardened and durability properties), the following materials were selected: white cement (CEM II/A-L 52.5N); two white mineral additions, metakaolin and limestone filler; polycarboxylate superplasticizer; and non-reactive aggregates.

White Portland cement is especially used for applications where colour is one of the requirements (Neville, 1998). White cement differs from grey Portland cement by having lower content of Fe_2O_3 and Al_2O_3 and lower alkalis content. An often overlooked advantage of the much lower Fe_2O_3 content in white Portland cement is the higher relative volume of hydrate phases, and therefore a lower capillary porosity (Nielsen, 2004). Furthermore, white Portland cements have a low content of alkalis, which not only reduces the risk of alkali-silica reaction but also results in a higher degree of chloride binding, despite its lower content in Al_2O_3 (Nielsen, 2004). According to Nielsen (2004) the content of alkalis is the main governing parameter for the chloride binding capacity, and owing to the minor effect of Al_2O_3 on chloride binding, low-alkali low-aluminate Portland cements are expected to result in extended service life in marine environments, providing higher protection to both chloride

transport and sulphate attack. However, on the other hand, a study conducted by Andrade and Buják (2013) shows that in natural wet and dry chloride tests, reinforced concrete specimens produced with white cement depassivate first than specimens with ordinary Portland cement and, also, chloride threshold was found to be lower for white cement.

Supplementary cementing materials, like limestone filler and metakaolin, are often used in concrete mixes to reduce cement content, improve workability and enhance mechanical or durability properties. Limestone filler is regularly used as mineral addition in SCC, which although relatively inert appears to contribute directly to concrete properties through three main mechanisms: particle packing effect which could improve mechanical and transport properties; nucleation effects, in which hydration products of traditional cement reactions are slightly accelerated; chemical reaction, which only occurs to a minor extent, producing carboaluminate phases (Schutter, 2011; Tennis *et al.*, 2011). According to some studies, notwithstanding the positive effect of particle packing, a large amount of limestone filler in concrete could affect some concrete durability aspects, especially thaumasite sulphate attack (RILEM-Report 38, 2007; Tennis *et al.*, 2011). This however, should not be a degradation mechanism of great relevance in the case of the new cruise terminal building, since the expected average temperature is around 15ºC. High-reactive metakaolin is one of the more recent types of mineral additions that have been used to produce high-performance concrete. Investigations carried out up to the present show that the use of metakaolin helps in enhancing mechanical and durability properties of concrete. The partial replacement of cement with metakaolin reduces water penetration into concrete by capillary action. Metakaolin modifies the pore structure of the cement matrix and significantly reduces permeability. Although total porosity may be increased by metakaolin blending, the process causes a refinement of the pore structure (Siddique and Klaus, 2009). The chloride ion permeability decreased considerably with increase content of metakaolin (Siddique and Klaus, 2009), but on the contrary, carbonation depth increases, which it is probably due to the fact that the replacement of cement by metakaolin decreases the content of $Ca(OH)_2$ in hydrate products due to pozzolanic reaction (Siddique and Khan, 2012). Also, according to some researches (Siddique and Khan, 2012), metakaolin had been found effective in reducing concrete expansion by

sulphate attack. The use of metakaolin increases the heat evolved during hydration, which may lead to thermal stress cracking (Parande *et al.*, 2009).

The presence of a superplasticizer in concrete composition could also improve durability by a refinement of the pore structure. This tensio-active material gets adsorbed on cement particles, yielding a negative charge that causes the cement particles to repel each other. As a consequence, less cement particles remain unhydrated and a more homogeneous distribution of the hydration products is developed (RILEM-Report 38, 2007).

3.4.1.4. Degradation models and limit state functions

The durability of concrete structures is determined by the transport of aqueous and gaseous substances in the pore system of concrete and their interaction with the hydrated paste matrix, aggregate or steel reinforcement. Chlorides can penetrate in hardened concrete by permeation, diffusion or capillary absorption and by mixed modes of transport mechanisms (CEB-FIP, 2012). In marine environment, when reinforced concrete is exposed to tidal or splash zones (XS3 exposure class) the main transport mechanisms of chlorides into concrete are diffusion and capillarity. Capillary suction occurs in concrete surface layers that are subjected to wetting and drying cycles affecting a thin outer layer of cover concrete (10-20 mm). Therefore, beyond this capillary suction zone, the diffusion process is the most important transport mechanism for the penetration of chlorides (Tuutti referred by Saassouh and Zoubir Lounis (2012)). If chloride penetration is diffusion-controlled, the Fick's second law of diffusion can be used to predict the variation of chloride concentration in time for one dimensional flow. Under the assumption of homogeneous concrete, constant chloride concentration at the exposure surface, linear chloride binding, constant effect of co-existing ions and one dimensional diffusion into semi-infinite space, the error function solution to Fick's second law yields (Luping and Gulikers, 2007):

$$C(x,t) = C_0 + (C_s - C_0)\left(1 - erf\frac{x}{2\sqrt{D_{app}(t)\cdot t}}\right) \tag{3.5}$$

where $C(x,t)$ is the chloride content in percentage of cement by weight (%), at a distance x (m) from the concrete surface after being exposed for a period of time t (s); C_s is the chloride content on the concrete surface in percentage of cement by weight

(%); C_o is the initial chloride content in percentage of cement by weight (%); erf is the error function; $D_{app}(t)$ is the apparent chloride diffusion coefficient in concrete as a function of exposure time (m²/s).

The chloride content C_s at the concrete surface depends on geometrical and environmental conditions, and according to the specification of the Portuguese National Annex to the NP EN 206-1 (IPQ, 2007), E 465 (LNEC, 2007), C_s can be obtained using the following equation:

$$C_s = C_b \cdot 2.5(w/b) \cdot k_{vert} \cdot k_{hor} \cdot k_{temp} \tag{3.6}$$

where C_b is the surface chloride content in percentage (%) that accounts for the salinity of the seawater at the Portuguese coast (21g/l), seawater mean temperature (16±2)ºC and the environmental exposure classes (XS1, XS2 and XS3); w/b is the water/binder ratio; k_{vert} and k_{hor} are coefficients related to environmental exposure considering the concrete location with reference to sea level and its distance to sea coast, respectively; and k_{temp} is the coefficient that accounts for concrete temperature.

The influence of curing and environmental conditions and the time dependence of $D_{app}(t)$ are introduced, according to E 465 (LNEC, 2007), by the following equation:

$$D_{app}(t) = k_{D,c} \cdot k_{D,RH} \cdot k_{D,T} \cdot D_0 \cdot \left(\frac{t_0}{t}\right)^n \tag{3.7}$$

where $k_{D,c}$ is the factor that considers the influence of curing conditions; $k_{D,RH}$ and $k_{D,T}$ are coefficients related to the influence of relative humidity and temperature on the diffusion coefficient, respectively; D_0 is the apparent diffusion coefficient (m²/s), obtained from migration laboratory tests performed at the reference age t_0; and n is the concrete's ageing factor, which represents the time dependence of the diffusion coefficient or the increasing ability of the concrete to resist chloride penetration over time. Several effects have been attributed to time dependence of the concrete chloride diffusion coefficient, mainly the evolution with time of the concrete pore refinement, changes in binding ability of cement phases towards chlorides and the possible changes of chloride surface concentration (Andrade *et al.*, 2011). The n coefficient in equation (3.7) is a constant, and it depends on the type of cementitious materials used, the mixture proportions and the concrete exposure conditions. The way concrete's ageing

factor is introduced has been discussed by the scientific community and there is still a need to clarify issues such as the solution of the differential equation of Fick's second law when this factor is applied (Luping and Gulikers, 2007; Andrade *et al.*, 2011) or the period of time that should be considered for the time dependence of chloride diffusion coefficient (Andrade *et al.*, 2013). Given the lack of consensus on this issue, in the present work the solution of the Fick´s second law presented in equation (3.5) will be considered and the ageing factor will be applied to a period of time equal to the exposure period of time, t in equation (3.7).

Therefore, for concrete mixture design of new structures, the required chloride diffusion coefficient of the composition, $\mathrm{Dcl}_{\mathrm{concrete}}$ ($\mathrm{Dcl}_{\mathrm{concrete}}$ and D_0 are the same parameter in the present work) can be determined using equation (3.8), developed from equations (3.5), (3.6) and (3.7), considering that x is the concrete cover thickness c, the initial chloride content (C_o) is zero and, for the limit state of depassivation, which is the limit state considered for this structure, the exposure period of time t is equal to the initiation period t_i and $C(x,t)$ is equal to the chloride threshold level necessary to depassivate reinforcing steel (C_r). The depth of the capillary suction zone is also taken into account in the model by the parameter Δx. The model uncertainty is taken into account by the parameter λ.

$$Dcl_{concrete} = \left(\frac{(c - \Delta x)^2}{4 \cdot t_i \cdot \left(erf^{-1}\left(\frac{C_s - C_r}{C_s}\right)\right)^2 \cdot k_{D,c} \cdot k_{D,RH} \cdot k_{D,T} \cdot \left(\frac{t_0}{t_i}\right)^n} \right) \cdot \lambda \qquad (3.8)$$

Electrical resistivity limit value can be computed using the relationship between diffusivity and resistivity, based on the Nernst-Einstein equation and assuming the square root relation between diffusivity and penetration depth of the aggressive agent (Einstein´s theory to the Brownian motion of a particle) (Andrade *et al.*, 2000). For the limit state of depassivation, where the service lifetime is equal to the initiation period t_i and based on the model proposed by Andrade *et al.* (Andrade *et al.*, 2000; Andrade *et al.*, 2013), the required electrical resistivity of the concrete could be obtained by equation (3.9):

$$\rho_{concrete} = \frac{t_i \cdot k_{cl}}{(c - \Delta x)^2 \cdot \left(\frac{t_{hydr}}{t_0}\right)^q \cdot r_{cl} \cdot k_{\rho,c} \cdot k_{\rho,RH} \cdot k_{\rho,T}} \qquad (3.9)$$

where $\rho_{concrete}$ (Ω.m) is the "effective" resistivity measured under saturated conditions at time t_0 (years); t_i (years) is the exposure period of time equal to the initiation period; k_{cl} is a factor which depends on the external ionic concentration; c (m) is the concrete cover thickness; Δx (m) is the depth of the capillary suction zone; r_{cl} is a reaction or binding factor; q is the ageing factor of resistivity which can be deduced from the ageing factor n of chloride diffusion by means of an experimental expression (Andrade *et al.*, 2011) (q=0.798n-0.0072); t_{hydr} (years) is the period of time the ageing factor should be applied in the electrical resistivity model (Andrade *et al.*, 2013); $k_{\rho,c}$ is the curing factor; $k_{\rho,RH}$ is the humidity factor; and $k_{\rho,T}$ is the temperature factor. It should be noted that the period of time the ageing factor is applied in the chloride diffusion coefficient model is different to the electrical resistivity model.

3.4.1.5. Limit values of selected durability indicators

Limit values of the durability indicators selected for the design of the terminal cruise concrete were specified using the mathematical models (limit state functions) presented in the previous section, and adopting a full probabilistic approach for the concrete apparent chloride diffusion coefficient ($Dcl_{concrete}$) and a partial safety factor approach for the concrete electrical resistivity ($\rho_{concrete}$).

The probabilistic analysis approach was implemented with a Latin Hypercube simulation method, using a commercial software (@Risk, 2013) and applying a set of 10^5 simulations, thus ensuring a high accuracy of the result. The Kolmogorov-Smirnov test was performed to evaluate the quality of the generated samples. Table 3.1 shows the input parameters characterization of the chloride diffusion coefficient model. In the case of stochastic variables a statistical characterization is presented, namely the distribution type, the average and standard deviation. The values adopted for characterization of the model parameters were based on data provided by E 465 (LNEC, 2007), *fib*-Model Code (CEB-FIP, 2012), DuraCrete (2000), Nokken *et al.* (2006) and Marques *et al.* (2012).

Table 3.1 – Parameters characterization of chloride diffusion coefficient model for a probabilistic analysis.

Variable	Distribution	Mean value (μ)	Stand. deviation (σ)	Observations
λ	normal	1	0.15	
c	lognormal	60 mm	7 mm	c=c_{nom} according to NP EN 1992-1-1 (IPQ, 2010b), value that should be considered for the construction project drawings and specifications, in order to take into account any expected deviation
Δx	beta	8.901 mm	5.604 mm	
t_i	deterministic	75 years	-	t_i=t_g for a serviceability limit state of depassivation
t_o	deterministic	28 days	-	
$k_{D,c}$	deterministic	1.0	-	corresponding to 7 days curing
$k_{D,RH}$	deterministic	1.0	-	corresponding to the exposure class XS3
$k_{D,T}$	normal	0.8	0.16	corresponding to a mean concrete temperature of 15ºC
n	normal	0.54	0.06	
C_r	normal	0.4%	0.048%	
C_s	normal	3.24%	0.324%	
C_b=3.0%				corresponding to 21g/l salinity, 16±2ºC and XS3
w/b=0.36				maximum value of water/binder ratio expected for the concrete composition
k_{vert}=1.0				corresponding to the exposure class XS3
k_{hor}=1.0				corresponding to a distance of the concrete surface from the coast of 0 km
k_{temp}=1.2				corresponding to a mean surface concrete temperature of 15ºC

In the case of electrical resistivity, a partial safety factor approach was carried out due to an insufficient amount of statistical information on some of the model parameters. The analysis was performed using a safety factor γ=2.8, provided by E 465 (LNEC, 2007) for RC3 reliability class. The definition of the safety factor was based on the assumption that the lifetime of the structure is following a lognormal distribution with a coefficient of variation of 0.5 (LNEC, 2007). Table 3.2 shows the values adopted for the model parameters, which are based on Andrade *et al.* (2013), DuraCrete (2000), Nokken *et al.* (2006) and E 465 (LNEC, 2007).

Table 3.2 – Parameters characterization of electrical resistivity model, for a partial safety factor analysis.

Variable	Design value	Observations
c	50 mm	c=$c_{min,dur}$ is the characteristic value of the concrete cover
Δx	8.9 mm	
t_i	210 years	t_i=$t_g \cdot \gamma$ for a serviceability limit state of depassivation and RC3 reliability class (t_g=75 years and γ=2.8)
t_{hydr}	10 years	
t_o	28 days	
q	0.424	
k_{Cl}	25000 Ω.cm^3/year	corresponding to the exposure class XS3
r_{cl}	1.5	
$k_{\rho,c}$	1.0	corresponding to 7 days curing
$k_{\rho,RH}$	1.0	corresponding to the exposure class XS3
$k_{\rho,T}$	1.25	corresponding to a mean concrete temperature of 15ºC

Figure 3.5 presents the variation of the two durability indicators, $Dcl_{concrete}$ and $\rho_{concrete}$, as a function of nominal concrete cover (c_{nom}), determined by a full probabilistic approach and a partial safety factor approach, respectively. Given all the constraints imposed to the structure and for a c_{nom} of 60 mm (see Figure 3.5), concrete composition of the new cruise terminal building should exhibit a $Dcl_{concrete}$ lower than 3.26x10^{-12} m^2/s and $\rho_{concrete}$ higher than 210.5 Ω.m. Noteworthy that if a semi-probabilistic approach had been performed to determine $Dcl_{concrete}$, using the same safety factor used in electrical resistivity analysis and the characteristic value of the concrete cover, presented in Table 3.1, the threshold value would be higher than that obtained by a full probabilistic analysis (4.82x10^{-12} m^2/s). Contrary to what would be expected, the safety factor approach was less conservative than the full probabilistic approach. According to Marques *et al.* (2012) in the performance-based approaches for chloride action, the statistical distribution of service life should be analysed considering a calibration of safety factors so that both approaches, probabilistic and safety factor, could converge.

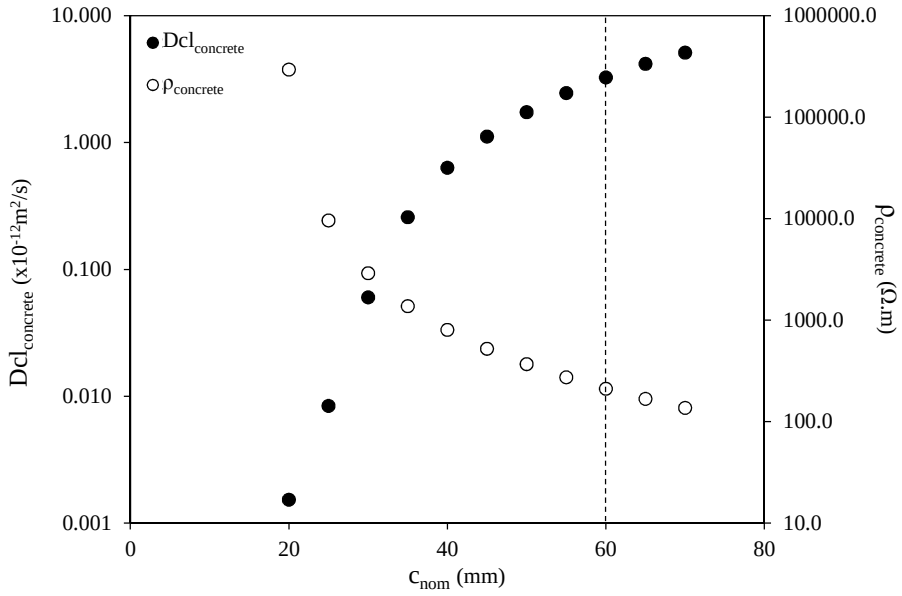

Figure 3.5 – $Dcl_{concrete}$ and $\rho_{concrete}$, for different nominal concrete cover values (c_{nom}), determined by a full probabilistic approach and a partial safety factor approach, respectively.

Despite probabilistic analysis can provide a more accurate analysis and, in some cases, even represent cost savings, minor changes in the values of model parameters (average or standard deviation) can lead to very different results. A probabilistic analysis needs to be supported by a sufficiently reliable database that allows confidence in the input data and in the corresponding model outcome. A careful characterization of the model parameters is very important to obtain realistic threshold values and a sensitivity analysis helps to define the most influential parameters, and therefore to take an additional care in the characterisation of these parameters (distribution type, average value and standard deviation). A sensitivity analysis of the main chloride diffusion coefficient model parameters was performed by analysing the model outcome in a probabilistic way, using the same probability of failure (2.3x10^{-2}). Each parameter average value was varied of $\pm\sigma_j$ (standard deviation of parameter j) with respect to the reference average value, whereas keeping constant the respective standard deviation and the other model parameters (distribution type, average value and standard deviation). The sensitivity coefficient φ_j, determined according to equation (3.10), provides a measure of the significance of the stochastic model parameter on the model outcome ($Dcl_{concrete}$).

$$\varphi_j = \delta_j \left|\frac{\Delta Y}{\Delta X_j}\right| = \delta_j \left|\frac{\Delta y / y_o}{\Delta x_j / x_{j,0}}\right| = \delta_j \left|\frac{(y_{\alpha\sigma} - y_0)/y_0}{(x_{j,\alpha\sigma} - x_{j,0})/x_{j,0}}\right| \quad (3.10)$$

Where in δ_j is the coefficient of variation of the stochastic model parameter j; $x_{j,0}$ is the average value of model parameter j; $x_{j,\alpha\sigma}$ is the value of model parameter j, result of a change of the average value of $\pm\alpha\sigma_j$, with α being equal to 1 in the present study; y_0 is the model outcome value performed in a probabilistic analysis and using the parameters characterization present in Table 3.1; $y_{\alpha\sigma}$ is the model outcome value performed in a probabilistic analysis and using the parameters characterization present in Table 3.1, except for the average value of parameter j which was replaced by $x_{j,\alpha\sigma}$ value.

The normalized sensitivity coefficient φ_j^{rel}, is determined dividing φ_j by the maximum absolute value of the obtained sensitivity coefficients of the model parameters, φ_{max} (equation (3.11)).

$$\varphi_j^{rel} = \frac{\varphi_j}{\varphi_{max}} \quad (3.11)$$

In Figure 3.6, the normalized sensitivity coefficients for positive and negative variation of each model parameters are presented. The most influential model parameters and, therefore, the most critical in a probabilistic performance-based design, are the concrete's ageing factor (n) and the concrete cover thickness (c), while the least influential model parameters are the chloride threshold (C_r) and the chloride content on the concrete surface (C_s). The influence of temperature ($k_{D,T}$) and model uncertainty (λ) on $Dcl_{concrete}$ is considered to be significant. Similar results were obtained by Ferreira (2007), although using a different procedure to evaluate the sensitivity of the model parameters.

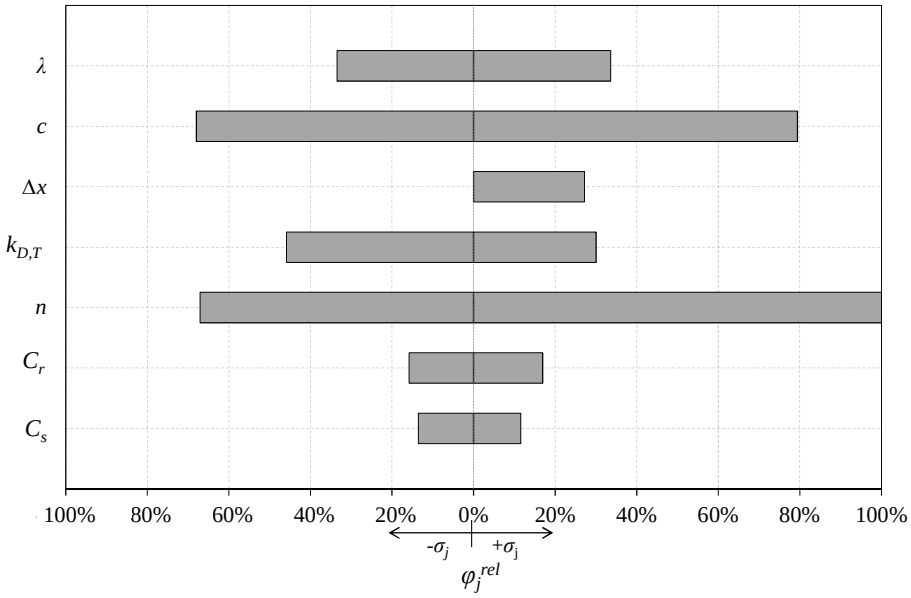

Figure 3.6 – Normalized sensitivity coefficient φ_j^{rel} for positive and negative variation of each model parameters ($\pm\sigma_j$).

3.5. Statistical experimental design

Given the numerous factors affecting flow properties of SCC, the mixture design and production of this type of concrete can involve balancing several factors to achieve adequate fresh properties (Khayat *et al.*, 1999). The mix-design process has become even more complex with the increasing variety of materials available to produce concrete, namely, several kinds of cements and mineral additions (including recycled waste materials) and a new generation of chemical admixtures (superplasticizers, viscosity agents, etc.). Therefore, to facilitate material selection and mixture optimization protocols, efforts have been developed to correlate the flow properties of SCC to those of mortar or paste (Okamura *et al.*, 2000; Saak *et al.*, 2001; Grünewald and Walraven, 2007; Erdem *et al.*, 2009; Nunes *et al.*, 2009b; Nunes *et al.*, 2011; Figueiras *et al.*, 2014). Indeed, SCC can be considered as a suspension of aggregates in paste (see Figure 3.7), where sufficient paste must be provided to fill the voids between the compacted aggregates and to form a thin layer of paste around the aggregate particles (excess paste). This excess paste layer lubricates aggregate particles, which reduces interparticle friction allowing their relative movement and increases flowability of the mixture (Grünewald and Walraven, 2007; Koehler and Fowler, 2007). The required

paste volume to achieve adequate fresh properties is determined by the rheological properties of cement paste and the aggregate volume fraction, packing density and surface area.

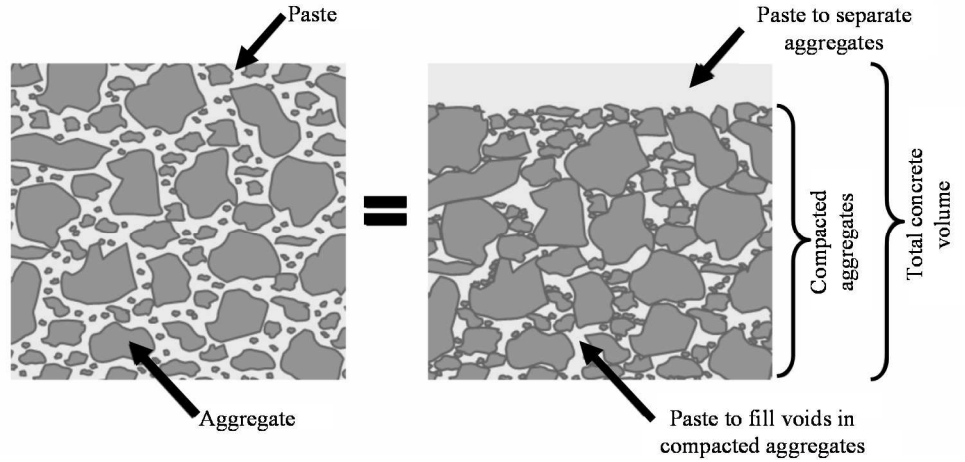

Figure 3.7 – Schematic representation of concrete as a suspension of aggregate particles in paste (Koehler and Fowler, 2007).

In fact, paste workability plays a major role in concrete and therefore it is reasonable to expect that there is a direct relationship between paste and concrete flow behaviour (Hidalgo *et al.*, 2008). Besides controlling concrete workability, paste composition also has a large influence on the early-age and long-term properties, including durability. Using paste or mortar testing as a previous step in SCC design simplifies experimental work involved, mainly because concrete tests are reduced to a minimum and mortar or paste tests are easier to carry out, less time and material consuming (Okamura *et al.*, 2000; López *et al.*, 2009). However, the prediction of concrete behaviour, based on paste properties, is not yet fully established, especially with regard to hardened properties. Fresh mortar properties adequate for SCC were well defined by Professor Okamura and his co-workers in the Japanese SCC-designing method (Okamura *et al.*, 2000).

The SCC mixture design approach followed in this study is developed in two phases: in the first phase, at mortar level (mortar mix-design), paste mixture proportions are optimized, and in the second phase, at concrete level, mixture parameters related with the aggregate skeleton are adjusted (concrete mix-design). A flow chart of the statistical performance-based design approach used in this study is presented in Figure 3.8.

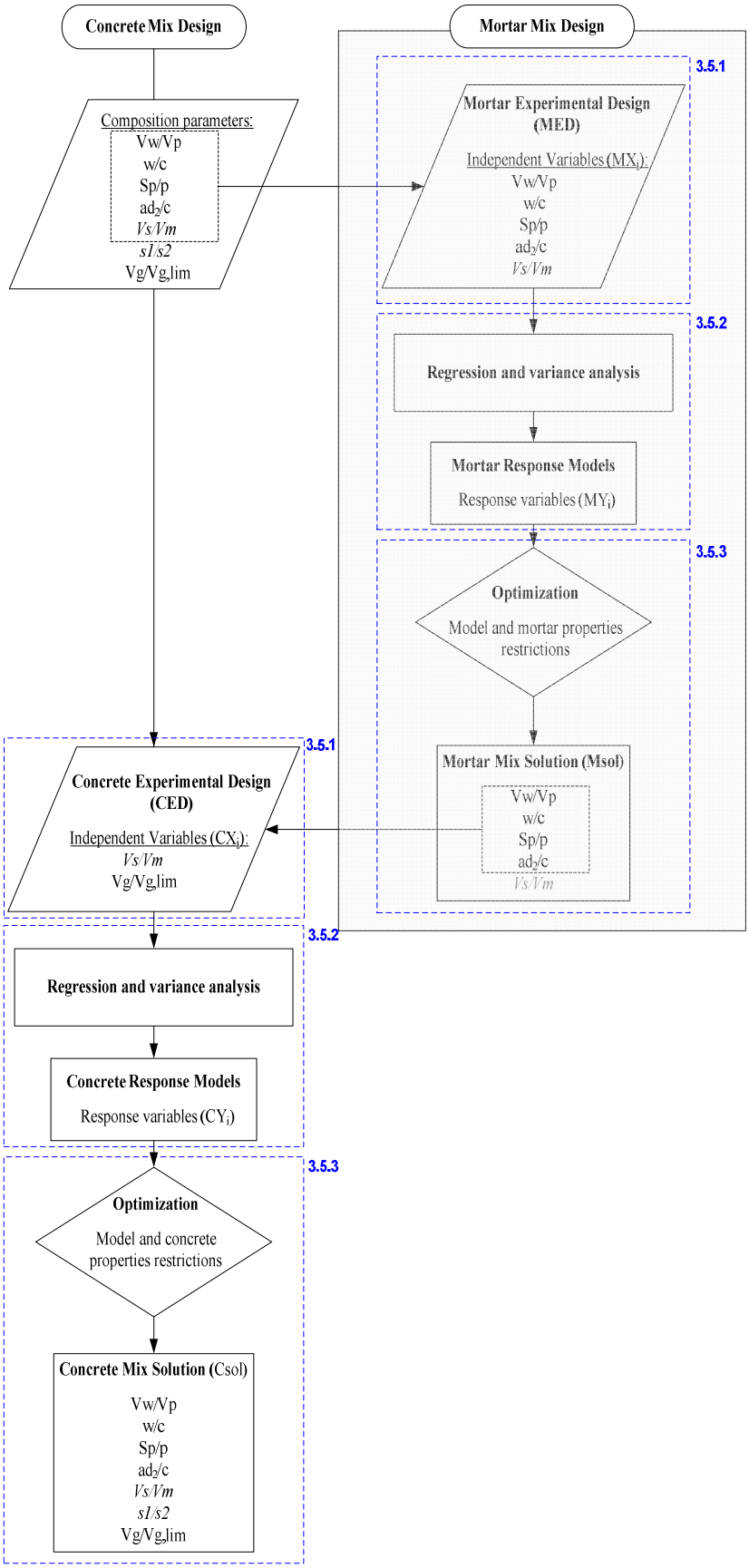

Figure 3.8 – Flow chart of the statistical performance-based design approach used in this study.

Mortar and concrete mixtures were designed based on statistical experimental design techniques that have been applied to self-compacting mortar and concrete (Khayat *et al.*, 2000; Nehdi and Summer, 2002; Sonebi, 2004; Nunes, 2008). These techniques provide a way of planning experiments in order to collect the appropriate data to derive statistical models, evaluate individual and interaction effects of mixture parameters on fresh and hardened properties and optimize mix-proportions for a given set of constraints (fresh and hardened properties and economic constraints). Thereby, for mortar and concrete level the design methodology is developed in three steps: first step, definition and implementation of the experimental plan (see Section 3.5.1); second step, statistical data analysis and model fitting of data collected during the experimental phase (see Section 3.5.2); and, third step, the numerical optimization of mixture parameters, using the models derived in the previous phase (see Section 3.5.3). A brief outline of the overall methodology is presented herein and more detailed information can be found in Nunes (2008).

3.5.1. Definition and implementation of the experimental plan

Based on the Japanese SCC-designing method (Okamura *et al.*, 2000), SCC composition can be defined using the following independent variables: water to powder volume ratio (Vw/Vp); water to cement weight ratio (w/c); superplasticizer to powder weight ratio (Sp/p); sand to mortar volume ratio (Vs/Vm); and coarse aggregate to dry rodded coarse aggregate volume ratio (Vg/Vg,lim). Additional variables must be considered when fine aggregate is a combination of two sands (s_1/s_2) or whenever two or more types of additions (ad_2/c) are used. The air content (Va) is generally set at 2%. The study conducted at mortar level, performed with standard sand, will permit determining variables of the optimized paste mix-proportions, namely, Vw/Vp, w/c, Sp/p and ad_2/c. These paste mix-proportions are maintained at concrete level and only the parameters related with the aggregate content and aggregate skeleton (Vs/Vm, Vg/Vg,lim and s_1/s_2) are defined as variables. As will be discussed later, the volumetric ratio Vs/Vm set at mortar level will affect the total aggregate content of concrete, since it influences paste fresh properties.

Mortar and concrete mix-designs were performed through a statistical experimental design, which allows to derive statistical models for mortar/concrete properties

(response variables) from mixture parameters (independent variables) (Montgomery, 2001). Since expected responses, fresh and hardened properties of mortar and concrete, do not vary in a linear manner with the selected variables, experiments were designed according to a factorial central composite design (2^k, where k is the number of independent variables x_i) adequate to fit a second order model. When the number of factors (variables) in a 2^k factorial plan increases, the number of experiments needed to perform the full factorial plan grows rapidly, becoming a very time consuming process. If the effect of higher order terms in the model is negligible in regard to lower order terms, it is possible to consider only part of the plan to establish response models, for example a 2^{k-1} fractional factorial plan. The effect of each factor is evaluated at five different levels, codified as $-\alpha$, -1, 0, $+1$, $+\alpha$. In order to make the design rotatable (i.e. the standard deviation of the predicted response is constant in all points at the same distance from the center of the design) the α value should be taken equal to $n_f^{1/4}$, where n_f is the number of points in the factorial part of the design. The range of variables variation ($-\alpha$ to $+\alpha$) was established based on a set of preliminary tests where extreme mixtures, least fluid mixture and most fluid mixture, were tested to ensure that it was possible to achieve their characterization in the fresh state. Some prior knowledge of the materials to be used and SCC proportioning helped to define the range of variables variation (Koehler and Fowler, 2007). The transformation of coded into absolute values is performed according to the following equation:

$$a = a_0 + x \cdot \Delta_a \tag{3.12}$$

with a being the absolute value in normal units; a_0 being the absolute value of the variable at the centre of the design; x being the coded variable measured with the step like units; and Δ_a the variable variation (in absolute values) corresponding to a unit change in the coded variable. Experimental programs also include central point replication in order to evaluate the experimental error associated to conditions and test procedures variability (Montgomery, 2001).

3.5.2. Data analysis and fitted response models

In this work a commercial software (Design-Expert-Software, 2007) was used to analyse the results of each response variable, by examining summary plots of the data,

fitting a model by using regression analysis and analysis of variance (ANOVA), validating the model by examining the residuals for trends and outliers and interpreting the model graphically.

For each response variable, a quadratic model can be estimated from the central composite design data. The generic form of a second order model is presented in equation (3.13), where: y is the response of the material; x_i are the independent variables; β_0 is the independent term; β_i, β_{ii} and β_{ij} are the coefficients of independent variables and interactions, representing their contribution to the response; and ε is the random residual error term representing the effects of variables or higher order terms not considered in the model.

$$y = \beta_0 + \sum_{i=1}^{k} \beta_i x_i + \sum_{i=1}^{k} \beta_{ii} x_i^2 + \sum_{i<j} \sum \beta_{ij} x_i x_j + \varepsilon \tag{3.13}$$

The model parameters (β_0, β_i, β_{ii} and β_{ij}) are estimated by means of a multilinear regression analysis. The significance of each factor on a given response can be evaluated using a Student's *t*-test and a backward elimination was used in this work to eliminate non-significant terms in the regression model (Design-Expert-Software, 2007), i.e. those terms associated with a *p*-value greater than the defined significance level (in this study, α=0.05). An analysis of variance is used to evaluate the regression model in several aspects, namely, the significance of regression, lack of fit and significance of each variable in the model. The hypothesis-testing procedure involved in regression analysis is based on the assumptions that the errors are independent and normally distributed with zero mean and constant variance.

3.5.3. Mixtures optimization

The fitted numerical models are used to define mix-proportions (mortar or concrete) that meet certain performance requirements defined in advance. These requirements may be set in terms of fresh properties (deformability and viscosity), hardened properties (mechanical and durability properties) and economic requirements. A last constraint should be implemented in the optimization process due to the fact that the error function that is associated to each response model increases with the distance to the center of the modelled region (D_{center}). In the present work numerical optimization

was performed using a software developed in MATLAB 2011b, which is based on a subroutine provided by the program in the Optimization Toolbox Solvers (MATLAB 2011b, 2011). In fact, this optimization process is a general problem of solving a system of non-linear multidimensional equations, with the same number of equality conditions as variables in the model.

3.6. Experimental programme

3.6.1. Materials characterization

The mortar and concrete mixes investigated in this study were prepared with white cement (CEM II/A-L 52.5N) according to EN 197-1 (IPQ, 2012) and two mineral additions, metakaolin and limestone filler, with a specific gravity of 3.04, 2.21 and 2.68, respectively. The mean particle size dimension of cement, metakaolin and limestone filler was 11.03 μm, 7.12 μm and 6.53 μm, respectively. A polycarboxylate type high range water reducing admixture was used having a specific gravity of 1.07 and 26.5% solid content. Standard sand (IPQ, 2006) used in mortar mixes is a siliceous round natural sand (0.08-2 mm) with a specific gravity of 2.63 and an absorption value of 0.30%. Crushed calcareous aggregate, a siliceous natural fine sand (sand 1) with a fineness modulus of 2.01 and natural coarse sand (sand 2) with a fineness modulus of 3.94 were used in concrete mixes (see Table 3.3). The specific gravity of the coarse aggregate, sand 1 and sand 2 were 2.68, 2.59 and 2.66, and the absorption values were 0.60%, 0.80% and 0.20%, respectively, according to EN 1097-6 (IPQ, 2003a). Bulk density of compacted coarse aggregate was 1.54.

Table 3.3 – Grading of aggregates.

Sieve size (mm)	0.063	0.125	0.250	0.500	1.000	2.000	4.000	8.000	11.200	16.000
Sand 1	3.97	9.23	28.37	65.92	95.57	99.63	100.00	100.00	100.00	100.00
Sand 2	0.86	1.10	1.85	6.60	31.15	70.97	94.35	100.00	100.00	100.00
Coarse aggre.	0.72	0.78	0.83	0.87	0.92	0.99	1.35	31.05	79.53	100.00

3.6.2. Experimental design

SCC mortar mix-proportions were established based on the following five variables x_i: Vw/Vp, w/c, Sp/p, Vs/Vm and metakaolin to cement weight ratio, mtk/c. At concrete level two independent variables were studied, namely, Vs/Vm and Vg/Vg,lim, keeping constant the ratio between the two sands (s1/s=0.400). This value was fixed following a set of preliminary tests carried out at mortar level, aimed at finding the weight ratio of sands leading to the greater spread flow area. Table 3.4 presents the experimental plans adopted to study mortar (MED) and concrete (CED) mixtures, namely the characterization of the factorial statistical design, independent variables and respective range of variation. Mix-proportions of mortars and concretes prepared in this study were obtained using the formulation presented in the Appendix.

Table 3.4 – Mortar and concrete experimental designs characterization.

Designation	Experimental design	Independent variables	$[-\alpha; +\alpha]$
Mortar Experimental Design (MED)	2^{5-1} α=2.000 n_c=6 n_f=16 n_a=10	Vw/Vp w/c Sp/p mtk/c Vs/Vm	[0.800; 1.000] [0.360; 0.460] [0.680%; 0.720%] [3.0%; 15.0%] [0.400; 0.500]
Concrete Experimental Design (CED)	2^2 α=1.414 n_c=4 n_f=4 n_a=4	Vs/Vm Vg/Vg,lim	[0.400; 0.480] [0.480; 0.580]

n_c: number of central points; n_f: number of factorial points; n_a: number of axial points

3.6.3. Mixing procedure, response variables and testing methods

Mortar mixes were prepared in 2.42 l batches and mixed in a two-speed mixer complying the NP EN 196-1 (IPQ, 2006), according to the following procedure: (i) mix sand and powder materials (cement, limestone filler and metakaolin) with 0.80 of the mixing water during 60 s; (ii) stop the mixer to scrape material adhering to the mixing bowl; (iii) mixing for another 60 s; (iv) add the rest of the water with the

superplasticizer and mix for 60 s; (v) stop the mixer again to scrape adherent material; (vi) mix for 60 s; (vii) stop the mixer for 5 min; and (viii) mix mortar during 90 s. The mixer was always set at low speed except in the last 90 s of mixing sequence where it was set at high speed. Mortar tests using the flow cone and the V-funnel, with the same internal dimensions as the Japanese equipment, were then carried out to characterize fresh state (see Okamura and Ouchi (2003) for details on equipment and testing procedures). The mortar flow test ($D_{flow,mortar}$) was used to assess deformability by calculating the flow diameter as the mean of two diameters in the spread area and the V-funnel test was used to assess the viscosity and passing ability of the mortar. Test flow time was recorded ($T_{funnel,mortar}$). After fresh mortar tests, specimens were moulded: three prisms (40x40x160 mm^3) to evaluate electrical resistivity ($\rho_{28d,mortar}$) and compressive strength ($fc_{28d,mortar}$) at 28 days, and three cylinders (ϕ=100 mm; h=50 mm) to evaluate chloride diffusion coefficient (Dcl_{mortar}). Mortar specimens were demoulded one day after casting and kept under water in a chamber under controlled environmental conditions (T=20ºC) until testing age.

Concrete mixes were prepared in the laboratory in batches with total volume of 33 l using an open pan mixer with vertical axis. The mixing sequence was as follows: (i) mix both sands and coarse aggregate with 0.15 of the mixing water during 2.5 min; (ii) stop mixing for 2.5 min for aggregates absorption; (iii) add powder materials followed by the rest of water with the superplasticizer; (iv) mix for 5 min; (v) stop the mixer for 1 min to clean mixer paddles; and (vi) mix concrete during 3 min. Self-compacting properties were evaluated through the slump-flow, the V-funnel, the L-box and the segregation tests according to the standards NP EN 12350-8 (IPQ, 2010c), NP EN 12350-9 (IPQ, 2010d), NP EN 12350-10 (IPQ, 2010e) and NP EN 12350-11 (IPQ, 2010f), respectively. The slump-flow test was used to evaluate the deformation capacity, with slump-flow diameter ($D_{flow,concrete}$) being recorded. The V-funnel test was used to assess viscosity and passing ability of SCC, with test flow time ($T_{funnel,concrete}$) being recorded, and the L-box was used to assess the ability of concrete to pass through tight openings between reinforcing bars (filling ability), by recording a relative filling height (H_2/H_1). To assess concrete segregation resistance (Sr) the sieve segregation test was performed. After fresh concrete tests some specimens were moulded to characterize hardened concrete, namely, electrical resistivity ($\rho_{28d,concrete}$), compressive strength ($fc_{28d,concrete}$) and chloride diffusion coefficient ($Dcl_{concrete}$). Concrete specimens were demoulded one day

after casting and kept under water in a chamber under controlled environmental conditions (T=20ºC) until testing age, 28 days.

Mixtures from both experimental plans, MED and CED, were tested in a random order. Table 3.5 presents a summary of mortar and concrete properties that have been analysed and modelled (response variables, y_{Mi} and y_{Ci}), as well as, the followed standard, test equipment and/or specimens used.

Table 3.5 – Mortar and concrete response variables: testing methods.

	Test designation	Test equipment and specimens
Mortar response variable (y_{Mi})		
$D_{flow,mortar}$	Mortar flow test (Okamura and Ouchi, 2003)	mini-slump flow cone
$T_{funnel,mortar}$	Mortar V-funnel test (Okamura and Ouchi, 2003)	mini-V-funnel
$fc_{28d,mortar}$	Mortar compressive strength (IPQ, 2006)	3 prisms (40x40x160 mm^3)
$\rho_{28d,mortar}$	Mortar electrical resistivity	3 prisms (40x40x160 mm^3)
Dcl_{mortar}	Mortar chloride diffusion coefficient (LNEC, 2004)	3 cylinders (ϕ=100mm; h=50mm)
Concrete response variable (y_{Ci})		
$D_{flow,concrete}$	Concrete slump-flow test (IPQ, 2010c)	Abrams cone and plate
$T_{funnel,concrete}$	Concrete V-funnel test (IPQ, 2010d)	V-funnel
H_2/H_1	L-Box test (IPQ, 2010e)	L-box
Sr	Sieve segregation test (IPQ, 2010f)	perforated plate sieve and balance
$fc_{28d,concrete}$	Concrete compressive strength (IPQ, 2011)	3 cubs (150x150x150 mm^3)
$\rho_{28d,concrete}$	Concrete electrical resistivity	3 cubs (150x150x150 mm^3)
$Dcl_{concrete}$	Concrete chloride diffusion coefficient (LNEC, 2004)	3 cylinders (ϕ=100mm; h=50mm)

Mortar and concrete electrical resistivity was assessed by the two electrodes technique, using stainless steel meshes embedded on opposite faces of the specimen to work as electrodes. Resistivity was assessed by imposing a current passing through the specimen, between the two electrodes, and measuring the potential difference. Electrical resistivity, inverse of conductivity, is a volumetric measurement of electrical resistance, which, by Ohm's law, is expressed as the ratio between the voltage and the applied current (see equation (3.14)).

$$R = \frac{V}{I} = \rho \cdot \left(\frac{L}{A}\right) \Rightarrow \rho = \frac{V \cdot A}{I \cdot L} \tag{3.14}$$

where R is the electrical resistance, (Ω); I, current (Amp.); V, voltage (Volts); ρ, electrical resistivity (Ω·m); L, length between electrodes (m); and A (m^2) the cross-section area of the test specimen through which current passes. If all tested specimens are in the same moisture (saturated) and temperature conditions, electrical resistivity can be used to compare the porous structure, and therefore constitutes a measure of the amount and interconnectivity of the cementitious matrix pores. After completing the electrical resistivity test, the specimens were used to assess mortar or concrete compressive strength. Resistance to chloride ion penetration was carried out using a non-steady migration test, CTH Rapid Method (Chalmers University of Technology, Sweden) described in NT BUILD 492 (NORDTEST, 1999) and adopted in Portugal through a LNEC specification, E 463 (LNEC, 2004). The CTH Rapid Method is based on a theoretical relationship between diffusion and migration, which enables the calculation of the chloride diffusion coefficient (Dcl_{mortar} and $Dcl_{concrete}$ for mortar and concrete, respectively) from an accelerated test.

3.7. Mortar mix-design

3.7.1. Mortar test results

The coded values of the independent mix variables and the test results of the 32 mixes prepared in MED are summarized in Table 3.6. Concerning the tests conducted under this experimental plan, it was not possible to perform the V-funnel test of mixture MCC10, due to the excessive viscosity of this mixture, and the electrical resistivity tests of mixtures MC1 and MC5 were also not carried out, due to problems with the mesh embedded in the specimens.

Table 3.6 – Coded values of the independent mix variables and properties of fresh and hardened mortar specimens of MED.

Mix number	Ref.	Vw/Vp	w/c	Sp/p	Vs/Vm	mtk/c	$D_{flow,mortar}$ (mm)	$T_{funnel,mortar}$ (s)	$fc_{28d,mortar}$ (MPa)	$\rho_{28d,mortar}$ (Ω.m)	Dcl_{mortar} ($\times 10^{-12} m^2/s$)
1	MC1	0	0	0	0	0	268.3	6.95	86.5	***	***
2	MC2	0	0	0	0	0	297.5	6.10	89.6	168.5	***
3	MC3	0	0	0	0	0	270.8	7.31	90.2	167.2	***
4	MC4	0	0	0	0	0	269.8	6.97	86.2	165.5	3.18
5	MC5	0	0	0	0	0	275.8	6.68	79.5(*)	***	3.08
6	MC6	0	0	0	0	0	270.8	7.19	86.6	171.3	3.10
7	MF1	-1	-1	-1	-1	1	143.3	37.45	91.3	290.8	1.40
8	MF2	1	-1	-1	-1	-1	306.0	3.91	89.6	107.2	4.57
9	MF3	-1	1	-1	-1	-1	343.5	4.24	82.2	87.9	6.59
10	MF4	1	1	-1	-1	1	230.0	6.34	83.9	205.9	2.47
11	MF5	-1	-1	1	-1	-1	336.8	5.19	89.9	105.2	4.83
12	MF6	1	-1	1	-1	1	187.3	11.11	87.8	277.3	1.53
13	MF7	-1	1	1	-1	1	244.8	8.84	85.0	217.6	2.28
14	MF8	1	1	1	-1	-1	344.0	2.87	83.9	82.0	6.29
15	MF9	-1	-1	-1	1	-1	278.5	8.10	90.6	133.0	4.28
16	MF10	1	-1	-1	1	1	163.3	16.23	88.5	295.5	1.77
17	MF11	-1	1	-1	1	1	223.0	11.25	85.7	228.2	2.65
18	MF12	1	1	-1	1	-1	330.3	3.55	79.4	93.5	6.48
19	MF13	-1	-1	1	1	1	140.5	38.08	89.9	336.7	1.27
20	MF14	1	-1	1	1	-1	282.5	5.82	85.8	112.4	4.68
21	MF15	-1	1	1	1	-1	333.5	5.74	81.7	102.8	6.65
22	MF16	1	1	1	1	1	237.0	7.99	79.7	228.2	2.64
23	MCC1	-2	0	0	0	0	292.0	7.95	90.4	155.2	3.47
24	MCC2	2	0	0	0	0	273.5	4.56	83.1	154.5	3.31
25	MCC3	0	-2	0	0	0	210.8	11.00	93.4	247.9	1.97
26	MCC4	0	2	0	0	0	312.3	5.00	80.6	146.2	4.47
27	MCC5	0	0	-2	0	0	260.0	7.08	84.3	176.0	3.56
28	MCC6	0	0	2	0	0	305.0	5.73	84.5	158.0	3.64
29	MCC7	0	0	0	-2	0	307.8	5.34	84.0	158.3	3.15
30	MCC8	0	0	0	2	0	258.5	8.50	80.8	181.7	3.34
31	MCC9	0	0	0	0	-2	340.8	3.35	80.0	49.0	10.21
32	MCC10	0	0	0	0	2	101.8	**	87.7	336.6	1.31

* observation identified as an outlier; ** test not performed due to excessive viscosity; *** test not performed due to problems in the data-acquisition equipment

An overall statistical analysis of the test results concerning statistics of the results for the total points and central points, including minimum and maximum values, mean value, standard deviation and coefficient of variation is presented in Table 3.7. From these statistics it may be observed that the variations introduced in the independent variables of the experimental plan allow covering a wide range of mortars with $D_{flow,mortar}$ ranging from 101.8 to 344.0 mm, $T_{funnel,mortar}$ ranging from 2.87 to 38.08 s, $fc_{28d,mortar}$ ranging from 79.4 to 93.4 MPa, $\rho_{28d,mortar}$ ranging from 49.1 to 336.7 Ω.m and Dcl_{mortar} ranging from 1.33 to 10.00×10^{-12} m²/s. As stated before (Section 3.5.1), central point replication is used to evaluate the experimental error associated to conditions and test procedures variability and the coefficient of variation, as a measure of the relative dispersion of data, can be used to make comparisons of repeatability and reproducibility of the tests. The highest coefficient of variation of the central points were associated to $D_{flow,mortar}$ and $T_{funnel,mortar}$, while $\rho_{28d,mortar}$ and Dcl_{mortar} exhibited the lower coefficient of variation.

Table 3.7 – Statistics of the results for the total points and central points from MED.

	Minimum	Maximum	Mean	Stand. deviation	Coeff. of variation
Total points from MED					
$D_{flow,mortar}$ (mm)	101.8	344.0	263.7	62.9	23.9%
$T_{funnel,mortar}$ (s)	2.87	38.08	8.92	8.18	91.7%
$fc_{28d,mortar}$ (MPa)*	79.4	93.4	85.9	3.84	4.5%
$\rho_{28d,mortar}$ (Ω.m)	49.1	336.7	178.0	75.6	42.5%
Dcl_{mortar} ($\times10^{-12}$ m²/s)	1.33	10.00	3.72	1.98	53.2%
Central points from MED					
$D_{flow,mortar}$ (mm)	268.3	297.5	275.5	11.1	4.0%
$T_{funnel,mortar}$ (s)	6.10	7.31	6.87	0.43	6.3%
$fc_{28d,mortar}$ (MPa)*	86.2	90.2	87.8	1.9	2.2%
$\rho_{28d,mortar}$ (Ω.m)	165.5	171.3	168.1	2.5	1.5%
Dcl_{mortar} ($\times10^{-12}$ m²/s)	3.08	3.18	3.12	0.06	1.8%

*excluding the outlier

3.7.2. Mortar fitted models

The results of the estimated models, including the residual error term, along with the correlation coefficient, are given in Table 3.8.

Table 3.8 – Fitted numerical models for response variables from MED (coded variables).

	$D_{flow,mortar}$ (mm)	$[T_{funnel,mortar}$ (s)$]^{-0.5}$	$fc_{28d,mortar}$ (MPa)	log10[$\rho_{28d,mortar}$ (Ω·m)]	log10[Dcl_{mortar} ($\times 10^{-12}$ m^2/s)]
independent term	278.411	0.382	87.640	2.227	0.506
Vw/Vp	-0.021 (*0%*)	0.038 (*15%*)	-1.341 (*-14%*)	-0.010 (*-3%*)	0.006 (*2%*)
w/c	27.125(*18%*)	0.047 (*18%*)	-3.222 (*-34%*)	-0.058 (*-16%*)	0.093 (*22%*)
Sp/p	7.438 (*5%*)	0.005 (*2%*)	-0.301 (*-3%*)	-0.004 (*-1%*)	-0.003 (*-1%*)
Vs/Vm	-10.229 (*-7%*)	-0.026 (*-10%*)	-0.787 (*-8%*)	0.022 (*6%*)	NS
mtk/c	-61.000 (*-40%*)	-0.094 (*-36%*)	0.997 (*10%*)	0.203 (*56%*)	-0.225 (*-54%*)
(Vw/Vp)×(w/c)	NS	NS	NS	NS	-0.012 (*-3%*)
(Vw/Vp)×(Sp/p)	NS	NS	NS	NS	NS
(Vw/Vp)×(Vs/Vm)	NS	NS	-0.704 (*-7%*)	NS	NS
(Vw/Vp)×(mtk/c)	5.969 (*4%*)	NS	NS	NS	0.014 (*3%*)
(w/c)×(Sp/p)	NS	NS	NS	NS	NS
(w/c)×(Vs/Vm)	4.375 (*3%*)	NS	NS	NS	NS
(w/c)×(mtk/c)	9.563 (*6%*)	0.012 (*5%*)	NS	-0.009 (*-3%*)	0.019 (*5%*)
(Sp/p)×(Vs/Vm)	-5.719 (*-4%*)	-0.012 (*-5%*)	NS	NS	NS
(Sp/p)×(mtk/c)	NS	NS	NS	0.008 (*2%*)	-0.012 (*-3%*)
(Vs/Vm)×(mtk/c)	NS	0.011 (*4%*)	NS	NS	NS
$(Vw/Vp)^2$	NS	0.006 (*2%*)	NS	-0.008 (*-2%*)	NS
$(w/c)^2$	-4.763 (*-3%*)	NS	NS	0.015 (*4%*)	-0.011 (*-3%*)
$(Sp/p)^2$	NS	NS	-0.539 (*-6%*)	NS	0.010 (*2%*)
$(Vs/Vm)^2$	NS	NS	-1.041 (*-11%*)	NS	NS
$(mtk/c)^2$	-14.826 (*-10%*)	-0.009 (*-4%*)	-0.678 (*-7%*)	-0.028 (*-8%*)	0.011 (*-3%*)
residual error, ε *					
Mean	0	0	0	0	0
standard deviation	8.028	0.014**	1.374	0.013**	0.019**
R^2/ $R^2_{adjusted}$	0.984 / 0.975	0.979 / 0.969	0.872 / 0.817	0.995 / 0.993	0.989/0.986

NS non-significant terms; * error term is a random and normally distributed variable and no evidence of auto-correlation was found in the residues; ** corresponding value for $T_{funnel,mortar}$, $\rho_{28d,mortar}$ and Dcl_{mortar} is 1.591, 5.076 and 0.1584, respectively; (%) relative influence of the variable on the response variation

An analysis of variance showed that these models are significant when describing the effect of Vw/Vp, w/c, Sp/p, Vs/Vm and mtk/c on the modelled responses. Notice that the observed value of 79.5 in the variable $fc_{28d,mortar}$ (marked with * in Table 3.6) is not typical of the rest of the data. This value was identified as an outlier in the statistical analysis and has been excluded from the data when fitting the model. Residual analysis did not reveal any obvious model inadequacies or indicate serious violations of the normality assumptions, except in the cases of $T_{funnel,mortar}$, $\rho_{28d,mortar}$ and Dcl_{mortar}. The problem was overcome after a variable transformation, as indicated in Table 3.8.

Even though the majority of the fitted models presented considerably high correlation coefficients (see R^2 and $R^2_{adjusted}$ in Table 3.8) their accuracy must be verified. The results of the central points included in the experimental design were analysed in order to estimate the experimental error and the accuracy of the derived models (see Table 3.7). The estimated residual standard deviation (see Table 3.8) does not exceed the experimental error by far, so a good fitting can be expected.

Based on the derived models, the relative influence of each variable on the response variation was computed and is presented (in brackets and italic) in Table 3.8. Naturally, higher values indicate greater influence of this parameter in the response and on the other hand, a negative value reflects a response decrease to an increase in this parameter. The results clearly show that w/c and mtk/c exhibit a great effect on all measured responses, being the only exception $fc_{28d,mortar}$, where the relative influence of mtk/c does not exceed 10%. It should be noted, however, that these two variables have opposite effects on the response. In the case of $\rho_{28d,mortar}$ and Dcl_{mortar}, the variable mtk/c explains almost 50% of the variation of these responses. Besides w/c and mtk/c, the variable that most influences $T_{funnel,mortar}$, was Vw/Vp. The aggregate content in mortar (Vs/Vm) has some influence in mortar response variables, except in the case of Dcl_{mortar}, where the range of variation introduced in Vs/Vm (0.400 to 0.500, see Table 3.4) seems to have no major influence on mortar chloride ingress. Sp/p exhibits the lowest influence on mortar properties, as compared to other mixture parameters, which can be explained by the short variation range of Sp/p in the experimental plan (see Table 3.4) triggered by its strong dispersion action. Significant interaction and quadratic effects are found in all responses.

3.7.3. Mortar mix optimization

After building the regression models that establish relationships between mix-design variables and responses, a numerical optimization technique (described in Section 3.5.3) was used to define mortar composition. Indeed, one of the key stages of the concrete mix-design approach presented in this work is the way in which mortar performance requirements should be defined to ensure a concrete composition that complies with the previously established requirements, fresh and hardened concrete properties (see Section 3.4).

Mortar fresh requirements that lead to SCC were defined based on the values recommended by the Japanese SCC-design method (Okamura and Ouchi, 2003), the European Guidelines for SCC (EFNARC, 2005) and previous experience (Nunes *et al.*, 2009b). The values of Vw/Vp and Sp/p that lead to the optimum mixtures in fresh state, $D_{flow,mortar}$=260.0 mm and $T_{funnel,mortar}$=10.0 s, were searched for each combination of (w/c, mtk/c, Vs/Vm). In a first stage, no restriction was established for the other response variables. Note that since the response models were expressed as a function of five independent variables, a multiple optimum will hardly occur. The use of the models was limited to an area bounded by coded values -2.5 to +2.5 (D_{center}). The range of mortar mixture parameters, defined in coded values, where deformability and viscosity coexist in a balanced manner to achieve self-compacting mortar, while the distance to center of the modelled region is less than 2.5, is presented in Figure 3.9.

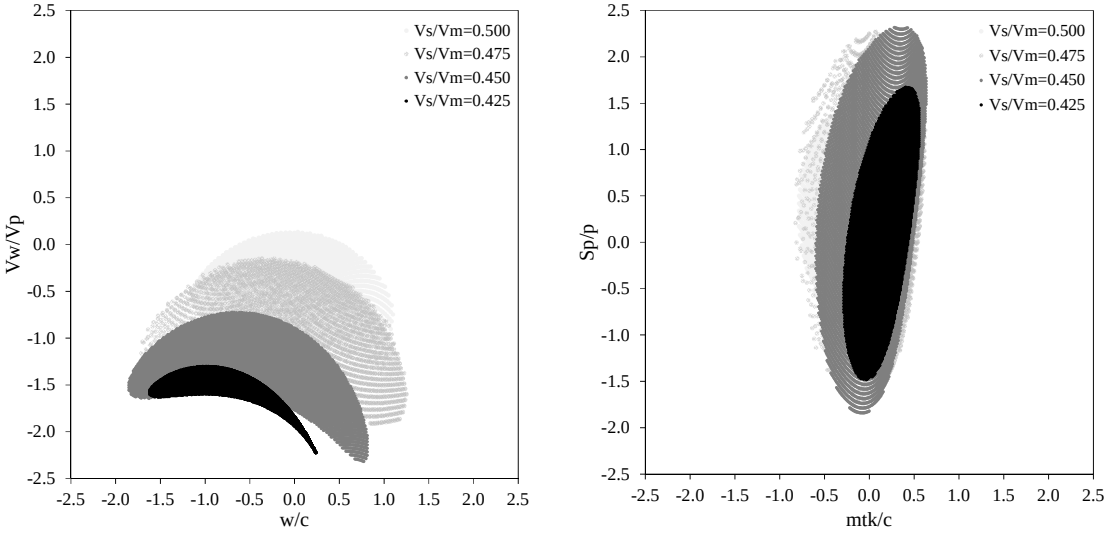

Figure 3.9 – Range of mixture variables, in coded values, for optimized self-compacting mortars.

This type of representation enables a more global picture of the solutions and a quick identification of the optimal solutions zone, its location and extension on the modelled region. The results were grouped in four values of Vs/Vm namely, 0.425, 0.450, 0.475 and 0.500, corresponding in coded values to -1, 0, +1 and +2, respectively. No solutions were found for aggregate volume fraction of 0.400 (-2 in coded values), while the wider region of optimized solution are found for a Vs/Vm of 0.450 and 0.475. The parameter with lower variation in coded values within the region of optimized solutions was mtk/c, ranging between -0.78 and 0.64, corresponding, in absolute values, to a variation between 6.7% and 10.9%. The range of mixture parameters included in the region of optimized solutions varies with the aggregate content (Vs/Vm), where an increase of Vs/Vm seems to demand solutions with higher w/c and Vw/Vp and lower mtk/c. In fact, as the aggregate volume fraction increases the flowability of the paste should also increase, to ensure the same workability of the mortar ($D_{flow,mortar}$ and $T_{funnel,mortar}$) (Figueiras *et al.*, 2014).

Alternatively, the mixture parameters of optimized solutions in fresh state can be represented in contour plots as shown in Figure 3.10 for a Vs/Vm of 0.500, where the grey shading represents the distance to the center of the modelled region (D_{center}). The corresponding contour plots for estimated $fc_{28d,mortar}$ is presented in Figure 3.11 and for estimated $\rho_{28d,mortar}$ and Dcl_{mortar} are presented in Figure 3.12.

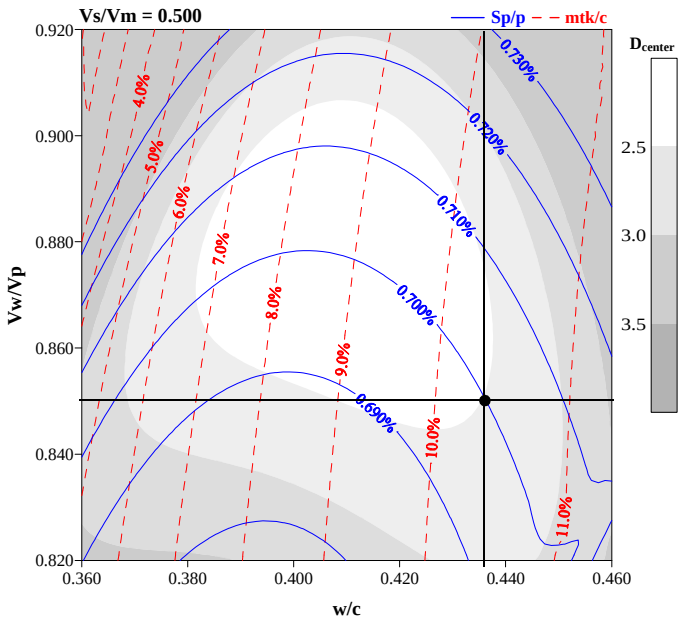

Figure 3.10 – Range of mixture variables, in absolute values, for optimized self-compacting mortars containing 0.500 of Vs/Vm.

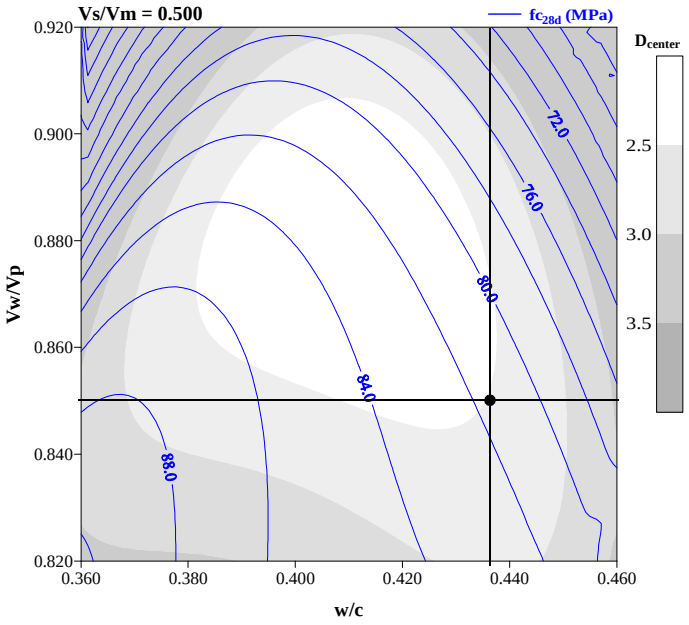

Figure 3.11 – Estimated values of $fc_{28d,mortar}$ for optimized self-compacting mortars containing 0.500 of Vs/Vm.

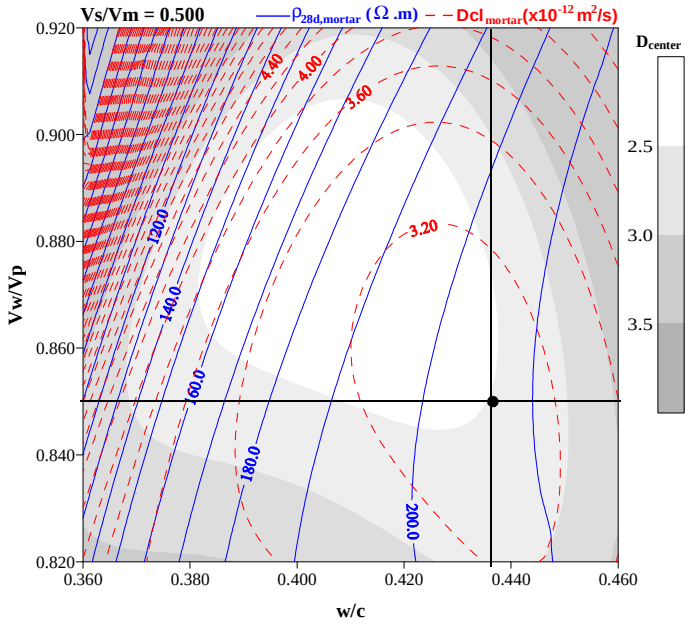

Figure 3.12 – Estimated values of $\rho_{28d,mortar}$ and Dcl_{mortar} for optimized self-compacting mortars containing 0.500 of Vs/Vm.

Given the restrictions imposed on the concrete composition (see Section 3.4), mortar requirements may be set in terms of fresh state properties, but also in terms of hardened state properties, namely, compressive strength, electrical resistivity and chloride diffusion coefficient. A Vs/Vm=0.500 was set for the optimized mortar

solution, considering the fact that pastes corresponding to a higher sand content (Vs/Vm), in the optimized mortar mixtures, can lead to SCCs with higher aggregate surface (usually representing higher total aggregate content) and lower paste volume (Nunes, 2008; Figueiras *et al.*, 2014). In fact, a composition with higher total aggregate content results in more economic SCC mixtures and also reduces the heat release due to cement hydration and shrinkage deformation, resulting in a lower cracking risk and therefore better durability of the structure. Furthermore, according to the adjusted models, the aggregate content (fine aggregate) seems to have little influence on Dcl_{mortar} but a positive effect in $\rho_{28d,mortar}$, i.e. a greater volume of aggregate leads to compositions with higher electrical resistivity. The presence of aggregate in a cement paste matrix has two opposite effects on the transport properties: firstly, the dilution and tortuosity effects that reduce the permeability; and secondly, the presence of a porous interfacial transition zone (ITZ) between paste and aggregate that facilitates the movement of ions and increases mortar conductivity (Garboczi *et al.*, 2000; RILEM-Report 38, 2007). In the presence of low water/cement ratios or fine mineral addition, like in SCC, some studies appear to indicate that the porosity and width of the ITZ is significantly smaller than in vibrated concrete (RILEM-Report 38, 2007). However, on the other hand, as the proportion of larger size aggregate increases in the mix, the local porosity at the ITZ increases and the overall durability decreases (Basheer *et al.*, 2005). In the case of the apparent chloride diffusion coefficient, an additional effect shall be taken in consideration. This coefficient depends on the diffusivity of chloride ion in liquid-saturated concrete, as well as on the chloride binding capacity of the cement paste matrix, which can take place by chemical reaction with the hydration products of cement (such as C_3A or C_4AF) or physical adsorption. Thus, an increase in aggregate volume content represent, for the same mixture volume, a decrease in paste volume and therefore a reduction in the chloride binding capacity (higher apparent chloride diffusion coefficient). The influence of the aggregate content and aggregate skeleton on the durability behaviour of the mixture composition is therefore dictated by the balance between several effects. With regard to the electrical resistivity and diffusivity properties, one of the approaches that has begun to be used to establish this link between paste and concrete is through the Effective Medium Theory (EMT) (Garboczi and Berryman, 2000; Figueiras *et al.*, 2013b). Additionally, by analysing the contour plot of estimated durability indicators for Vs/Vm=0.500, it is observed that the values estimated at mortar level are quite close to desired values at concrete level ($Dcl_{concrete}$

lower than 3.26×10^{-12} m²/s and $\rho_{28d,concrete}$ higher than 210.5 Ω.m). Thus, in view of the durability performance requirements, mortar mix-proportions were optimized to satisfy the following criteria: minimize Dcl_{mortar} and maximize $\rho_{28d,mortar}$. With regard to mortar compressive strength, and given the range of optimized solutions in the fresh state, this response variable does not vary significantly and always displays a value higher than the target value established for the concrete composition (70 MPa defined in Section 3.4), see Figure 3.11. Hence, no restriction was established for $fc_{28d,mortar}$ in the mortar optimization process.

In summary, mortar mix-proportions were optimized to satisfy the following criteria: $D_{flow,mortar}$ equal to 260.0 mm; $T_{funnel,mortar}$ equal to 10.0 s; Vs/Vm equal to 0.500; maximize $\rho_{28d,mortar}$; minimize Dcl_{mortar}; D_{center} lower or equal to 2.5. Optimized mortar, marked in the contour plots of Figure 3.10 to Figure 3.12 has a Vw/Vp=0.851, w/c=0.435, Sp/p=0.700%, Vs/Vm=0.500 and mtk/c=10.4%, and it is expect to exhibits $D_{flow,mortar}$ of 260.0 mm, $T_{funnel,mortar}$ of 10.0 s, $fc_{28d,mortar}$ of 81.7 MPa, $\rho_{28d,mortar}$ of 206.3 Ω.m and Dcl_{mortar} of 3.12×10^{-12} m²/s.

3.8. Concrete mix-design

The paste mixture proportions (Vw/Vp; w/c, Sp/p and mtk/c) optimized at mortar level were maintained at concrete level and a central composite design was carried out to mathematically model the influence of the two parameters, Vs/Vm and Vg/Vg,lim, and their coupled effects on $D_{flow,concrete}$, $T_{funnel,concrete}$, H_2/H_1, Sr, $fc_{28d,concrete}$, $\rho_{28d,concrete}$ and $Dcl_{concrete}$. It should be noted that it was necessary to perform an adjustment of the superplasticizer content due to the lower mixing efficiency exhibited by the concrete mixer, when compared with the used mortar mixer.

3.8.1. Concrete test results

The coded values of the independent mix variables and the test results of the 12 mixes prepared in CED are summarized in Table 3.9. Concerning the tests conducted under this experimental plan, it was not possible to perform the electrical resistivity test and the chloride migration test of mixture CC3, due to problems with the specimens.

Table 3.9 – Coded values of the independent mix variables and properties of fresh and hardened concrete specimens of CED.

Mix number	Ref.	Vs/Vm	Vg/Vg,lim	$D_{flow,concrete}$ (mm)	$T_{funnel,concrete}$ (s)	H_2/H_1	Sr (%)	$fc_{28d,concrete}$ (MPa)	$\rho_{28d,concrete}$ (Ω.m)	$Dcl_{concrete}$ ($\times 10^{-12} m^2/s$)
1	CC1	0	0	750.0	16.94	0.851	10.30	80.7	244.9	3.58
2	CC2	0	0	772.5	18.00	0.927	11.30	77.6	246.1	3.53
3	CC3	0	0	767.5	18.47	0.896	11.25	84.1	*	*
4	CC4	0	0	772.5	16.73	0.916	11.08	83.2	243.9	3.56
5	CF1	-1	-1	845.0	10.97	0.966	27.91	82.8	212.7	3.54
6	CF2	1	-1	722.5	23.85	0.842	6.78	82.6	231.0	3.63
7	CF3	-1	1	792.5	17.00	0.989	18.29	84.3	227.5	3.69
8	CF4	1	1	612.5	35.57	0.614	1.55	82.7	257.0	3.50
9	CCC1	-1.414	0	827.5	10.30	0.971	31.24	80.6	235.7	3.34
10	CCC2	1.414	0	627.5	32.45	0.658	2.43	77.8	267.3	3.37
11	CCC3	0	-1.414	807.5	13.96	0.949	16.11	83.0	214.6	3.47
12	CCC4	0	1.414	712.5	31.60	0.813	8.87	88.4	250.1	3.59

* test not performed due to problems with the specimens

An overall statistical analysis of the response variables is presented in Table 3.10. With this experimental plan a wide range of SCC was covered, with $D_{flow,concrete}$ ranging from 612.5 to 845.0 mm, $T_{funnel,concrete}$ ranging from 10.30 to 35.57 s, H_2/H_1 ranging from 0.614 to 0.989 and Sr ranging from 1.55% to 31.24%. On the contrary, hardened properties values varied little, being $\rho_{28d,concrete}$ the variable with the greater variation, ranging from 212.7 to 267.3 Ω.m. The highest coefficient of variation of the central points were associated to $T_{funnel,concrete}$, H_2/H_1, Sr and $fc_{28d,concrete}$ while $\rho_{28d,concrete}$ and $Dcl_{concrete}$ exhibited the lower coefficient of variation.

Table 3.10 – Statistics of the results for the total points and central points from CED.

	Minimum	Maximum	Mean	Stand. deviation	Coeff. of variation
Total points from CED					
$D_{flow,concrete}$ (mm)	612.5	845.0	750.8	72.3	9.6%
$T_{funnel,concrete}$ (s)	10.30	35.57	20.49	8.49	41.4%
H_2/H_1	0.614	0.989	0.866	0.121	14.0%
Sr (%)	1.55	31.24	13.09	9.09	69.4%
$fc_{28d,concrete}$ (MPa)	77.6	88.4	82.3	2.9	3.6%
$\rho_{28d,concrete}$ (Ω.m)	212.7	267.3	239.2	16.9	7.1%
$Dcl_{concrete}$ ($\times 10^{-12}$ m²/s)	3.34	3.69	3.53	0.10	2.9%
Central points from CED					
$D_{flow,concrete}$ (mm)	750.0	772.5	765.6	10.7	1.4%
$T_{funnel,concrete}$ (s)	16.73	18.47	17.54	0.84	4.8%
H_2/H_1	0.851	0.927	0.898	0.034	3.7%
Sr (%)	10.30	11.30	10.98	0.47	4.2%
$fc_{28d,concrete}$ (MPa)	77.6	84.1	81.4	2.9	3.6%
$\rho_{28d,concrete}$ (Ω.m)	243.9	246.1	245.0	1.1	0.5%
$Dcl_{concrete}$ ($\times 10^{-12}$ m²/s)	3.53	3.58	3.56	0.02	0.7%

3.8.2. Concrete fitted models

The results of the estimated models, including the residual error term, along with the correlation coefficient, are given in Table 3.11. Residual analysis did not reveal any obvious model inadequacies or indicate serious violations of the normality assumptions. The majority of the fitted models presented considerably high correlation coefficients except in the cases of $fc_{28d,concrete}$ and $Dcl_{concrete}$. Variations introduced in Vs/Vm and Vg/Vg,lim yielded minor variations in these two response variables, whereby in this case the experimental average value provides a better fit to the experimental results.

Table 3.11 – Fitted numerical models for response variables from CED (coded variables).

	$D_{flow,concrete}$ (mm)	$T_{funnel,concrete}$ (s)	H_2/H_1	Sr (%)	$fc_{28d,concrete}$ (MPa)	$\rho_{28d,concrete}$ (Ω·m)	$Dcl_{concrete}$ ($\times 10^{-12}$ m²/s)
independent term	763.250	17.535	0.892	11.380	80.655	245.716	3.581
Vs/Vm	-73.168 (*-51%*)	7.847 (*41%*)	-0.118 (*-44%*)	-9.827 (*-59%*)	NS	11.555 (*36%*)	-0.009 (*-11%*)
Vg/Vg,lim	-37.106 (*-26%*)	5.337 (*28%*)	-0.049 (*-18%*)	-3.139 (*-19%*)	1.143 (*31%*)	11.388 (*36%*)	NS
Vs/Vm×Vg/Vg,lim	-14.375 (*-10%*)	1.423 (*7%*)	-0.063 (*-23%*)	1.098 (*7%*)	NS	NS	NS
$(Vs/Vm)^2$	-18.625 (*-13%*)	1.863 (*10%*)	-0.039 (*-14%*)	2.570 (*15%*)	NS	NS	-0.073 (*-89%*)
$(Vg/Vg,lim)^2$	NS	2.565 (*13%*)	NS	NS	2.506 (*69%*)	-9.022 (*-28%*)	NS
residual error, ε*							
Mean	0	0	0	0	0	0	0
standard deviation	7.050	0.888	0.019	0.855	1.957	4.947	0.086
R^2/ $R^2_{adjusted}$	0.990 / 0.985	0.989 / 0.980	0.974 / 0.959	0.991 / 0.986	0.554 / 0.455	0.914 / 0.878	0.309 / 0.136

(NS) non-significant terms; (*) error term is a random and normally distributed variable and no evidence of auto-correlation was found in the residues

It is expected that the established models are sufficiently accurate to predict $D_{flow,concrete}$, $T_{funnel,concrete}$, H_2/H_1, Sr and $\rho_{28d,concrete}$ because the standard deviation measured on the central points (see Table 3.10) was always higher or close to the residual standard deviation.

The relative influence of each variable on the response variation is presented, in brackets and italic, in Table 3.11. The results show that an increase in aggregate volume content increases the $T_{funnel,concrete}$ and decrease the $D_{flow,concrete}$, H_2/H_1 and Sr, being Vs/Vm the variable with the highest effect on all responses of the fresh state. As expected, higher aggregate volume content increases electrical resistivity values (positive values of Vs/Vm and Vg/Vg,lim), although the model shows that there is also a negative component associated with an increase in the volume of coarse aggregate, represented by the quadratic term $(Vg/Vg,lim)^2$. In the case of $Dcl_{concrete}$, as previously mentioned, the range of variation introduced in the aggregate content and skeleton seems to have no major influence on chloride ingress, which is in agreement with the results obtained at mortar level. Moreover, by comparing the average value obtained in concrete with the value of the optimized mortar, 3.53×10^{-12} and 3.12×10^{-12} m²/s, respectively, values are quite similar. The influence of the aggregate content and aggregate skeleton on the electrical resistivity and apparent chloride diffusion coefficient is discussed in more detail in Figueiras *et al.* (2013b).

3.8.3. Concrete mix optimization

Concrete mix optimization was carried out using the same numerical technique applied for mortar mix optimization in order to meet requirements set out in Section 3.4. In summary, concrete composition for the new cruise terminal building should satisfy the following requirements: $D_{flow,concrete}$ between 750.0 and 850.0 mm, $T_{funnel,concrete}$ between 10.00 and 15.00 s, H_2/H_1 higher than 0.900, Sr lower than 15.00%, $fc_{28d,concrete}$ higher than 70 MPa, $\rho_{28d,concrete}$ higher than 210.5 Ω.m and $Dcl_{concrete}$ lower than 3.26×10^{-12} m²/s. The use of the models was limited to an area bounded by coded values -2.0 to +2.0 (D_{center}). As previously mentioned, due to the fact the fitted models of the response variables $fc_{28d,concrete}$ and $Dcl_{concrete}$ are not sufficiently accurate, the experimental average values will be taken as the predictive responses, which according to the values presented in Table 3.10 are 82.3 MPa and 3.53×10^{-12} m²/s, respectively.

Despite the $Dcl_{concrete}$ requirement not being fully complied, it can be considered satisfactory since values are relatively close. Furthermore, it should be emphasised that the Portuguese specification E 465 (LNEC, 2007) is more restrictive than NP EN 1990 (IPQ, 2009) or *fib*-Model Code (CEB-FIP, 2012) with respect to the minimum reliability index β associated with reliability class RC3 for the serviceability limit state. The range of SCC mix-proportions that satisfies concrete optimization requirements is given in Figure 3.13. It should be stressed that the target area presented in Figure 3.13 will probably change if different paste mixture proportions are used or changes in the aggregate type are made.

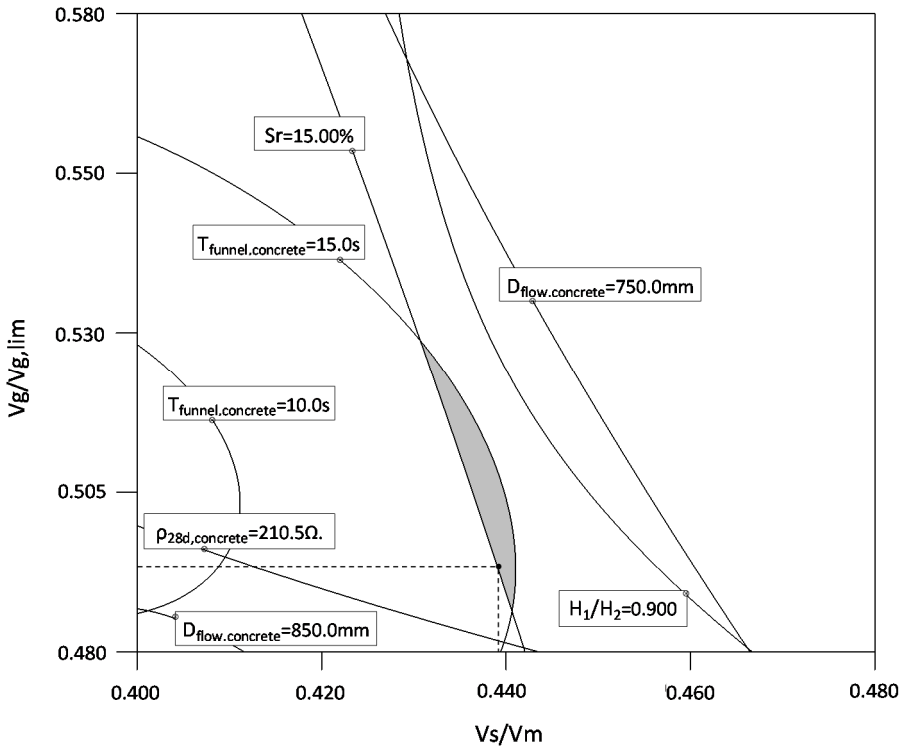

Figure 3.13 – Range of mix-proportions that satisfy concrete optimization requirements.

Among the set of optimal solutions, the selected composition is pointed out in Figure 3.13, which corresponds to Vs/Vm=0.439 and Vg/Vg,lim=0.493. Table 3.12 shows the final concrete optimized composition and the respective predicted values for fresh and hardened properties. The final composition was tested and the measured values of fresh and hardened properties are also presented in Table 3.12. Measured values are within the prediction intervals corresponding to a 95% confidence level.

Table 3.12 – Optimized mix-proportions and concrete properties, predicted and experimental values.

Constituent materials (kg/m³)		
cement	416	
limestone filler	151	
metakaolin	44	
water	185	
superplasticizer	6.10	
sand 1	325	
sand 2	487	
coarse aggregate	744	
Fresh and hardened properties		
	Predicted [prediction interval]*	Experimental
$D_{flow,concrete}$ (mm)	803.4 [792.2; 814.6]	805.0
$T_{funnel,concrete}$ (s)	14.63 [13.01; 16.24]	13.96
H_2/H_1	0.945 [0.914; 0.975]	0.927
Sr (%)	14.90 [13.54; 16.26]	13.90
$fc_{28d,concrete}$ (MPa)	82.3	80.4
$\rho_{28d,concrete}$ (Ω.m)	223.6 [216.6; 230.6]	220.3
$Dcl_{concrete}$ ($\times 10^{-12}$ m²/s)	3.53	3.54

*prediction interval corresponding to a 95% confidence level

3.9. Conclusions

Based on the results previously presented, the following conclusions can be drawn:

- The performance-based design methodology presented in this work enables the systematization of the mixture design process of SCC considering environmental exposure. Although the methodology has been developed for structures exposed to severe marine environment, its application to other types of environmental exposure is only limited by the accuracy of the mathematical models for modelling degradation mechanisms.

- For an adequate specification of durability requirements it is crucial to carry out a correct identification of the major degradation mechanisms and to select most representative durability indicators. For structures in severe marine environment the reinforcement corrosion is the main degradation mechanism and a serviceability limit state of depassivation should be considered. In these cases the most often used durability indicator is the

apparent chloride diffusion coefficient measured by the migration test ($Dcl_{concrete}$), although the electrical resistivity under saturated conditions ($\rho_{concrete}$) turns out to be an interesting alternative. Assessment of $\rho_{concrete}$ is performed by a straightforward and non-destructive test, with good reproducibility and accuracy. However, to use $\rho_{concrete}$ as a durability indicator in the initiation period requires a prior knowledge of the chloride binding capacity of the mixture.

- Limit values of the durability indicators were specified through a probabilistic calculation of the limit state functions, established on the basis of the target service life, limit state criterion and degradation mathematical models. In the case of $\rho_{concrete}$, a partial safety factor approach was carried out due to insufficient statistical characterization of some model parameters. The limit value of $Dcl_{concrete}$ was determined adopting a full probabilistic analysis and a partial safety factor analysis. Contrarily to what would be expected, the $Dcl_{concrete}$ value obtained with the partial safety factor analysis was the least conservative. A careful characterization of the model parameters is very important to obtain realistic threshold values. A sensitivity analysis helps to define the most influential parameters, and therefore to take additional care in their characterisation (distribution type, average value and standard deviation). In $Dcl_{concrete}$ model, the most influential parameters are n and c, while the least influential parameters are C_r and C_s. The influence of temperature ($k_{D,T}$) and model uncertainty (λ) on $Dcl_{concrete}$ was found to be significant.

- Experimental factorial design provides a systematic methodology to identify optimal mixes given a set of constituents and performance constraints. Data collected during the experimental plan, conducted according to a central composite design, can be used to establish numerical models relating mixture parameters with fresh and hardened properties of mortar and concrete. Such numerical models provide an adequate representation of mixture properties (fresh, mechanical and durability properties) over the region of interest.

- This statistical experimental approach, generally used to model fresh properties, was extended to durability properties of paste, mortar and concrete. In this research work the methodology was extended to the chloride diffusion coefficient and electrical resistivity, however its application has also been validated to water absorption by capillarity, porosity accessible to water and carbonation. The ability to mathematically model the influence of mixture parameters on a given response variable, through an experimental design methodology, is determined mainly by the choice of the relevant factors, the range of variation of the response in the experimental plan, accuracy of test methods and experience of the operator performing tests.

- The SCC mixture design was developed in a first phase at mortal level, in which paste mixture proportions were optimized, and in a second phase at concrete level, where the aggregate skeleton was adjusted. Using mortar tests as a previous step in SCC design greatly simplifies experimental work, however requires prior knowledge of the link between mortar/paste and concrete performance requirements. SCC mortar requirements in the fresh state are fairly well defined and in the hardened state, selection of values will be further optimized as knowledge on the link between paste/mortar and concrete durability properties is deepened.

- Concrete mixture designed for the new cruise terminal building satisfied all the specified requirements. The final optimized mixture was tested and, as expected, the measured values of fresh and hardened properties were within the prediction intervals of the respective models.

Chapter 4

Linking fresh and durability properties of paste to SCC mortar

4.1. Synopsis

In the last years many approaches to design SCC have been developed, but it remains a very complex process since it is necessary to manipulate several variables and understand their effects on concrete behaviour (fresh and hardened states). The prediction of concrete or mortar behaviour based on paste properties will be a significant contribution to simplify SCC design. With this purpose, two statistical experimental designs were carried out, one at paste level and the other at mortar level, to mathematically model the influence of mixture parameters on fresh and durability properties. The derived numerical models were used to define an area, labelled by self-compacting zone at paste level (SCZ), where fresh properties of the paste enable the design SCC mortar. Furthermore, in order to extend this link to durability properties, the effect of including aggregate in cement paste was evaluated by means of the electrical resistivity test.

4.2. Introduction

Durability of concrete structures is presently looked at with great concern as it represents a challenge to achieve sustainable development in construction. Self-compacting concrete (SCC), initially developed in Japan, corresponds to an advanced special concrete type as it leads to technological, economic and environmental benefits.

The main advantage of this sustainable technology lies in the unneeded compaction during placing, thus leading to a homogeneous and more durable material. In the fresh state, SCC must show filling ability, resistance to segregation and passing ability (EFNARC, 2005). The selection of constituent materials and the design of mix-proportions are essential factors to achieve adequate fresh properties. To produce SCC, a good balance between deformability and resistance to segregation has to be accomplished, which can be made possible by the use of chemical admixtures (superplasticizers, viscosity agents, etc.) combined with high concentrations of fine particles (cement and mineral admixtures) (Okamura and Ouchi, 2003). In addition, the characteristics of fine and coarse aggregate are also very important. With the growing variety of materials available to produce concrete, the mix-design process has become complex since it is necessary to manipulate several variables and their interaction is difficult to predict. Indeed, to achieve the adequate performance in fresh and hardened states further work is needed to better understand the effect of mixture parameters governing material performance (Khayat *et al.*, 2000).

Several different mix-design methods have been developed by many academic institutions and construction industry companies, but still, there is no standard method for SCC mix-design (EFNARC, 2005). Typically, mixture optimization is based on a trial an error approach where each parameter is changed one at a time to assess its influence on concrete properties. This process does not permit to understand interactions of the mixture parameters, may involve carrying out a large and unpredictable number of trial batches and does not guarantee an optimal general solution. One of the methodologies that lately has been applied in the SCC mix-design is the statistical experimental design. The derived statistical models established on the basis of a factorial design, highlight not only the significance of the mixture parameters but also their interactions on concrete properties. Using such numerical models, a multi-parametric optimization can be carried out, with the user controlling the goal of the optimization and the significance of each experimental parameter. In fact, this approach increases the efficiency in selecting the optimum mix-proportions for a given set of constraints (related to fresh and hardened properties and economic limitations) based on a limited number of experimental data points (Khayat *et al.*, 2000; Nehdi and Summer, 2002; Sonebi, 2004). An additional advantage of the factorial experimental design is that there is some freedom to define the mixture parameters (it can be applied

to paste, mortar or concrete) and to select the responses to be analysed (e.g. rheological parameters, empirical fresh tests results, durability properties, etc.) (Nunes, 2008). This mix-design approach was followed in the present work.

Several different design methods found in the literature consider SCC as a suspension of aggregates in paste, separating optimization of the granular skeleton grading, paste volume and paste composition. In fact, paste plays a major role in concrete workability and therefore it is reasonable to expect that there is a direct relationship between paste and concrete flow behaviour (Hidalgo *et al.*, 2008). The prediction of the concrete behaviour based on paste properties facilitates the design of SCC, reduces the volume of material required for testing and takes advantage of the greater accuracy and precision of paste rheology tests (Grünewald and Walraven, 2007; Hidalgo *et al.*, 2008). The rheological behaviour of cement paste is controlled by the same factors that control any other suspension, namely, by macro-level factors such as particle size, size distribution, shape, texture, density, water content, etc., and by micro-level forces such as colloidal, Brownian and viscous forces. Depending on the size of the particles, on their volume fraction in the mixture and on external forces (applied stress or strain rate), one or several of these interactions dominate (Flatt referred by Roussel *et al.* (2010)). Colloidal particles forces dominate, to a large extent, the complex and time dependent behaviour of cement paste, while for most aggregate sizes, only viscous forces are relevant (Nunes, 2008). According to Wallevik and Wallevik (2011) rheology of fresh concrete or mortar is much simpler than rheology of cement paste, due to the fact that the time-dependent behaviour (thixotropy and structural breakdown) is more pronounced in cement paste because of the absence of aggregates, which act as a very effective grinder and/or dispersant.

The objective of this chapter is therefore to establish a link between paste and mortar that exhibit adequate fresh properties (deformability and viscosity) to produce self-compacting concrete. Furthermore, in order to extend this link to durability properties, the effect of including aggregate in cement paste was evaluated by means of the electrical resistivity test. With this purpose, two statistical experimental designs were conducted, with the same set of materials, one at paste level and the other at mortar level (including reference sand). At paste level, numerical models were established relating mixture parameters to rheological properties (yield stress and plastic viscosity), empirical fresh properties (flow diameter and free water content) and to a durability

property (electrical resistivity). At mortar level empirical fresh properties (flow diameter and flow time), a mechanical property (compressive strength) and the same durability property evaluated in paste (electrical resistivity) were assessed. The mortar numerical models were used to find optimal solutions that satisfy SCC fresh requirements, i.e. to determine the range of mortar mixture parameters where deformability and viscosity coexist in a balanced manner. By using the mixture parameters of the optimized mortars and the derived numerical models to describe paste properties, it was possible to define an area, labelled by self-compacting zone at paste level, where the rheological properties of the paste enable the design a self-compacting mortar. Furthermore, the influence of the aggregate in the electrical resistivity of mortar was studied, which allowed to draw contour plots that aid in the design of SCC mortar with defined durability requirements, based on tests at paste level only. Additionally, the correlation between rheological and empirical tests results was discussed and the evolution of paste rheological behaviour during the hydration process was assessed.

4.3. Experimental program

4.3.1. Materials characterization

The mortar and paste mixes investigated in this study were prepared with ternary mixtures including white cement (CEM II/A-L 52.5N according to EN 197-1 (IPQ, 2012)) and two mineral additions, metakaolin and limestone filler. The chemical composition and some physical properties of the cement and the two mineral additions are presented in Table 4.1. The particle size distribution performed by a laser diffraction granulometer is shown in Figure 4.1. A polycarboxylate type high range water reducing admixture was used having a specific gravity of 1.07 and 26.5 % of solid content. In mortar mixes a reference sand was employed, conforming to EN 196-1 (IPQ, 2006). Reference sand used is a siliceous round natural sand (0.08-2 mm) with a specific gravity of 2.63 and an absorption value of 0.30%. Distilled water was used for all paste and mortar mixes.

Table 4.1 – Chemical and physical properties of the cement, metakaolin and limestone filler.

	CEM II/A-L 52.5N (white) *	Metakaolin	Limestone filler*
SiO_2 (%)	18.80	52.00	--
Al_2O_3 (%)	2.23	45.00	--
Fe_2O_3 (%)	0.20	0.46	0.02
CaO (%)	66.42	<0.50	--
MgO (%)	0.66	<0.50	--
SO_3 (%)	2.17	<0.10	--
Na_2O (%)	--	<0.50	--
Na_2O_{eq} (%)	0.30	--	--
$CaCO_3$ (%)	--	--	99.00
$MgCO_3$ (%)	--	--	0.30
K_2O (%)	--	<0.50	--
TiO_2	--	1.50	--
MnO	--	<0.30	--
P_2O_5	--	<0.30	--
Cl^- (%)	0.03		<0.001
S^{2-} (%)	--		<0.04
Loss on ignition (%)	8.60	1.50	43.10
Insoluble residue (%)	0.31	61	0.20
Specific density (g/cm³)	3.04	2.21	2.68
Blaine (cm²/g)	5011	31678	5150
Residue 90 µm (%)	0.00	0.00	0.01
Residue 45 µm (%)	1.80	1.09	2.44
Residue 32 µm (%)	7.38	2.55	4.41
Mean size (µm)	11.03	7.12	6.53
Vicat test			
initial set (min.)	154	--	--
final set (min.)	214	--	--

* information provided by the supplier

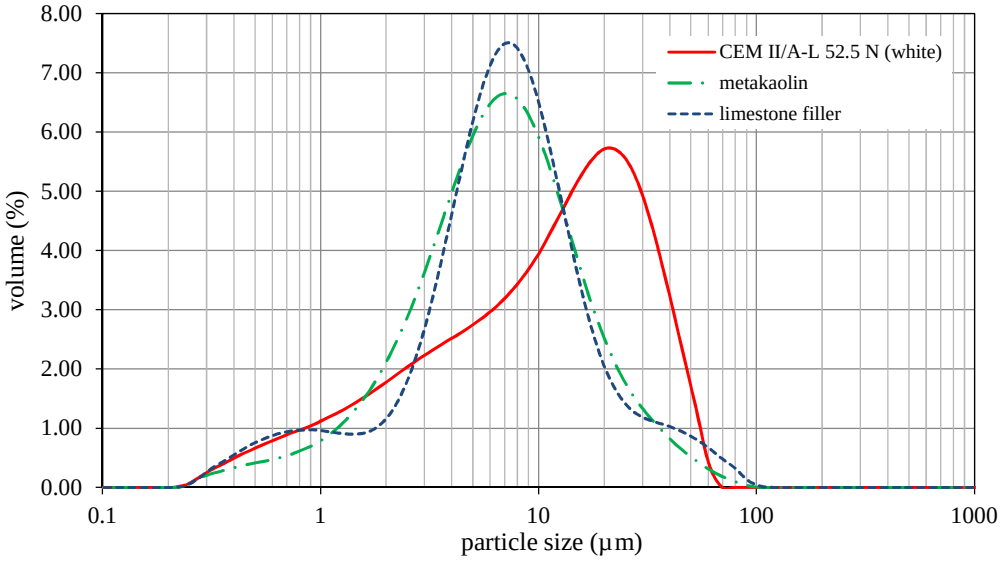

Figure 4.1 – Particle size distribution curves of cement, metakaolin and limestone filler, in terms of volume.

4.3.2. Experimental design

The experiments were designed according to a statistical design approach known as two-level factorial design (2^k). This is a process of planning experiments in order to collect appropriate data that can be analysed by statistical tools, such as analysis of variance, resulting in a valid basis for deriving an empirical numerical model that expresses the relationship between the input variables (e.g. mixture parameters) and response variables (e.g. fresh or hardened properties of paste/mortar). Factorial design is frequently used in experiments involving large number of parameters (input variables) and when it is important to study not only the isolated significance of each parameter in response but also their interaction (Montgomery, 2001). According to studies conducted by some authors (Sonebi, 2001; Yahia and Khayat, 2001b; Nehdi and Summer, 2002; Nunes *et al.*, 2006b) the response surface of mortar and paste properties, fresh and hardened properties, exhibit some curvature. Therefore, in this study experiments were designed according to a factorial central composite design adequate to fit a second order model. The generic form of a second order model is:

$$y = \beta_0 + \sum_{i=1}^{k} \beta_i x_i + \sum_{i=1}^{k} \beta_{ii} x_i^2 + \sum_{i<j} \sum \beta_{ij} x_i x_j + \varepsilon \qquad (4.1)$$

where y is the response of the material; x_i are the independent variables; β_0 is the independent term; β_i, β_{ii} and β_{ij} are the coefficients of independent variables and interactions, representing their contribution to the response and ε is the random residual error term representing the effects of variables or higher order terms not considered in the model.

To define paste composition, four independent variables x_i were selected, namely, water to powder volume ratio (Vw/Vp), water to cement weight ratio (w/c), superplasticizer to powder weight ratio (Sp/p) and metakaolin to cement weight ratio (mtk/c). For mortar mixtures it was necessary to include an additional variable to define the composition completely, which was sand to mortar volume ratio (Vs/Vm). The selection of these parameters, used widespread in the design of SCC mixtures, was based on the method developed by Okamura and Ouchi (2003). A complete 2^4 factorial statistical design, corresponding to four factors at two levels, was selected for the studies carried out at paste level whereas for the study of mortar mixes a 2^{5-1} fractional

factorial statistical design was adopted. The fractional factorial design was selected for mortar experimental design since it involves fewer runs than the complete set of 2^5=32 runs, while it can still be used to obtain information on the main effects and on the two-factor interactions. Axial points and central points were added to both experimental designs (Central Composite Design), thereby allowing a second-order model fitting. The effect of each factor was evaluated at five different levels, codified in $-\alpha$, -1, 0, $+1$ and $+\alpha$. In order to make the design rotatable (i.e. the standard deviation of the predicted response is constant in all points at the same distance from the centre of the design) the α value should be taken equal to $n_f{}^{1/4}$, where n_f is the number of points in the factorial part of the design (Montgomery, 2001; Sonebi, 2004). The absolute value of each variable corresponding to a given level depends on the variable itself and the specific experimental plan. For a given variable and a given experimental plan the transformation of coded into absolute values is of the form:

$$a = a_0 + x \cdot \Delta a \tag{4.2}$$

with a being the absolute value in normal units; a_0 being the absolute value of the variable at the centre of the design; x being the coded variable measured with the step like units and Δa the variable variation (in absolute values) corresponding to a unit variation in the coded variable. The range of variables variation (-α to +α) was established based on a set of preliminary tests where extreme mixtures, in terms of fresh state behaviour, were searched (least fluid mixture and most fluid mixture), but ensuring performance of characterization testing. Experimental programs also included central point replication in order to evaluate the experimental error associated to conditions and test procedures variability (six replicate central runs were prepared) (Montgomery, 2001). Table 4.2 presents the experimental plans adopted to study paste (PED) and mortar (MED) mixtures.

SCC mix-proportions are generally established based on the volumetric composition of the mix, due to the SCC core concept of overfilling the voids between the aggregate skeleton (EFNARC, 2005). Mix-proportions of paste and mortar prepared in this study were obtained using the formulation presented in the Appendix.

Table 4.2 – Characterization of the experimental designs.

Designation	Experimental design	Independent variables	[-α; +α]
Paste Experimental Design (PED)	2^4 α =2.000 n_c=6 n_f=16 n_a=8	Vw/Vp w/c Sp/p mtk/c	[0.783; 0.904] [0.364; 0.440] [0.682%; 0.724%] [6.44%; 10.89%]
Mortar Experimental Design (MED)	2^{5-1} α =2.000 n_c=6 n_f=16 n_a=10	Vw/Vp w/c Sp/p mtk/c Vs/Vm	[0.800; 1.000] [0.360; 0.460] [0.680%; 0.720%] [3.00%; 15.00%] [0.400; 0.500]

n_c: number of central points; n_f: number of factorial points; n_a: number of axial points

4.3.3. Response variables

Given the main objectives of this study, the selected response variables (y) of the paste experimental plan (PED) were: flow diameter ($D_{flow,paste}$), free water content (w_{free}), yield stress at 10 minutes ($\tau_{0,10min}$), plastic viscosity at 10 minutes ($\eta_{pl,10min}$), yield stress at 23 minutes ($\tau_{0,23min}$), plastic viscosity at 23 minutes ($\eta_{pl,23min}$) and resistivity at 28 days ($\rho_{28d,paste}$). In the mortar experimental plan (MED) assessed response variables were: flow diameter ($D_{flow,mortar}$), flow time with the V-funnel test ($T_{funnel,mortar}$), resistivity at 28 days ($\rho_{28d,mortar}$) and compressive strength at 28 days (fc_{28d}). A brief explanation of the tests performed on paste and mortar is presented below.

4.3.3.1. Paste test methods

Paste flow test

The deformability of paste was assessed by the paste flow test, also known as mini-slump flow test. This test is carried out by using a truncated cone with 19 mm top diameter, 38 mm lower diameter and 57 mm height (Gomes, 2002). After filling the cone and lifting it vertically to let the paste flow freely, the paste flow diameter ($D_{flow,paste}$) was taken as the average of two perpendicular diameters of the spread area.

Centrifugal consolidation test

The centrifugal consolidation test was used to determine the free water of the paste, i.e. the water that is not restricted by particles and can move around them (Grünewald, 2004; Fennis, 2011). The paste is poured into four plastic containers of the centrifuge equipment (approximately 30 ml on each container) and centrifuging was carried out at 3500 rpm during 15 min. During the centrifugal cylinder separation, the particles in the paste are compacted and the free water rises up to the surface of the paste, and is, removed with a pipette after the test. The weight of the containers before and after centrifuging was determined. The free water content (w_{free}) was calculated from,

$$w_{free} = \frac{w_{final} - w_{initial}}{V_{paste}} \tag{4.3}$$

where $w_{initial}$ and w_{final} are the weight of containers before and after removing the surplus of water, respectively, and V_{paste} the volume of paste on each container. A strong relation between paste flow time assessed by the Marsh cone flow test and free water content (centrifuge test) was found by Nunes *et al.* (2011). Therefore, the centrifugal consolidation test is a promising substitute of the Marsh cone with the advantage of being equally precise for lower and higher fluidity pastes.

Rheological test

The rheological flow behaviour of viscoplastic non-Newtonian fluids such as cement paste is often characterized by the yield stress (τ_0) and plastic viscosity (η_{pl}), in accordance with the Bingham model. More complex analytical rheological models have been applied to characterize cement paste behaviour with different degrees of success. In general, the use of the Bingham model offers a less favourable fitting for highly pseudoplastic mixtures or for tests performed in a wide range of shear rates, due to the inability to fit the nonlinear portion of the flow curve observed at low shear rates (Yahia and Khayat, 2001a; Ferraris, 2005). Despite all the shortcomings of the Bingham equation, it is still the most used method on account of its simplicity (a low number of adjustable parameters). In the present study, the Bingham model was selected to fit the flow curve data. According to this model, the relationship between shear stress and shear rate is of the form (equation (4.4)),

$$\tau = \tau_0 + \eta_{pl}\dot{\gamma} \tag{4.4}$$

where τ (in Pa) is the shear stress applied to the material; τ_0 is the yield stress (in Pa); η_{pl} (in Pa·s) is the plastic viscosity and $\dot{\gamma}$ (in s^{-1}) is the shear strain rate. The yield stress corresponds to the minimum required shear stress to initiate flow, while the plastic viscosity measures the resistance of the paste to flow under external stress.

Rheological tests were carried out with a rotational rheometer, using a cone and plate geometry measuring device (cone with 40 mm diameter and 4º angle, providing a gap of 150 μm). This geometry measuring device has the major advantage of imposing a constant shear rate through the entire sample, important in the case of time-dependent and non-Newtonian fluids such as cement paste (Chhabra and Richardson, 1999). However, according to Chhabra and Richardson (1999) the use of the cone and plate tool may be subject to some criticism, especially due to limitations of the maximum particle size. For this geometry (cone and plate 4º/40mm) the corresponding gap size is 150 μm, allowing for a maximum particle size of 15 μm. The gap size must be at least 10 times larger than the mean particles size (Bohlin Instruments Ltd., 1994), and this may conflict with the gap size required to ensure near constant shear rate. As can be observed in Table 4.1, the coarser powder materials have few particles with sizes as high as 35 μm, and the mean particle size is lower than 15 μm. Furthermore, a superplasticizer was always included preventing the formation of large floccules.

A viscometry shear stepped test in shear rate control mode with controlled temperature (25 ± 0.1 ºC) was implemented to obtain equilibrium flow curves. The rheometer was programmed to perform a 12-step logarithmic increase of shear rate ranging from 0.1 to 200 s^{-1} and back again to complete a full cycle. The complete testing sequence is illustrated in Figure 4.2. The descending part of the obtained flow curves were fitted to the Bingham model (see equation (4.4)) and the adjusted model parameters, τ_0 and η_{pl}, were taken as the rheological test results for the present study. An example of the up- and down-flow curves of a cement paste tested in this study is presented in Figure 4.3.

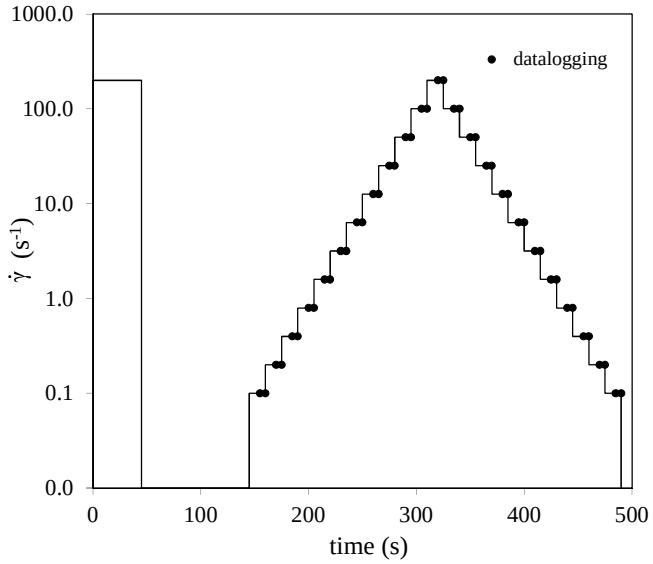

Figure 4.2 – Testing sequence for the rheological tests.

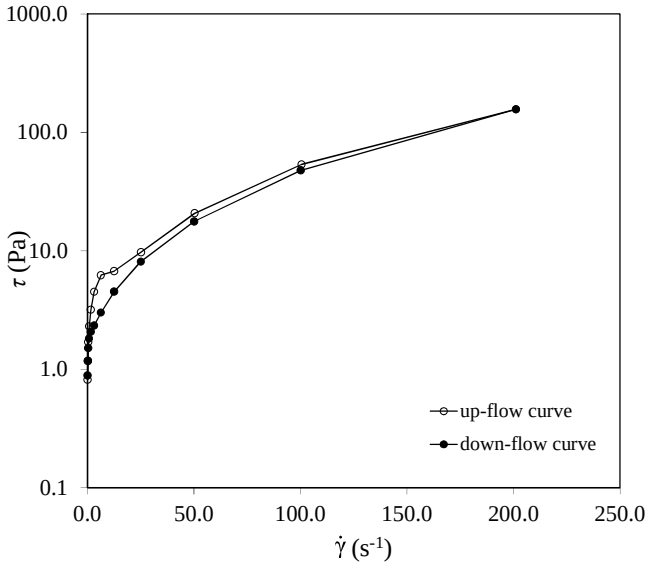

Figure 4.3 – Up- and down-flow curves of a cement paste during the rheological test.

An important feature of cement paste flow behaviour is the extent of hysteresis that is generally observed between the up and down flow curves in a shear ramp test. This hysteresis reflects a reversible time-dependent behaviour of cementitious materials, called thixotropy. In the present study, thixotropy effects were mitigated, as can be observed in Figure 4.3 by appropriate pre-conditioning of samples (pre-shear was applied to the sample during 45 s at a shear rate of 200 s^{-1}), shear stepped test and using only the down-curve data to adjust model parameters. A more detailed description of

the measuring sequence setup and of the procedure used to fit the flow-curves by the Bingham model is given in Nunes *et al.* (2011).

Paste electrical resistivity at 28 days

Electrical resistivity is an intrinsic property of the material that relates to the ability of cement paste to carry electric charge and it depends mainly on the hydration process (nature and topography of the pore structure), changes in pore solution composition and moisture and temperature conditions. Electrical resistivity was assessed by the two electrodes technique on cubic specimens (40×40×40 mm^3) in which stainless steel meshes were embedded to work as electrodes. Applying Ohm's Law, as shown in equation (4.5), the relationship between the intensity of the applied current and the potential difference measured, gives the electrical resistance of the material. The resistivity is obtained applying to the electrical resistance a geometric factor, which depends on the dimensions of the specimen and the electrodes used.

$$R = \frac{V}{I} = \rho \cdot \left(\frac{L}{A}\right) \Rightarrow \rho = \frac{V.A}{L.I} \tag{4.5}$$

where R is the electrical resistance (Ω); I, current (Amp.); V, voltage (Volts); ρ, electrical resistivity (Ω·m); L, length between electrodes (m) and A (m^2) the cross-section area of the test specimen through which current passes. The measurement was carried out at 28 days old paste ($\rho_{28d,paste}$). Paste cubes were demoulded one day after casting and kept under water in a chamber under controlled environmental conditions (T=20ºC) until testing. Since all the specimens were at the same moisture (saturated) and temperature conditions, resistivity can be used to compare the porous structure of various paste specimens and therefore, constitute a measure of the amount and interconnectivity of the cementitious matrix pores.

In fact, according to Andrade (2004), electrical resistivity of water saturated specimens provides indications on the pore connectivity and therefore, on the concrete resistance to penetration of liquid or gas substances. Thus, resistivity is a parameter which accounts for the main key properties related to concrete durability. Regarding the influence of the chemical composition of the pore solution, Andrade (2004) stated that its impact in the total resistivity is small providing concrete remains alkaline. At high pH values the pore solution resistivity varies from 0.3 to 1.0 Ω.m, which is

comparatively very small taking into account that mortar resistivity after several days of hardening is in the range of few dozen Ω.m. Rajabipour and Weiss (2007) also found in their work that the pore connectivity, for saturated specimens, is the single most important parameter governing the overall conductivity of a cement paste specimen. However some authors (Shi *et al.*, 1998) called attention to the fact that the replacement of Portland cement with supplementary cementing materials, such as silica fume, fly ash and ground blast furnace may have a significant effect on electrical conductivity of the pore solution, depending on the alkali content of the supplementary cementing material, replacement level and age.

4.3.3.2. Mortar test methods

Mortar flow and V-funnel tests

The mortar flow test ($D_{flow,mortar}$) was used to assess deformability by calculating the flow diameter as the mean of two diameters in the spread area and the V-funnel test ($T_{funnel,mortar}$) was used to assess the viscosity and passing ability of the mortar. The used flow cone and V-funnel have the same internal dimensions as the Japanese equipment (see (Okamura and Ouchi, 2003) for details on equipment and test procedures).

Mortar electrical resistivity and compressive strength at 28 days

Mortar resistivity ($\rho_{28d,mortar}$) was assessed at 28 days on prismatic specimens (40×40×160 mm^3), using the same technique used on paste specimens. Mortar specimens were demoulded one day after casting and kept under water in a chamber under controlled environmental conditions (T=20ºC) until testing. After completing the electrical resistivity test, a non-destructive test, the specimens were used to assess mortar compressive strength (fc_{28d}).

4.3.4. Mixing and testing sequence

Paste mixes were prepared in 0.31 l batches using a vertical paddle mixer, according to the following procedure: (i) powder materials were mixed with mixing water for 120 s at 750 rpm; (ii) superplasticizer was added and mixed during 120 s at 750 rpm; (iii) the mixer was stopped for 60 s and (iv) mixing was resumed for 120 s at 2000 rpm. Mortar

mixes were prepared in 2.42 l batches and mixed in a two-speed mixer complying to EN 196-1 (IPQ, 2006). The mixing sequence was as follows: (i) sand and powder materials were mixed with 0.80 of the mixing water during 60 s; (ii) the mixer was stopped to scrape material adhering to the mixing bowl and mixed for another 60 s; (iii) the rest of the water was added with the superplasticizer and mixed for 60 s; (iv) the mixer was stopped again to scrape material adhering to the bowl and mixed for 60 s; (v) the mixer was then stopped for 5 min and (vi) the mortar was mixed during a further 90 s. The mixer was always set at low speed except in the last 90 s of the mixing sequence where it was set at high speed (as defined in EN 196-1(IPQ, 2006)). Mixtures (paste and mortar) from experimental plans were tested in a random order to reduce effects of extraneous variables not explicitly included in the experiment. Paste tests were performed according to the following sequence: (a) 0 min: paste mixing procedure was started; (b) 10 min: 1st rheological test in the rheometer; (c) 12 min: paste flow test; (d) 23 min: 2nd rheological test in the rheometer; (e) 26 min: centrifuge test and (f) 36 min: moulding of three cubic test specimens with embedded stainless steel meshes (40×40×40 mm^3). Mortar testing sequence was approximately the following: (a) 0 min: mortar mixing procedure was started; (b) 10 min: mortar flow test; (c) 15 min: mortar V-funnel test and (d) 17 min: moulding of three prismatic test specimens with embedded stainless steel meshes (40×40×160 mm^3). Before the beginning of each test the sample was re-mixed by hand with a paddle to destroy any structure formed during resting (thixotropic effects).

4.4. Discussion of results

4.4.1. Tests results

Test results of the mixes prepared in the PED and the MED are summarized in Table 4.3 and Table 4.4, respectively. In the case of the MED it was not possible to perform the V-funnel test of mixture MCC10, due to the excessive viscosity of the mixture, and the electrical resistivity tests of mixtures MC1 and MC5 were also not carried out, due to problems with the mesh embedded in the specimens.

Table 4.3 – Coded values of the independent variables and fresh and hardened paste results.

Mix number	Ref.	Vw/Vp	w/c	Sp/p	mtk/c	$D_{flow,paste}$ (mm)	w_{free} (kg/m^3)	$\tau_{0,10min}$ (Pa)	$\eta_{pl,10min}$ (Pa.s)	$\tau_{0,23min}$ (Pa)	$\eta_{pl,23min}$ (Pa.s)	$\rho_{28d,paste}$ (Ω.m)
1	PC1	0	0	0	0	191.0	59.25	0.240	0.240	1.084	0.283	68.7
2	PC2	0	0	0	0	208.5	63.42	0.231	0.234	1.140	0.272	68.8
3	PC3	0	0	0	0	197.3	67.17	0.210	0.222	0.946	0.270	72.0
4	PC4	0	0	0	0	200.8	66.08	0.259	0.225	1.090	0.275	75.4
5	PC5	0	0	0	0	206.0	63.67	0.197	0.242	1.330	0.248	65.6
6	PC6	0	0	0	0	204.5	62.75	0.208	0.242	1.036	0.301	72.7
7	PF1	-1	-1	-1	-1	194.8	57.56	0.294	0.264	1.398	0.305	68.4
8	PF2	1	-1	-1	-1	191.8	65.67	0.205	0.246	1.319	0.282	67.4
9	PF3	-1	1	-1	-1	210.8	69.33	0.098	0.205	0.547	0.232	53.2
10	PF4	1	1	-1	-1	209.3	74.08	0.101	0.177	0.672	0.206	51.7
11	PF5	-1	-1	1	-1	190.7	55.92	0.199	0.266	1.303	0.309	64.2
12	PF6	1	-1	1	-1	195.5	69.33	0.148	0.215	1.057	0.268	66.3
13	PF7	-1	1	1	-1	225.8	75.83	0.113	0.207	0.261	0.221	56.3
14	PF8	1	1	1	-1	205.3	83.08	0.071	0.164	0.244	0.185	62.6
15	PF9	-1	-1	-1	1	154.0	44.08	1.663	0.347	4.681	0.442	99.7
16	PF10	1	-1	-1	1	170.0	53.17	0.942	0.296	3.249	0.396	93.4
17	PF11	-1	1	-1	1	173.5	54.00	0.320	0.261	1.354	0.303	78.0
18	PF12	1	1	-1	1	192.8	66.25	0.271	0.224	1.385	0.278	69.7
19	PF13	-1	-1	1	1	163.5	45.08	1.335	0.279(*)	4.407	0.449	97.1
20	PF14	1	-1	1	1	175.0	54.08	0.726	0.282	2.615	0.358	97.8
21	PF15	-1	1	1	1	190.3	57.83	0.267	0.263	1.470	0.255	76.4
22	PF16	1	1	1	1	201.5	72.83	0.145	0.217	0.779	0.227	74.8
23	PCC1	-2	0	0	0	184.5	52.67	0.328	0.286	2.110(*)	0.364	76.0
24	PCC2	2	0	0	0	209.0	76.50	0.183	0.198	0.679	0.222	71.9
25	PCC3	0	-2	0	0	158.0	48.00	1.412	0.338	4.538	0.485	87.8
26	PCC4	0	2	0	0	198.5	75.83	0.130	0.200	0.471	0.226	60.5
27	PCC5	0	0	-2	0	193.5	61.83	0.230	0.255	1.264	0.295	76.8
28	PCC6	0	0	2	0	213.8	67.83	0.199	0.232	0.755	0.259	66.3
29	PCC7	0	0	0	-2	216.8	71.42	0.077	0.199	0.460	0.218	50.5
30	PCC8	0	0	0	2	156.8	46.83	1.120	0.319	3.596	0.402	102.8

* observation identified as an outlier

Table 4.4 – Coded values of the independent variables and fresh and hardened mortar results.

Mix number	Ref.	Vw/Vp	w/c	Sp/p	Vs/Vm	mtk/c	$D_{flow,mortar}$ (mm)	$T_{funnel,mortar}$ (s)	fc_{28d} (MPa)	$\rho_{28d,mortar}$ (Ω.m)
1	MC1	0	0	0	0	0	268.3	6.95	86.5	***
2	MC2	0	0	0	0	0	297.5	6.10	89.6	168.5
3	MC3	0	0	0	0	0	270.8	7.31	90.2	167.2
4	MC4	0	0	0	0	0	269.8	6.97	86.2	165.5
5	MC5	0	0	0	0	0	275.8	6.68	79.5(*)	***
6	MC6	0	0	0	0	0	270.8	7.19	86.6	171.3
7	MF1	-1	-1	-1	-1	1	143.3	37.45	91.3	290.8
8	MF2	1	-1	-1	-1	-1	306.0	3.91	89.6	107.2
9	MF3	-1	1	-1	-1	-1	343.5	4.24	82.2	87.9
10	MF4	1	1	-1	-1	1	230.0	6.34	83.9	205.9
11	MF5	-1	-1	1	-1	-1	336.8	5.19	89.9	105.2
12	MF6	1	-1	1	-1	1	187.3	11.11	87.8	277.3
13	MF7	-1	1	1	-1	1	244.8	8.84	85.0	217.6
14	MF8	1	1	1	-1	-1	344.0	2.87	83.9	82.0
15	MF9	-1	-1	-1	1	-1	278.5	8.10	90.6	133.0
16	MF10	1	-1	-1	1	1	163.3	16.23	88.5	295.5
17	MF11	-1	1	-1	1	1	223.0	11.25	85.7	228.2
18	MF12	1	1	-1	1	-1	330.3	3.55	79.4	93.5
19	MF13	-1	-1	1	1	1	140.5	38.08	89.9	336.7
20	MF14	1	-1	1	1	-1	282.5	5.82	85.8	112.4
21	MF15	-1	1	1	1	-1	333.5	5.74	81.7	102.8
22	MF16	1	1	1	1	1	237.0	7.99	79.7	228.2
23	MCC1	-2	0	0	0	0	292.0	7.95	90.4	155.2
24	MCC2	2	0	0	0	0	273.5	4.56	83.1	154.5
25	MCC3	0	-2	0	0	0	210.8	11.00	93.4	247.9
26	MCC4	0	2	0	0	0	312.3	5.00	80.6	146.2
27	MCC5	0	0	-2	0	0	260.0	7.08	84.3	176.0
28	MCC6	0	0	2	0	0	305.0	5.73	84.5	158.0
29	MCC7	0	0	0	-2	0	307.8	5.34	84.0	158.3
30	MCC8	0	0	0	2	0	258.5	8.50	80.8	181.7
31	MCC9	0	0	0	0	-2	340.8	3.35	80.0	49.0
32	MCC10	0	0	0	0	2	101.8	**	87.7	336.6

* observation identified as an outlier; ** test not performed due to excessive viscosity; *** test not performed due to problems with the embedded mesh

An overall statistical analysis of the response variables, including minimum and maximum values, mean value, standard deviation and coefficient of variation is presented in Table 4.5 for PED and MED. From these statistics it may be observed that the variations introduced in the independent variables of the experimental plans allow covering a wide range of pastes and mortars with regard to the fresh and hardened states. For example, in the case of the mortar experimental design, $D_{flow,mortar}$ ranged from 101.8 to 344.0 mm, $T_{funnel,mortar}$ between 2.87 to 38.08 s, fc_{28d} between 79 to 93 MPa and $\rho_{28d,mortar}$ between 49 to 337 Ω.m.

Table 4.5 – Statistics of the results for the total points from PED and MED.

	Minimum	Maximum	Mean	Stand. deviation	Coeff. of variation
Paste Experimental Design (PED)					
$D_{flow,paste}$ (mm)	154.0	225.8	192.8	18.6	9.7%
w_{free} (kg/m^3)	44.08	83.08	62.71	10.18	16.2%
$\tau_{0,10min}$ (Pa)	0.071	1.663	0.397	0.437	109.9%
$\eta_{pl,10min}$ (Pa.s)	0.164	0.347	0.244	0.045	18.3%
$\tau_{0,23min}$ (Pa)	0.244	4.681	1.556	1.287	82.7%
$\eta_{pl,23min}$ (Pa.s)	0.185	0.485	0.295	0.077	26.0%
$\rho_{28d,paste}$ (Ω·m)	50.5	102.8	73.1	14.0	19.2%
Mortar Experimental Design (MED)					
$D_{flow,mortar}$ (mm)	101.8	344.0	263.7	62.9	23.9%
$T_{funnel,mortar}$ (s)	2.87	38.08	8.92	8.18	91.7%
fc_{28d} (MPa)	79.4	93.4	85.9	3.8	4.5%
$\rho_{28d,mortar}$ (Ω·m)	49.1	336.7	178.0	75.6	42.5%

4.4.2. Empirical vs. rheological paste test results

The characterization and control of fresh state behaviour of SCC is critical for the final quality of the structure, and it is usually performed through some empirical tests such as the slump flow or the V-funnel. Although these methods are relatively inexpensive and practical to use in the field, the most accurate way to describe the behaviour of fresh concrete is through rheological tests. The use of rheometers or viscometers allow a quantitative characterization of the material behaviour in terms of fundamental physical measures, less dependent on the details of the apparatus and on the experience and ability of the operator for their implementation and interpretation (Wallevik and Wallevik, 2011). A rheological test is an excellent method to characterize cement-based materials since it describes the fresh properties with at least two parameters, i.e., yield

stress and plastic viscosity, in contrast to e.g., the slump test which measures the flow of a fluid under a single set of conditions (one point test) (Banfill, 2006). However, rheological test methods have some drawbacks, namely that they are more expensive, require a careful experimental procedure, are rather time consuming and not suited to use at construction sites. Given the advantages and limitations of empirical and rheological tests it is important to find suitable workability test methods for continuous use in the field, and calibrate them with rheological parameters (Utsi *et al.*, 2003; Saak *et al.*, 2004; Zerbino *et al.*, 2009).

In order to verify if the different test results obtained on pastes correlate with each other, in particular, empirical and rheological test results, a correlation matrix with the Spearman's correlation coefficient was computed (see Table 4.6). Spearman's correlation coefficient ($\rho_{Spearman}$) is a non-parametric correlation coefficient that determines the degree to which a monotonic relationship exists between two variables (coefficient ranges between -1 and 1). This coefficient does not require the assumption that the relationship between variables is linear and is less sensitive to asymmetries or presence of outliers. It is important to note that if there is a strong correlation between two variables (absolute value of $\rho_{Spearman}$ is close to 1) merely indicates that variables are associated, not implying that one variable causes another (Sheskin, 2003).

Table 4.6 – Spearman's correlation matrix within PED results.

	$D_{flow,paste}$	w_{free}	$\tau_{0,10min}$	$\eta_{pl,10min}$	$\tau_{0,23min}$	$\eta_{pl,23min}$	$\rho_{28d,paste}$
$D_{flow,paste}$	1.000	0.858	-0.858	-0.847	-0.880	-0.859	-0.810
w_{free}		1.000	-0.907	-0.965	-0.924	-0.941	-0.773
$\tau_{0,10min}$			1.000	0.888	0.933	0.906	0.880
$\eta_{pl,10min}$				1.000	0.929	0.929	0.773
$\tau_{0,23min}$					1.000	0.885	0.810
$\eta_{pl,23min}$						1.000	0.781
$\rho_{28d,paste}$							1.000

all correlations are significant at the 0.01 level (two-tailed)

Spearman's correlation coefficients presented in Table 4.6 indicated on one hand that the empirical test results are related to each other to some degree, the $\rho_{Spearman}$ of spread flow ($D_{flow,paste}$) against free water results (w_{free}) was 0.858 with a significance at the 0.01 level, and, on the other hand, a strong relation was found between empirical and rheological tests. The highest correlation was found between free water results (w_{free})

and plastic viscosity at 10 minutes ($\eta_{pl,10min}$) with a $\rho_{Spearman}$ of -0.965. In fact, empirical tests, to some extent, provide information about rheology, and this has been shown by many investigators. Several analytical models have been developed to relate slump, as well as spread flow (of concrete, mortar or paste) to yield stress (Saak *et al.*, 2004; Roussel, 2005), but more recent studies seem to indicate that, especially at low viscosity, the final spread diameter is controlled by both yield stress and plastic viscosity (Esping, 2007; Bouvet *et al.*, 2010). According to Roussel and Roy (2005) the flow time of fresh paste tested in the Marsh cone can be directly linked to plastic viscosity and yield stress for Bingham fluids, which is a simple approximation of the fresh cement paste behaviour. The Spearman's correlation coefficient computed with the data collected in the present work supports these conclusions. Actually $D_{flow,paste}$ and w_{free} have a strong relation with plastic viscosity but also with yield stress (see Table 4.6). Similar correlation coefficients were found between empirical and rheological tests performed at 10 and 23 minutes.

It is also noteworthy the relation found between paste electrical resistivity at 28 days and fresh paste properties (empirical and rheological), especially with yield stress and spread flow ($\rho_{Spearman}$=0.882 and $\rho_{Spearman}$=-0.810 for $\tau_{0,10min}$ and $D_{flow,paste}$, respectively) see Table 4.6, Figure 4.4(a) and Figure 4.4(b). A strong correlation between resistivity and spread diameter was also found from the results collected in the mortar experimental plan, with a $\rho_{Spearman}$ of -0.956 (see Figure 4.4(c)).

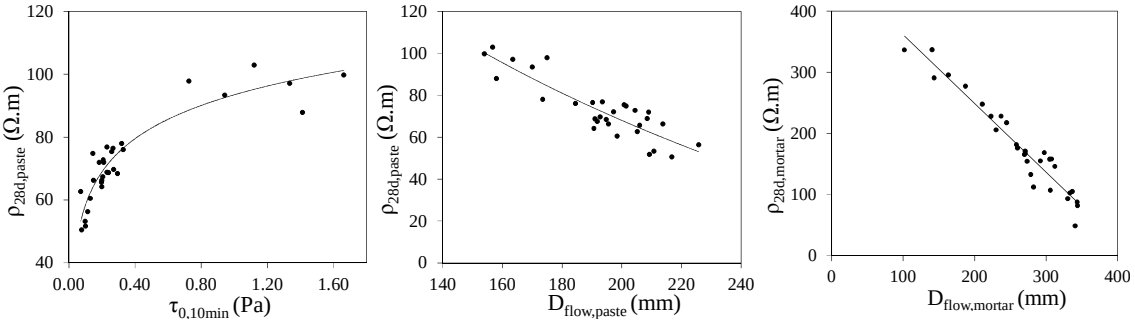

Figure 4.4 – Relation between (a) $\tau_{0,10min}$ and $\rho_{28d,paste}$ ($\rho_{Spearman}$=0.882); (b) $D_{flow,paste}$ and $\rho_{28d,paste}$ ($\rho_{Spearman}$=-0.810); (c) $D_{flow,mortar}$ and $\rho_{28d,mortar}$ ($\rho_{Spearman}$=-0.956).

4.4.3. Time-dependent rheological behaviour of cement pastes

In order to assess the differences in the paste rheological behaviour during the hydration process, two rheological tests were performed in the PED, at 10 and 23 minutes. The experimental results presented in the graphs below, show that yield stress (Figure 4.5) and plastic viscosity (Figure 4.6) measured at 23 minutes are higher than those measured at 10 minutes.

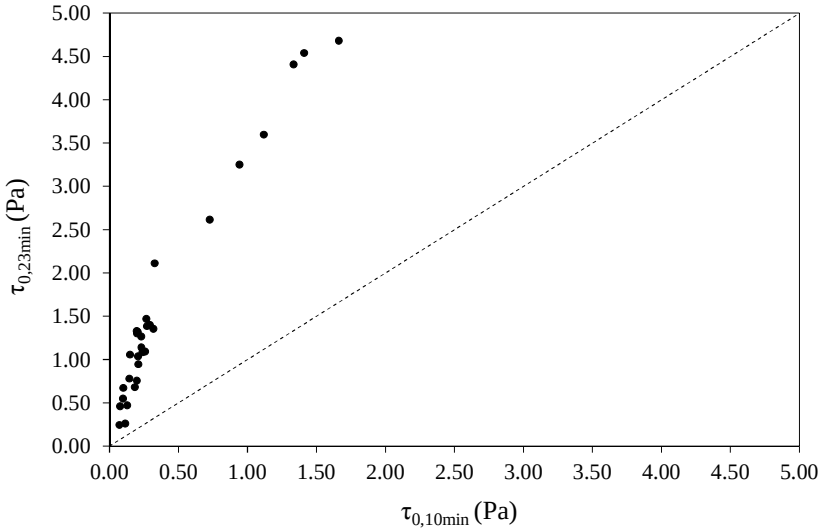

Figure 4.5 – Relation between the τ_0 measured at 10 and 23 minutes in paste mixtures of the PED.

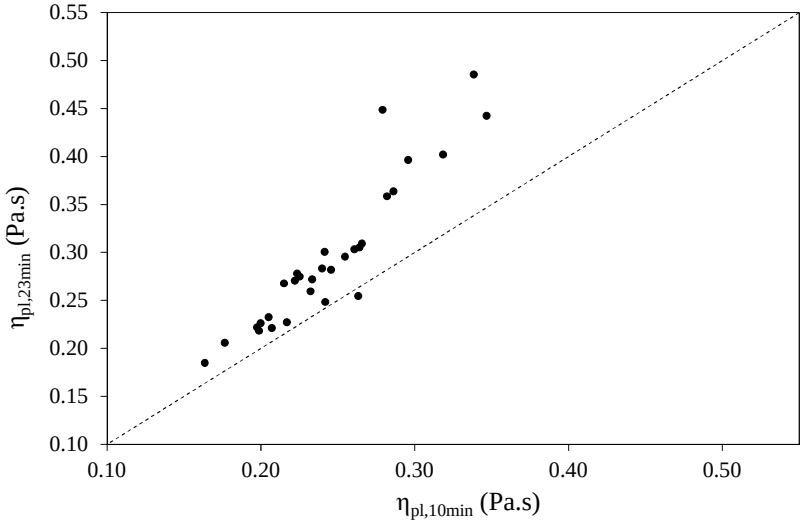

Figure 4.6 – Relation between the η_{pl} measured at 10 and 23 minutes in paste mixtures of the PED.

As expected, this time-dependent behaviour is markedly more evident in yield stress than in plastic viscosity. For the range of paste mixtures studied in this PED, yield stress in some cases increased almost 6 times, whereas plastic viscosity increased less than 1.6 times. Early cement hydration increases both, yield stress and plastic viscosity, but it is yield stress that is particularly sensitive to hydration and its associated microstructural changes. The increase in paste yield stress reflects both the attractive colloidal forces between the cement and other submicron particles that cause them to flocculate, as well as the strength of these attractive interparticle forces (Struble and Lei, 1995; Struble *et al.*, 1996; Petrou *et al.*, 2000).

In cementitious materials, a reversible rheological behaviour is often observed during the dormant period of the hydration process. As long as the available mixing power is sufficient to break the chemical links between cement particles, the hydration process has a reversible macroscopic time-dependent behaviour referred to as thixotropy (Saak, 2000; Roussel *et al.*, 2012). Thixotropy is a reversible macroscopic phenomenon which is associated to reversible physico-chemical phenomena such as colloidal flocculation and de-flocculation of the cement particles in combination with the structural breakdown of the chemically formed linkages between the particles (Roussel, 2005; Wallevik, 2009; Roussel *et al.*, 2012). However at a microscopic scale, it is a nonreversible chemical reaction that can create new bonds between particles, as long as the reservoir of chemical species is sufficient (Roussel *et al.*, 2012). Besides the reversible time-dependent behaviour (thixotropy), cementitious materials also show a time-dependent irreversible behaviour. As stated before, in rheological tests performed in this experimental programme, thixotropy effects were mitigated by appropriate pre-conditioning of samples and shear stepped tests, therefore the observed differences in τ_0 and η_{pl} between 10 minutes and 23 minutes, corresponds mainly to the irreversible time-dependent behaviour of cement paste. This irreversible rheological transient behaviour observed in suspensions subjected to chemical reactions or particles absorptions is due to concurrent processes like the growth of hydration products and water consumption during cement hydration, the loss of water by evaporation and the loss of dispersing efficiency of the superplasticizer or other water reducing admixtures (Esping, 2007).

4.5. Response models

In the present study a commercial software (Design-Expert-Software, 2007) was used to analyse the results for each response variable, by examining summary plots of the data, fitting a model using regression analysis and ANOVA, validating the model by examining the residuals for trends and outliers and, finally, interpreting the model graphically.

4.5.1. Fitted models

For each response variable, a quadratic model can be estimated from the central composite design data (see equation (4.1) in Section 4.3.2). The model parameters (β_0, β_i and β_{ij}) are estimated by means of a multilinear regression analysis. It may happen that, for some response variables, some of the terms in equation (4.1) may not be significant. The significance of each factor on a given response can be evaluated using a Student's *t*-test. A backward elimination was used in this work to eliminate non-significant terms in the regression model (Design-Expert-Software, 2007), i.e. those terms associated with a *p*-value greater than the chosen significance level (in this study, α=0.05). The results of the estimated models, including the residual error term, along with the correlation coefficients, are given in Table 4.7 and Table 4.8, for the PED and MED, respectively.

Notice that the observed values marked with * in Table 4.3 and Table 4.4 (Section 4.4.1) are not typical of the rest of the data. These values were identified as outliers in the statistical analysis and for this reason they have been excluded from the data when fitting the model. Residual analysis did not reveal any obvious model inadequacies or indicate serious violations of the normality assumptions, except in some cases such as $\tau_{0,10min}$ where the problem was overcome after a variable transformation of the form $\log_{10}(y)$, as indicated in Table 4.7.

Table 4.7 – Fitted numerical models for response variables from PED (coded variables).

	$D_{flow,paste}$ (mm)	w_{free} (kg/m^3)	$\log_{10}[\tau_{0,10min}$ (Pa)]	$\eta_{pl,10min}$ (Pa.s)	$[\tau_{0,23min}$ (Pa)]$^{0.5}$	$[\eta_{pl,23min}$ (Pa.s)]$^{-0.5}$	$\rho_{28d,paste}$ (Ω·m)
independent term	200.399	63.657	-0.654	0.237	1.035	1.907	72.086
Vw/Vp	3.618 *(8%)*	5.272 *(23%)*	-0.076 *(-9%)*	-0.021 *(-19%)*	-0.083 *(-7%)*	0.080 *(17%)*	-0.739 *(-3%)*
w/c	10.618 *(23%)*	6.834 *(30%)*	-0.253 *(-29%)*	-0.034 *(-30%)*	-0.336 *(-28%)*	0.174 *(36%)*	-7.759 *(-29%)*
Sp/p	3.799 *(8%)*	1.744 *(8%)*	-0.045 *(-5%)*	-0.004 *(-4%)*	-0.072 *(-6%)*	0.037 *(8%)*	-0.293 *(-1%)*
mtk/c	-13.465 *(-29%)*	-6.360 *(-28%)*	0.287 *(32%)*	0.030 *(27%)*	0.312 *(26%)*	-0.135 *(-28%)*	12.556 *(46%)*
(Vw/Vp)×(w/c)	NS	NS	NS	NS	0.046 *(4%)*	NS	NS
(Vw/Vp)×(Sp/p)	NS	NS	-0.025 *(-3%)*	-0.004 *(-4%)*	-0.040 *(-3%)*	NS	1.548 *(6%)*
(Vw/Vp)×(mtk/c)	4.885 *(11%)*	NS	-0.024 *(-3%)*	-0.003 *(-3%)*	-0.067 *(-6%)*	NS	NS
(w/c)×(Sp/p)	NS	1.373 *(6%)*	NS	NS	NS	0.027 *(6%)*	NS
(w/c)×(mtk/c)	NS	NS	-0.082 *(-9%)*	-0.004 *(-4%)*	-0.082 *(-7%)*	NS	-2.912 *(-11%)*
(Sp/p)×(mtk/c)	NS	NS	NS	NS	NS	NS	NS
$(Vw/Vp)^2$	NS	NS	NS	NS	NS	NS	NS
$(w/c)^2$	-5.835 *(-13%)*	NS	0.067 *(8%)*	0.008 *(7%)*	0.095 *(8%)*	-0.029 *(-6%)*	NS
$(Sp/p)^2$	NS	NS	NS	NS	NS	NS	NS
$(mtk/c)^2$	-3.710*(-8%)*	-1.180 *(-5%)*	0.026 *(3%)*	0.005 *(4%)*	0.065 *(5%)*	NS	1.254 *(5%)*
residual error, ε *							
mean	0	0	0	0	0	0	0
standard deviation	4.909	1.888	0.044**	0.006	0.051**	0.045**	2.980
R^2/ $R^2_{adjusted}$	0.930 / 0.908	0.966 / 0.958	0.986 / 0.980	0.984 / 0.977	0.988 / 0.981	0.960 / 0.949	0.955 / 0.941

(NS) non-significant terms; (*) error term is a random and normally distributed variable and no evidence of auto-correlation was found in the residues; (**) corresponding value for $\tau_{0,10min}$, $\tau_{0,23min}$ and $\eta_{pl,23min}$ is 0.045, 0.108 and 0.015, respectively; (%) relative influence of the variable on the response variation.

Table 4.8 – Fitted numerical models for response variables from MED (coded variables).

	$D_{flow,mortar}$ (mm)	$[T_{funnel,mortar}$ (s)$]^{-0.5}$	f_{c28d} (MPa)	$\log_{10}[\rho_{28d,mortar}$ (Ω·m)]
independent term	278.411	0.382	87.640	2.227
Vw/Vp	-0.021 *(0%)*	0.038 *(15%)*	-1.341 *(-14%)*	-0.010 *(-3%)*
w/c	27.125 *(18%)*	0.047 *(18%)*	-3.222 *(-34%)*	-0.058 *(-16%)*
Sp/p	7.438 *(5%)*	0.005 *(2%)*	-0.301 *(-3%)*	-0.004 *(-1%)*
Vs/Vm	-10.229 *(-7%)*	-0.026 *(-10%)*	-0.787 *(-8%)*	0.022 *(6%)*
mtk/c	-61.000 *(-40%)*	-0.094 *(-36%)*	0.997 *(10%)*	0.203 *(56%)*
(Vw/Vp)×(w/c)	NS	NS	NS	NS
(Vw/Vp)×(Sp/p)	NS	NS	NS	NS
(Vw/Vp)×(Vs/Vm)	NS	NS	-0.704 *(-7%)*	NS
(Vw/Vp)×(mtk/c)	5.969 *(4%)*	NS	NS	NS
(w/c)×(Sp/p)	NS	NS	NS	NS
(w/c)×(Vs/Vm)	4.375 *(3%)*	NS	NS	NS
(w/c)×(mtk/c)	9.563 *(6%)*	0.012 *(5%)*	NS	-0.009 *(-3%)*
(Sp/p)×(Vs/Vm)	-5.719 *(-4%)*	-0.012 *(-5%)*	NS	NS
(Sp/p)×(mtk/c)	NS	NS	NS	0.008 *(2%)*
(Vs/Vm)×(mtk/c)	NS	0.011 *(4%)*	NS	NS
$(Vw/Vp)^2$	NS	0.006 *(2%)*	NS	-0.008 *(-2%)*
$(w/c)^2$	-4.763 *(-3%)*	NS	NS	0.015 *(4%)*
$(Sp/p)^2$	NS	NS	-0.539 *(-6%)*	NS
$(Vs/Vm)^2$	NS	NS	-1.041 *(-11%)*	NS
$(mtk/c)^2$	-14.826 *(-10%)*	-0.009 *(-4%)*	-0.678 *(-7%)*	-0.028 *(-8%)*
residual error, ε *				
mean	0	0	0	0
standard deviation	8.028	0.014**	1.374	0.013**
R^2/ $R^2_{adjusted}$	0.984 / 0.975	0.979 / 0.969	0.872 / 0.817	0.995 / 0.993

(NS) non-significant terms; (*) error term is a random and normally distributed variable and no evidence of auto-correlation was found in the residues; (**) corresponding value for $T_{funnel,mortar}$ and $\rho_{28d,mortar}$ is 1.591 and 5.076, respectively; (%) relative influence of the variable

4.5.2. Accuracy of the proposed models

Even though the majority of the fitted models presented considerably high correlation coefficients (see R^2 and $R^2_{adjusted}$ in Table 4.7 and Table 4.8) their accuracy must be verified. The results of the central points included in the experimental design were analysed in order to estimate the experimental error and the accuracy of the derived models. The corresponding minimum, maximum and mean value, standard deviation and coefficient of variation for PED and MED are presented in Table 4.9. The estimated residual standard deviation (see Table 4.7 and Table 4.8) does not exceed the experimental error by far, so a good fitting can be expected.

It must be stressed that the highest coefficients of variation of the central points were associated to $\tau_{0,10min}$ and $\tau_{0,23min}$, 10.4% and 11.7%, respectively. The yield stress was determined by the extrapolation of experimental shear stress vs. shear rate data to zero shear rate, using a numerical fitting to the Bingham model. In fact, the yield stress value obtained by this extrapolation technique is obviously more sensitive to small deviations of the shear stress measured values, which may explain the higher coefficient of variation.

Table 4.9 – Statistics of the results for central points from PED and MED.

	Minimum	Maximum	Mean	Stand. deviation	Coeff. of variation
Paste Experimental Design (n=6 central points)					
$D_{flow,paste}$ (mm)	191.0	208.5	201.3	6.4	3.2%
w_{free} (kg/m³)	59.25	67.17	63.72	2.77	4.4%
$\tau_{0,10min}$ (Pa)	0.197	0.259	0.224	0.023	10.4%
$\eta_{pl,10min}$ (Pa.s)	0.222	0.242	0.234	0.009	3.7%
$\tau_{0,23min}$ (Pa)	0.946	1.330	1.104	0.129	11.7%
$\eta_{pl,23min}$ (Pa.s)	0.248	0.301	0.275	0.017	6.2%
$\rho_{28d,paste}$ (Ω·m)	65.6	75.3	70.5	3.49	5.0%
Mortar Experimental Design (n=5 central points)					
$D_{flow,mortar}$ (mm)	268.3	297.5	275.5	11.1	4.0%
$T_{funnel,mortar}$ (s)	6.10	7.31	6.87	0.43	6.3%
fc_{28d} (MPa)	86.2	90.2	87.8	1.9	2.2%
$\rho_{28d,mortar}$ (Ω·m)	165.5	171.3	168.1	2.5	1.5%

4.5.3. Individual and interaction effects

Based on the derived models, the relative influence of each variable on the response variation was computed and is presented (in brackets) in Table 4.7 and Table 4.8 for PED and MED, respectively. Naturally, higher values indicate greater influence of this parameter in the response and on the other hand, a negative value reflects a response decrease to an increase in this parameter. The results clearly show that w/c and mtk/c exhibited a great effect on all measured responses, being the only exception fc_{28d} of MED where the relative influence of mtk/c does not exceed 10%. It should be noted, however, that these two variables have opposite effects on the response. In the case of $\rho_{28d,paste}$ and $\rho_{28d,mortar}$, the variable mtk/c explains almost 50% of the variation of these responses. The partial replacement of cement by a pozzolanic material, like metakaolin, causes substantial changes on the pore structure of the paste and on the chemistry of the hydration products. Metakaolin contributes to the microstructure improvement by the filler effect (like limestone filler) and by the pozzolanic reaction of metakaolin with calcium hydroxide, and this is reflected in the resistivity values. According to some authors, although total porosity may be increased by metakaolin blending, the partial replacement of cement with metakaolin also causes a refinement of pore structure (Frías and Cabrera, 2000). Metakaolin modifies the pore structure of the cement matrix and significantly reduces permeability, resulting in higher resistance to transportation of water and diffusion of harmful ions which lead to the deterioration of the matrix (Siddique and Klaus, 2009).

Besides w/c and mtk/c, the variable that most influenced w_{free}, $\eta_{pl,10min}$ and $\eta_{pl,23min}$ on PED and $T_{funnel,mortar}$ on MED, was Vw/Vp. A global analysis of the distribution of the relative influence of each parameter on the variation of the response variables of fresh state on PED, has revealed a distribution quite similar to the responses $D_{flow,paste}$, $\tau_{0,10min}$ and $\tau_{0,23min}$, as well as quite similar to the responses w_{free}, $\eta_{pl,10min}$ and $\eta_{pl,23min}$. In the mortar experimental plan the variable Vs/Vm had some influence, but w/c e mtk/c remain the most prevalent variables in all measured responses. Significant interaction and quadratic effects were found in all responses. The interaction effects represent, on average, a weight of 13% on the variation of the responses and quadratic terms a weight of 11%.

4.6. SCC mortar design using paste rheological models

4.6.1. Influence of paste rheology on the workability of mortar

The influence of the rheology of the cement paste matrix on the workability of fresh mortar can be assessed linking the two experimental designs results. In order to understand this influence, the values of independent variables that define the mixture composition of paste tested in the PED, were used in the mortar fitted numerical models to obtain the corresponding $D_{flow,mortar}$ and $T_{funnel,mortar}$. The paste mix proportions were maintained at the mortar level and only the mixture parameter related with the aggregate skeleton (Vs/Vm) was established. Figure 4.7 shows the flow chart used to assess the influence of paste rheology on the workability of mortar.

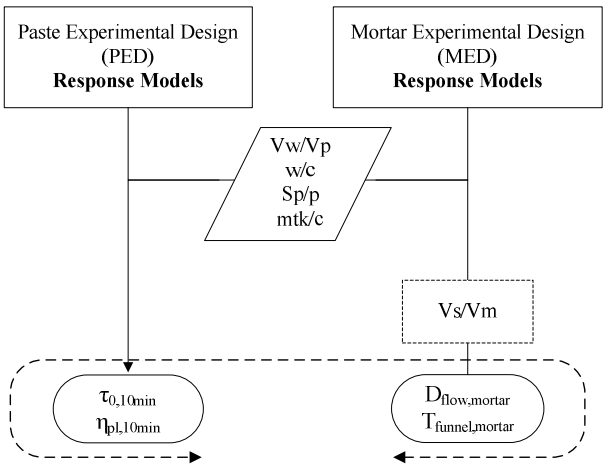

Figure 4.7 – Flow chart used to assess the influence of paste rheology on the workability of mortar.

In Figure 4.8(a) and Figure 4.8(b) the range of rheological parameters, $\tau_{0,10min}$ and $\eta_{pl,10min}$, were plotted against the corresponding mortar workability parameters, $D_{flow,mortar}$ and $T_{funnel,mortar}$, for a Vs/Vm=0.45. From these figures it is clear that there is a strong correlation between the parameters that define the fresh behaviour of paste and mortar. It is also noteworthy that, paste mixtures considered within the PED led to a wide range of mortars in the fresh state, with $D_{flow,mortar}$ ranging between 328 mm and 216 mm and $T_{funnel,mortar}$ ranging between 5.4 s and 16.0 s, for a Vs/Vm=0.45.

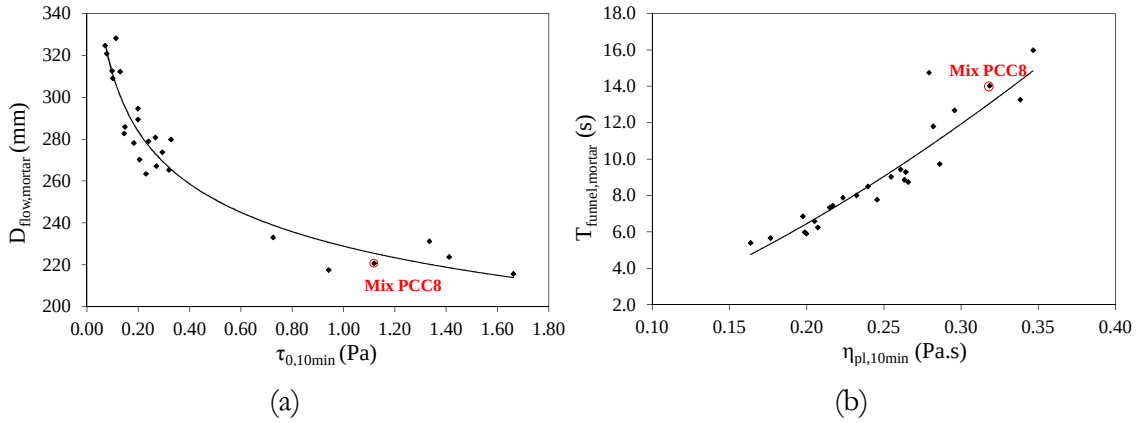

Figure 4.8 – Relation between: (a) $\tau_{0,10min}$ measured in paste and $D_{flow,mortar}$; (b) $\eta_{pl,10min}$ measured in paste and $T_{funnel,mortar}$, for Vs/Vm=0.45.

The same procedure was performed for Vs/Vm values from 0.40 to 0.50, and the results are presented in Figure 4.9. For each paste mixture, the flow properties were described by the ratio of the rheological parameters ($\tau_{0,10min}/\eta_{pl,10min}$) and the workability of the corresponding mortar defined as the ratio of the empirical parameters ($D_{flow,mortar}/T_{funnel,mortar}$). As observed in the previous figures, for each Vs/Vm there is a clear correlation between fresh properties of paste and mortar. As Vs/Vm used in mortar increases, the trend line shifts in the direction of lower values of the $D_{flow,mortar}$ to $T_{funnel,mortar}$ ratio. Observing, for example PCC8, one can conclude that mortars with lower aggregate content exhibited a greater ratio (247.2 mm/10.28 s, with Vs/Vm=0.40), while mortars with higher aggregate content showed a lower ratio (194.4mm/20.26s, with Vs/Vm=0.50).

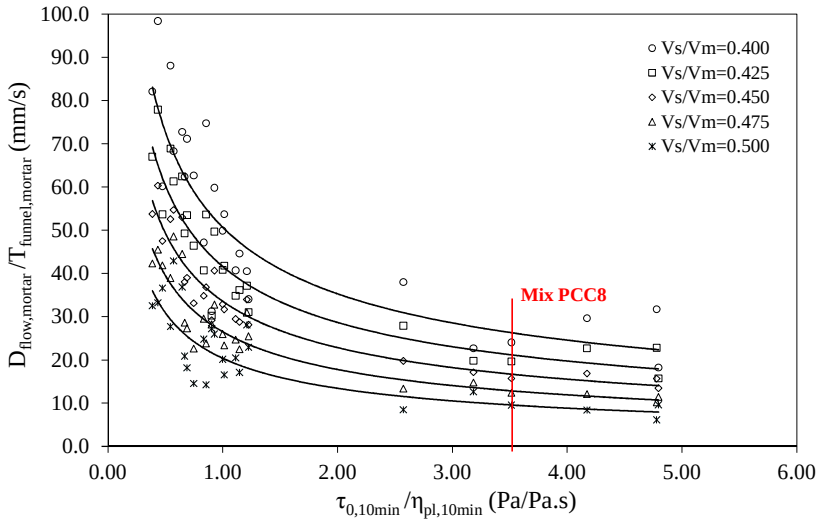

Figure 4.9 – Relation between fresh properties of paste and mortar, for various Vs/Vm.

In fact, increasing $\eta_{pl,10min}$ increases the value of $T_{funnel,mortar}$, at an increasing rate of Vs/Vm, and increasing $\tau_{0,10min}$ decreases the value of $D_{flow,mortar}$, at an increasing rate of Vs/Vm. Similar results were also found by Ferrara *et al.* (2007), when trying to establish correlations between fresh properties of paste (paste mini-cone flow and paste viscosity), the average size and spacing of the solid skeleton particles and the fresh behaviour of the concrete (concrete slump flow and time needed to reach a 500 mm diameter spread, T_{50}). According to these authors, increasing the paste viscosity increases the value of T_{50} in concrete, and decreasing paste mini-cone flow (higher yield stress values) decreases concrete slump flow, at decreasing rate of average aggregate spacing (increasing rate of aggregate content).

4.6.2. Self-compacting zone at paste level

After building the regression models that establish relationships between mix-design variables and the responses (see Section 4.5), a numerical optimization technique was used to determine the range of mortar mixture parameters where deformability and viscosity coexist in a balanced manner to achieve self-compacting mortar, i.e. to determine the best mixtures which exhibit a spread flow of 260 mm and a flow time of 10 s. Mortar fresh requirements that lead to self-compacting concrete were defined based on the values recommended by the Japanese SCC-design method (Okamura and Ouchi, 2003), the European Guidelines for SCC (EFNARC, 2005) and previous experience of other authors (Nunes *et al.*, 2009b). In the present work, a slightly higher target spread flow value was adopted, when compared to the value recommended by the Japanese SCC-designing method (245 mm).

Numerical optimization was performed using a software developed on MATLAB 2011b, which is based on a subroutine provided by the program in the Optimization Toolbox Solvers (MATLAB 2011b, 2011). In fact, this optimization process is a general problem of solving a system of nonlinear multidimensional equations, with the same number of equality conditions as variables in the model. The values of Vw/Vp and Sp/p that lead to the optimum mixtures in fresh state ($D_{flow,mortar}$=260 mm and $T_{funnel,mortar}$=10 s), were searched for each combination of (w/c, mtk/c, Vs/Vm). Note that since the response models were expressed as a function of five independent variables, a multiple optimum will hardly occur. A last constraint should be

implemented in the optimization process due to the fact that the error function that is associated to each response model increases with the distance to the center of the modelled region. Therefore, only solutions with a distance to the center of the modelled region (D_{center}) less than 2.5, defined in coded values, were accepted (Figure 4.10

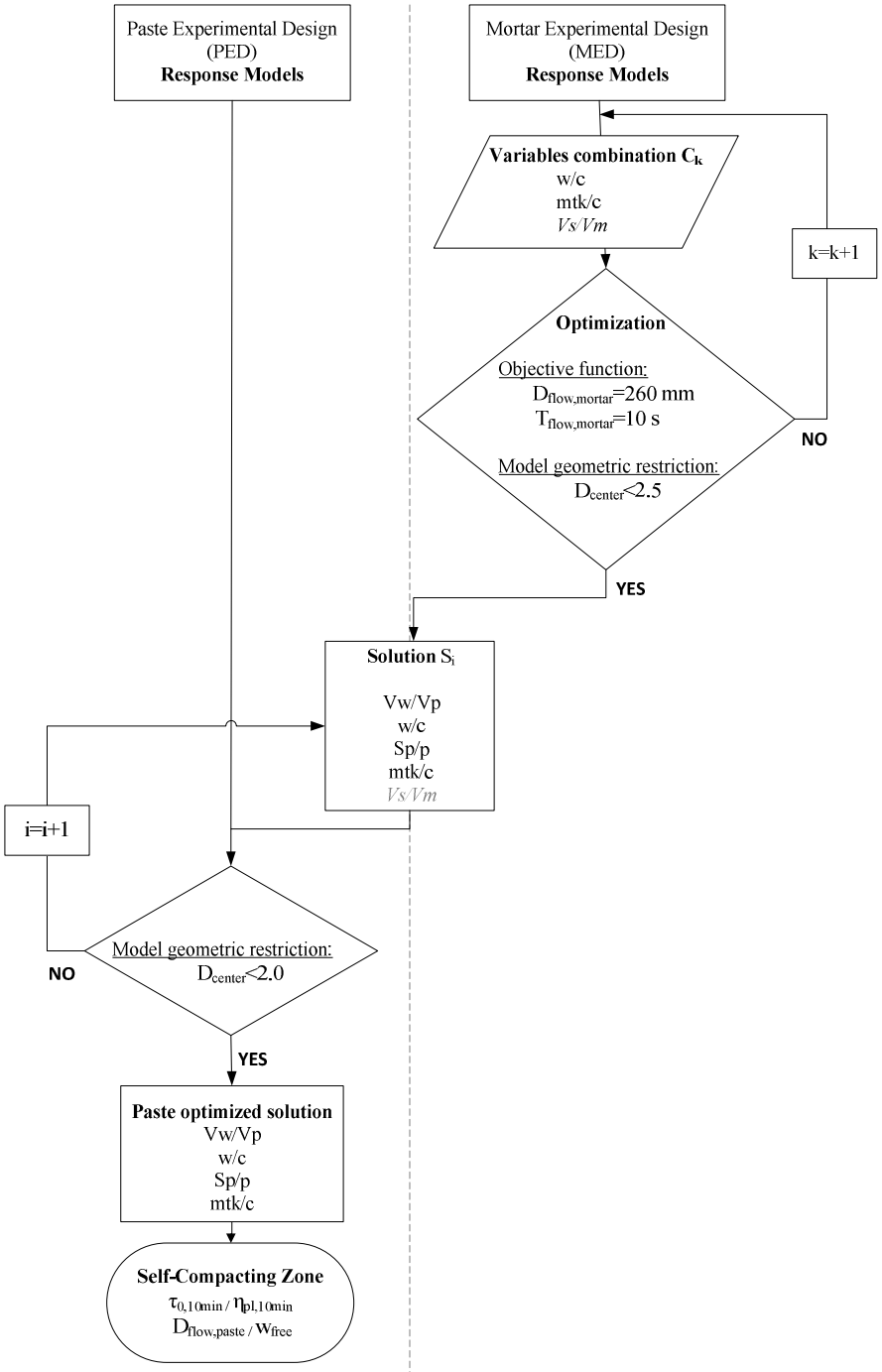

Figure 4.10 – Flow chart used to determine fresh properties of paste to achieve SCC mortar ($D_{flow,mortar}$=260 mm and $T_{funnel,mortar}$=10 s).

The range of paste mixtures that lead to compositions with self-compacting properties are established from the mortar optimized mixtures (solutions S_i with variables defined in real values). Using the mixture parameters of optimized solutions, the corresponding paste fresh properties were determined using the fitted numerical models from PED. In the same way as performed with mortar models, the use of the paste models was limited to an area bounded by coded values -2.0 to +2.0 (D_{center}<2.0, see Figure 4.10), ensuring that the error in predicting the responses is not relevant. The rheological properties ($\tau_{0,10min}$ and $\eta_{pl,10min}$) of the optimized paste mixtures are plotted in Figure 4.11. The results are grouped according to the aggregate content (Vs/Vm) of the mortars that gave rise to paste optimized solutions.

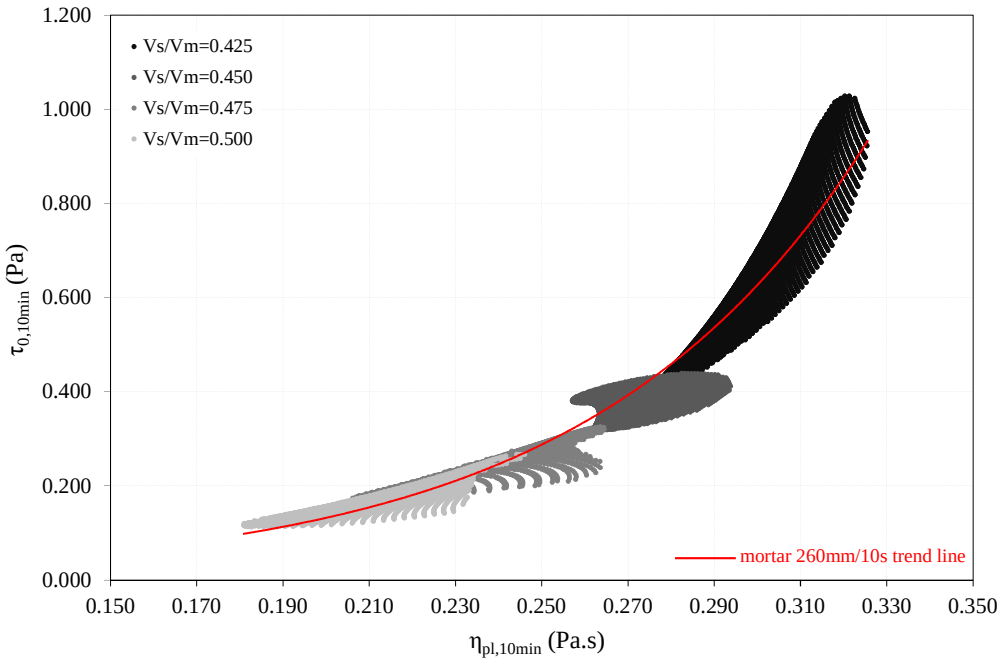

Figure 4.11 – Rheological properties of paste mixtures to achieve SCC mortars ($D_{flow,mortar}$=260 mm and $T_{funnel,mortar}$=10 s).

According to these results, higher aggregate contents (Vs/Vm), which correspond to a shorter average distance between aggregate particles, demands a paste with lower yield stress and lower plastic viscosity (more fluid paste), to achieve self-compacting mortars, while lower aggregate contents require a paste with higher yield stress and viscosity (more viscous paste). Therefore, the rheological properties of the paste (yield stress and viscosity) have to be optimized with respect to aggregate content to obtain mortar with the desired flowability and stability characteristics. Indeed, these conclusions meet the fundamentals of the "Excess Paste Theory" proposed by Kennedy in 1940 (Oh *et al.*,

1999) and applied by Oh *et al.* (1999) to SCC. This theory explained the fact that to reach sufficient workability, it is necessary to have not only enough cement paste to fill all the spaces between the particles, but a volume of cement paste that ensures a very thin lubricating layer around the particles, by virtue of which the friction between the particles is greatly reduced. This cement paste excess layer lubricates the relative movement of the aggregate particles, but also increases flowability of the mixture. Figure 4.12 shows the formation of the cement paste excess layer around the aggregate particles. In fact, the characteristics of SCC in the fresh state are affected by two factors: first, the rheological properties of cement paste, and second, the "relative" layer thickness, a parameter proposed by Oh *et al.* (1999) that depends on the excess paste volume and the diameter and surface area of the aggregate. It can however be noted that the cement paste layer thickness is in fact another way to express the average distance between aggregate particles, which is directly related to the aggregate volume fraction. This means that in a mortar with a given workability, as the aggregate volume fraction (Vs/Vm) increases, the paste layer thickness around aggregate decreases, and this reduction must be balanced with an increase in the paste flowability (lower yield stress and plastic viscosity) to ensure the same workability.

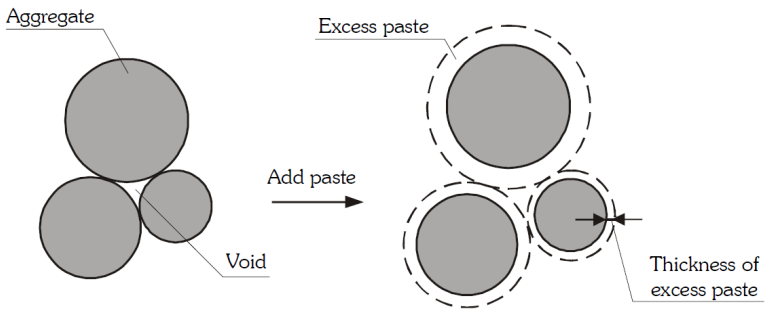

Figure 4.12 – Excess paste theory (Oh *et al.*, 1999).

According to Figure 4.11, for a given aggregate content (Vs/Vm) it is possible to achieve self-compacting mortar from paste with different rheological properties, i.e., there are different combinations of $\tau_{0,10min}$ and $\eta_{pl,10min}$ that can ensure the desired workability in mortar. However $\tau_{0,10min}$ and $\eta_{pl,10min}$ cannot be varied independently, since for this set of materials, paste rheological properties should vary according to the trend line drawn in Figure 4.11 to ensure self-compacting mortar (in this case mortar with 260 mm and 10 s). The shape of the trend line reflects the need of compromise between yield stress and plastic viscosity, which seems to indicate that the increase in

aggregate content decreases the $\tau_{0,10min}$ to $\eta_{pl,10min}$ ratio and decreases the influence of the plastic viscosity on the workability of the mortar as compared to yield stress. Similar conclusions can be found if, instead of rheological variables, empirical variables are used, in this case $D_{flow,paste}$ and w_{free}, as shown in Figure 4.13. In fact others authors, using a different methodology, have reached similar conclusions (Bui *et al.*, 2002). Bui *et al.* (2002) developed a segregation-controlled design methodology for SCC based on the paste rheology criteria, which include minimum apparent viscosity, minimum slump flow diameter, and optimum slump flow diameter to viscosity ratio. According to these authors the optimum slump flow diameter to viscosity ratio of paste is related to the average aggregate diameter and aggregate spacing (aggregate content), where higher aggregate spacing requires lower slump flow diameter to viscosity ratio.

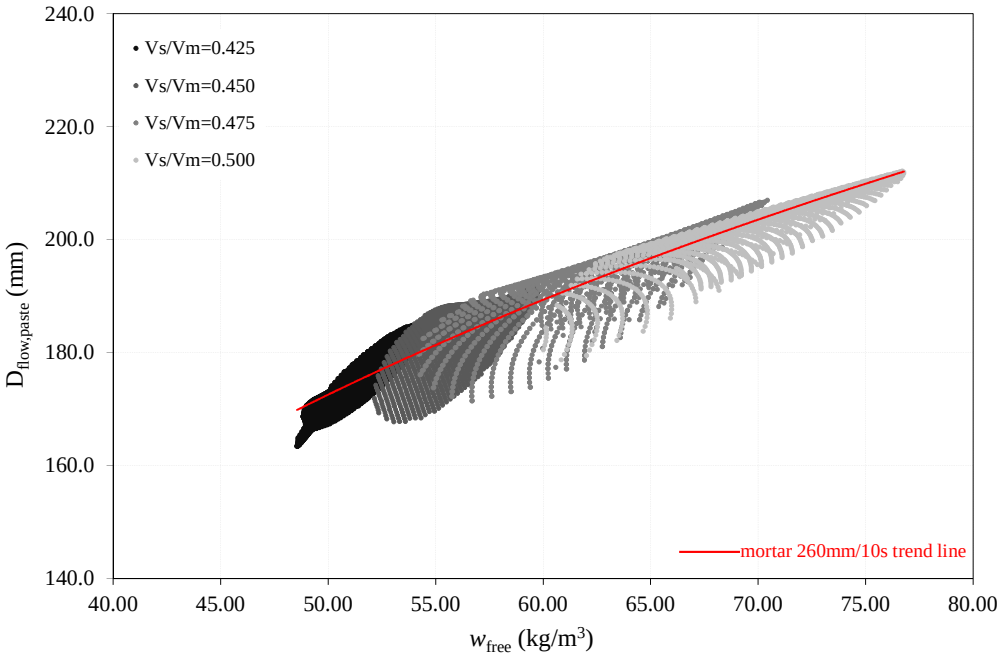

Figure 4.13 – Empirical fresh properties of paste mixtures to achieve SCC mortars ($D_{flow,mortar}$=260 mm and $T_{funnel,mortar}$=10 s).

Specifications of fresh SCC properties should depend on the type of application and on requirements such as, confinement conditions, placing equipment, placing method or finishing method (IPQ, 2010a). A low SCC viscosity may be of interest when good surface finish is required, while a viscous SCC with lower slump flow and higher funnel time is more appropriate to be used under a strong inclination such as ramps in parking houses. Indeed, based on these borderline situations, in terms of fresh SCC properties it is possible to establish a self-compacting zone. Applying the procedure described

above to both situations, a very fluid self-compacting mortar (e.g. a mortar with $D_{flow,mortar}$=280 mm and $T_{funnel,mortar}$=8 s) and a very viscous self-compacting mortar (e.g. a mortar with $D_{flow,mortar}$=240 mm and $T_{funnel,mortar}$=12 s), the respective trend lines can be computed as illustrated in Figure 4.14, which allows to define a self-compacting zone at paste level (SCZ), for the set of materials used in this study.

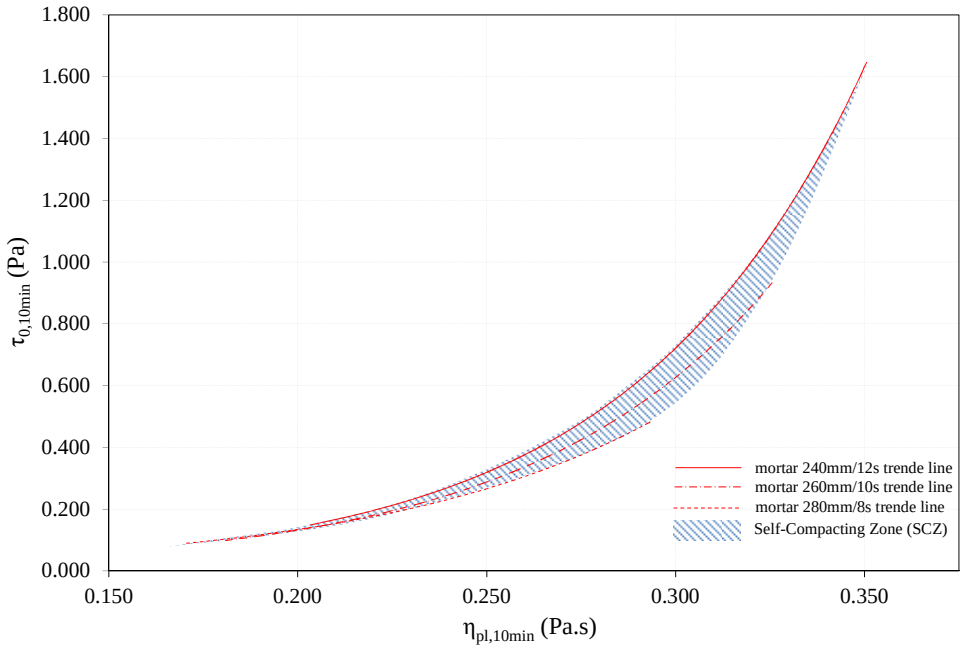

Figure 4.14 – Self-compacting zone at paste level (SCZ) for the set of materials used in this study.

This SCZ has a great applicability when producing SCC, since it allows an expeditious design of mortar mixtures, and therefore of concrete, with the desired self-compacting properties. This design approach can simplify the test protocol required to optimize a given SCC mixture, namely, to select the combination of powder materials with admixtures and to design tailor-made and economic SCC mixtures. It should be mentioned that this SCZ will probably change if a different set of materials is used (addition, superplasticizer or viscosity agent). In fact, studies conducted by Saak *et al.* (2001), allowed to conclude that there is a variation in the relative size and position of the SCZ for a different set of materials. The effect of a new admixture or a new superplasticizer could be assessed at the paste level based on this SCZ although it would demand some adjustments at mortar level in order to achieve the final mortar mixture.

4.6.3. Mixture proportions of optimized SCC mortar

The adjusted values of mtk/c and Sp/p for each pair of (w/c, Vw/Vp) were used to obtain the contour plots presented in Figure 4.15. The mixtures which exhibit a spread flow of 260 mm and a flow time of 10 s are marked with small (+). This figure shows that the increase in sand content led to an adjustment of the variable range where SCC mortars can be found, namely, the range of w/c and Vw/Vp move to higher values and the range of mtk/c move to lower values.

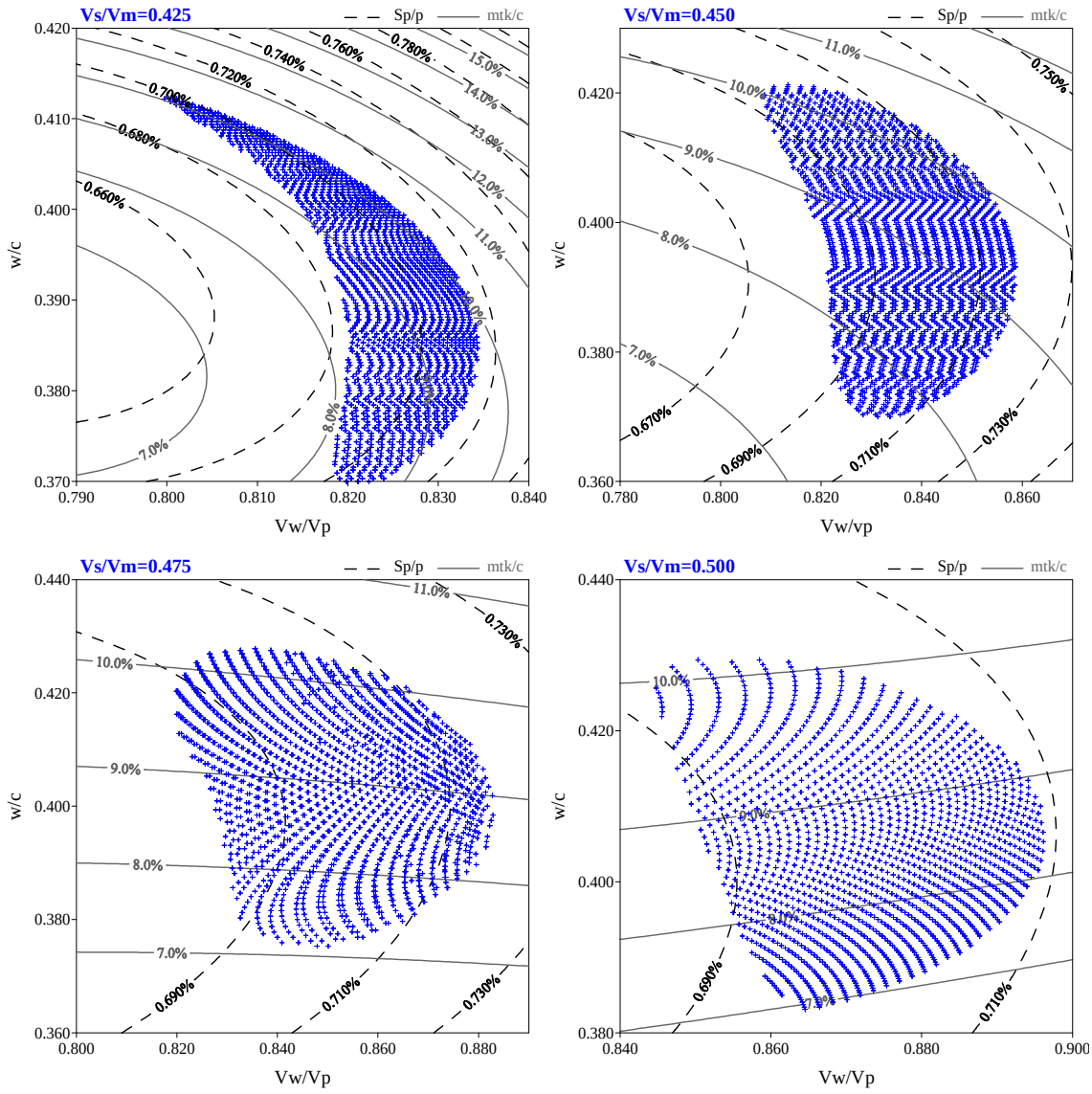

Figure 4.15 – Range of mixture variables (absolute values) for optimized mortars, marked with (+) ($D_{flow,mortar}$=260 mm and $T_{funnel,mortar}$=10 s).

After selecting the paste mix proportions, a SCC concrete mixture can be achieved substituting reference sand (sand used in this study) by real aggregates, fine and coarse aggregate. Tests on concrete are then necessary to optimize the aggregate skeleton and aggregate content. Paste mixtures corresponding to a higher sand content (Vs/Vm) in the optimized mortar mixtures can lead to SCCs with higher total aggregate content and lower paste volume, thus resulting in more economic mixtures (Nunes *et al.*, 2009b). On the other hand, increasing the paste volume increases mixture robustness and allows the accommodation of poorly graded or poorly shaped aggregates (Koehler and Fowler, 2007).

4.7. Influence of aggregate content on the electrical resistivity

With the purpose of evaluating the influence of aggregate on electrical resistivity, the correlation between paste and mortar resistivity was assessed, for different aggregate contents. The correlation was obtained based on the results provided by paste and mortar fitted models (see Section 4.5), applied to the experimental mixtures carried out on the paste experimental design (PED). Figure 4.16 shows the electrical resistivity results for paste mixtures and respective mortars with different aggregate contents, as well as the respective trend lines.

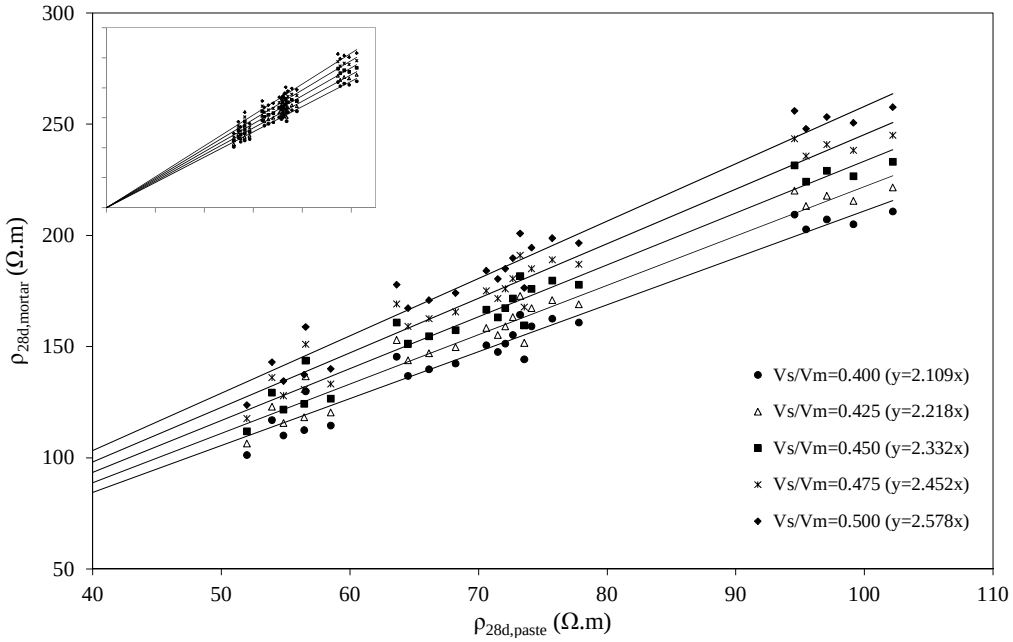

Figure 4.16 – Relation between paste and mortar electrical resistivity as a function of Vs/Vm.

For each Vs/Vm a good correlation between paste and mortar resistivity was found, following a linear trend line with a correlation coefficient above 0.96. The trend line slope increases as more aggregate are added to the paste, which means that the aggregate contributes to increase mixture resistivity.

Indeed, the inclusion of aggregates in the cement paste matrix has an effect of dilution (blocking) and tortuosity (redirecting). The dilution effect depends on the aggregate volume fraction, and it occurs because the aggregate conductivity (inverse of resistivity) is much lower compared with the cement paste conductivity. Paste electrical conductivity (σ_{paste}=$1/\rho_{28d,paste}$) is affected by the dilution effect, according to the equation (4.6):

$$\frac{\sigma_{mortar}}{\sigma_{paste}} = (1 - Vs/Vm) \tag{4.6}$$

where σ_{mortar} ($1/\rho_{28d,mortar}$) is the electrical conductivity of the mortar. The tortuosity effect occurs due to the presence of these "insulating" elements, the aggregate particles, forcing a redirection of conduction around them, making the conduction paths more tortuous.

The effect of including aggregates in the cement paste matrix can be predicted by the Differential Effective Medium Theory (D-EMT), also known as asymmetric Bruggeman formulation (Giordano, 2003b). For the case of a two-phase mixture (cement paste and aggregate), of not diluted dispersion of insulating spherical inclusions (aggregate) the D-EMT formulation leads to the formula presented in equation (4.7). This model also assumes that the inclusion of spherical particles (aggregate) does not change the matrix electrical conductivity (paste).

$$\frac{\sigma_{mortar}}{\sigma_{paste}} = (1 - Vs/Vm)^{3/2} \tag{4.7}$$

In Figure 4.17 the $\sigma_{mortar}/\sigma_{paste}$ results are plotted as a function of the volume fraction of aggregate, and are compared with the theoretical equations that express the dilution effect (equation (4.6)) and both the dilution and tortuosity effect (equation (4.7)).

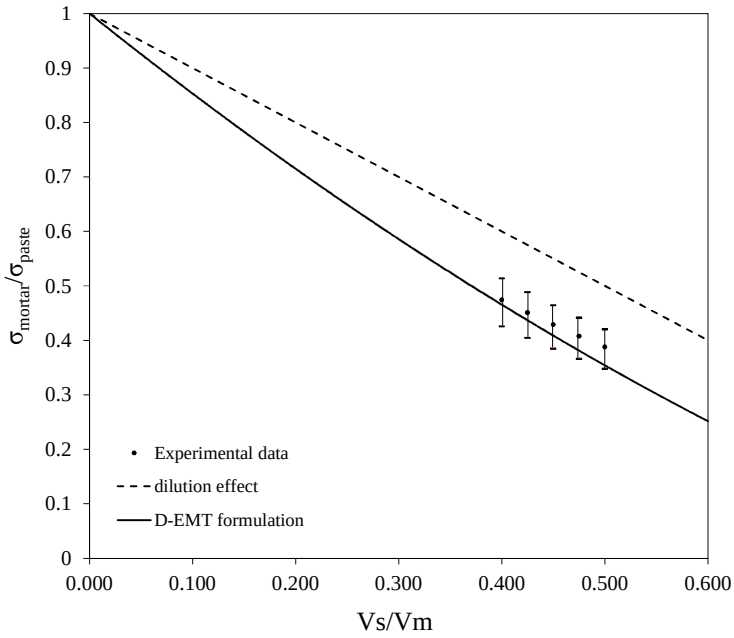

Figure 4.17 – Comparison of experimental results with D-EMT formulation.

Comparing the average value of the experimental data with the theoretical models it seems that the main effect of adding more sand is blocking and redirecting conductive flow. Average values of the experimental data are very close to the $(1\text{-}Vs/Vm)^{3/2}$ power line law. However, although in the vicinity, the results are always above the line and the distance appears to increase as more aggregate is added to paste. Indeed, the presence of aggregate in a cement paste matrix has two opposite effects on the transport properties: firstly, the dilution and tortuosity effects that reduce the permeability; secondly, the presence of a porous interfacial transition zone (ITZ) between paste and the aggregate that facilitates the movement of ions and increases mortar conductivity (Garboczi *et al.*, 2000; RILEM-Report 38, 2007). The volume and properties of the ITZ are influenced by the w/c ratio, addition of pozzolanic or inert fine particles, aggregate volume fraction or the stability of fresh mix. In the presence of low w/c ratios or fine mineral addition, as in SCC, some studies appear to indicate that the porosity and width of the ITZ is significantly smaller than in vibrated concrete. Furthermore, the ITZ formed around the aggregate increases locally the w/c ratio, but this is usually accompanied by a decrease in w/c ratio of bulk matrix, and therefore a decrease in the conductivity because of the lower porosity (Garboczi *et al.*, 2000; RILEM-Report 38, 2007). Another aspect that should be taken into consideration is the fact that the model presented in equation (4.7) considers spherical aggregate, but in fact, aggregate shape

can be more ellipsoidal or aggregate particles could be packed in clusters that behave as individual ellipsoids.

Once established this link between paste and mortar, it is possible to design mortar mixtures with the desired resistivity requirement, by simply conducting some trials at paste level. In Figure 4.18 the mortar resistivity predictions were added to the contour plot presented in Figure 4.15 (Section 4.6.3) for a Vs/Vm=0.475, allowing to simplify the test protocol required to optimize a given self-compacting mortar mixture with the desired durability requirement (resistivity). Although not presented in this work, it is important to emphasize that this link could be extended to concrete level.

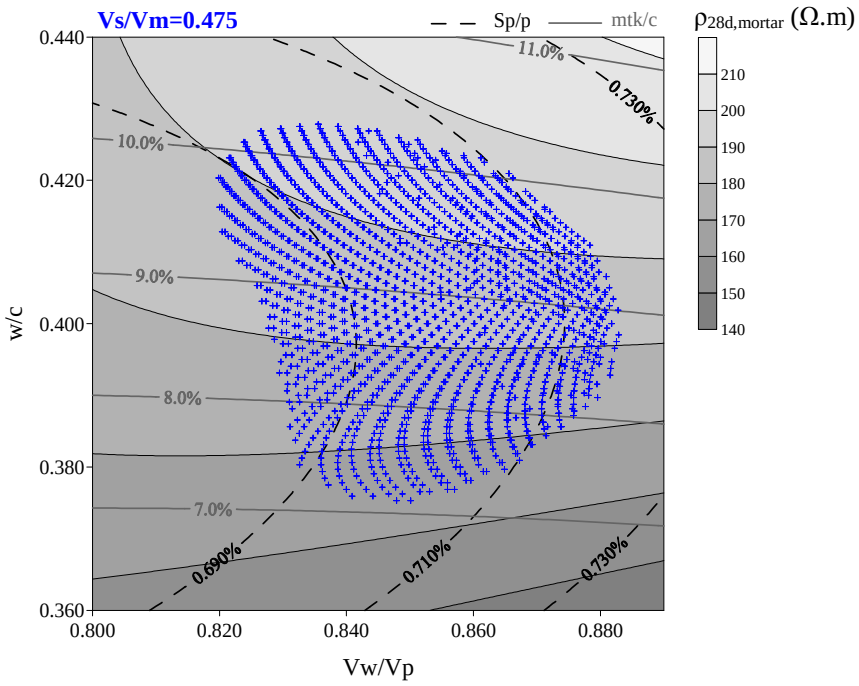

Figure 4.18 – Optimized mixture parameters for SCC mortars, marked with (+) ($D_{flow,mortar}$=260 mm; $T_{funnel,mortar}$=10 s; Vs/Vm=0.475), and estimated values of $\rho_{28d,mortar}$.

4.8. Conclusions

Based on the results presented in this chapter, the following conclusions can be drawn:

- Empirical tests performed in paste ($D_{flow,paste}$ and w_{free}) correlate with the rheological parameters of paste, namely, yield stress and plastic viscosity,

which seems to indicate that both types of tests can be used to characterize fresh paste behaviour.

- Rheological tests performed at 10 and 23 minutes, after starting mixing, showed an increase of both, yield stress and plastic viscosity, but it is the yield stress that seems particularly sensitive due to the hydration reaction and associated microstructural changes, loss of water by evaporation and loss of dispersing efficiency of the superplasticizer.

- Data collected during the experimental plan, conducted according to a central composite design, can be used to establish numerical models relating mixture parameters with fresh and hardened properties of paste and mortar. Such numerical models provide an effective mean to design paste and mortar mixtures by determining the influence of key parameters on the desired fresh and durability properties.

- A link between fresh properties of paste and SCC mortar was established using paste and mortar fitted numerical models. Fresh properties of paste (rheological and empirical) have to be optimized with respect to aggregate content to obtain mortar with the desired flowability and stability characteristics. For a given aggregate content it is possible to achieve SCC mortar from paste mixtures with different rheological properties, although yield stress and plastic viscosity cannot be varied independently. For given mortar target properties ($D_{flow,mortar}$ and $T_{funnel,mortar}$) a trend line establishing the relationship between paste rheological parameters was computed.

- The link established between fresh properties of paste and SCC mortar allowed the definition of a self-compacting zone at paste level (SCZ). This SCZ can simplify the test protocol required to optimize a given SCC mixture, reducing the extent of laboratory work, testing time and materials used.

- Although the SCZ was defined for a specific set of materials, variations in material characteristics are expected to change the relative size of the SCZ.

Depending on the level of deviation, a limited number of mixtures can be prepared to adjust the final composition. The SCZ can also provide the basis for quality control and further behaviour assessment of new materials (addition, superplasticizer or viscosity agent).

- A link between durability properties of paste and SCC mortar was established using electrical resistivity numerical models of paste and mortar. For each Vs/Vm a good correlation between resistivity of paste and mortar was found, showing that aggregate increases mixture resistivity. Comparing experimental data with D-EMT formulation, it seems that the ITZ has little influence on the electrical resistivity of SCC mortar and the main effect of aggregate is blocking and redirecting conductive flow.

Chapter 5

Effective medium theories to assess aggregate influence on SCC resistivity and chloride diffusion

5.1. Synopsis

The possibility of predicting concrete properties from cement paste behaviour has great advantages, as it simplifies and makes easier the materials selection process and the performance-based design of concrete mixtures. In this work the ability of some of the effective medium theories to predict the influence of aggregate on the electrical resistivity and chloride ion diffusion properties of self-compacting concrete (SCC) is assessed. With this purpose an experimental programme was conducted, with self-compacting concrete and mortar mixes, designed based on four reference paste mixtures. Experimental results are compared with the values predicted by different models derived from the Differential Effective Medium Theory (D-EMT). A D-EMT formulation for insulating spherical inclusions and a D-EMT formulation for insulating ellipsoidal inclusions with an aligned orientation seems to predict fairly accurately the durability properties of self-compacting mortar and concrete, respectively. A good approximation has also been found with the predictions provided by the Hashin-Shtrikman lower bound.

5.2. Introduction

SCC, initially developed in Japan, corresponds to an advanced special concrete type as it leads to technological, economic and environmental benefits. In fresh state, SCC has the ability to fill the form and consolidate under its own weight with no compaction. Several different design methods found in the literature consider SCC as a suspension of aggregates in paste, separating optimization of the granular skeleton grading, paste volume and paste composition. In fact, paste plays a major role in concrete workability and therefore it is reasonable to expect that there is a direct relationship between paste and concrete flow behaviour (Hidalgo *et al.*, 2008). Therefore, to facilitate materials selection and mixture optimization protocols, efforts have been developed to correlate flow properties of SCC to those of mortar or paste (Okamura *et al.*, 2000; Saak *et al.*, 2001; Grünewald and Walraven, 2007; Erdem *et al.*, 2009; Nunes *et al.*, 2009b; Nunes *et al.*, 2011; Figueiras *et al.*, 2014). Besides controlling concrete workability, paste composition also has a large influence on early-age and long-term properties, including durability. If in fresh state, mortar requirements that lead to self-compacting concrete are fairly well defined, in hardened state, the link between paste/mortar and concrete durability properties is still at an early stage. The presence of aggregate in a cement paste matrix has two opposite effects on the transport properties: firstly, the dilution and tortuosity effects that reduce the permeability; secondly, the presence of a porous interfacial transition zone (ITZ) between paste and aggregate that facilitates the movement of ions and increases conductivity (Garboczi *et al.*, 2000; RILEM-Report 38, 2007). In order to establish this link it is necessary to know how to predict the influence of the aggregate (aggregate content and aggregate skeleton) in the mixture. With regard to the resistivity and diffusivity properties, one of the approaches that has begun to be used to establish this link between paste and concrete is through the effective medium theories (EMT) (Garboczi and Berryman, 2000). The work developed by Garboczi and Berryman (2000) included the application of Differential Effective Medium Theory (D-EMT) formulation with insulating spherical inclusions for normal vibrated concrete. Indeed, there are many different effective medium theories, each of them being more or less accurate in different conditions. Nevertheless, all theories assume that a material composed by a mixture of distinct homogeneous media can be regarded as an homogeneous one at a sufficiently large observation scale (Giordano, 2003b). The EMT, which is a semi-analytic method, has been applied in many different areas to

describe the physical properties of diphasic or multiphasic materials starting from the knowledge of the physical property of each phase composing the mixture, as well as of the structural properties of the mixture itself (percentage, shape and distribution of each phase). Ideally, the aim is to construct a theory that employs general microstructural information to make some accurate property predictions (Giordano, 2003b). EMTs are commonly used because of their relative simplicity compared to numerical computations, even though it is very important to establish the conditions of validity and the microstructures for which the theories yield accurate predictions (Giordano, 2003a).

The objective of this work is to conduct an exploratory analysis to assess the ability of some of the EMTs to predict the influence of the aggregate on the electrical resistivity and chloride ion diffusion properties of SCC. With this purpose, an experimental programme was conducted with self-compacting concrete and mortar mixes, designed based on four reference paste mixtures. Mortar and concrete mixtures, which included aggregate with different granular skeleton grading, aggregate with different shapes and different aggregate volume contents, were assessed for electrical resistivity and the apparent chloride diffusion coefficient, obtained in a non-steady-state migration test. Experimental results were compared with the values predicted by different models derived from the D-EMT, which seems to be the EMT that best fits the concrete problem. The assessed models include: the D-EMT formulation for not diluted suspension of insulating spherical inclusions; the D-EMT formulation for not diluted suspension of insulating ellipsoidal inclusions with an aligned orientation; and the D-EMT formulation for not diluted suspension of insulating ellipsoidal inclusions with a random orientation. Besides the models derived from D-EMT, experimental results were also compared to the bounds provided by Hashin and Shtrikman variational analysis (Hashin and Shtrikman, 1962).

5.3. Effective medium theories

Prediction for physical properties of heterogeneous media has been attracting the attention of many scientific areas leading to the development of a number of different EMTs. Contrary to other numerical approaches, such as the finite element method

(FEM), which are based on an approximate discretization of the study medium, in EMTs it is assumed that the effect of heterogeneities existing in the study medium can be captured by a basic morphological unit that constitutes a representative elementary volume (Coenza *et al.*, 2009). The direct consequence of this physical conceptualization is that EMTs do not explicitly account for the size of heterogeneities (inclusions) but rather for their shape (Coenza *et al.*, 2009). According to Hashin (Hashin, 1983) the properties of a composite material are determined by the internal phase geometry, i.e. the phase interface geometry and the physical properties of the phases, i.e. their constitutive relations. Figure 5.1, presents for the case of a geomaterial sample (unsaturated soil), the scheme of these two sets of theoretical formulations (numerical modelling and effective medium theory by the Maxwell-Garnett rule) for modelling the relationships between electromagnetic properties and hydrological variables.

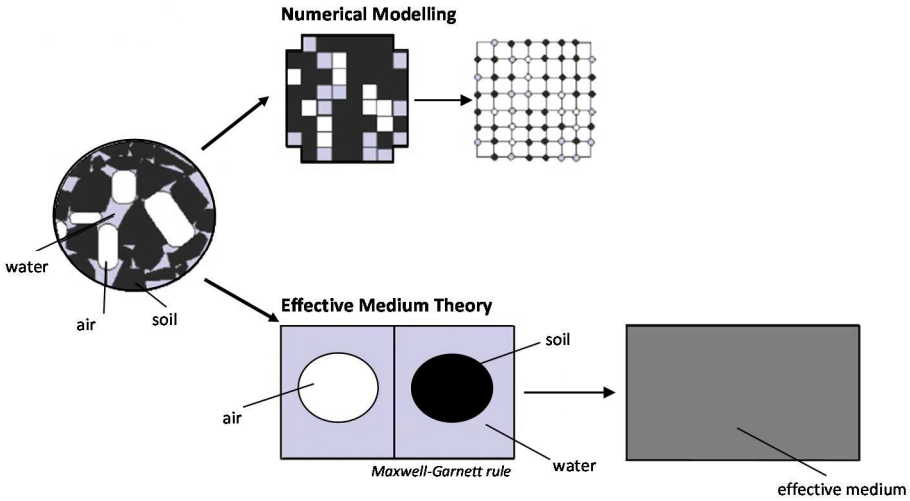

Figure 5.1 – Schematic representation of numerical modelling and effective medium theory formulations applied to a geomaterial (unsaturated soil) (adapted from (Coenza *et al.*, 2009)).

While the discussion presented in this section will be in the context of electrostatics, it should be realized that the problems of electrostatics, thermal conduction, electrical conduction, magnetostatics and diffusion are mathematically analogous (Hashin, 1983). The different EMTs mainly differ by the way they account for the effect of spatial distribution, orientation and shape of inclusions, and by the way interactions between heterogeneities are considered, which is not explicitly considered in the representative elementary volume. Two different effective medium theories are presented, the Effective Medium Approximation (EMA) and the Differential Effective Medium Theory (D-EMT). The first EMA developed was the Maxwell-Garnett model, which is

an extension of the Clausius-Mossotti relation that connects the macroscopic property of a material (e.g. effective dielectric constant ε_{ef} of inhomogeneous medium) with a microscopic property (e.g. the polarizability of a inclusion, particle) (Choy, 1999). The Maxwell-Garnett formulation is based on the assumption that the dielectric constant of N particles disperse in a host material (matrix) is equal to an equivalent volume having the effective dielectric constant ε_{ef} (see Figure 5.2). If the spherical particles and the external medium (matrix) have dielectric constants ε_p and ε_m, respectively, and considering φ_p the volumetric content of the particles, Maxwell-Garnett equation corresponds to expression (5.1), only valid for a strongly diluted suspension of spherical inclusions since the electromagnetic interactions between the heterogeneities are neglected.

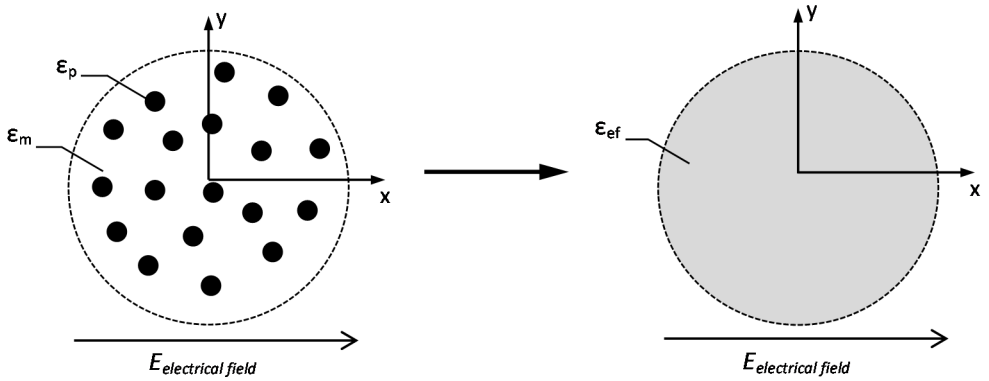

Figure 5.2 – Maxwell-Garnett equivalent principle (adapted from (Qin *et al.*, 2005)).

$$\frac{\varepsilon_{ef} - \varepsilon_m}{\varepsilon_{ef} + 2\varepsilon_m} = \varphi_p \frac{\varepsilon_p - \varepsilon_m}{\varepsilon_p + 2\varepsilon_m} \tag{5.1}$$

An alternative EMT is provided by the differential method, which derives from the mixture characterization approach used by Bruggeman, named the Differential Effective Medium Theory (D-EMT) approach or asymmetric Bruggeman formulation, also valid for less diluted suspensions (Giordano, 2003b). In the D-EMT procedure the initial low concentration is gradually increased by infinitesimal additions of the dispersed component. Given a known effective dielectric constant of the inhomogeneous material ε_{ef}, if a small additional volume of inclusions is embedded in the matrix, the change in the dielectric constant is approximately equal to that which would arise if an infinitesimal volume of inclusions were added to a uniform,

homogeneous matrix with dielectric constant ε_{ef} (Giordano, 2003b). Both theories, EMA and D-EMT, correspond to realizable microgeometries in which the composite is built up incrementally through a process of homogenization (Norris *et al.*, 1984). In contrast with EMA, in the microgeometry of D-EMT one phase acts as a backbone which always percolates (Norris *et al.*, 1984). For the case of a two-phase mixture of not diluted dispersion of spherical inclusions the D-EMT formulation leads to the formula presented in equation (5.2):

$$\frac{\varepsilon_{ef}-\varepsilon_p}{\varepsilon_m-\varepsilon_p}\left(\frac{\varepsilon_m}{\varepsilon_{ef}}\right)^{1/3}=1-\varphi_p \tag{5.2}$$

In the particular case of insulating spherical inclusions ($\varepsilon_p = 0$), equation (5.2) reduces to equation (5.3):

$$\varepsilon_{ef}=\varepsilon_m(1-\varphi_p)^{3/2} \tag{5.3}$$

The D-EMT approach has been extended for a two-phase mixture of aligned ellipsoidal inclusions and randomly oriented ellipsoids, prolate and oblate ellipsoids. Giordano (2003b) has presented in his work the explicit relationships, translated by equations (5.4) to (5.7). For a two-phase mixture of aligned ellipsoidal inclusions with the external surface of the mixture being an ellipsoid with the same shape of the inclusions (see Figure 5.3(a)):

$$\frac{\varepsilon_{ef,j}-\varepsilon_p}{\varepsilon_m-\varepsilon_p}\left(\frac{\varepsilon_m}{\varepsilon_{ef,j}}\right)^{\alpha^a_{f,j}}=1-\varphi_p \qquad (j=x,y,z) \tag{5.4}$$

where $\varepsilon_{ef,j}$ is the effective dielectric constant and $\alpha^a_{f,j}$ the depolarisation factor, along the x, y and z axes. The depolarization factor $\alpha^a_{f,j}$ for inclusions shaped as ellipsoids of revolution is computed as follows:

$$\alpha^a_{f,x}=\alpha^a_{f,y}=\begin{cases}\dfrac{e}{4p^3}\left[2ep+ln\left(\dfrac{e-p}{e+p}\right)\right] & if\ e>1\ (prolate\ ellipsoid)\\[2ex] \dfrac{e}{4q^3}\left[\pi-2eq-2arctg\left(\dfrac{e}{q}\right)\right] & if\ e<1\ (oblate\ ellipsoid)\end{cases} \tag{5.5}$$

$$\alpha_{f,z}^{a} = \begin{cases} \dfrac{1}{2p^3}\left[e\ ln\left(\dfrac{e+p}{e-p}\right) - 2p\right] & if\ e{>}1\ (prolate\ ellipsoid) \\ \dfrac{1}{2q^3}\left[2q - e\pi + 2e\ arctg\left(\dfrac{e}{q}\right)\right] & if\ e{<}1\ (oblate\ ellipsoid) \end{cases} \tag{5.6}$$

where $e = {a_z}/{a_x} = {a_z}/{a_y}$; $p = \sqrt{e^2 - 1}$ and $q = \sqrt{1 - e^2}$, being a_x, a_y and a_z the lengths of the ellipsoids semi-axes, with $a_x = a_y$. For the case of insulating ellipsoidal inclusions ($\varepsilon_p = 0$), equation (5.4) reduces to equation (5.7):

$$\varepsilon_{ef,j} = \varepsilon_m(1 - \varphi_p)^{1/(1-\alpha_{f,j}^{a})} \qquad (j = x, y, z) \tag{5.7}$$

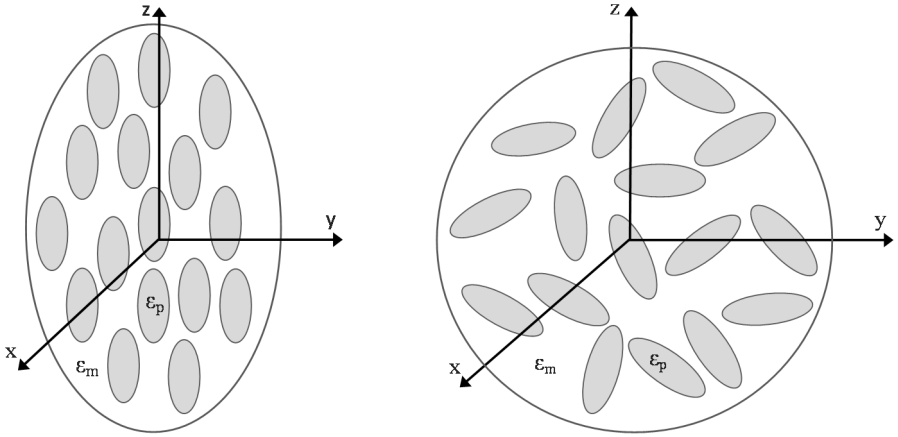

(a) (b)

Figure 5.3 – Structure of a dispersion of ellipsoids: (a) aligned ellipsoids; (b) randomly oriented ellipsoids (Giordano, 2003a).

For a two-phase mixture of randomly oriented ellipsoidal inclusions with the external surface of the mixture being spherical (see Figure 5.3(b)):

$$\frac{\varepsilon_{ef} - \varepsilon_p}{\varepsilon_m - \varepsilon_p}\left(\frac{\varepsilon_m}{\varepsilon_{ef}}\right)^{3\alpha_f^r(1-2\alpha_f^r)/(2-3\alpha_f^r)} \times \left[\frac{(1 + 3\alpha_f^r)\varepsilon_m + (2 - 3\alpha_f^r)\varepsilon_p}{(1 + 3\alpha_f^r)\varepsilon_{ef} + (2 - 3\alpha_f^r)\varepsilon_p}\right]^{2(3\alpha_f^r-1)^2/(2-3\alpha_f^r)(1+3\alpha_f^r)} = 1 - \varphi_p \tag{5.8}$$

For insulating ellipsoidal inclusions ($\varepsilon_p = 0$), equation (5.8) reduces to equation (5.9):

$$\varepsilon_{ef} = \varepsilon_m(1-\varphi_p)^{\Bigg/\left(1-\left(\frac{3\alpha_f^r\left(1-2\alpha_f^r\right)}{2-3\alpha_f^r}+\frac{2\left(3\alpha_f^r-1\right)^2}{(2-3\alpha_f^r)(1+3\alpha_f^r)}\right)\right)^1} \tag{5.9}$$

where α_f^r is the depolarisation factor along the x-axis or y-axis for randomly oriented ellipsoids of revolution, given by equation (5.5).

The Bruggeman formulation of ellipsoids mixtures has been used to characterize the dielectric response of water-saturated rocks with a good agreement with Archie´s law, an empirical expression that relates the electrical conductivity of a brine-saturated sedimentary rock to its porosity (Giordano, 2003b; Coenza *et al.*, 2009). In the concrete field, also Andrade and d'Andréa (2010) have been applying Archie´s law to estimate concrete electrical resistivity, based on the knowledge of the pore solution electrical resistivity, concrete porosity and a coefficient related to the connectivity and tortuosity of the porous network. The percolation theory has also been used to design numerical experiments and applied to transport processes in cement paste (Elsener *et al.*, 2005)

A fundamental result for effective properties of composite materials is given by the Hashin-Shtrikman variational analysis (Hashin and Shtrikman, 1962), which provides an upper and lower bound, irrespective of the microstructure (Giordano, 2003a). The Hashin-Shtrikman variational approach is an alternative representation of the effective energy of the heterogeneous medium in terms of suitably chosen polarization fields regarding a homogeneous comparison material (Duan *et al.*, 2006). The multiphase material is replaced by a homogeneous and isotropic material, without changing the surface potential (the stored energy is equal). The permeability (or dielectric constant, conductivity, resistivity, etc.) of the homogeneous comparison material is defined as the effective permeability of the multiphase material (Hashin and Shtrikman, 1962). The Hashin-Shtrikman bounds were derived for a macroscopically homogeneous and isotropic multiphase material, in terms of volume fraction and permeability of the constituting phases (Hashin and Shtrikman, 1962). In particular, for a two-phase material the upper and lower dielectric constant bounds (ε_{ef}^h and ε_{ef}^l) are given by two expressions of Maxwell type (equation (5.10). According to Hashin (1983) the variational approach is in a certain sense more powerful than the direct approach (exact calculation of effective properties) since it leads to bounds on effective properties when exact calculation is not possible.

$$\begin{cases} \varepsilon_{ef}^{l} = \varepsilon_m + \dfrac{\varphi_p}{\dfrac{1}{\varepsilon_p - \varepsilon_m} + \dfrac{1-\varphi_p}{3\varepsilon_m}} \\ \varepsilon_{ef}^{h} = \varepsilon_p + \dfrac{(1-\varphi_p)}{\dfrac{1}{\varepsilon_m - \varepsilon_p} + \dfrac{\varphi_p}{3\varepsilon_p}} \end{cases} \quad (5.10)$$

5.4. Experimental programme

5.4.1. Materials characterization

The paste, mortar and concrete mixes investigated in this study were prepared with white cement (CEM II/A-L 52.5N according to EN 197-1 (IPQ, 2012)) and two mineral additions, metakaolin and limestone filler, with a specific gravity of 3.04, 2.21 and 2.68, respectively. The mean size of the cement, metakaolin and limestone filler particles was 11.03 μm, 7.12 μm and 6.53 μm, respectively. A polycarboxylate type high range water reducing admixture was used having a specific gravity of 1.07 and 26.5% of solid content.

The present work was developed within a study devoted for designing SCC compositions with defined requirements (fresh and hardened concrete properties) (Figueiras *et al.*, 2013a). In order to simplify SCC design, the study was developed in two phases, first at mortar level and then at concrete level. At mortar level standard sand was employed, conforming to EN 196-1 (IPQ, 2006). Standard sand is a siliceous round natural sand (0.08-2 mm) with a specific gravity of 2.63 and an absorption value of 0.30%. Crushed calcareous aggregate, a siliceous natural fine sand (sand 1) with a fineness modulus of 2.01 and natural coarse sand (sand 2) with a fineness modulus of 3.94 were used in concrete mixes. The specific gravity of the coarse aggregate, sand 1 and sand 2 were 2.68, 2.59 and 2.66, and the absorption values were 0.60%, 0.80% and 0.20%, respectively, according to EN 1097-6 (IPQ, 2003a). Bulk density of compacted coarse aggregate was 1.54. Figure 5.4 shows the particle size distribution curves, in terms of accumulated volume, of standard sand, sand 1, sand 2 and coarse aggregate.

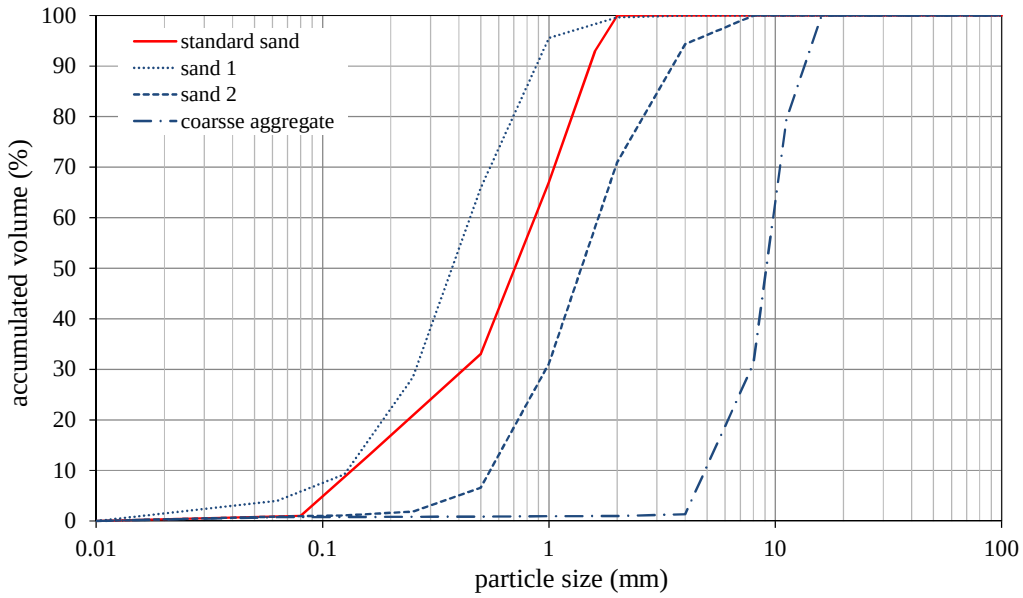

Figure 5.4 – Aggregate particle size distribution curves in terms of accumulated volume.

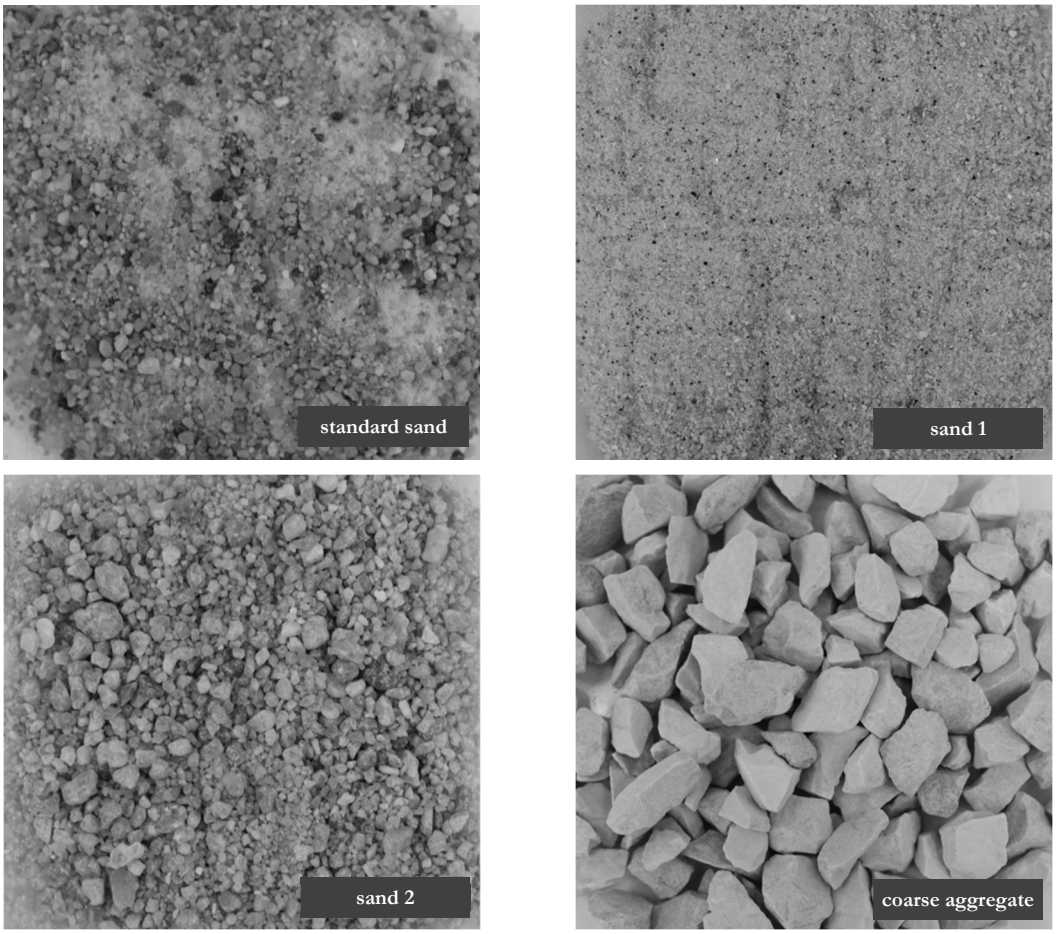

Figure 5.5 – Aggregates used in this study: standard sand; fine sand (sand 1); coarse sand (sand 2); and coarse aggregate.

With regard to the aggregate shape, it was considered that standard sand, fine sand (sand 1) and coarse sand (sand 2) are predominantly constituted by spherical particles, while coarse aggregate shape is closer to a prolate ellipsoid of revolution. The main differences in particle shape of aggregate used in this study can be observed in Figure 5.5. The particles shape of the coarse aggregate, in particular the ratio of ellipsoids semi-axes lengths which will be used in the application of effective medium theories, was determined using a random sampling of 100 particles (see Figure 5.6). This sampling resulted in an average value for a_z/a_x, considering $a_z > a_x$ and $a_x = a_y$, of 2.319 with a standard deviation of 0.865.

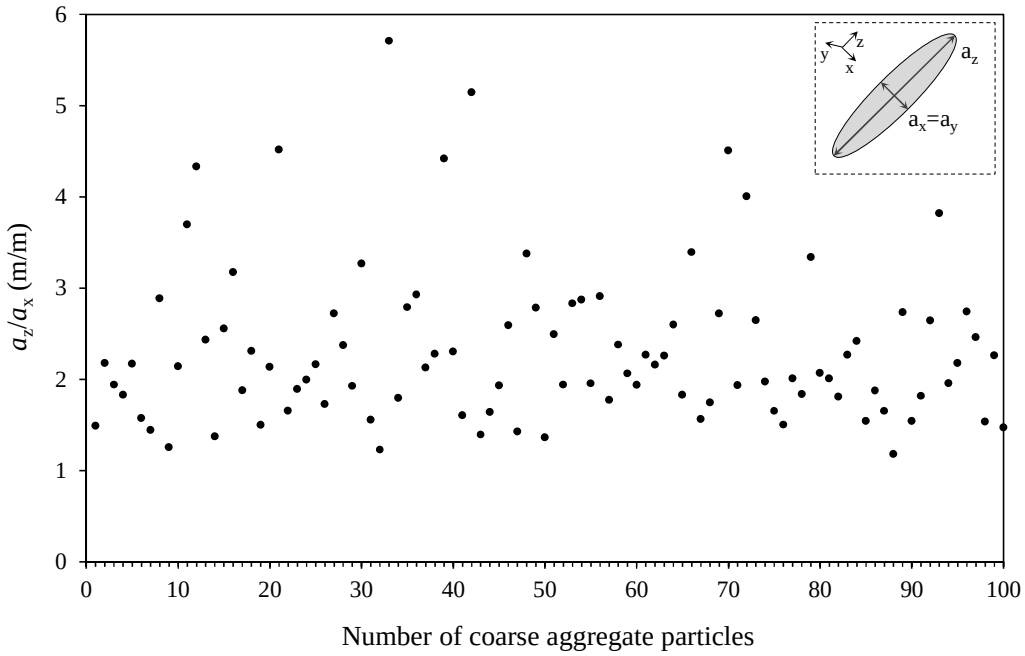

Figure 5.6 – Ratio of semi-axes lengths of coarse aggregate particles.

5.4.2. Mixture proportions

The testing programme included 27 concrete, mortar and paste mixes. Self-compacting concrete and mortar mixes were designed based on four reference paste mixtures (A-P1, B-P1, C-P1 and D-P1). Sand volume content (Vs), coarse aggregate volume content (Vg) and total aggregate volume content ($Vaggr_{total}$) used in the mixtures prepared under this study are presented in Table 5.1. At concrete level the ratio between both sands was kept constant, with s1/s been equal to 0.400. The experimental programme also included a few mixture replications in order to evaluate

the experimental error associated to variability of conditions and test procedures, A-M1 to A-M4 at mortar level and B-C1 to B-C3 at concrete level.

Table 5.1 – Aggregate volume content of mortar and concrete mixtures.

Paste	Mortar		Concrete			
Mix reference	Mix reference	Vs (m^3/m^3)	Mix reference	Vs (m^3/m^3)	Vg (m^3/m^3)	$Vaggr_{total}$ (m^3/m^3)
A-P1	A-M1	0.450	-	-	-	-
	A-M2	0.450				
	A-M3	0.450				
	A-M4	0.450				
	A-M5	0.400				
	A-M6	0.500				
B-P1	B-M1	0.500	B-C1	0.300	0.298	0.598
			B-C2	0.300	0.298	0.598
			B-C3	0.300	0.298	0.598
			B-C4	0.289	0.279	0.567
			B-C5	0.328	0.279	0.607
			B-C6	0.272	0.318	0.591
			B-C7	0.310	0.318	0.628
			B-C8	0.273	0.318	0.571
			B-C9	0.327	0.298	0.626
			B-C10	0.312	0.270	0.583
			B-C11	0.287	0.327	0.614
			B-C12	0.303	0.302	0.605
C-P1	C-M1	0.500	C-C1	0.309	0.278	0.587
D-P1	D-M1	0.450	D-C1	0.259	0.298	0.557

In the present study, the parameters used to design paste, mortar and self-compacting concrete mixtures, were based on the Japanese SCC-designing method (Okamura *et al.*, 2000). Paste mix-proportions were established based on the following four variables: water to powder volume ratio (Vw/Vp); water to cement weight ratio (w/c), superplasticizer to powder weight ratio (Sp/p) and metakaolin to cement weight ratio (mtk/c). Paste mix-proportions were maintained at mortar and concrete levels and only the parameters related to the aggregate content and aggregate skeleton were modified, namely, sand to mortar volume ratio (Vs/Vm) and coarse aggregate to dry rodded coarse aggregate volume ratio (Vg/Vg,lim). The mix-proportions of paste, mortar and concrete were established based on the mixture parameters values presented in Table 5.2 and according to the formulation presented in the Appendix.

Table 5.2 – Paste, mortar and concrete mixture parameters and mix-proportions.

Mix reference	Vw/Vp	w/c	Sp/p (%)	mtk/c (%)	Vs/Vm	Vg/Vg,lim	Wc (kg/m³)	Wf (kg/m³)	Wmtk (kg/m³)	Ww (kg/m³)	Wsp (kg/m³)	Wsd,stan (kg/m³)	Wsd1 (kg/m³)	Wsd2 (kg/m³)	Wgd (kg/m³)
A-P1	0.900	0.410	0.70	9.00	-	-	1155	265	104	466	10.67	-	-	-	-
A-M1	0.900	0.410	0.70	9.00	0.450	-	635	146	57	260	5.87	1184	-	-	-
A-M2	0.900	0.410	0.70	9.00	0.450	-	635	146	57	260	5.87	1184	-	-	-
A-M3	0.900	0.410	0.70	9.00	0.450	-	635	146	57	260	5.87	1184	-	-	-
A-M4	0.900	0.410	0.70	9.00	0.450	-	635	146	57	260	5.87	1184	-	-	-
A-M5	0.900	0.410	0.70	9.00	0.400	-	693	159	62	283	6.40	1052	-	-	-
A-M6	0.900	0.410	0.70	9.00	0.500	-	578	133	52	237	5.34	1315	-	-	-
B-P1	0.851	0.435	0.70	10.40	-	-	1057	382	110	452	10.84	-	-	-	-
B-M1	0.851	0.435	0.70	10.40	0.500	-	528	191	55	230	5.42	1315	-	-	-
B-C1	0.851	0.435	1.00	10.40	0.440	0.530	403	146	42	179	5.91	-	316	473	800
B-C2	0.851	0.435	1.00	10.40	0.440	0.530	403	146	42	179	5.91	-	316	473	800
B-C3	0.851	0.435	1.00	10.40	0.440	0.530	403	146	42	179	5.91	-	316	473	800
B-C4	0.851	0.435	1.00	10.40	0.412	0.495	436	158	45	193	6.39	-	304	456	747
B-C5	0.851	0.435	1.00	10.40	0.468	0.495	394	143	41	176	5.78	-	345	518	747
B-C6	0.851	0.435	1.00	10.40	0.412	0.565	411	149	43	183	6.03	-	287	431	853
B-C7	0.851	0.435	1.00	10.40	0.468	0.565	372	135	39	167	5.45	-	326	489	853
B-C8	0.851	0.435	1.00	10.40	0.400	0.530	432	156	45	191	6.33	-	287	430	800
B-C9	0.851	0.435	1.00	10.40	0.480	0.530	375	135	39	167	5.49	-	344	517	800
B-C10	0.851	0.435	1.00	10.40	0.440	0.480	420	152	44	186	6.16	-	329	493	724
B-C11	0.851	0.435	1.00	10.40	0.440	0.580	387	140	40	173	5.67	-	303	454	875
B-C12	0.851	0.435	1.00	10.40	0.439	0.493	416	151	44	185	6.10	-	325	487	744
C-P1	0.890	0.389	0.71	7.02	-	-	1212	246	85	463	10.94	-	-	-	-
C-M1	0.890	0.389	0.71	7.02	0.500	-	606	123	43	235	5.47	1315	-	-	-
C-C1	0.890	0.389	1.00	7.02	0.439	0.493	478	97	34	189	6.08	-	325	487	744
D-P1	0.863	0.398	0.72	9.84	-	-	1164	273	115	455	11.17	-	-	-	-
D-M1	0.863	0.398	0.72	9.84	0.450	-	640	150	63	254	6.14	1184	-	-	-
D-C1	0.863	0.398	0.90	9.84	0.380	0.530	492	115	48	199	5.90	-	273	409	800

5.4.3. Testing methods

5.4.3.1. Electrical resistivity

Electrical resistivity is an intrinsic property of the material that is related to the ability of cement paste to carry electric charge and it depends mainly on the hydration process (nature and topography of the pore structure), changes in the pore solution composition and moisture and temperature conditions. Electrical resistivity was assessed by the two electrodes technique, using stainless steel meshes embedded on opposite faces of a specimen to work as electrodes (see Figure 5.7). Applying Ohm's Law, as shown in equation (5.11), the relationship between the applied electrical voltage and the measured current intensity, gives the electrical resistance of the material. The resistivity is obtained by applying to the electrical resistance a geometric factor, which depends on the dimensions of the specimen and the electrodes used.

$$R = \frac{V}{I} = \rho \cdot \left(\frac{L}{A}\right) \Rightarrow \rho = \frac{V.A}{L.I} \tag{5.11}$$

where R is the electrical resistance (Ω); I, current (Amp.); V, voltage (Volts); ρ, electrical resistivity (Ω·m); L, length between electrodes (m); and A (m^2) the cross-section area of the test specimen through which current passes. This equation is valid for a constant cross-section of the specimen along its length and for electrodes with the same cross-section as the test specimen.

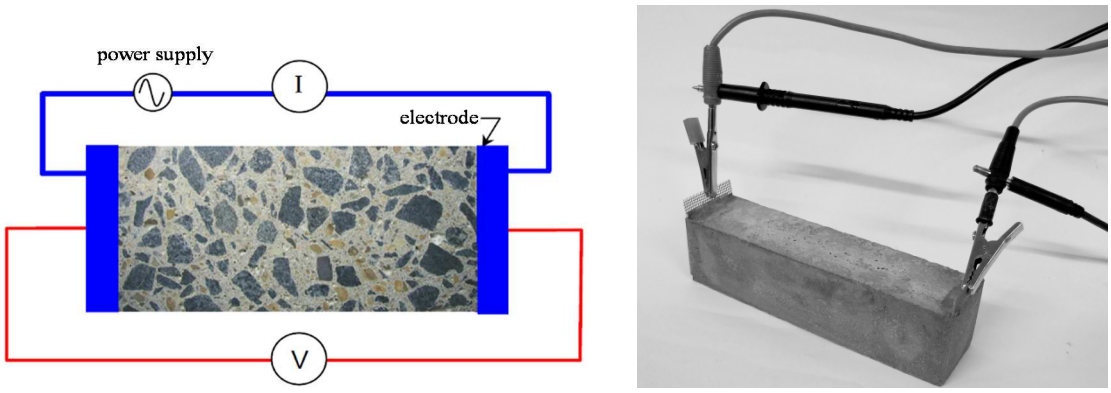

Figure 5.7 – Electrical resistivity test: schematic representation of the measuring set-up (left); mortar specimen during the test (right).

Paste electrical resistivity was assessed on cubic specimens with 40×40×40 mm^3, mortar resistivity was assessed on prismatic specimens with 40×40×160 mm^3 and concrete resistivity was assessed on cubic specimens with 150×150×150 mm^3, 3 specimens per mixture. Specimens were demoulded one day after casting and kept under water in a chamber with controlled environmental conditions (T=20ºC) until testing (28 days). Since all specimens were at the same moisture (saturated) and temperature conditions, resistivity can be used to compare the pore structure of various paste specimens, and therefore constitute a measure of the amount and interconnectivity of the cementitious matrix pores.

5.4.3.2. Chloride ion penetration

Resistance to chloride ion penetration was carried out using a non-steady migration test, CTH Rapid Method (Chalmers University of Technology, Sweden) described in NT BUILD 492 (NORDTEST, 1999) and adopted in Portugal through a LNEC specification, E 463 (LNEC, 2004). The CTH Rapid Method is based on a theoretical relationship between diffusion and migration, which enables the calculation of the chloride diffusion coefficient from an accelerated test. It is based on measuring the depth of colour change of a silver nitrate solution sprayed on specimens previously submitted to a migration test (disc specimens were submitted to an electric current during a certain time) and application of the following equations:

$$\mathrm{Dcl_{ns}} = \frac{RT}{zFE} \cdot \frac{x_d - \alpha\sqrt{x_d}}{t} \tag{5.12}$$

where,

$$E = \frac{U - 2}{L} \tag{5.13}$$

$$\alpha = 2\sqrt{\frac{RT}{zFE}} \cdot erf^{-1}\left(1 - \frac{2C_d}{C_0}\right) \tag{5.14}$$

where $\mathrm{Dcl_{ns}}$ is the apparent chloride diffusion coefficient obtained in a non-steady-state migration test (m^2/s); R is the gas constant (R=8.314 J/(mol.K)); T is the average value

of the initial and final temperatures in the anolyte solution (K); L is the thickness of the specimen (m); z is the absolute value of valence ion, for chloride (z=1); F is the Faraday constant (F=9.648×10^4 J/(V.mol)), U is the absolute value of the applied voltage (V); x_d is the average depth of chloride penetration measured by using a colorimetric method (m); t is the test duration (s); C_d is the concentration of free chloride at which the colour changes when using the colorimetric method to measure the chloride penetration depth (C_d≈0.07 N); and C_0 is the concentration of free chloride in the catholyte solution (C_0≈2 N). Mortar and concrete chloride diffusion coefficient was assessed on cylinders specimens with ϕ=100 mm and h=50 mm (3 specimens per mixture). Specimens were demoulded one day after casting and kept under water in a chamber with controlled environmental conditions (T=20ºC) until testing (28 days).

5.4.4. Mixing procedure

Paste mixes were prepared in 0.31 l batches using a vertical paddle mixer, according to the following procedure: (i) powder materials were mixed with mixing water for 120 s at 750 rpm; (ii) superplasticizer was added and mixed during 120 s at 750 rpm; (iii) mixer was stopped for 60 s; and (iv) mixing was resumed for 120 s at 2000 rpm.

Mortar mixes were prepared in 2.42 l batches and mixed in a two-speed mixer complying to EN 196-1 (IPQ, 2006). The mixing sequence was as follows: (i) sand and powder materials were mixed with 0.80 of the mixing water during 60 s; (ii) mixer was stopped to scrape material adhering to the mixing bowl and mixed for another 60 s; (iii) the rest of the water was added with the superplasticizer and mixed for 60 s; (iv) mixer was stopped again to scrape material adhering to the bowl and mixed for 60 s; (v) mixer was then stopped for 5 min; and (vi) mortar was mixed during a further 90 s. The mixer was always set at low speed except in the last 90 s of the mixing sequence where it was set at high speed (as defined in (IPQ, 2006)).

Concrete mixes were prepared in the laboratory in batches with total volume of 33 l using an open pan mixer with vertical axis. The mixing sequence was as follows: (i) both sands and coarse aggregate were mixed with 0.15 of the mixing water during 2.5 min; (ii) mixing was stopped for 2.5 min for aggregate absorption; (iii) powder materials were added followed by the rest of the water with the superplasticizer;

(iv) mixing was resumed for more 5 min; (v) mixer was stopped for 1 min to clean the mixer paddles; and (vi) concrete was mixed for a further 3 min.

5.4.5. Experimental results

Experimental results of electrical resistivity and apparent chloride diffusion coefficient for the mixes prepared under the experimental programme are summarized in Table 5.3. An overall statistical analysis of the results for the mixtures replication is presented in Table 5.4, including minimum and maximum values, mean value, standard deviation and coefficient of variation.

Table 5.3 – Paste, mortar and concrete test results: electrical resistivity (ρ) and apparent chloride diffusion coefficient (Dcl_{ns}).

Paste			Mortar			Concrete		
Mix reference	$\rho_{exp,p}$ (m.Ω)	$Dcl_{ns,p}$ (x10^{-12} m^2/s)	Mix reference	$\rho_{exp,m}$ (m.Ω)	$Dcl_{ns,m}$ (x10^{-12} m^2/s)	Mix reference	$\rho_{exp,c}$ (m.Ω)	$Dcl_{ns,c}$ (x10^{-12} m^2/s)
A-P1	70.2	-	A-M1	168.5	3.08	-	-	-
			A-M2	167.2	-			
			A-M3	165.5	3.18			
			A-M4	171.3	3.10			
			A-M5	158.3	3.15			
			A-M6	181.7	3.34			
B-P1	73.1	-	B-M1	206.3	3.12	B-C1	244.9	3.58
						B-C2	246.1	3.53
						B-C3	243.9	3.56
						B-C4	212.7	3.54
						B-C5	231.0	3.63
						B-C6	227.5	3.69
						B-C7	257.0	3.50
						B-C8	235.7	3.34
						B-C9	267.3	3.37
						B-C10	214.6	3.47
						B-C11	250.0	3.59
						B-C12	223.6	3.54
C-P1	53.0	-	C-M1	139.2	-	C-C1	148.9	-
D-P1	88.9	-	D-M1	205.9	-	D-C1	232.0	-

Table 5.4 – Statistics of the results for the mixture replication.

	Minimum	Maximum	Mean	Stand. deviation	Coeff. of variation
Mortar Mixtures (A-M1 to A-M4)					
$\rho_{exp,m}$ (Ω.m)	165.5	171.3	168.1	2.5	1.5%
$Dcl_{ns,m}$ ($\times 10^{-12}$ m²/s)	3.08	3.18	3.12	0.05	1.7%
Concrete Mixtures (B-C1 to B-C3)					
$\rho_{exp,c}$ (Ω.m)	243.9	246.1	245.0	1.1	0.5%
$Dcl_{ns,c}$ ($\times 10^{-12}$ m²/s)	3.53	3.58	3.56	0.02	0.7%

As stated before, mixture replication can be used to evaluate the experimental error associated to the variability of conditions and test procedures, and the coefficient of variation, as a measure of the relative dispersion of data, can be used to make comparisons of repeatability and reproducibility of the tests. Coefficients of variation of both test results are relatively low, with the concrete test results exhibiting lower values.

5.5. Appraisal of effective medium theories

On a macro scale, concrete can be assumed as a composite material with at least three phases: cement paste matrix, aggregate grains of various sizes and a thin shell of altered matrix material surrounding each aggregate (ITZ) (Garboczi and Berryman, 2000). The ITZ is characterized, generally, by a higher concentration of calcium hydroxide and an increased porosity relative to the matrix paste (Garboczi *et al.*, 2000), which facilitates the movement of ions and consequently increases conductivity. The volume and properties of the ITZ are influenced by the w/c ratio, addition of pozzolanic or inert fine particles, aggregate volume fraction and the stability of the fresh mix. In the presence of low water/cement ratios or fine mineral additions, like in SCC, some studies appear to indicate that the porosity and width of the ITZ is significantly smaller than in vibrated concrete (RILEM-Report 38, 2007). Furthermore, the ITZ formed around the aggregate increases locally the w/c ratio, but this is usually accompanied by a decrease of w/c ratio in the bulk matrix, and therefore by a decrease in the conductivity because of the lower porosity (Garboczi *et al.*, 2000; RILEM-Report 38, 2007). However, as the proportion of larger size aggregate increases in the mix, the local porosity at the ITZ increases and the overall durability decreases (Basheer *et al.*,

2005). The volume of coarse aggregate used in SCC usually ranges between 30 to 34 % of the concrete volume. This is significantly less than typical values of 40 to 45 % for normal workability concrete (RILEM-Report 38, 2007). For these reasons it is expected that in the present study the ITZ has minor influence on mortar/concrete resistivity and diffusivity, and therefore the ITZ will be considered as part of the cement paste matrix, with the same properties.

In the case of normal vibrated concrete, the application of EMTs can become a much more complicated problem, due to the greater influence that the ITZ may have on the final properties. In this case the ITZ may have to be considered as a third phase of the composite material, with the additional disadvantage of having a gradient of properties extending out its width (Garboczi and Berryman, 2000). Furthermore it should be taken into account that the ITZ regions could themselves percolate (Garboczi and Berryman, 2000).

In the present study the aggregate particles will be treated as insulating elements, with high resistivity and low diffusivity. In fact, although the aggregate is a conductive element, the high conductivity of cement paste allows to consider it as an insulating phase. The same simplification could be performed for the diffusivity since the diffusivity of cement paste is much higher than aggregate diffusivity. Mortar/concrete will be assumed as a composite material with two distinct phases, a cement paste matrix phase in which insulating aggregate particles of various sizes and shapes are embedded. Moreover, mortar/concrete can be regarded as a composite material consisting of discrete aggregate particles dispersed in a continuous cement matrix, i.e. inclusions are always discontinuities embedded in a continuous matrix (Garboczi and Berryman, 2000). Therefore, to predict aggregate influence on mortar/concrete properties the D-EMT seems to be the EMT that best fits the concrete problem, once this formulation is used for materials in which one phase always percolates (Norris *et al.*, 1984) and it is also valid for less diluted suspensions (Giordano, 2003b). Besides the models derived from D-EMT, experimental results were also compared with the predictions provided by the Hashin-Shtrikman bounds. Thus, experimental results (electrical resistivity and apparent chloride diffusion coefficient) of mixtures prepared under the experimental programme were compared with the values predicted by the following models:

i. Model 1 – D-EMT formulation for not diluted suspension of insulating spherical inclusions, equation (5.3), considering spherical particles of sand and coarse aggregate;

ii. Model 2 – D-EMT formulation for not diluted suspension of insulating ellipsoidal inclusions with an aligned orientation and electrical field aligned with x-axis or y-axis, equation (5.5) and equation (5.7), considering spherical particles of sand and ellipsoidal particles of coarse aggregate. The depolarization factor was determined from a weighted average taking into account the shape and volume of the inclusion phases;

iii. Model 3 – D-EMT formulation for not diluted suspension of insulating ellipsoidal inclusions with an aligned orientation and electrical field aligned with z-axis, equation (5.6) and equation (5.7), considering spherical particles of sand and ellipsoidal particles of coarse aggregate. The depolarization factor was determined from a weighted average taking into account the shape and volume of the inclusion phases;

iv. Model 4 – D-EMT formulation for not diluted suspension of insulating ellipsoidal inclusions with a random orientation, equation (5.5) and equation (5.9), considering spherical particles of sand and ellipsoidal particles of coarse aggregate. The depolarization factor was determined from a weighted average taking into account the shape and volume of the inclusion phases;

v. Model 5a – Lower bound of the Hashin-Shtrikman variational analysis for insulating inclusions, equation (5.10);

vi. Model 5b – Upper bound of the Hashin-Shtrikman variational analysis for insulating inclusions, equation (5.10).

Mortar properties were compared with the values given by the D-EMT formulation for not diluted suspension of insulating spherical inclusions (equation (5.3)), which corresponds to Model 1.

5.5.1. Effective medium theories to assess electrical resistivity

The electrical resistivity of mortar mixtures was determined from the electrical resistivity of the corresponding reference cement paste matrix (denoted as $\rho_{exp,p}$), using the D-EMT formulation for not diluted suspension of insulating spherical inclusions (Model 1). Experimental results of mortar electrical resistivity tests ($\rho_{exp,m}$), as well as, the corresponding values obtained by means of Model 1 ($\rho_{ef,m}$) are presented in Table 5.5. The prediction error ($\Delta\varepsilon$) is calculated according to equation (5.15) and is also presented in Table 5.5.

Table 5.5 – Experimental results $\rho_{exp,m}$, predicted values $\rho_{ef,m}$ and prediction error $\Delta\varepsilon$.

Paste		Mortar			
Mix reference	$\rho_{exp,p}$ (m.Ω)	Mix reference	$\rho_{exp,m}$ (m.Ω)	$\rho_{ef,m}$ (m.Ω)	$\Delta\varepsilon$ (%)
A-P1	70.2	A-M1	168.5	172.1	2.1
		A-M2	167.2	172.1	2.9
		A-M3	165.5	172.1	4.0
		A-M4	171.3	172.1	0.5
		A-M5	158.3	151.1	-4.6
		A-M6	181.7	198.6	9.3
B-P1	73.1	B-M1	206.3	206.8	0.2
C-P1	53.0	C-M1	139.2	149.9	7.7
D-P1	88.9	D-M1	205.9	218.0	5.8

$$\Delta\varepsilon = \frac{\rho_{ef,m} - \rho_{exp,m}}{\rho_{exp,m}} \tag{5.15}$$

The average of the prediction error ($|\Delta\varepsilon|_{average}$) is 4.1%, which seems to indicate that the D-EMT formulation for not diluted suspension of insulating spherical inclusions (Model 1) predicts fairly accurately the electrical resistivity of mortars based on the knowledge of $\rho_{exp,p}$ and aggregate volume content (φ_p). It is worth emphasising that the experimental error associated to variability of conditions and test procedures is also included in the prediction error. According to Table 5.4, the coefficient of variation obtained for mortar mixtures replication was 1.5%, which already accounts for a significant share of the error.

For the prediction of concrete electrical resistivity through the different effective medium theories, Model 1 to Model 5b, paste experimental results ($\rho_{exp,p}$) were used as

the electrical resistivity of the cement paste matrix. Experimental results of concrete electrical resistivity tests conducted under the experimental plan ($\rho_{exp,c}$), as well as the corresponding values obtained by each model ($\rho_{ef,c}$) are presented in Figure 5.8. The prediction error ($\Delta\varepsilon$) of each model is presented in Table 5.6, as well as the corresponding average ($|\Delta\varepsilon|_{average}$). According to Table 5.4, the coefficient of variation obtained for concrete mixtures replication was 0.5%, which means that the experimental error does not represent a significant share of the error.

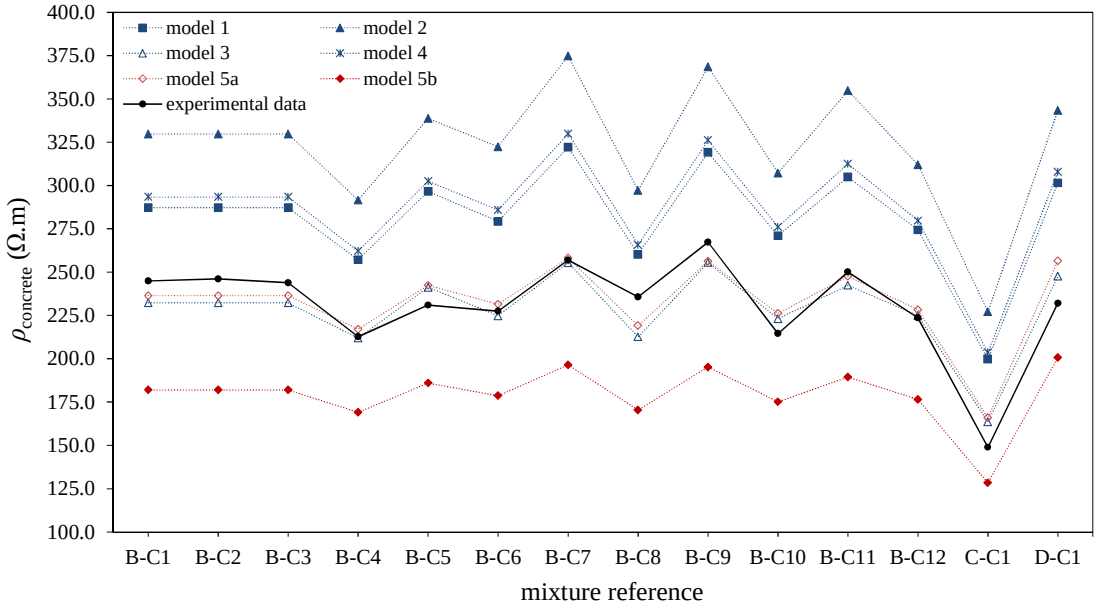

Figure 5.8 – Experimental data $\rho_{exp,c}$ and predicted values obtained by the models $\rho_{ef,c}$.

Table 5.6 – Models prediction error $\Delta\varepsilon$ for concrete electrical resistivity.

Mix reference	$\Delta\varepsilon_{model\ 1}$ (%)	$\Delta\varepsilon_{model\ 2}$ (%)	$\Delta\varepsilon_{model\ 3}$ (%)	$\Delta\varepsilon_{model\ 4}$ (%)	$\Delta\varepsilon_{model\ 5a}$ (%)	$\Delta\varepsilon_{model\ 5b}$ (%)
B-C1	17.3	34.6	-5.2	19.8	-3.5	-25.7
B-C2	16.7	34.0	-5.6	19.2	-3.9	-26.0
B-C3	17.7	35.2	-4.8	20.3	-3.1	-25.4
B-C4	20.9	37.1	-0.3	23.3	2.1	-20.5
B-C5	28.4	46.6	4.4	31.0	4.9	-19.5
B-C6	22.8	41.7	-1.2	25.7	1.7	-21.5
B-C7	25.3	45.8	-0.6	28.3	0.4	-23.6
B-C8	10.4	26.1	-9.8	12.8	-7.0	-27.7
B-C9	19.4	37.8	-4.4	22.0	-4.1	-27.0
B-C10	26.3	43.1	4.0	28.7	5.4	-18.4
B-C11	21.9	41.9	-3.1	24.9	-1.0	-24.3
B-C12	22.7	39.5	0.6	25.1	2.1	-21.0
C-C1	34.1	52.5	9.9	36.7	11.5	13.8
D-C1	29.9	48.0	6.7	32.7	10.6	13.5
$\|\Delta\varepsilon\|_{average}$	22.4%	40.0%	4.3%	25.0%	4.4%	22.0%

The model derived from D-EMT with the lowest prediction error was Model 3 ($|\Delta\varepsilon|_{average}$=4.3%), a D-EMT formulation for ellipsoidal inclusions with an aligned orientation and electrical field aligned with z-axis (aligned according to the semi-major axis of the ellipsoids). On the contrary, Model 2, a D-EMT formulation for orientated ellipsoidal inclusions but with the electrical field aligned with a semi-minor axis of the ellipsoid (aligned according to x-axis or y-axis) exhibited the highest prediction error. Against to what might be expected, Model 3 correlates better with experimental data than the D-EMT formulation for ellipsoidal inclusions with a random orientation (Model 4). One possible explanation for the best fit presented by Model 3 could be closely linked to the way the specimens were cast, usually preformed from the faces, where the stainless steel meshes were positioned, towards the center of the specimen. Furthermore, the application of these models requires the knowledge/determination of paste electrical resistivity, which has an associated error with influence in the final error of each model. As expected, Model 1 does not predict, in an appropriate manner, the influence of aggregate volume and aggregate skeleton on resistivity ($|\Delta\varepsilon|_{average}$ =22.4%), which could be associated to the fact that the model only assumes spherical inclusions. The lower and upper bounds established by the Hashin-Shtrikman variational analysis (Model 5a and Model 5b) cover a substantially wide range of resistivity values, nevertheless, experimental data are very close to the lower bound ($|\Delta\varepsilon|_{average}$ =4.4%). In fact, according to Hashin (1983), if a random two-phase composite contains a small amount of highly conducting inclusions, the effective conductivity will be governed by the poorly conducting matrix and will be close to the lower bound. If the relative volume of conducting inclusions is increased it could start to form a continuous skeleton and thus the effective conductivity would increase dramatically and become close to the upper bound. In the case of the present study, if the relative volume of the highly resistive inclusions is small, the effective resistivity (inverse of conductivity) will be governed by the poorly resistive matrix and will be close to the lower bound (Model 5a). According to Torquato and Rubinstein (1991) the Hashin-Shtrikman variational analysis derived rigorous upper and lower bounds of the effective conductivity. However special care has to be taken on the limits of infinite contrast between the conductivity of the two phases (matrix and inclusions) for microgeometries in which one of the phases is not continuously connected (Torquato and Rubinstein, 1991).

5.5.2. Effective medium theories applied to chloride diffusion coefficient

The output of CTH test is a chloride diffusion coefficient calculated based on the chloride penetration depth of a specimen subjected to an ionic migration induced by an external electrical voltage. This chloride diffusion coefficient depends on the diffusivity of chloride ions in liquid-saturated concrete, as well as on the chloride binding capacity of the cement matrix, which can take place by chemical reaction with the hydration products of cement (such as C_3A or C_4AF) or physical adsorption (on the surface of CSH gel). Thus, the effective medium theories cannot be directly applied to predict the apparent or non-steady-state chloride diffusion coefficient obtained through the CTH test (Dcl_{ns}). Only the diffusivity, also called effective or steady-state chloride diffusion coefficient (Dcl_s) can be predicted. The relation between Dcl_{ns} and Dcl_s can be established through the reaction or binding factor r_{cl}, according to equation (5.16). The r_{cl} represents the number of times the Dcl_s is apparently decreased due to the chloride binding effect. When establishing the relationship between Dcl_s and Dcl_{ns} it has to be considered that Dcl_s is referred to the concentration in the pore solution and Dcl_{ns} is referred to the aggressive ion concentration in the mass of concrete (Andrade *et al.*, 2013).

$$Dcl_{ns} = \frac{Dcl_s}{r_{cl}} \tag{5.16}$$

Therefore, the influence of aggregate on the Dcl_{ns} has in fact two opposite effects. On the one hand, the dilution and tortuosity effect that reduce the diffusion coefficient, apparently able to be predicted by EMTs and, on the other hand, the fact that an increase in aggregate volume content represents, for the same mixture volume, a decrease in paste volume and therefore a reduction in the chloride binding capacity. To derive the chloride binding capacity of a concrete mixture ($r_{cl,c}$) from the chloride binding capacity of, for example, a mortar mixture ($r_{cl,m}$), the differences in the water to cement weight ratio and cement content should be taken into account (Andrade, 2004), according to equation (5.17).

$$r_{cl,c} = r_{cl,m} \frac{(W/C)_m}{(W/C)_c} \cdot \frac{C_c}{C_m} \tag{5.17}$$

Where $(w/c)_c$ is the water to cement weight ratio in the concrete mixture; $(w/c)_m$ is the water to cement weight ratio in the mortar mixture; C_c is the cement content in the concrete mixture (kg/m³); and C_m is the cement content in the mortar mixture (kg/m³). In the present study, which aims to predict mortar or concrete behaviour based on a reference paste, the water to cement weight ratio of mortar and concrete are the same (same paste composition) and the relation between C_c and C_m is proportional to the corresponding paste volume content of the mixture. Thus, equation (5.17) can be simplified and written as equation (5.18):

$$r_{cl,c} = r_{cl,m}\frac{(1-\varphi_{p,c})}{(1-\varphi_{p,m})} \tag{5.18}$$

where $\varphi_{p,c}$ is the aggregate volume fraction in the concrete mixture and $\varphi_{p,m}$ is the aggregate volume fraction in the mortar mixture. Unlike the electrical resistivity study, no paste experimental tests were performed, whereby the experimental result of chloride diffusion coefficient of mortar in non-steady-state conditions ($Dcl_{ns,m}$), obtained through the CTH test, was used to determine the chloride diffusion coefficient in steady-state conditions of the cement paste matrix (matrix diffusivity). Thus, from $Dcl_{ns,m}$ experimental results presented in Table 5.3 and using equation (5.16) and equation (5.18), the mortar chloride diffusion coefficient in steady-state conditions ($Dcl_{s,m}$) was obtained through equation (5.19):

$$Dcl_{s,m} = Dcl_{ns,m} \cdot r_{cl,c}\frac{(1-\varphi_{p,m})}{(1-\varphi_{p,c})} \tag{5.19}$$

The paste chloride diffusion coefficient in steady-state conditions ($Dcl_{s,p}$) was then determined from $Dcl_{s,m}$ and using the D-EMT formulation for not diluted suspension of insulating spherical inclusions (Model 1), equation (5.20):

$$Dcl_{s,p} = \delta_{model,m}\left(Dcl_{s,m}\right) = \delta_{model,m}\left(Dcl_{ns,m} \cdot r_{cl,c}\frac{(1-\varphi_{p,m})}{(1-\varphi_{p,c})}\right) \tag{5.20}$$

where $\delta_{model,m}$ is a parameter that represents de application of Model 1 to obtain $Dcl_{s,p}$. Thus, the chloride diffusion coefficient in steady-state conditions of a concrete mixture from the experimental programme ($Dcl_{s,ci}$) was predicted by applying equation (5.21),

where $\delta_{model,ci}$ is a parameter that represents the application of the models (Model 1 to Model 5b) to the concrete composition c_i.

$$Dcl_{s,ci} = \delta_{model,ci}(Dcl_{s,p}) = \delta_{model,ci}\left(\delta_{model,m}\left(Dcl_{ns,m} \cdot r_{cl,c}\frac{(1-\varphi_{p,m})}{(1-\varphi_{p,c})}\right)\right) \quad (5.21)$$

Finally, from $Dcl_{s,ci}$ value, the chloride diffusion coefficient obtained in non-steady-state conditions of the concrete mixture c_i from the experimental programme ($Dcl_{ns,ci}$) was determined by applying equations (5.16) and (5.17), adapted for the case of two concretes with the same w/c but different aggregate content (see equation (5.22)):

$$\mathrm{Dcl_{ns,ci}} = Dcl_{s,ci}/\left[r_{cl,c}\frac{(1-\varphi_{p,ci})}{(1-\varphi_{p,c})}\right] = \delta_{model,ci}\left(\delta_{model,m}\left(Dcl_{ns,m} \cdot \frac{(1-\varphi_{p,m})}{(1-\varphi_{p,ci})}\right)\right) \quad (5.22)$$

where $\varphi_{p,ci}$ is the aggregate volume fraction in a concrete mixture c_i from the experimental programme. Therefore, according to equation (5.22), $Dcl_{ns,ci}$ can be obtained without assessing the binding capacity of the mixture. Experimental results of concrete chloride diffusion coefficient tests conducted under the experimental programme ($Dcl_{ns,exp,ci}$), as well as the corresponding values predicted by means of each model ($Dcl_{ns,ci}$) are presented in Figure 5.9.

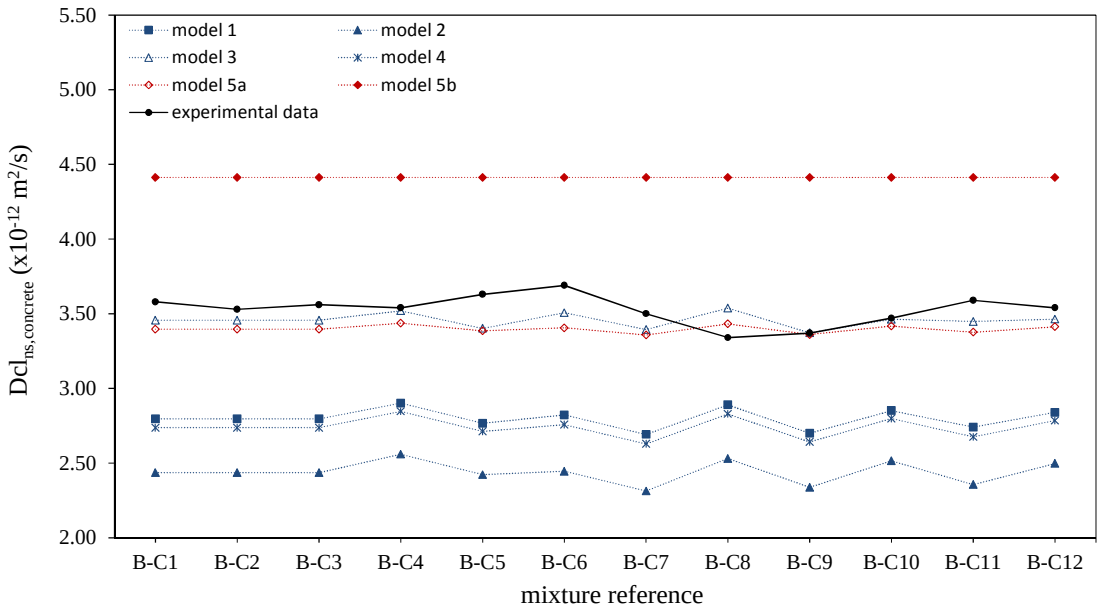

Figure 5.9 – Experimental data $Dcl_{ns,exp,ci}$ and predicted values obtained by the models $Dcl_{ns,ci}$.

The prediction error ($\Delta\varepsilon$) of each model is presented in Table 5.7, as well as the respective average ($|\Delta\varepsilon|_{average}$). According to Table 5.4 the coefficient of variation obtained for mortar and concrete mixtures replication was 1.7% and 0.7%, respectively, which already accounts for a significant share of the error in the case of Model 3 and Model 5a.

Table 5.7 – Models prediction error $\Delta\varepsilon$ for concrete chloride diffusion coefficient, obtained in non-steady-state conditions.

Mix reference	$\Delta\varepsilon_{model\ 1}$ (%)	$\Delta\varepsilon_{model\ 2}$ (%)	$\Delta\varepsilon_{model\ 3}$ (%)	$\Delta\varepsilon_{model\ 4}$ (%)	$\Delta\varepsilon_{model\ 5a}$ (%)	$\Delta\varepsilon_{model\ 5b}$ (%)
B-C1	-21.9	-32.0	-3.4	-23.5	-5.1	23.2
B-C2	-20.8	-31.0	-2.1	-22.5	-3.8	25.0
B-C3	-21.4	-31.6	-2.9	-23.1	-4.6	23.9
B-C4	-18.0	-27.7	-0.6	-19.6	-2.9	24.6
B-C5	-23.8	-33.3	-6.3	-25.3	-6.7	21.6
B-C6	-23.5	-33.7	-5.0	-25.3	-7.7	19.6
B-C7	-23.1	-33.9	-3.0	-24.9	-4.1	26.1
B-C8	-13.5	-24.2	5.9	-15.3	2.8	32.1
B-C9	-19.9	-30.6	0.1	-21.6	-0.3	30.9
B-C10	-17.8	-27.5	-0.2	-19.4	-1.5	27.2
B-C11	-23.6	-34.4	-3.9	-25.5	-6.0	22.9
B-C12	-19.8	-29.5	-2.1	-21.3	-3.6	24.6
$\lvert\Delta\varepsilon\rvert_{average}$	20.6%	30.8%	3.0%	22.3%	4.1%	25.1%

The behaviour of the models applied to the chloride diffusion coefficient proved to be very similar to that observed for electrical resistivity. The prediction errors of Models 3 and 5a are relatively small, 3.0 and 4.1%, respectively, which seems to indicate that these two models can predict with fair accuracy the influence of the aggregate volume and aggregate skeleton in the concrete chloride diffusion coefficient of a SCC.

Considering the precision and versatility of the models, Model 3 is suggested for prediction of the influence of aggregate volume and aggregate skeleton on SCC electrical resistivity and chloride diffusion coefficient. Nevertheless, the lower and upper bounds established by the Hashin-Shtrikman variational analysis (Hashin and Shtrikman, 1962) (Model 5a and Model 5b) can be a good guideline to select paste/mortar durability properties (electrical resistivity and chloride diffusion coefficient) that ensure a concrete composition with the previously established requirements. Despite Hashin-Shtrikman bounds cover a substantially wide range of values, this formulation has the advantage of only using as input parameters, paste

property (electrical resistivity or diffusivity) and aggregate volume content. In the present study, the lower bound (Model 5a) has provided a very similar prediction compared to experimental results.

5.6. Conclusions

The possibility of predicting concrete properties from cement paste behaviour has great advantages, as it facilitates the materials selection process and the performance-based design of concrete mixtures. In this work the possibility of using EMTs to establish the link between paste and self-compacting concrete was studied in terms of durability properties namely, electrical resistivity and chloride diffusion. Different models derived from the D-EMT were investigated and the predictions provided by the Hashin-Shtrikman bounds were also assessed. From the results presented in this chapter the following conclusions can be drawn:

- EMT has been applied in many different areas to describe the physical properties of composite materials however it is still under exploitation in the field of concrete as a material. The EMTs allow determining the properties of a multiphasic material starting from the knowledge of the physical property of each phase composing the mixture, as well as, of the structural properties of the mixture itself (percentage, shape and distribution of each phase).

- Self-compacting concrete and mortar were assumed as composite materials with two distinct phases, a cement paste in which insulating aggregate grains of various sizes and shapes are discontinuously embedded. Aggregate was considered as an insulating phase, given its high resistivity and low diffusivity compared with cement paste. It was considered that the ITZ has minor influence on SCC resistivity and diffusivity, and therefore the ITZ was assumed as part of the cement paste matrix, with the same properties.

- To predict aggregate influence on mortar/concrete properties the D-EMT seems to be the EMTs that best fits the concrete problem, since this

formulation is used for materials in which one phase always percolates and is also valid for less diluted suspensions.

- Mortar properties were predicted by the D-EMT formulation for not diluted suspension of insulating spherical inclusions (Model 1). The average prediction error was 4.1%, which seems to indicate that the model predicts fairly accurately the electrical resistivity of mortars based on the knowledge of paste electrical resistivity and aggregate volume content.

- Considering the precision and versatility of the models, Model 3 is suggested for predicting the influence of aggregate volume and aggregate skeleton on SCC electrical resistivity and chloride diffusion coefficient, which is a D-EMT formulation for ellipsoidal inclusions with an aligned orientation and electrical field aligned according to the semi-major axis of the ellipsoids. The average prediction error was 4.3% for the electrical resistivity and 3.0% for the chloride diffusion coefficient. It should be noted that a share of the error concerns to the experimental error.

- The lower bound established by the Hashin-Shtrikman variational analysis (Model 5a) has also provided prediction values very similar to experimental results.

- Concrete resistance to chloride ion penetration is generally evaluated using a non-steady migration test. However, EMTs cannot be directly applied to predict the non-steady-state chloride diffusion coefficient. Only the diffusivity, also called steady-state chloride diffusion coefficient can be predicted. A relationship has been established to determine concrete non-steady-state chloride diffusion coefficient by EMTs, without the explicit assessment of the binding factor.

- The applied formulations may also be extended to evaluate other SCC durability properties, transport properties, such as the oxygen permeability coefficient or the carbon dioxide coefficient.

Chapter 6

Durability monitoring to improve service life predictions of concrete structures

6.1. Synopsis

In this chapter a durability monitoring system is presented and its working principle and the methodologies of analysis and interpretation of the acquired data are discussed. The monitoring system integrates a sensorial component (corrosion kit-sensor), a data acquisition component and a communication and data processing component. Laboratory tests were conducted to establish the corrosion kit-sensor measuring protocol, assess its behaviour with temperature and humidity variations and appraise its performance to detect corrosion activity. This durability monitoring system was implemented in two structures, the Lezíria Bridge and a yachting harbour structure. Results collected during the construction and service phase were analysed and interpreted in the light of available information on surrounding environmental conditions. Service life of the yachting harbour structure was predicted and validated using data collected by the continuous monitoring system and during a periodic inspection.

6.2. Introduction

After decades aiming at improving of concrete strength, today researchers, civil engineers and construction technicians are mainly concerned with durability-related issues. Insufficient attention at durability of concrete structures has led to expensive

repair and even demolition and replacement, with great impact on resources, environment and human safety (Walraven, 2009; Gjørv, 2010). An effective action in the prevention of degradation and maintenance of concrete structures becomes crucial to achieve longer service life with low maintenance costs. Implementation of durability monitoring systems in new and existing concrete structures could reduce costs by enabling a more rational approach for the assessment of repair options and scheduling of inspections and maintenance programmes (Chrisp *et al.*, 2010). Also, important concrete infrastructures are increasingly being designed for long service life, by modelling the degradation process and using a probabilistic assessment of uncertainties (DuraCrete, 2000). However, aggressive loads or material resistance can, in reality, be very different from those assumed in the design phase. Hereupon monitoring of structure performance could provide added value for their management (Polder *et al.*, 2008b). The development of a probabilistic modelling approach supported by durability monitoring could improve service life predictions of concrete structures (Cusson *et al.*, 2011).

Monitoring of concrete structures can be performed at three different levels designated as low, intermediate and high level (Jensen and Andersen referred by Bertolini *et al.* (2005)). The low-level procedure essentially integrates periodic visual inspections and is still the basis of most structures management programs. The intermediate level of monitoring combines periodic visual inspection with more detailed inspections using non-destructive or semi-destructive techniques. In the high-level monitoring procedure, embedded sensors are installed within the covercrete, during structure construction or after repair works.

Monitoring of reinforced-concrete structures through embedded sensors has the disadvantage of providing a pre-set and more limited sampling. However, this allows resorting to automatic data acquisition systems which enable the collection of detailed information over long periods of time without access to the structure. Monitoring systems, eventually with continuous and automatic data acquisition, could be a key tool to achieve different objectives, such as: monitoring durability of a structure and its condition in order to make timely decisions for preventive and/or repair actions; monitoring the effect of preventive or repair actions; monitoring the condition of structures made of new materials and/or built with novel technologies; improving

service life prediction models; and following the ageing effects in zones where access is difficult (Bertolini *et al.*, 2005).

In recent years a great progress has been accomplished concerning durability monitoring systems using embedded sensors and automatic data acquisition systems. However, monitoring objectives and strategy have to be clearly defined, otherwise heavily instrumented structures will produce large amount of data with little or no practical value (Bertolini *et al.*, 2005). Furthermore, there is still a long way to go with regard to the results reliability, data interpretation and adequate decision in terms of timely rehabilitation actions. In this sense, this study aims at discussing the working principle and the methodologies of analysis and interpretation of data collected by the designated corrosion kit-sensor. The installation of this device in a structure provides measurements of galvanic current, corrosion potential and temperature, enabling to monitor the advance of aggressive agents into the concrete cover, to predict the time for corrosion initiation and to evaluate the corrosion state of the most external reinforcing bar. The durability monitoring system presented in this work includes, in addition to the sensorial component, a data acquisition component and a communication and data processing component. Laboratory tests were conducted to establish the corrosion kit-sensor measuring protocol, assess its behaviour for temperature and humidity variations and appraise its performance to detect corrosion activity. This durability monitoring system was installed in two structures, the Lezíria Bridge over the Tejo River and a yachting harbour structure implanted in Leixões Port. Results collected during the construction and service phase were analysed and interpreted in the light of available information on the surrounding environmental conditions. In order to demonstrate the effective use of the data obtained from field monitoring, the service life prediction of the yachting harbour structure was performed and updated using data collected in the continuous monitoring system and during a periodic inspections.

6.3. Durability monitoring system

Corrosion of a metal in an electrolytic medium, such as corrosion of reinforcement embedded in concrete (Figure 6.1), is an electrochemical reaction involving four

complementary partial processes (Bertolini *et al.*, 2005): (i) the oxidation of iron (anodic process) that liberates electrons in the metallic phase and gives rise to the formation of iron ions ($Fe \rightarrow Fe^{2+} + 2e^-$), and whose hydrolysis produces acidity ($Fe^{2+} + 2H_2O \rightarrow Fe(OH)_2 + 2H^+$); (ii) the reduction of oxygen (cathodic process) that consumes these electrons and produces alkalinity ($O_2 + 2H_2O + 4e^- \rightarrow 4OH^-$); (iii) the transport of electrons within the metal from the anodic regions where they become available, to the cathodic regions where they are consumed and (iv) in order to complete the circuit, the flow of current inside the concrete from the cathodic to the anodic regions, transported by ions in the pore solution. Note that this is an idealized figure because, in fact, the corroding zone is never a pure anode, but rather is composed by several micro-anodes and micro-cathodes.

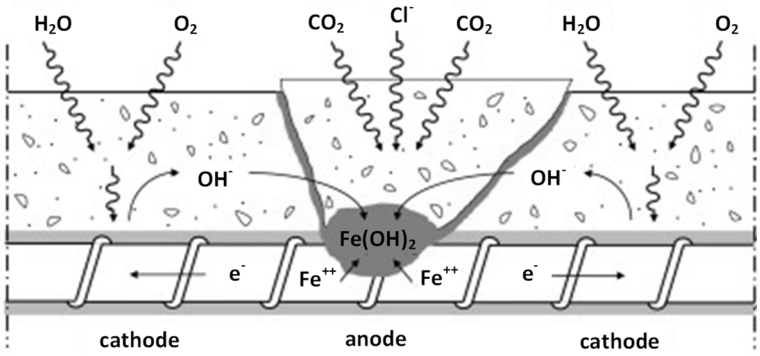

Figure 6.1 – Schematic representation of corrosion of steel in concrete (Cao *et al.*, 2013).

The corrosion evaluation of a reinforced concrete structure, during the initiation and propagation periods, can be performed by measuring electrochemical parameters of steel and the physicochemical properties of concrete. Steel electrochemical parameters enable monitoring the corrosion process itself. Examples of such parameters are the corrosion potential, corrosion rate and galvanic current of the macrocell. The physicochemical parameters of the concrete, as the chloride content, pH, resistivity, temperature, humidity, are factors that control the corrosion process. As many factors contribute to the durability of a reinforced concrete structure, information from different corrosion evaluation techniques should be gathered for an accurate assessment of the state of corrosion-induced damage (Qian *et al.*, 2003; Basheer *et al.*, 2009). Selection of parameters to be monitored should depend on the type of structure, exposure environment and whether it is a new structure or to be repaired, and, in this case, the type of intervention.

The first measurements of corrosion parameters in concrete were those of the electrical resistivity (Monfore, 1968), corrosion potential and polarization curves (Baumell, 1959; Gouda, 1970; Kaesche, 1973). The main interest was to know the effect of concrete humidity and of admixtures on corrosion. According to Gurulsamy and Geoghegan (referred by Pereira (2004)) the early applications of embedded sensors in concrete structures occurred at the end of the '70s with the introduction of reference electrodes to monitor corrosion potential in cathodic protection systems. Andrade and González (1978) were the first to apply the polarization resistance technique to quantify and monitor bars embedded in concrete, allowing the non-destructive assessment of the bars cross section loss (corrosion rate). Short *et al.* (1991) designed a laboratory device for detecting carbonation through the measurement of the galvanic current between a stainless steel bar and a ring of mild steel. This idea was later used by Schiessl and Raupach (1992) to develop a sensor based on the measurement of galvanic current in macrocells to continuously monitor corrosion risk of the reinforcement, depending on its distance from the concrete surface. This was followed by the development of sensors for in-depth measurements of concrete electrical resistivity (McCarter *et al.*, 1992; McCarter *et al.*, 1995; Raupach and Schiessl, 2000), corrosion rate by electrochemical techniques (Videm and Myrdal, 1997; Broomfield *et al.*, 2002), limiting current of oxygen reduction (Myrdal *et al.*, 1997; Correia *et al.*, 2006) and chloride content (Climent-Llorca *et al.*, 1996; Zimmermann *et al.*, 1997; Montemor *et al.*, 2006). Well-documented reviews on the electrochemical techniques and sensors for corrosion assessment and their application to concrete structures are presented in Broomfield *et al.* (2002), McCarter and Vennesland (2004), Song and Saraswathy (2007), Basheer *et al.* (2009) and Figueiras and Nunes (2010). Temperature and humidity sensors are currently used in corrosion monitoring applications given the nature of the corrosion process. In the last few years novel optical fiber sensor systems have been developed for monitoring concrete durability parameters, namely, temperature, humidity, pH, chloride content and corrosion of rebars (Basheer *et al.*, 2009).

Indeed, to be effective, a permanent monitoring system must include a number of sensors installed in the structure, but also a data acquisition and transfer system and an integrated software for analysis and processing of information (Comisu, 2005). In the next sections the durability monitoring system which has already been installed in some structures, will be described. The monitoring system integrates a sensorial component

(corrosion kit-sensor), a data acquisition component and a communication and data processing component, which are described in sections 6.3.1, 6.3.2 and 6.3.3, respectively.

6.3.1. Corrosion kit-sensor

The corrosion kit-sensor (CKS) is a commercial device (Force Technology) that incorporates a galvanic current sensor (sensor 1), a reference electrode (sensor 2) and a temperature sensor (sensor 3), see Figure 6.2 and Figure 6.3. The installation of this device in a structure provides measurements of galvanic current, corrosion potential and temperature, enabling to monitor the advance of aggressive agents into the concrete cover, to predict the time for corrosion initiation and to evaluate the corrosion state of the outermost reinforcing bar.

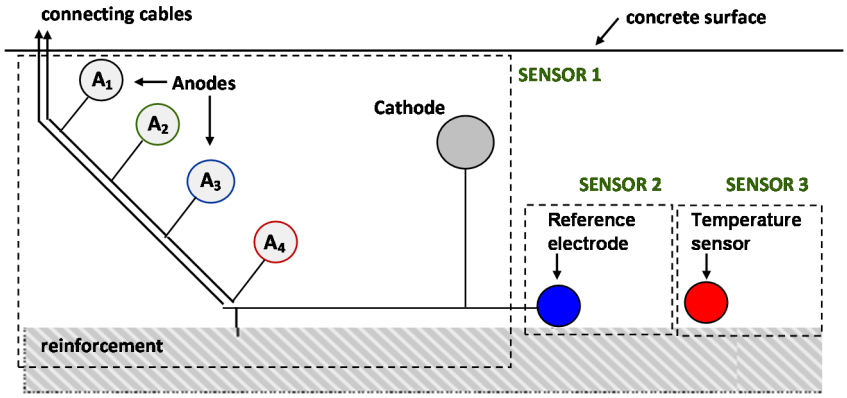

Figure 6.2 – Schematic representation of CKS (adapted from Cost Action 521 (2003)).

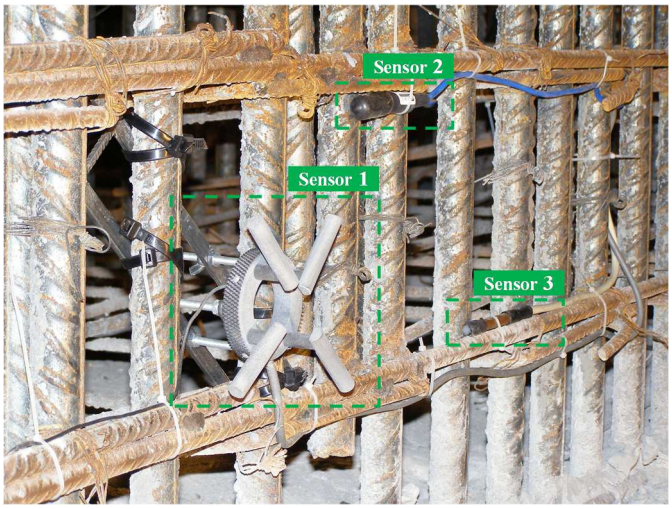

Figure 6.3 – CKS installed in situ, before concrete casting.

6.3.1.1. Galvanic current sensor

The operation principle of a galvanic current sensor is based on the measurement of electric current of a macrocell composed by two metals with different electrical potential, placed in contact through an electrolyte, such as concrete (see Figure 6.4). The magnitude of current flowing between the less noble metal (anode) and the more noble metal (cathode), is an indicative measure of the corrosion rate process. This current is known as galvanic current or macrocell current.

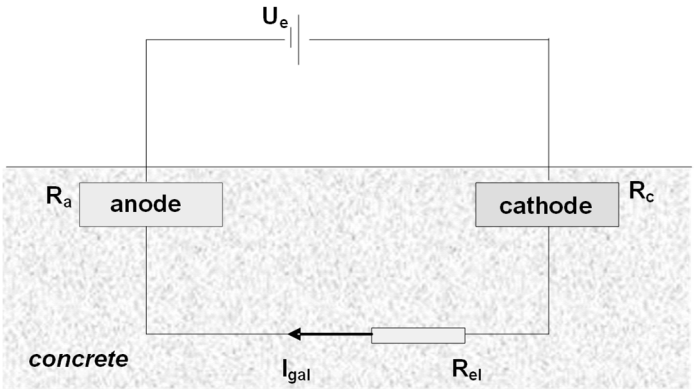

Figure 6.4 – Simplified electric circuit model of a macrocell.

Based on a simplified electric circuit model of a macrocell, the galvanic current I_{gal} (electric macrocell current) circulating between anode and cathode is given by the driving voltage U_e ($U_e = U_c - U_a$) and the resistances of the corroding system, namely, the electrolyte resistance (R_{el}), the anode polarization resistance (R_a) and the cathode polarization resistance (R_c), as expressed in equation (6.1) (Andrade *et al.*, 1992; Raupach, 1996):

$$I_{gal} = \frac{U_c - U_a}{R_{el} + R_a + R_c} = \frac{U_c - U_a}{\rho/_k + r_a/_{A_a} + r_c/_{A_c}} \tag{6.1}$$

where U_c is the rest potential of the cathode (cathode equilibrium potential); U_a is the rest potential of the anode (anode equilibrium potential); ρ is the specific resistance of the electrolyte (concrete); k is the cell constant geometry; r_a and r_c are the specific anodic and cathodic polarization resistances, respectively; and A_a and A_c are the anodically and cathodically acting steel surface area, respectively. This equation is valid to a face to face arrangement of anode and cathode.

The electrochemical interaction between steel regions with different steady-state potentials can be explained by polarization curves for the anodic and cathodic components (Evans-diagram) (Gulikers, 1996), see Figure 6.5. As a consequence of macrocell action the cathodic component potential is shifted towards less positive values (cathodic polarization) and the anodic component potential is shifted towards less negative values (anodic polarization). From the polarization curves and electrolyte resistance, the potentials of the coupled steel electrodes and the galvanic current can be derived.

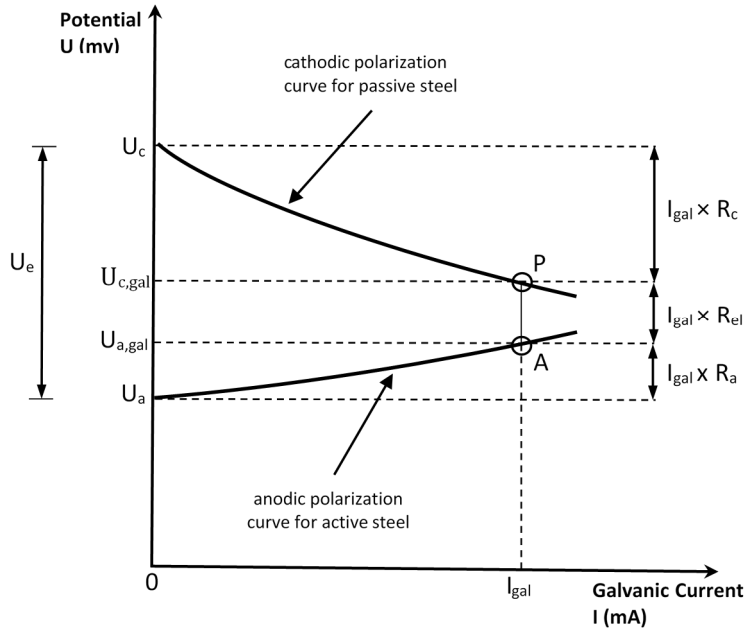

Figure 6.5 – Evans-diagram for a two-component macrocell (Gulikers, 1996).

From equation (6.1) it can be found that current flowing in a macrocell depends on the anodic and cathodic process ($U_c - U_a$), as well as the resistances of the anode, cathode and electrolyte. Therefore, the galvanic current may have very low values if the anode surface is not depassivated ($R_a \rightarrow \infty$), if the availability of oxygen in the electrolyte is low ($R_c \rightarrow \infty$) or if the concrete is totally dried out ($\rho \rightarrow \infty$) (Raupach, 1996). The intensity of the macrocell current in concrete structures is influenced by a large number of factors such as concrete quality (e.g. w/c, cement content and curing), chloride content, carbonation, environmental conditions and geometry of the corrosion cell. Thus, the prediction of the macrocell current is very difficult. Moreover, relationships between different influencing parameters and the anode, cathode and electrolyte resistances are not the same, e.g. the water saturation of the concrete leads to very low

electrolytic resistance but also to a high cathodic resistance (Raupach, 1996). Concrete quality or environmental conditions should be taken into consideration when designing the galvanic current sensor.

By measuring the current flow between the anode and cathode and considering Faraday´s law, it is possible to determine the corrosion rate, i.e. the amount of corroded metal per unit of area and time. However, determining the reinforcement corrosion rate from galvanic current measurements is not correct. Galvanic current established between corroding and passive metal represents only part of total corrosion activity (Andrade *et al.*, 1992; Cost Action 521, 2003). Galvanic current is a direct measure of the corrosion rate only when the corroding area is a pure anode, with no microcell activity, which only may happen in concrete with a completely oxygen-free atmosphere around the corroding areas, or when the corroding area is comparatively very small (Gulikers, 1996; Alonso *et al.*, 2000).

The principle of measuring galvanic current generated by a macrocell has been employed in the development of sensors for monitoring the depth of contaminated concrete with aggressive agents and thus assessing reinforcement corrosion risk. These sensors are essentially constituted by small carbon-steel anodes, placed at different depths of the concrete cover, and a more noble metal that will function as cathode, see Figure 6.2. By measuring the electric current that flows between each individual anode and the cathode, it is possible to know when depassivation of the carbon-steel anode occurs. In the course of time the deeper carbon-steel anodes will be depassivated one by one, enabling time to depassivation and critical depth of chlorides or carbonation front to be monitored (Cost Action 521, 2003; Bertolini *et al.*, 2005). The relationship between critical depth of chlorides or carbonation and time, can be determined and used to predict, by extrapolation, time to reinforcement depassivation (Schiessl and Raupach, 1992).

The galvanic current sensor used in the CKS comprises a circular polymer body on which four sandblasted carbon steel anodes are assembled using polymer spacers with different heights (see Figure 6.6). The area of the anodes is 21.3 cm^2, 60 mm long and 12 mm diameter. Around the circular polymer body a mixed-metal oxide coated titanium mesh (MMO-Ti) is assembled to function as cathode. Additionally, this sensor enables performing a connection to the reinforcement to assess its corrosion state.

When installed in new structures, this sensor is mounted on the outer reinforcement with the 4 anodes positioned in the cover concrete, between the outer reinforcement and the concrete surface (see Figure 6.3 and Figure 6.6).

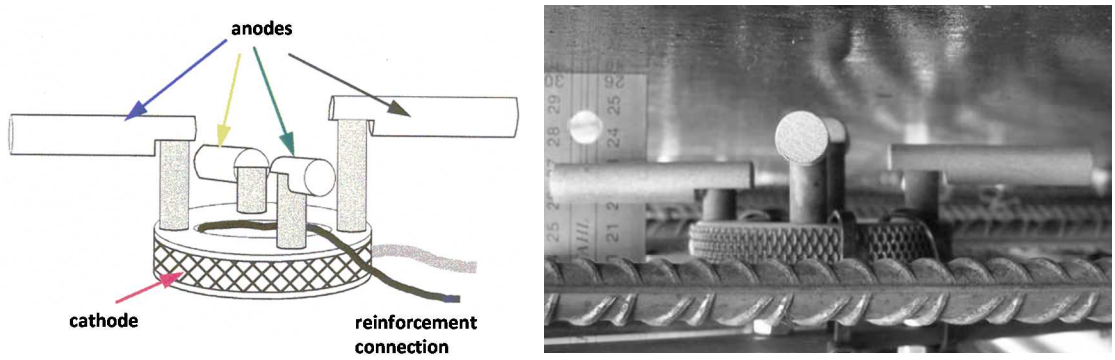

Figure 6.6 – Galvanic current sensor: schematic representation (Force Technology) (left); typical installation (right).

6.3.1.2. Reference electrode

The corrosion potential (E_{corr}), which provides qualitative information of the actual corrosion state of steel in concrete, is measured as a difference of potential against a reference electrode (RILEM TC 154-EMC, 2003). The reference electrode can be either an external reference electrode placed over a wet sponge on the concrete surface or an embeddable reference electrode.

Requirements for a reference electrode will depend mainly on the objective of the installation and the nature of the application. An electrode embedded in a concrete structure should exhibit stability, reversibility and reproducibility requirements, be adequately small, exhibit little sensitivity to changing variables inherent to concrete under service conditions and enabling passing of small currents with a minimum of polarization and hysteresis effects (referred by Ansuini and Dimond (Castro *et al.*, 1996)).

Concerning the CKS, an embeddable reference electrode of manganese dioxide (MnO_2) is coupled to the galvanic current sensor. The embeddable MnO_2 electrode for use in concrete was developed in 1986 during the BRITE programme (Arup *et al.*, 1997). This electrode is designed as a double junction electrode containing a MnO_2 in a stainless steel housing with a NaOH gel of pH 13.5. The electrolytic contact with the concrete is

performed through a porous cementitious plug, which ensures a good bond to concrete, allows an intimate contact with the interstitial pore solution, and minimizes the junction potential (Arup *et al.*, 1997), see Figure 6.7. Given the similarity between the pH of the solution inside the electrode (NaOH) and the pH of the interstitial pore solution, junction potential across the cementitious matrix is minimized.

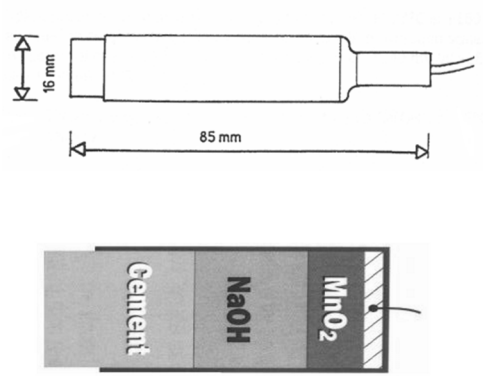

Figure 6.7 – Schematic representation of the MnO_2 reference electrode (Force Technology).

The typical potential value of the MnO_2 electrode used in the present work, measured in a saturated $Ca(OH)_2$ solution at 23 ºC versus a saturated calomel electrode (SCE) is of +175 mV, equal to +420 mV in hydrogen scale (NHE). The inclusion of the reference electrode in the CKS will enable automatic monitoring of corrosion potential of the reinforcement and of each of the anodes of the galvanic current sensor, see Figure 6.2.

6.3.1.3. Temperature sensor

Each CKS has also a temperature sensor to monitor concrete temperature at the level of the outermost reinforcing bar. The temperature detector used is made of platinum and presents a resistance of 100 Ω at 0 ºC, thus named Pt-100 sensor. Temperature sensors were encapsulated in small steel tubes sealed with epoxy resin.

Temperature is an important parameter given its influence on concrete deterioration and reinforcement corrosion process, and therefore, in measurements of corrosion potential and galvanic current. Actually, the three environmental parameters, temperature, moisture and oxygen availability, have a significant influence on the progress of the reinforcement corrosion process.

6.3.2. Automatic reading and data acquisition system

An electronic equipment, designated by DURABOX@ (Veiga *et al.*, 2011), was developed to enable automatic and continuous reading and data acquisition of CKS. This equipment comprises an acquisition module, a power module and corrosion and temperature reading modules. Corrosion modules operate simultaneously as a high impedance voltmeter and a zero resistance ammeter (ZRA), for corrosion potential and galvanic current readings, respectively. Each corrosion module enables measuring two CKSs, while the temperature module enables reading six temperature sensors. The data acquisition module deals with the process of measuring electrical values from corrosion and temperature modules and converts results into digital values, which can be read by the computer. As a modular system, DURABOX@ provides both the advantage of being adaptable to the type and number of sensors installed on the structure and also the ease of integrating new measuring modules. Communication with the computer is performed through Ethernet or RS232. The following figure presents a schematic representation of the overall architecture of DURABOX@.

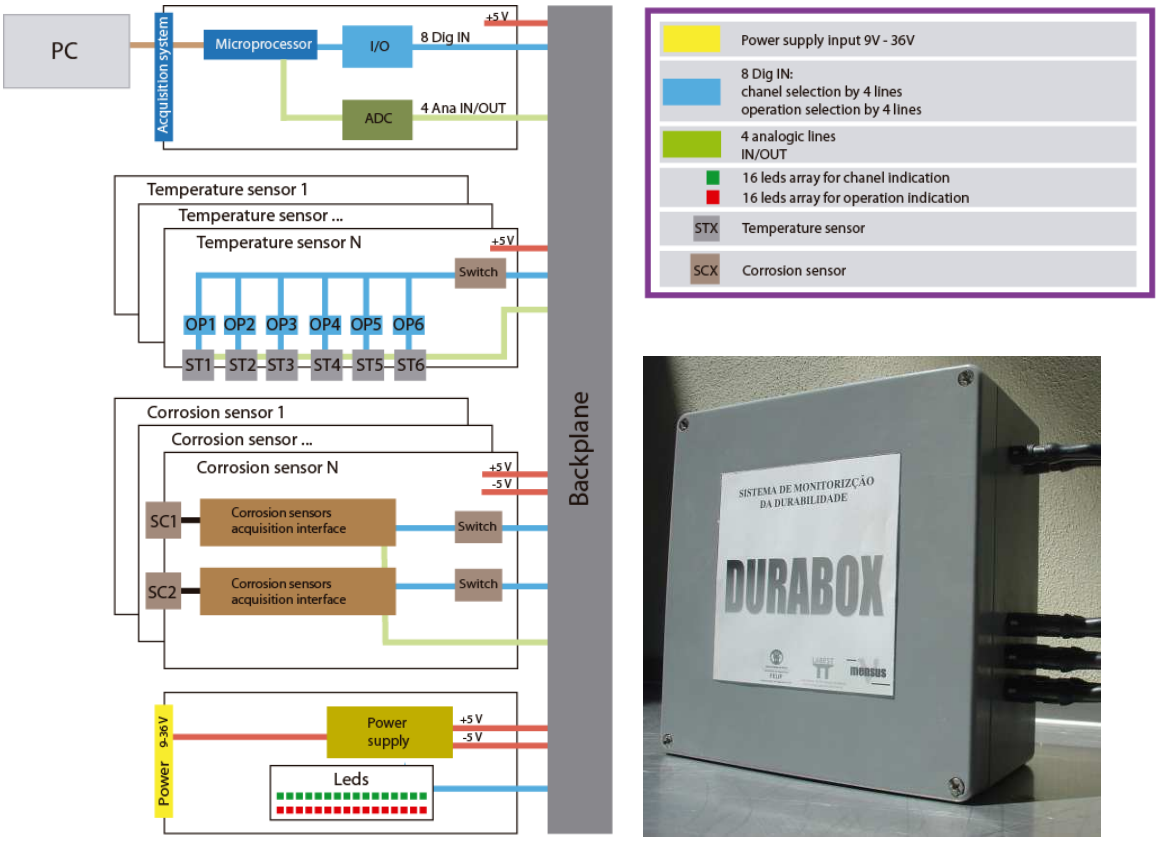

Figure 6.8 – DURABOX@: Schematic representation of the overall architecture.

6.3.3. Database and remote access

All data collected from the CKSs installed in the structure are sent to a database engine that runs on the open source software PostgreSQL. A web application was developed to provide access to the sensors data in quasi-real time. This application enables accessing monitoring results in the form of graphs and tables and complementarily, scheduling and automatic report generation with e-mail sending (Figueiras *et al.*, 2008). Figure 6.9 shows some of the layouts from the web application developed for the monitoring system installed in the Lezíria Bridge. The software for storage management, analysis and access to the sensors data was developed by a technical team including software and civil engineers from FEUP/LABEST and NewMensus (Figueiras *et al.*, 2008).

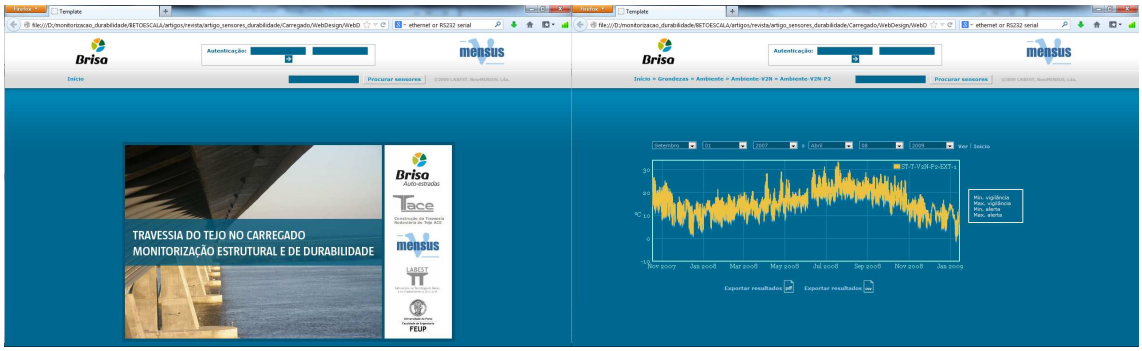

Figure 6.9 – Layouts from the web application developed for the monitoring system installed in the Lezíria Bridge.

6.4. Interpretation of CKS results

6.4.1. Galvanic current measurements

The galvanic current flow between both electrodes, anode and cathode, is negligibly low as long as anode is in the passive state. Once anode corrosion is initiated, the electron flow between anode and cathode grows, causing a significant increase of the galvanic current. Figure 6.11 shows the galvanic current measured, in a laboratory test, between a cathode and an anode with no corrosion and an anode with corrosion, during a short circuit time of 300 s. Measurements were performed on the first anode

(A_1 in Figure 6.2) of two CKSs installed on reinforcement concrete specimen panels ($30\times50\times10$ cm^3), see Figure 6.10. Upon short circuiting cathode and anode, galvanic current decreases with time (non-steady state) and thus the moment of measuring after closing the circuit (short circuit time) is important to allow correct corrosion detection.

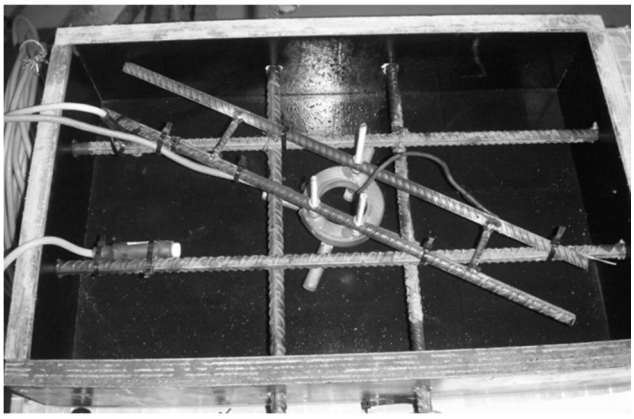

Figure 6.10 – CKS installed on the reinforcement concrete specimen panel.

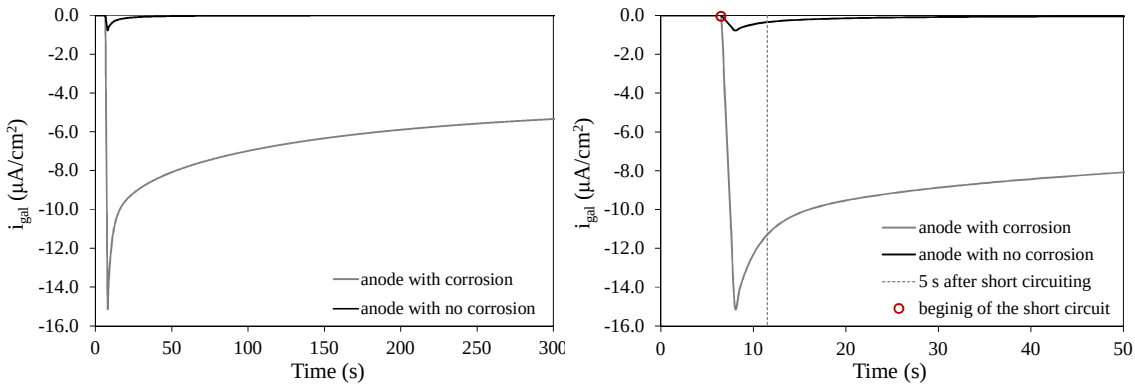

Figure 6.11 – Galvanic current records collected in an anode with no corrosion activity and an anode with corrosion activity: (a) the whole test; (b) the first 50 s of test.

According to the results it seems that all the studied short circuit times could be used to differentiate between the passive and active state, but for practical reasons, a short measuring time is the most convenient. In this work, the galvanic current was measured 5 s after short circuiting the anode and cathode (see Figure 6.11). Also Raupach and Schießl (2001) have investigated the most suitable short circuit time between 1 and 30 s, and concluded that, generally, all selected times will allow to differentiate between the passive and active state. However, it should be realized that the galvanic current

observed after a small short circuit time is a strong overestimation of the real steady state corrosion current density (Polder *et al.*, 2008a).

Nonetheless, in some situations the galvanic current measurements 5 s after short circuiting may lead to erroneous conclusions regarding anode corrosion state. An example of this situation is shown in Figure 6.12, measurements performed on the first anode of a CKS installed on a reinforcement concrete specimen panel (30×50×10 cm^3). The peak value of galvanic current and even the 5 s short circuiting value are relatively high (in absolute value), suggesting very active corrosion. However, the low value of galvanic current measure in steady-state condition (in absolute value) indicates that the anode may be corroding but with a low rate or with a small corroding area. In long-term monitoring these situations should be probed by a measure using longer short circuit time.

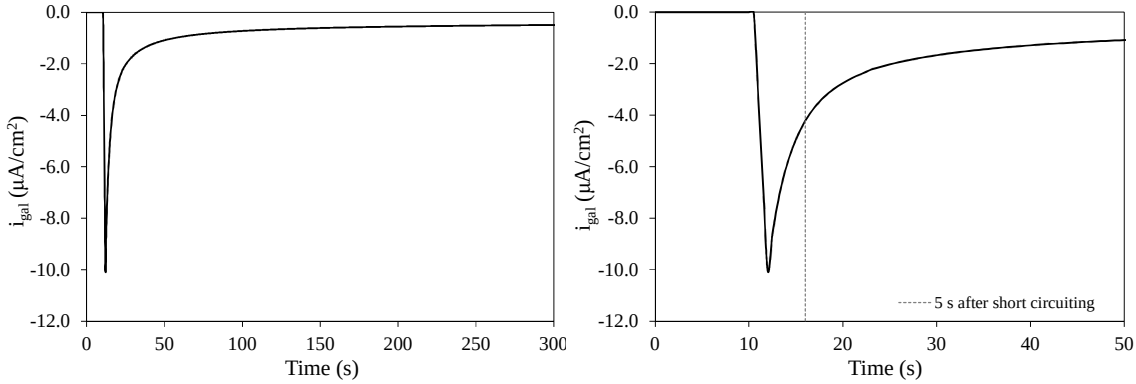

Figure 6.12 – Galvanic current records collected in anode A_1 of a CKS: (a) whole test; (b) the first 50 s of test.

6.4.2. Corrosion potential measurements

The corrosion potential measurement gives information on the probability of corrosion, since the transition of the steel from passive to active state will shift the potential to increasingly more negative values. Ranges of expectable values for corrosion potential associated to the probability of corrosion activity in atmospherically exposed structures are presented in Table 6.1. Corrosion potential values are presented for the reference electrode CSE ($Cu/CuSO_4$), as given by the ASTM 876-09 (ASTM,

2009), and for the reference electrode MnO_2. To convert corrosion potential from mV vs CSE to mV vs MnO_2, -105 mV were added to the corrosion potential values.

Table 6.1 – Probability of corrosion activity on atmospherically exposed structures from potential measurements, as given by ASTM C876-09 (ASTM, 2009).

Probability of corrosion activity	Potential (mV vs CSE)	Potential (mV vs MnO_2)
>90% probability of no corrosion occurring	>-200	>-305
Probability of corrosion uncertain	-200 a -350	-305 a -455
>90% probability of corrosion occurring	<-350	<-455

However, corrosion potential data can be misinterpreted and therefore lead to wrong or inadequate conclusions under some circumstances. To formulate conclusions concerning corrosion activity of embedded steel and its probable effect on the service life of the structure, it is often necessary to consider further data, such as chloride content, depth of carbonation or information on environmental exposure conditions (Uller *et al.*, 2000; RILEM TC 154-EMC, 2003; ASTM, 2009). Some typical ranges of corrosion potential of steel in concrete for different conditions are given by RILEM TC 154-EMC (2003) (see Table 6.2).

Table 6.2 –Typical ranges of potential of carbon steel in concrete (RILEM TC 154-EMC, 2003).

Concrete condition	Potential (mV vs CSE)
dry concrete	+200 to 0
dry and carbonated concrete	+200 to 0
wet and carbonated concrete	+100 to -400
wet and chloride free concrete	+100 to -200
wet and chloride contaminated concrete	-400 to -600
water saturated concrete without oxygen	-900 to -1000

The carbonation-induced corrosion initiation is one of the situations where potential values should be analysed with special care. Passive steel in concrete reacts as an oxygen electrode on variations in pH of the concrete pore solution, thus corrosion potential

increases with pH decrease ($\partial E/\partial pH$=-60 mV, at 25ºC) (RILEM TC 154-EMC, 2003). This means that measured potentials in carbonated concrete are less negative (more noble). In the case of submerged or buried structures, as the restricted oxygen availability is restricted the maintenance of the passive film can be prevented and steel may corrode (Pereira, 2004). Under these circumstances, corrosion potential lies in the range between -900 to -1000 mV vs CSE. The humidity condition of the concrete has also influence on the potential readings. As the moisture content increases the corrosion potential shifts to more negative values. Thereby, it is important to analyse changes in potential over time and not over consider single potential value (Vennesland *et al.*, 2007).

6.4.3. Temperature and humidity influence on CKS results

To investigate short-term impact of temperature and humidity on the corrosion process, two reinforcement concrete specimen panels (30×50×10 cm^3) instrumented with CKS were subjected to a set of tests with varying temperature and humidity.

A first experimental test was carried out on a concrete specimen panel with all the CKS anodes in passive state. During the test, the specimen was kept at a constant ambient humidity (50 %RH) and the temperature was varied between 10 and 40 ºC, a cycle of rise and fall in steps of 5ºC. Due to the relatively short duration at each temperature step the moisture content in the concrete specimen panel, at the depth of the sensor anodes, was assumed not to be affected by these temperatures. Corrosion potential and galvanic current records collected during the experimental test are given in Figure 6.13. Analysing results, it can be observed that, as temperature increases, the corrosion potential and the galvanic current become more negative, decreasing on average 1.5 mv/ºC and 0.0159 μA/cm^2/ºC, respectively. Although variations are consistent with temperature, no considerable impact on the corrosion process of passive anodes was found. The temperature rise increases galvanic current (in absolute values) as it improves ion mobility through the electrolyte and increases the kinetics of the anodic and cathodic reactions. Variations observed in corrosion potential depend mainly on how temperature affects the nature, composition and distribution of the anode oxide layer. Moreover, reference electrode potentials change with temperature, both

electrochemical reactions and chemical solubility of the inner reference electrode solution are affected (Myrdal, 2007).

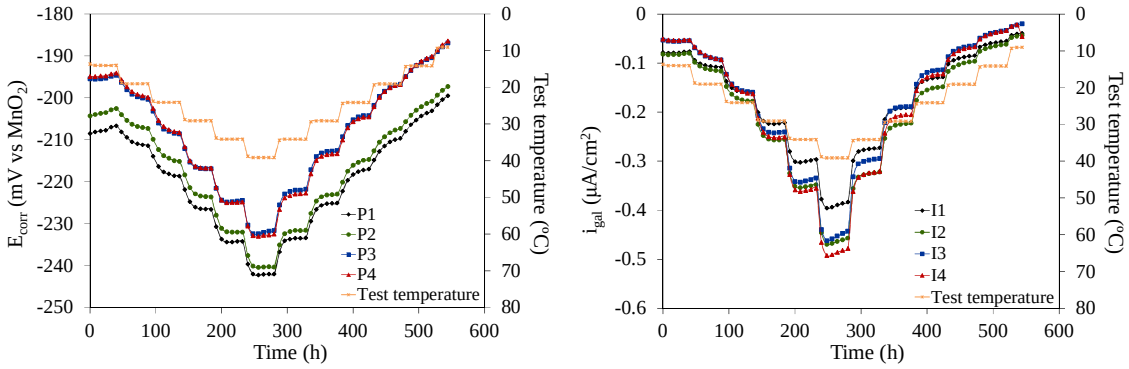

Figure 6.13 – Temperature influence on CKSs records: corrosion potential and galvanic current.

The durability parameters curves under the thermal action cycle on concrete specimen panel show some hysteresis, which is particularly evident in the case of corrosion potential. In addition, this parameter takes longer to reach a constant value at each temperature level than galvanic current. In fact, in the kinetics of electrochemical reactions of anode oxides layer, due to temperature variation, some reactions take place instantly while others will occur over time.

The other experimental test was conducted on a reinforcement concrete specimen panel previously subjected to a wetting period (simulating a rain period) and wherein only the outermost anode of CKS displayed values indicating and active corrosion process. After the wetting period, the test specimen was submitted to a drying period including periods of constant temperature (40 ºC) and a period with temperature cycles, approximately between 7 and 36 ºC (simulating daily cycles). Corrosion potential and galvanic current records collected from one of passive anodes, anode A_2, are shown in Figure 6.14. During the temperature cycles, a very consistent variation with temperature is observed again, where a temperature increase leads to more negative values of potential and galvanic current. Peak evolution during temperature cycles show that as concrete loses moisture, corrosion potential and galvanic current evolve into less negative values. Despite these variations with temperature and humidity, no considerable impact on the corrosion process of passive anodes was found during the test. Note that two systems may be distinguished in the concrete cover layer. An open system, corresponding to the outermost concrete layer (the first 3 cm depth

approximately), where humidity exchange occurs with the exterior, and a close system, in the innermost concrete cover layer, where fluctuations in water content due to temperature variations are reversible. In the innermost concrete the evaporated/condensed water due to temperature variations are not exchanged with the exterior.

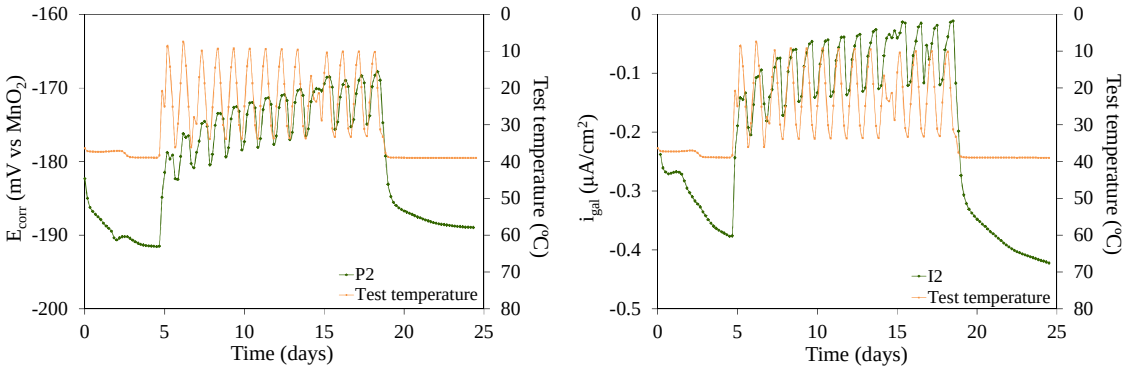

Figure 6.14 – Corrosion potential and galvanic current records collected in anode A_2 of a CKS, during an experimental test with varying temperature and humidity.

Figure 6.15 presents the corrosion potential and galvanic current values acquired in the outermost anode (A_1) of the CKS during this experimental test. The results indicate that concrete moisture has a very significant influence on the durability parameters. Also temperature displays a more pronounced effect in the anode in active corrosion process, especially on the galvanic current values.

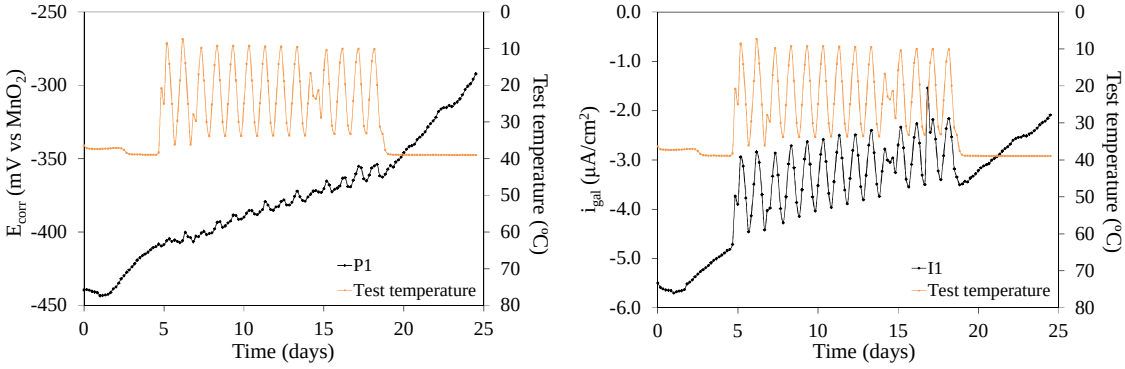

Figure 6.15 – Corrosion potential and galvanic current records collected in anode A_1 of a CKS, during an experimental test with varying temperature and humidity.

Temperature and humidity induce variations on the nature and composition of the anode oxides layer, ion mobility through the electrolyte, kinetics of corrosion reactions

and oxygen availability. Thus, variations observed in corrosion potential and galvanic current depend mainly on how environmental parameters affect these factors. Predicting the influence of humidity and temperature on the corrosion process is, however, complex as they may have opposite effects. For example, a higher moisture content facilitates ion mobility but prevents oxygen access, or a higher temperature increases kinetics of the reactions but decreases condensation (Uller *et al.*, 2000). This experimental test also highlights the importance of continuous monitoring, given the influence of environmental conditions on the corrosion process. Note that, corrosion potential and galvanic current values observed in the outermost anode at the beginning and at the end of the test are clearly different.

6.4.4. Corrosion detection on CKS

As long as the ingress of critical chlorides or carbonation has not reached the position of the outer anode, galvanic current between the anodes and the cathode is in the range of typical currents for passive state, i.e. very small. In this phase, variations in the galvanic current and corrosion potential values are mainly due to changes in the environmental conditions, such as temperature, concrete moisture and oxygen availability. As soon as the critical chloride content or carbonation reaches the surface of the outer anode (A_1 in Figure 6.2), and if sufficient moisture and oxygen are available, galvanic current and corrosion potential will decrease significantly (Raupach and Schiessl, 1997). Figure 6.16 presents the results of a CKS, installed on a reinforcement concrete specimen panel ($30\times50\times10$ cm^3), during an accelerated corrosion test conducted in the laboratory. The concrete specimen panel was subjected to wetting-drying cycles, using a 10 % NaCl solution, and under a constant temperature of 40 ºC.

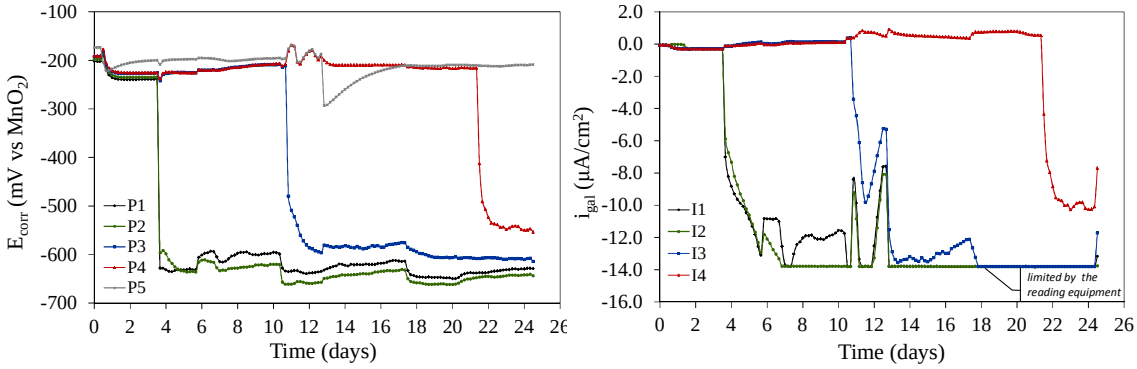

Figure 6.16 – CKS records acquired during an accelerated corrosion test: corrosion potential and galvanic current.

As would be expected, corrosion starts from the outermost anodes to the innermost anodes, and is detected by a significant and almost simultaneously variation of corrosion potential and galvanic current. According to the results the outer anode, anode A_1, and the following anode, anode A_2, seem to start corroding practically at the same time, which can be explained by two main reasons. On one hand, a solution with a very high chloride content was used, which may have greatly accelerated the corrosion process, especially in the outermost concrete cover layers. On the other hand, concrete has heterogeneities that, depending on the type of heterogeneity, may delay or accelerate chloride penetration in certain areas of the structure.

During the experimental test, galvanic current of active anodes shows greater fluctuations than corrosion potential. The wetting-drying cycles of the concrete or the passivation of a pit (localized corrosion) are situations that shall, in principle, be detected sooner in the galvanic current records. The galvanic current depends essentially on the rate of electron transfer reactions, wherefore a change in concrete electrical resistivity and cathode potential due to wetting-drying cycles or the occurrence of localized corrosion, has influence on its value.

6.5. Lezíria Bridge – Durability monitoring during the construction and exploration stages

6.5.1. Durability monitoring system

Lezíria Bridge, with a total length of 11670 m, comprises three concrete substructures with structural solutions adapted to the characteristics of each crossing area: the northern approach viaduct with 1700 m long; the main bridge crossing the Tejo River with a total length of 970 m; and the southern approach viaduct with 9160 m long (COBA-PC&A-CIVILSER-ARCAIS, 2005). The northern approach viaduct is constituted by a beamed slab deck cast in-situ over launching girders and supported by piers on piles. The main bridge comprises eight spans, six 130 m long and two 95 m long spans. The bridge deck, a box girder of variable inertia, was built by the balanced cantilever method using a movable scaffolding system. The concrete piers are constituted by four identical plates, with constant thickness and variable width, resting on pile caps. The southern approach viaduct is a partially precast structure composed by 22 elementary viaducts with a mean span length of 36 m. The viaduct deck is constituted by precast slabs and precast box girders monolithically connected to the piers. Figure 6.17 shows an overview of the Lezíria Bridge and a closer view of each of the three substructures.

(a) (b) (c)

Figure 6.17 – An overview of the Lezíria Bridge and each of the three structures: (a) northern approach viaduct; (b) main bridge; (c) southern approach viaduct.

In regard to the environmental aggressiveness where the Lezíria Bridge is implanted, the presence of a rather close thermoelectric power station and a railway line must be pointed out. Chemical analyses performed on the water of Tejo River indicated that it is generally not aggressive (Portugal *et al.*, 2006), although, soil water proved to be aggressive. The bridge is implanted in the east-west direction about 50 km away from the sea.

A monitoring system based on a limited number of sensors installed in a few sections of the structure requires a careful definition of their locations in order to gather information representing, as much as possible the global behaviour of the structure. The selection of the instrumented locations must take into account the environmental exposure conditions and specific aspects of structural design, in particular the geometry and structural behaviour of the elements. Specific aspects of construction practices such as casting joints or areas with high reinforcement density should also be taken into consideration. In the Lezíria Bridge 15 CKSs were installed in three distinct zones, namely, one section of the northern approach viaduct, one section of the main bridge

and two sections of the southern approach viaduct. For conciseness, only the results of the CKSs installed on the northern approach viaduct will be presented. The layout of the CKSs in the cross section of the northern approach viaduct is presented in Figure 6.18. CKSs anodes were placed along the concrete cover layer at the depth of: anode A_1 at 1.3 cm; anode A_2 at 1.8 cm; anode A_3 at 2.3 cm and anode A_4 at 2.8 cm (on average).

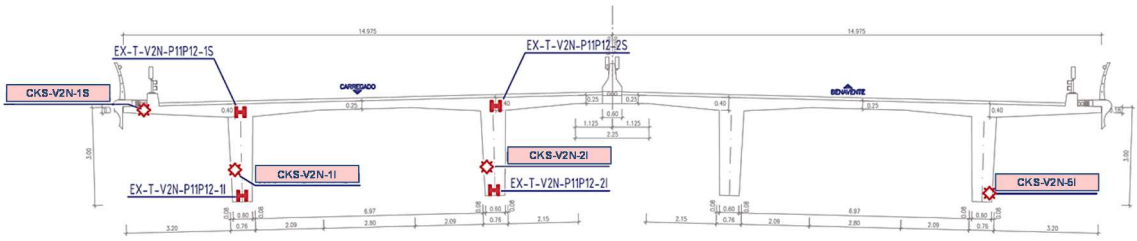

Figure 6.18 – Layout of the CKSs in the cross section of the northern approach viaduct.

The monitoring system installed in the Lezíria Bridge integrates, in addition to the durability monitoring system, a structural monitoring system comprising sensors to monitor structural parameters (strain, rotation, displacement), dynamic parameters (acceleration) and scour parameters (Figueiras *et al.*, 2007; Figueiras *et al.*, 2008). All the sensors are interrogated by automatic acquisition systems installed in selected points of the structure. Acquisition points communicate through a fibre optic local network and the information is recorded in a central acquisition unit (Figueiras *et al.*, 2007; Figueiras *et al.*, 2008). Remote access to the bridge monitoring system is established through the central acquisition unit.

6.5.2. Monitoring results during the early age phase

During the bridge construction, namely during concrete casting operations and concrete hardening (first 34 days), the corrosion potential and temperature of some CKSs installed in the northern approach viaduct were collected. Monitoring corrosion potential during an initial phase allows, from the outset, to verify good functioning of the CKSs and assess the passivation process evolution of the sensor anodes and most external reinforcing bar. Figure 6.19 and Figure 6.20 show the corrosion potential and temperature measurements of CKS-V2N-1S and CKS-V2N-1I respectively, acquired during concrete casting and in the following 34 days. In each CKS three potentials were monitored, namely the potential of the outermost anode (P1), the second outermost

anode (P2) and the most external reinforcing bar (P5). Deck casting was performed on 29th December around 7 a.m. and striking only occurred on 19th January. During this period, three power interruptions occurred, which prevented data acquisition for a few days (see Figure 6.19 and Figure 6.20).

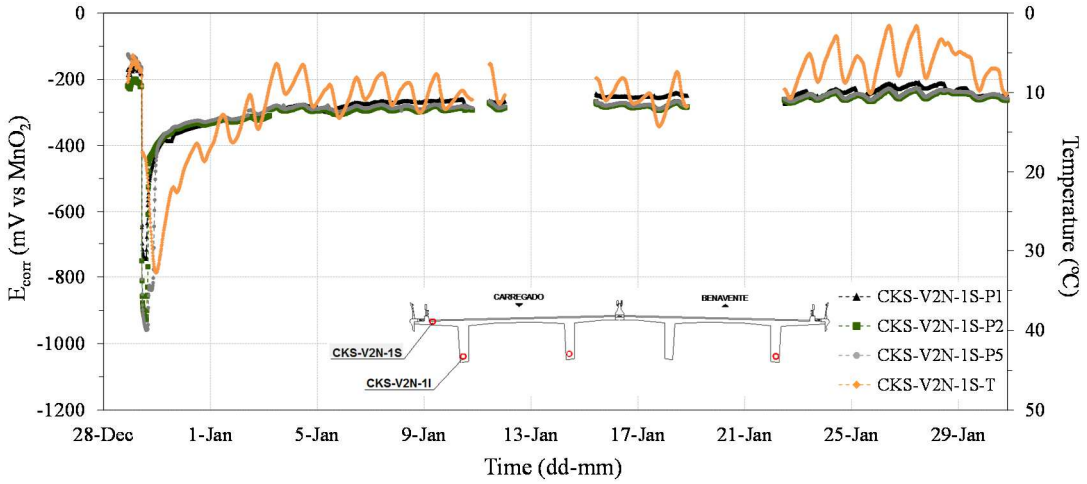

Figure 6.19 – Corrosion potential records collected in CKS-V2N-1S during concrete casting and within the following 34 days.

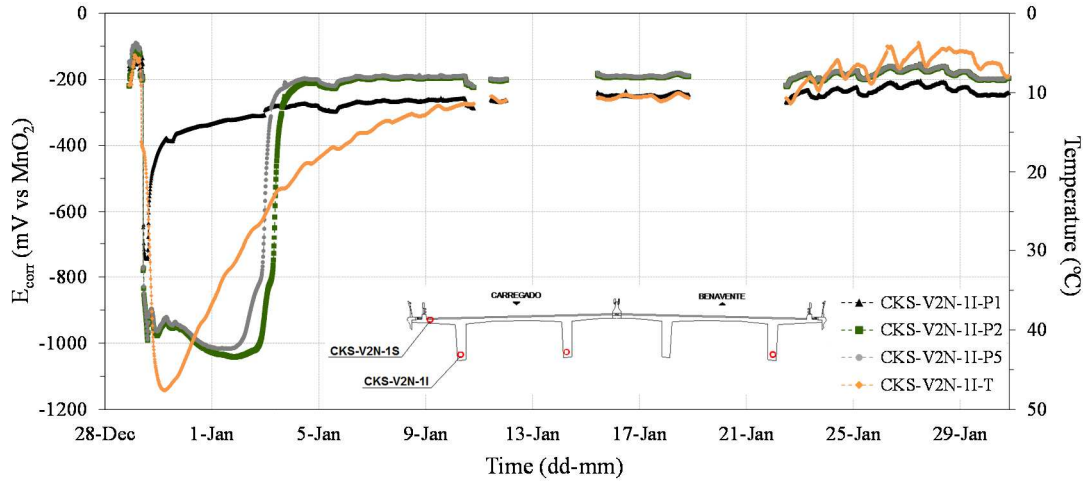

Figure 6.20 – Corrosion potential records collected in CKS-V2N-1I during concrete casting and within the following 34 days.

Temperature results in the early hours after concrete casting showed a significantly different heat evolution in the two instrumented zones, as expected, given the location of the CKSs in the structure. The maximum temperature observed in CKS-V2N-1S was 32.8 ºC, 15.5 hours after concrete casting, while in CKS-V2N-1I it was recorded

47.6 ºC, 21.5 hours after concrete casting. These temperatures were obtained at the level of the reinforcement bar nearest to the surface.

Regarding corrosion potential evolution, the concrete hardening stage can be basically divided into two periods. The first 3 a 7 days after concrete casting is a period where potential values undergo significant variations, whereas in the second period the average potential increases slightly becoming approximately constant, varying only with daily cycles. The minimum corrosion potential recorded by CKS-V2N-1S occurred about 14 hours after concrete casting, reaching -745.2 mV for anode A_1, -929.3 mV for anode A_2 and -958.8 mV for the reinforcing bar (vs MnO_2). The evolution of these potentials in the early hours after concrete casting seems to follow the temperature pattern. In the outermost anode of CKS-V2N-1I (P1) the potential evolution was similar to that observed in the CKS-V2N-1S anodes. In contrast, P2 and P5 potential recorded by CKS-V2N-1I reached more negative values, which remained over about 4 days, but like the other potential curves, evolved rapidly into values between -300 to -200 mV vs MnO_2. Also, temperature recorded by CKS-V2N-1I evolves more slowly until reaching values close to the external temperature. Based on results presented in Section 6.4, temperature alone is not likely to be responsible for the observed changes in corrosion potential however it can probably be a contributing factor. Indeed, some factors have been pointed out to explain potential changes in the first days after concrete casting. Pore solution of Portland cement concrete is mainly constituted by saturated $Ca(OH)_2$, but also Na^+ and K^+, which increases pH to more than 13 (Andrade *et al.*, 1995). This high alkalinity allows steel to develop a stable passive film as soon as fresh concrete involves the reinforcement, conferring a nobler corrosion potential, i.e., a less negative potential to the steel. However, temperature also plays an important role in the passive film development, since some of the oxides only will be formed when temperature drops to certain values. In addition to temperature and chemical structure changes of the reinforcement surface, humidity and oxygen availability also undergoes great transformations during the early days.

These results seem to indicate that CKSs, CKS-V2N-1S and CKS-V2N-1I, are providing a coherent response to daily cycles and, corrosion potential was within the range of expected values for a passive state.

6.5.3. Monitoring results during the exploration phase

Considering the CKS behaviour during the exploration or service phase, Figure 6.21 shows the results of the two innermost anodes of CKS-V2N-5I over an observation period of approximately 2 years. Along with corrosion potential and galvanic current values, Figure 6.21 presents the temperature records collected by CKS-V2N-5I and the daily precipitation records collected by a meteorological station located relatively near the structure.

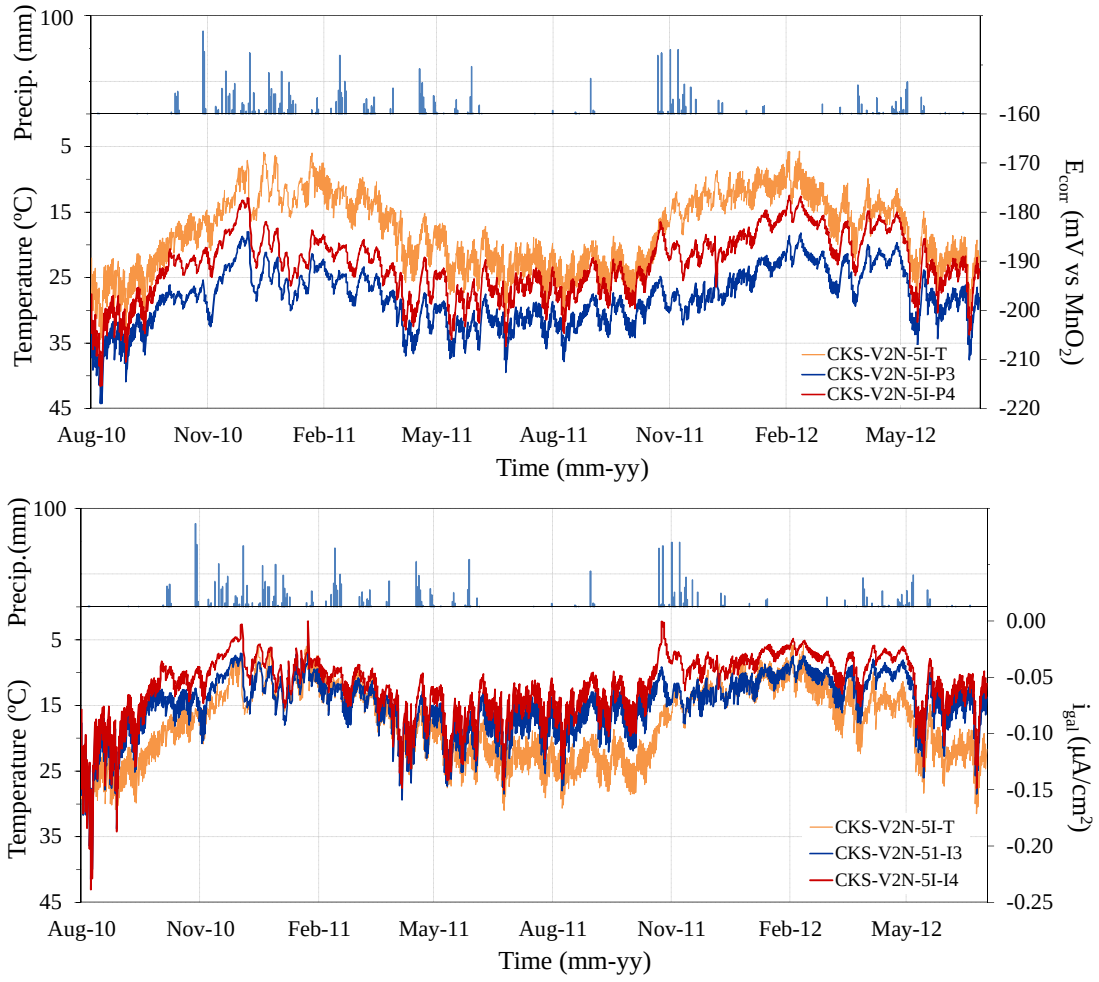

Figure 6.21 – Precipitation and long-term records of temperature, corrosion potential and galvanic current collected in CKS-V2N-5I.

Given the range of collected values, it seems that the two anodes of CKS-V2N-5I have remained passive during these two years of observation, i.e. low corrosion probability. It is also clear a good agreement between temperature and both durability parameters.

The seasonal and daily changes in temperature are in accordance with corrosion potential and galvanic current variations, registering more negative values during warm seasons (spring and summer) and less negative values during cold seasons (autumn and winter). However, durability parameters curves seem to diverge from the temperature evolution during periods of intense precipitation, this is, during autumn and winter seasons. This effect is particularly noticeable in the periods between December-10 to April-11 and November-11 to February-12. For more frequent and intense precipitation periods, corrosion potential and galvanic current become more negative, even if temperature decreases. The most important characteristic of the rain periods is not the amount of water but their length and frequency because each concrete has a maximum absorption capacity (Andrade *et al.*, 2002). In the periods with no significant precipitation, corrosion potential and galvanic current decreased on average 1.6 mv/ºC and 0.01 μA/cm²/ºC, respectively. These values are fairly similar to those observed in the laboratory (see Section 6.4).

An example of a CKS where records indicate a high corrosion probability of one of the anodes is presented in Figure 6.22. In order to assist the interpretation of results, the daily precipitation records are also presented. The continuous record of the durability parameters collected by CKS-V2N-1S seems to indicate that the three innermost anodes are passivated. In contrast, the outermost anode displays typical values of some corrosion activity, especially during periods of intense precipitation. In dry periods, the potential and galvanic current climbs up to typical values of low corrosion probability. It is interesting to observe that the precipitation records are almost mirrored with the corrosion potential and galvanic current curves.

These results show the great advantage of a continuous record in durability monitoring of concrete structures – an advanced warning in existing corrosion and corrosion development, which is difficult through discrete inspections, even with a careful selection of periods and areas to be inspected.

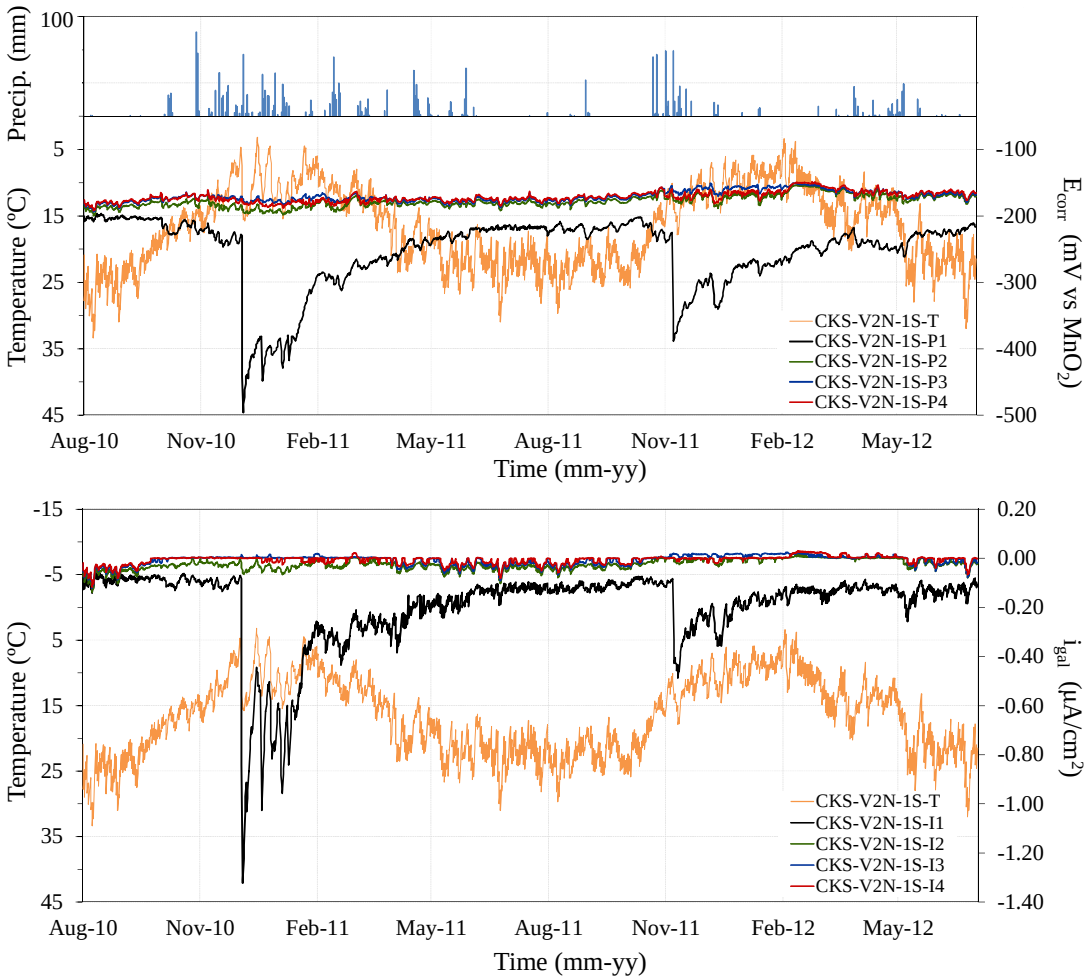

Figure 6.22 – Precipitation and long-term records of temperature, corrosion potential and temperature collected in CKS-V2N-1S.

6.6. Yachting harbour structure – Durability monitoring to improve service life prediction

6.6.1. Durability monitoring system

The main structure of the yachting harbour implanted in Leixões Port consists in a 22 m long and 30 cm thick curved wall (plan view). The wall is reinforced on each face with a Ø10//0.15 (horizontal) by Ø12//0.15 (vertical) mesh. Considering marine exposure, the lower part of the structure is a submerged zone, the middle part is in the

tidal zone, while the upper part corresponds to a splash and spray zone. Figure 6.23 shows an overview of the yachting harbour structure.

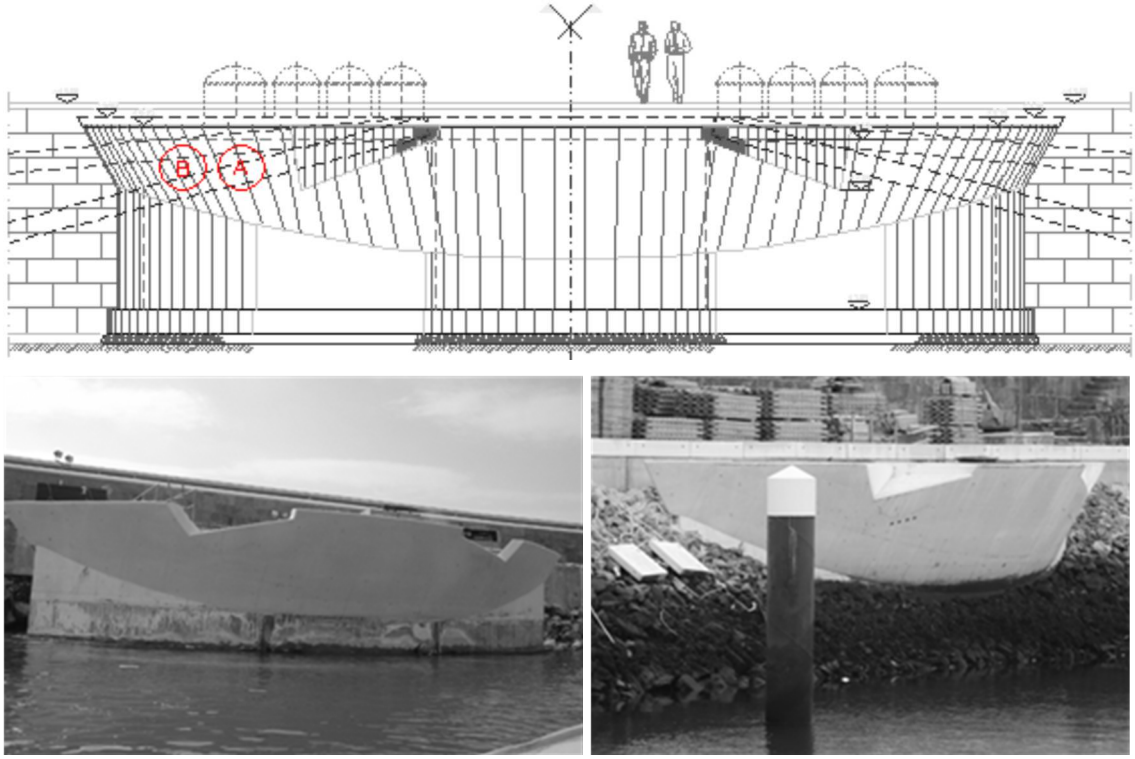

Figure 6.23 – An overview of the yachting harbour structure, including location of the instrumented areas (zone A and B).

Two areas located on the outer face of the wall, about 20 cm above maximum tide, were instrumented, zone A and B (see Figure 6.23). Each area was instrumented with a CKS and two vibrating wire strain gauges, one in the vertical alignment and the other in the horizontal alignment, see Figure 6.24. Concrete deformation given by the strain records will enable assessing concrete cracking risk. The measurements collected by the vibrating wire strain gauges must be corrected to eliminate the effect of the free thermal deformation of the wire and the concrete. For this purpose the strain gauges have an internal thermistor, which was used to measure concrete temperature. All sensors are interrogated by an automatic acquisition system installed in a central data acquisition point.

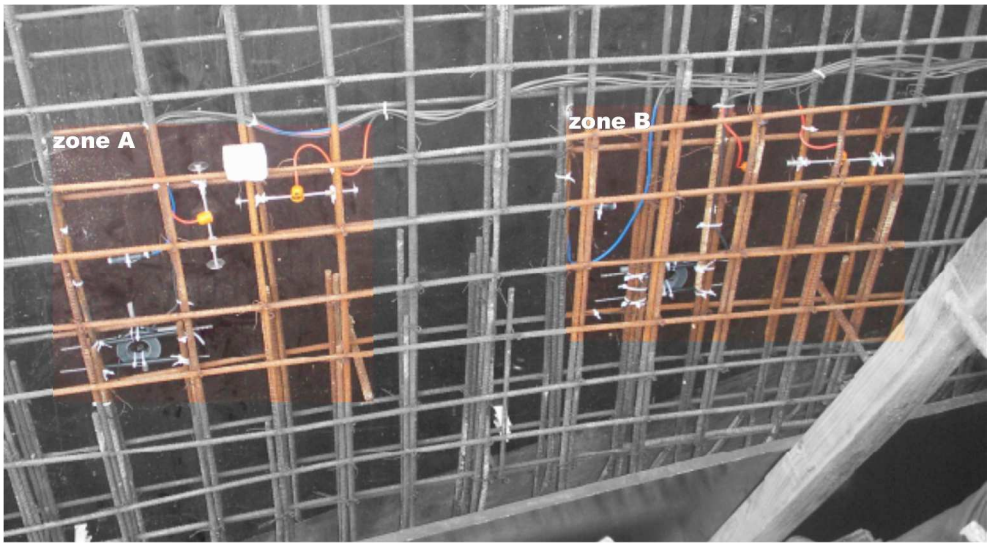

Figure 6.24 – Internal view of the instrumented areas in the yachting harbour structure (zone A and B).

In order to evaluate the influence of the reinforcement density in concrete deformations due to shrinkage, as well as, the behaviour concerning the advance of aggressive agents through the concrete cover and reinforcement corrosion, two wall models with a different amount of reinforcement were cast in-situ. The wall models were instrumented likewise the yachting harbour structure, with one CKS and two vibrating wire strain gauges (see Figure 6.23 right/below). These results are not presented in this work, for clarity's sake.

6.6.2. Concrete characterization

Concrete composition used in the yachting harbour structure was in fact, specifically designed, as an alternative solution, for the new cruise terminal building, also implanted within Leixões Port. The concrete to be used in the building was required to have special features in terms of architecture (white concrete with a good quality surface finishing), fresh state (self-compactability) and hardened state (compressive strength and high durability). A performance-based design approach, based on a probabilistic safety format, was applied to define concrete durability requirements subsequently, a central composite design was carried out to identify the best mixture, given a set of constituent materials and performance constraints (Figueiras *et al.*, 2013a). Concrete mix-proportions are presented in Table 6.3.

Concrete was produced, under normal working conditions, in a concrete plant located about 15 km from Leixões Port. Some differences in the fresh behaviour between mixes produced in the laboratory and on site were observed. Possible causes for these differences are mixing efficiency, consistency variations over time, material weighing errors, miss determination of humidity content in the aggregate and variation of materials characteristics. Regarding concrete hardened properties, slightly higher values of compressive strength and electrical resistivity and lower values of shrinkage and chloride migration coefficients were obtained compared to results of the laboratory study (see Table 6.3). Although concrete produced in-situ provided a slightly improved performance, results of tests performed with samples collected in-situ presented higher variation.

Table 6.3 – Concrete mix proportion and hardened properties characterization.

Constituent materials (kg/m³)		
Cement (CEM II/A-L 52.5N white)	416	
limestone filler	151	
Metakaolin	44	
Water	185	
superplasticizer	6.10	
sand 1	325	
sand 2	487	
coarse aggregate	744	
Hardened properties characterization		
	Laboratorial (28 days)	In situ (28 days)*
fcm [MPa]	80.4(a)	74.9(b)
fct,m [GPa]	--	5.8
Ecm [GPa]	--	44.1
Shrinkage 90d	345×10^{-6}	299×10^{-6}
Sorptivity [g/(m².min$^{1/2}$)]	--	51.11
Resistivity [Ω.m]	220.3	326.4
Dcl [m²/s] (c)	3.54×10^{-12}	2.88×10^{-12}

* tests were carried out on specimens casted in situ
(a) tests were carried out on cubes (150x150x150 mm³)
(b) tests were carried out on cylinders (ø=150 mm; h=300 mm)
(c) concrete chloride migration coefficient was determined according to LNEC E 463 (LNEC, 2004)

6.6.3. Monitoring results

Figure 6.25 and Figure 6.26 present corrosion potential, galvanic current and temperature records collected in the CKSs installed in the yachting harbour structure, during the service phase over a 2.5 years period. During this period, due to problems in the electric power supply of the acquisition system, some signal failures were observed.

A relatively significant variation in corrosion potential and galvanic current towards less negative values is observed in the early months. This increase is a consequence of variations of environmental conditions, but also should be related with the passive film development on the anodes and the variations in the moisture conditions of concrete (variations that are more pronounced in the early months). The exception is the galvanic current measured at CKS-B that starts with positive values and then tends toward negative values, near zero. The development of Fe^{3+} oxides on the surface of CKS anodes could justify this galvanic current evolution. These oxides, generally developed on steel exposed to a dry environment, may have arisen on the anodes before CKS installation in the structure. In atmospheric corrosion the proportion of Fe^{2+} and Fe^{3+} containing species is of major importance, as more Fe^{3+} is present in the rust a greater contribution of the Fe^{2+}/Fe^{3+} redox couple to the whole process is expected. This greater amount of rust (Fe^{3+} species) gives an extra source of cathodic reaction in dry conditions (Alonso *et al.*, 1998).

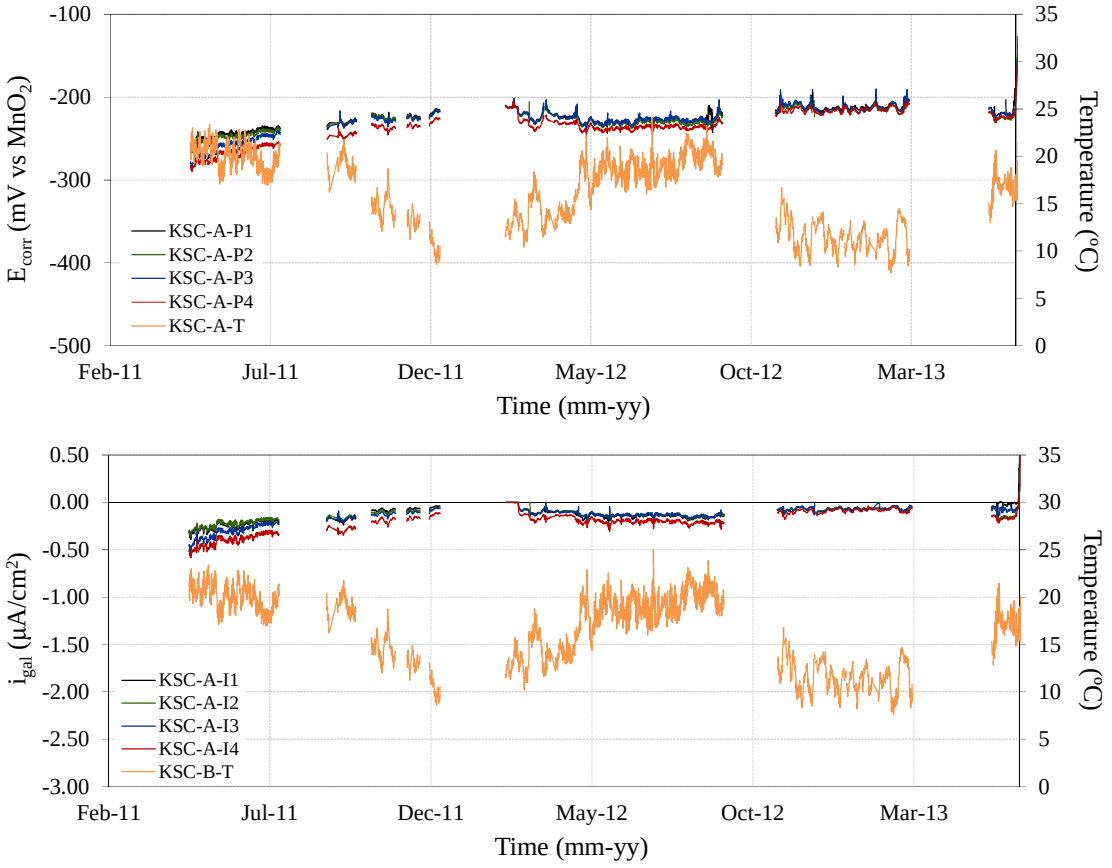

Figure 6.25 – Long-term records of temperature, corrosion potential and galvanic current collected in CKS-A.

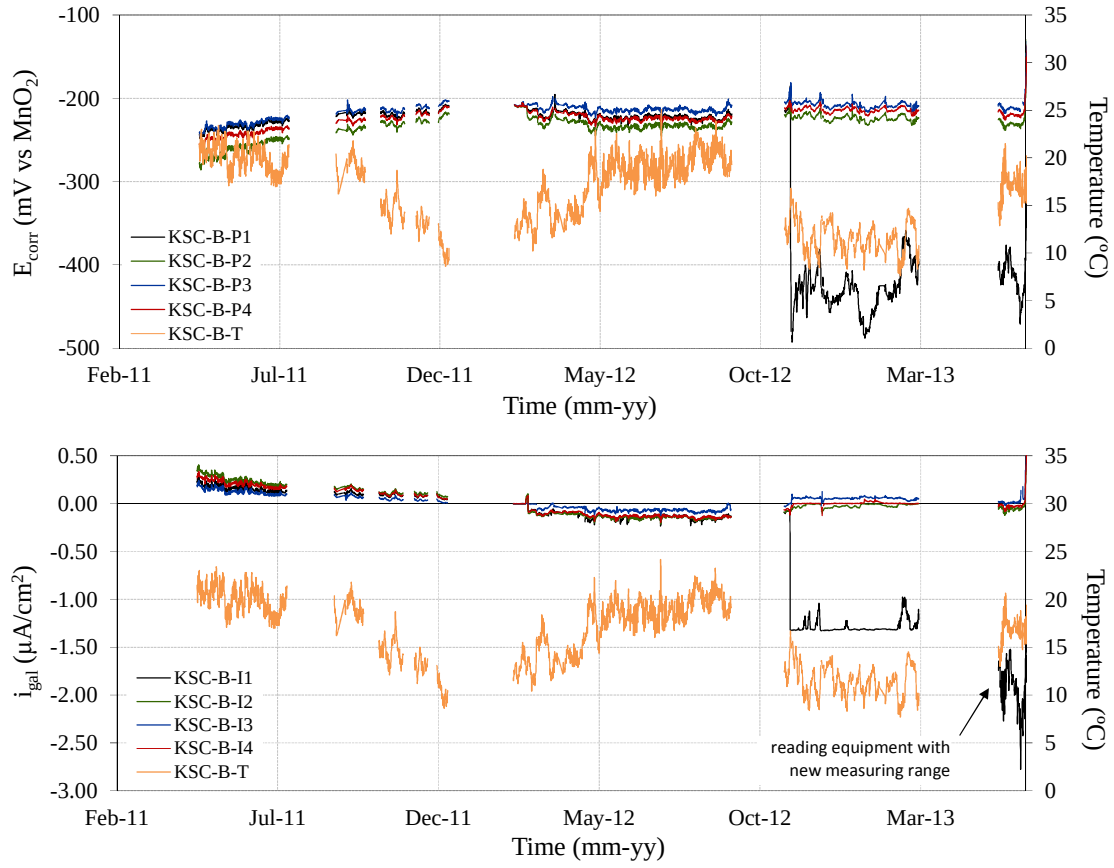

Figure 6.26 – Long-term records of temperature, corrosion potential and galvanic current collected in CKS-B.

After this initial period, corrosion potential and galvanic current values show a good agreement with the daily and seasonal cycles of temperature. Given the range of values collected in CKS-A, it seems that all the anodes are still in a passive state (low corrosion probability). However, in CKS-B a sudden change of corrosion potential and galvanic current values of the first anode was observed (CKS-B-P1 and CKS-B-I1 respectively), indicating some corrosion activity of this anode (probable anode depassivation). In the beginning of November 2012 corrosion potential of the first anode sharply decreases to values close to -500 mV, remaining in this range of values until the end of the observation period. Concerning galvanic current results, it should be mentioned that, initially, the acquisition system was designed for a maximum current of ±1.4 µA/cm² in order to have a good sensitivity in the range of passive state values. Albeit this limit, galvanic current measurements show a sudden decrease, simultaneously with the sudden decrease in corrosion potential. In June 2013 (see Figure 6.26), the acquisition system was re-designed to read values in the range of ±14 µA/cm², and during the

observation period values close to -2.5 μA/cm² were read. After depassivation of the first anode, variations observed in corrosion potential and galvanic current measurements were more significant, highlighting the greater influence of environmental conditions on the corrosion activity.

Indeed, results of the vibrating wire strain gauges may partially explain these differences in the behaviour of the CKSs installed in zone A and B. Besides the typical trend due to shrinkage and creep of concrete, results presented in Figure 6.27 show, from the outset, a clearly different behaviour of the vibrating wire strain gauge installed in zone A, in the horizontal direction. The strain evolution recorded by W-H-A is typically observed with the occurrence of a vertical crack (or a crack with a component in the vertical direction) close to the sensor head but outside its measurement field. In fact, given the adopted construction phasing, some cracks of this type it was expected to develop.

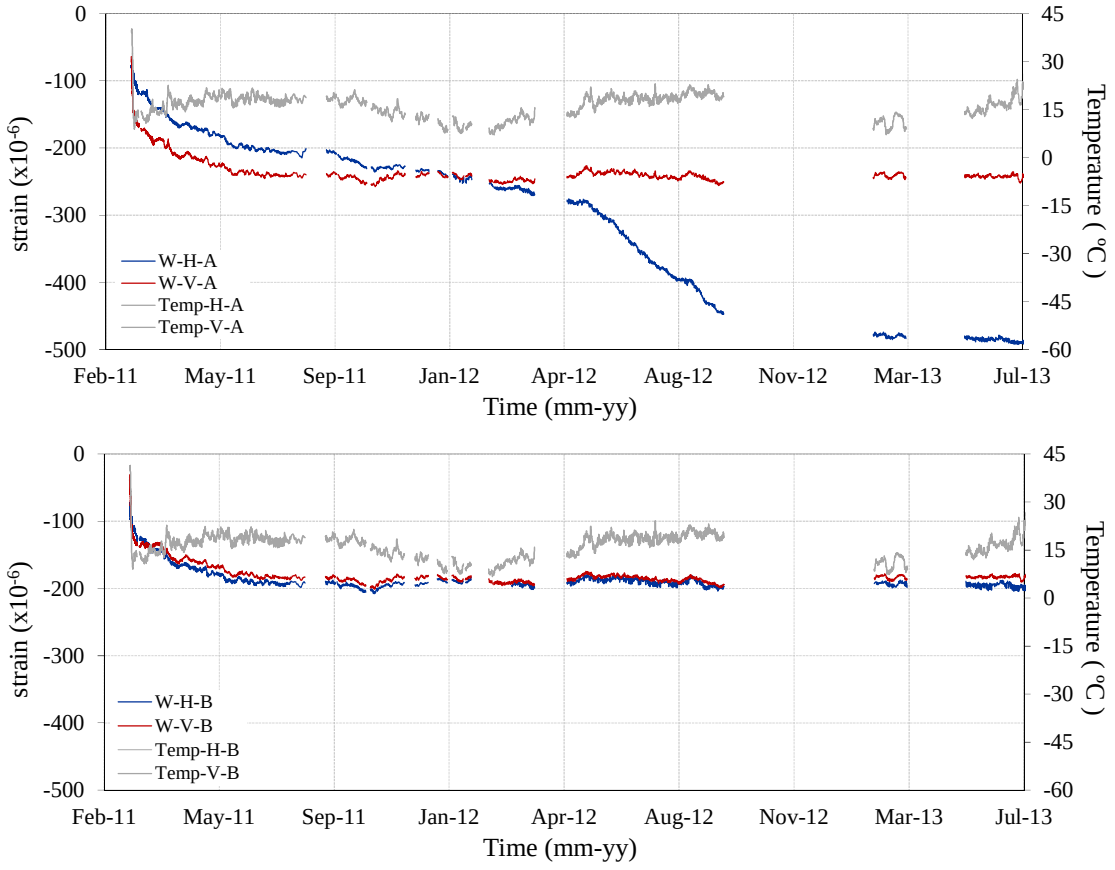

Figure 6.27 – Strain records collected by the vibrating wire strain gauge installed in zone A and B, during de service period.

Although, the pattern evolution of the strain measurements observed on the others strain gauges seems similar, values collected by strain gauges installed in zone B, W-B-H and W-B-V, are lower than those collected by the vertical strain gauge installed in zone A, W-A-V. The lowest values observed in W-B-H and W-B-V suggest that in zone B the concrete is under a greater constraint, which in this case could be provided by the higher reinforcement density. Actually, the instrumented zone B corresponds to a reinforcement overlapping zone, see Figure 6.24, and hence with a higher reinforcement density. This greater constraint might be the cause of some microcraking, not directly detected by the strain gauges. Microcraking, which usually takes place in a very wide area of the structure, facilitates the ingress of aggressive agents into concrete, which may justify the early corrosion detection in the first anode of CKS-B. It is important to consider the role of cracks in concrete, as they may reduce the effective capacity of the concrete cover layer and thereby reduce the service life of the structure, allowing a faster penetration of aggressive agents into concrete.

6.6.4. Service life prediction

Considering uncracked concrete and the spray zone where CKSs are installed, chloride penetration is essentially diffusion-controlled. Thus, the Fick's second law of diffusion can be used to predict the time variation of chloride concentration for one dimensional flow (Luping and Gulikers, 2007). Furthermore, in tidal or even splash and spray zones of marine structures, as the structure under analysis, service life is mainly determined by the initiation phase, since chloride induced corrosion rates can be very high (Andrade *et al.*, 1993). Therefore, in the present study, a serviceability limit state of depassivation was considered (structure service life equal to the initiation period). The limit state function with respect to chloride ingress and for a limit state of depassivation, can be defined by equation (6.2), according to fib-Model Code (CEB-FIP, 2012) and LNEC specification E 465 (LNEC, 2007):

$$t_L = t_i = \left(\left[\left(\frac{2}{c} erf^{-1}\left(1 - \frac{C_r - C_0}{C_s - C_0}\right)\right)^{-2} \frac{1}{k_{D,c} \cdot k_{D,RH} \cdot k_{D,T} \cdot D_0 \cdot {t_0}^n} \right]^{\frac{1}{1-n}} \right) \cdot \lambda \qquad (6.2)$$

where t_i is the initiation period equal to the design service life (t_L); c is the concrete cover (m); erf is the error function; C_r is the chloride threshold level necessary to depassivate reinforcing steel, in percentage of cement by weight (%); C_s is the chloride content on the concrete surface, in percentage of cement by weight (%); C_o is the initial chloride content, in percentage of cement by weight (%); $k_{D,c}$ is the factor that considers the influence of curing conditions; $k_{D,RH}$ and $k_{D,T}$ are coefficients related to the influence of relative humidity and temperature on the diffusion coefficient, respectively; D_0 is the apparent diffusion coefficient (m^2/s), obtained from migration laboratory tests performed at the reference age t_0 (s); n is the concrete's ageing factor, which represents the time dependence of the diffusion coefficient or the increasing ability of the concrete to resist chloride penetration over time; and λ is the model uncertainty. The chloride content C_s at the concrete surface depends on geometrical and environmental conditions, and according to the specification of the Portuguese National Annex of the NP EN 206-1 (IPQ, 2007), E 465 (LNEC, 2007), C_s can be obtained using the following equation (equation (6.3)):

$$C_s = C_b \cdot 2.5(w/b) \cdot k_{vert} \cdot k_{hor} \cdot k_{temp} \tag{6.3}$$

where C_b is the surface chloride content in percentage (%) that accounts for the salinity of the seawater at the Portuguese coast (21 g/l), seawater mean temperature (16±2)ºC and the environmental exposure classes (XS1, XS2 and XS3); w/b is the water/binder ratio; k_{vert} and k_{hor} are coefficients related to environmental exposure considering the concrete location related to sea level and distance to sea coast, respectively; and k_{temp} is the coefficient that accounts for concrete temperature.

Table 6.4 shows the input parameters characterization use in the concrete mix-design phase and presented in detail in Figueiras *et al.* (2013a). In the case of stochastic variables a statistical characterization is presented, namely the probability distribution type, the average and standard deviation. The values adopted for characterization of the model parameters were based on data provided by E 465 (LNEC, 2007), fib-Model Code (CEB-FIP, 2012), DuraCrete (2000), Nokken *et al.* (2006) and Marques *et al.* (2012).

Table 6.4 – Parameters characterization of chloride diffusion coefficient model for a probabilistic analysis.

Variable	Distribution	Mean value (μ)	Stand. deviation (σ)	Observations
λ	normal	1	0.15	
c	lognormal	60 mm	7 mm	design value
D_o	normal	3.54×10^{-12} m²/s	2.00×10^{-14} m²/s	value obtained in laboratory tests
t_o	deterministic	28 days	-	
$k_{D,c}$	deterministic	1.0	-	corresponding to 7 days curing
$k_{D,RH}$	deterministic	1.0	-	corresponding to the exposure class XS3
$k_{D,T}$	normal	0.8	0.16	corresponding to a mean concrete temperature of 15 ºC
n	normal	0.54	0.06	
C_r	normal	0.4%	0.048%	
C_s	normal	3.19%	0.319%	
C_b=3.0%				corresponding to 21 g/l salinity, 16±2 ºC and XS3
w/b=0.354				
k_{vert}=1.0				corresponding to the exposure class XS3
k_{hor}=1.0				corresponding to a distance of the concrete surface from the coast of 0 km
k_{temp}=1.2				corresponding to a mean surface concrete temperature of 15 ºC

As some parameters are uncertain and can also vary widely in space and time, some of the input data that are assumed in prediction models could be very different from reality and lead to inaccurate predictions. Service life predictions using probabilistic models updated with monitored field data can provide more reliable assessment of the reinforcement corrosion probability compared to the deterministic models. Such updated probabilistic models can help to optimize intervention strategies, thus improving life cycle performance, extending service life and reducing life-cycle cost (Cusson *et al.*, 2011). Field data can be obtained through periodic inspections, using non-destructive or limited destructive techniques, and from a long-term continuous monitoring durability system, as the system installed in this yachting harbour structure.

Two parameters considerably affected by the exposure conditions and with clear time dependence, are the concrete diffusion coefficient and the surface chloride content (Costa and Appleton, 1999; Cusson *et al.*, 2011). The time dependence of the diffusion coefficient is already taken into consideration in the prediction model presented in

equation (6.2) through the concrete ageing factor ***n***. However an accurate assessment of this parameter is critical due to its dependence on the type of cimentitious materials used, the mixture proportions and the concrete exposure conditions. Another concrete parameter with influence on service life is the chloride threshold, which is also highly uncertain as it depends on environmental conditions and properties of concrete and steel (Cusson *et al.*, 2011). According to Cusson *et al.* (2011) the use of deterministic parameters assessed in the structure at the age of 10 years could provide comparable estimates of service life to models using probabilistic values. Concrete cover thickness is a structure parameter, which is relatively easy to assess, and has a substantially importance in the service life prediction (Figueiras *et al.*, 2013a).

In order to initiate the update of the service life prediction model established during the concrete mix-design phase, some specimens were moulded in-situ to assess the 28 days hardened properties of the concrete used in the yachting harbour. Furthermore, an inspection was carried out on the structure after 820 days of exposure (approximately 2.2 years). During this inspection a local survey of concrete cover thickness was carried out on the structure and some cores were drilled from the wall models (see Figure 6.23) to evaluate the chloride diffusion coefficient and the surface chloride.

The apparent chloride diffusion coefficient obtained from migration tests performed at 28 days in specimens moulded in-situ was of 2.88×10^{-12} m^2/s with a standard deviation of 4.80×10^{-13} m^2/s (see Table 6.3). From the tests performed on the cores drilled after 820 days of exposure, a value of 8.88×10^{-13} m^2/s and 0.273% was obtained for the apparent chloride diffusion coefficient and the surface chloride content, respectively. These values do not enable in itself an accurate assessment of the time dependence of both the apparent chloride diffusion coefficient and the surface chloride content. This assessment will only be possible by providing more data from future inspections over time. The data of the cover thickness survey, presented in Figure 6.28, were adjusted to a normal probability density function with a mean of 48.81 mm and a standard deviation of 6.05 mm. It should be stressed that although cover thickness data does not strictly meet the normality tests (Kolmogrov-Smirnov and Shapiro-Wilk tests) a normal distribution was assumed.

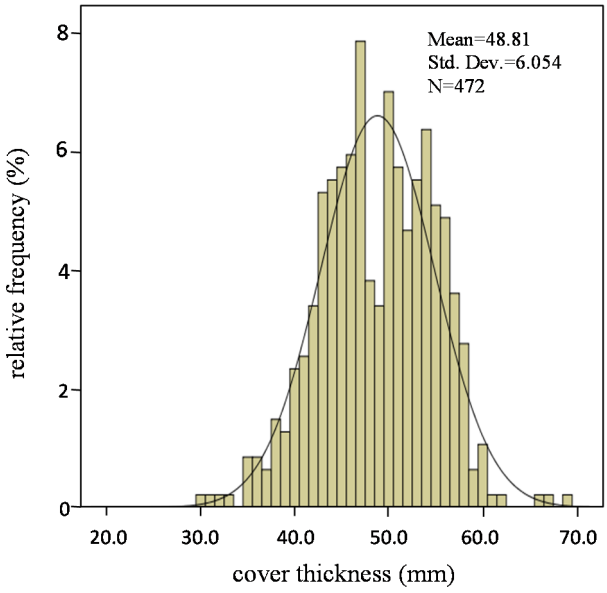

Figure 6.28 – Relative frequency of concrete cover thickness and the corresponding fitted normal probability density function.

Two service life predictions using probabilistic analysis were performed: the first analysis was performed using the available data in the design phase, data provided in Table 6.4; and the second analysis using the data of the design phase but updating the apparent chloride diffusion coefficient at 28 days and the concrete cover thickness. The probabilistic analysis were implemented through the Latin Hypercube simulation method, using a commercial software (@Risk, 2013) and applying a set of 10^5 simulations, thus ensuring a high accuracy of the result. The Kolmogorov-Smirnov test was performed to evaluate the quality of the generated samples. According to the European standard NP EN 1990 (IPQ, 2009), the yachting harbour structure fits into the RC1 reliability class, which means that the probability of failure for serviceability limit state should not exceed 12×10^{-2} (E 465 (LNEC, 2007)). The predictions of the penetration depth of the critical chloride content obtained by both analyses are presented in Figure 6.29. The results show less conservative predictions after this initial model update, although both analyses indicate that the reinforcement depassivation only occurs after 120 years of exposure. Both analyses also show that chloride ions soon reached 20 mm cover depth and thereafter concrete cover thickness plays a significant influence on the structure service life.

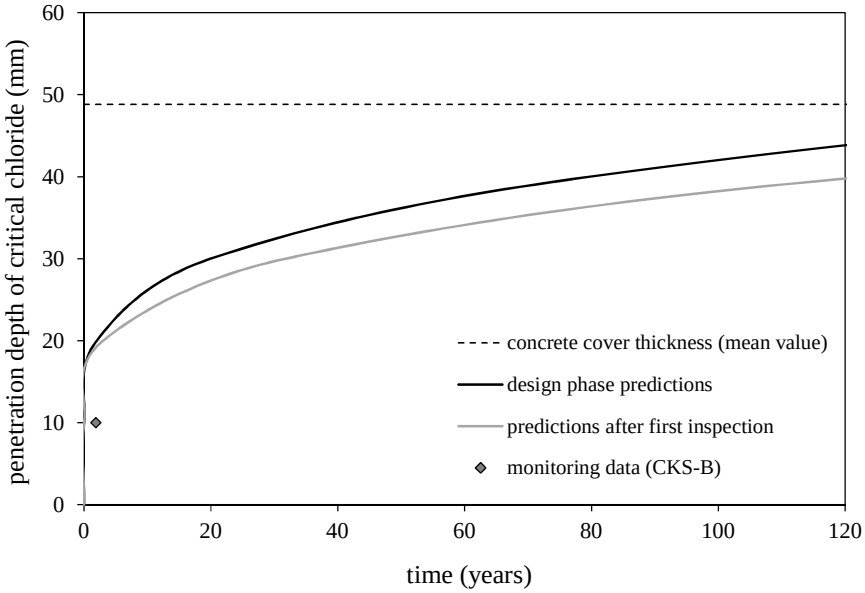

Figure 6.29 – Predictions of the critical chloride penetration over time.

The great advantage of long-term monitoring, using sensors like those presented in this work, is to provide permanent information of the real concrete critical depth (depassivation front). According to the records collected by CKS-B the depassivation front has reached, in the assessed area, the depth of 1 cm (depth of the first anode) after 1.9 years (see Figure 6.29). Nevertheless, records collected by CKS-A indicate that after 2.5 years the penetration depth of the critical chloride content has not yet reached 1 cm. It is therefore concluded, in the light of the monitoring results, that the predictions performed in the design stage and after first inspection are quite conservative. The results from the durability monitoring system installed in the structure could also be used to improve service life prediction of the structure however, further data will be necessary.

It should be noted that the great advantage of long-term monitoring, using sensors like those presented in this research work, is to provide permanent information of the real concrete critical depth (depth of the critical chloride content). As the critical chloride contents for reinforcement corrosion depends on many factors this information is a great advantage that cannot be replaced by data from chloride profiles obtained from the structures.

6.7. Conclusions

This chapter presented a durability monitoring system which integrates a sensorial component, a data acquisition component and a communication and data processing component. The sensorial component comprises corrosion kit-sensors that incorporate a galvanic current sensor, a reference electrode and a temperature sensor. The CKS provides information on the galvanic current and corrosion potential of small anodes placed along the concrete cover layer and of the most external reinforcing bar. Based on the results presented along this chapter the following conclusions can be drawn:

- This durability monitoring system enables monitoring the advance of aggressive agents into the concrete cover, predict the time to corrosion initiation and evaluate the corrosion state of the most external reinforcing bar. Implementation of this type of durability monitoring systems can be useful to assess concrete durability, predict service life more accurately and to take in due time, the decision on adequate protection.

- The great advantage of long-term monitoring, using sensors like those presented in this work, is to provide permanent information of the real concrete critical depth (depth of the critical chloride content). As the critical chloride content for reinforcement corrosion depends on many factors this information is a great advantage that cannot be replaced by chloride profiles obtained from the structure.

- Galvanic current and corrosion potential measurements are quite simple to perform and, as no external current is applied, anodes potential are always in the range of natural potential of the respective metal, which is an advantage compared with measuring certain durability parameters that require prior external polarization. Although galvanic current observed after a short circuit time is a large overestimation of the real steady state corrosion current density, for practical reasons, a short measuring time is the most convenient.

- Laboratory tests showed that galvanic current and corrosion potential are sensitive to environmental conditions (temperature and humidity), especially when CKS anodes are under active corrosion process. Temperature and humidity induce variations on the nature and composition of the anode oxides layer, ions mobility through the electrolyte, kinetics of corrosion reactions and oxygen availability. Thus, variations observed in corrosion potential and galvanic current depend mainly on how environmental parameters affect these factors.

- In a short-term temperature test, as temperature increases, the corrosion potential and the galvanic current become more negative, however corrosion potential takes longer to reach a constant value. In the kinetics of electrochemical reactions of the anode oxide layer, due to temperature variation, some reactions take place instantly while others will occur over time. The durability parameters curves corresponding to heating and cooling of concrete show some hysteresis.

- The accelerated corrosion test conducted in the laboratory demonstrated the good performance of the CKS against the advance of aggressive agents into the concrete cover.

- Laboratory and in-situ results highlight the importance of continuous monitoring, given the influence of environmental conditions on the corrosion process. The CKS, when installed in real structures, also proved to be quite sensitive to the environmental conditions and corrosion activity of the anodes.

- The durability monitoring systems presented in this work enable an automatic and continuous acquisition of CKSs measurements. After a proper processing, raw data collected by the monitoring systems can be provided through a website. Noteworthy that during these first years of service, the durability monitoring systems installed in two different structures, have presented a good electrical performance.

- The installation of concrete deformation transducers, e.g. vibrating wire strain gauges, along with the CKSs proved to be very useful since it enables assessing cracking risk, which may indicate possible reduction of the effective capacity of the concrete cover layer and thereby a cutback of the structure service life.

- Service life predictions performed during the design phase should be validated and updated by the effective use of data obtained from field monitoring, during periodic inspections or in long-term continuous monitoring systems. Some of the input data that are commonly assumed in the design phase, even those selected from the literature, may be quite different from reality and can also vary widely in space and time. Monitoring results from yachting harbour structure seems to indicate that the predictions performed in the design stage and after the first inspection are conservative.

Chapter 7

Conclusions and future research

7.1. Conclusions and main contributions

The present research work has been directed to contribute to performance-based design of SCC ensuring durability of concrete structures. The main purposes were to explore an integrated view of durability of concrete structures, to ensure durability and to predict service life of structures more accurately. In this sense, developments were performed in the concrete design phase, as well as, in the field assessment of concrete performance. Following the sequence of the four main objectives previously stated in Chapter 1, the main contributions and more relevant conclusions achieved by the current PhD research are the following:

Durability performance-based design

The performance-based design methodology presented in this research work enables the systematization of the mixture design process of SCC exposed to severe marine environment. Limit values of the durability indicators were specified through a probabilistic calculation of the limit state functions, established on the basis of target service life, limit state criterion and degradation mathematical models. Once the set of concrete requirements (fresh and hardened properties) was defined, mixture optimization was derived from numerical models established on the basis of a factorial central composite design. In order to simplify SCC design, the study was developed in

two phases: first at mortar level and then at concrete level. Based on the presented experimental studies and result analyses the following conclusions can be drawn:

- Although the methodology has been applied for a structure exposed to severe marine environment, application to other types of environmental exposure is only limited by the accuracy of the mathematical models for modelling relevant degradation mechanisms.

- For structures in severe marine environment, reinforcement corrosion is the main degradation mechanism and a serviceability limit state of depassivation should be considered. In these cases the most current durability indicator is the apparent chloride diffusion coefficient measured by the migration test, although the electrical resistivity under saturated conditions turns out to be an interesting alternative.

- Electrical resistivity proved to be a more rapid and economic method to predict resistance of concrete to chloride ion ingress. However, it requires a prior knowledge of the reaction factor of chlorides with cement phases and the transference number of chloride ions in concrete. Assessment of electrical resistivity is performed by a straightforward and non-destructive test, with good reproducibility and accuracy.

- In a full probabilistic analysis a careful characterization of the model parameters is very important to obtain realistic threshold values. A sensitivity analysis helps to define the most influential parameters, and therefore to take additional care in their characterisation (distribution type, average value and standard deviation). It was found that in the chloride diffusion coefficient model, the most influential parameters are the ageing factor (n) and the concrete cover thickness (c), while the least influential model parameters are the chloride threshold (C_r) and the chloride content on the concrete surface (C_s).

- In the case of electrical resistivity, a partial safety factor approach was carried out due to an insufficient amount of statistical information on some of the model parameters.

- An experimental plan conducted according to a central composite design provides a systematic methodology to identify optimal mixes given a set of constituents and performance constraints. Data collected during the experimental plan can be used to establish numerical models relating mixture parameters with fresh and hardened properties of paste, mortar and concrete.

- This statistical experimental approach, generally used to model fresh properties, was extended to durability properties of paste, mortar and concrete. In this research work the methodology was extended to the chloride diffusion coefficient and electrical resistivity, however its application has also been validated to water absorption by capillarity, porosity accessible to water and carbonation. The ability to mathematically model the influence of mixture parameters on a given response variable, through an experimental design methodology, is determined mainly by the choice of the relevant factors, the range of variation of the response in the experimental plan, accuracy of test methods and experience of the operator performing tests.

- Using mortar testing as a previous step in concrete design, greatly simplifies experimental work, however it requires prior knowledge of the link between mortar/paste and concrete performance requirements (fresh and hardened properties).

Linking fresh properties of paste and SCC mortar

A procedure, based on statistical experimental design, was used to establish the link between fresh properties of paste and SCC mortar, for a given set of materials. The statistical experimental design allows deriving numerical models relating mixture

parameters with fresh properties of paste and mortar. The derived numerical models were used to define an area, labelled by self-compacting zone at paste level (SCZ), where fresh properties of the paste enable the design of SCC mortar. From this study the following main conclusions can be drawn:

- As expected, empirical tests performed in paste ($D_{flow,paste}$ and w_{free}) correlate with the rheological parameters of paste, namely, yield stress and plastic viscosity, which seems to indicate that both types of tests can be used to characterize fresh paste behaviour.

- Rheological tests performed at 10 and 23 minutes, after starting mixing, showed an increase of both, yield stress and plastic viscosity, but it is the yield stress that seems particularly sensitive due to the hydration reaction and associated microstructural changes, loss of water by evaporation and loss of dispersing efficiency of the superplasticizer.

- Trend lines establishing the relationship between paste rheological parameters and mortar target properties ($D_{flow,mortar}$ and $T_{funnel,mortar}$) were computed. The shape of the trend line reflects the need of compromise between yield stress and plastic viscosity, which seems to indicate that the increase in aggregate content required an increase of yield stress to plastic viscosity ratio and decreases the influence of the plastic viscosity on the workability of the mortar as compared to yield stress. Similar conclusions were found when empirical tests were used to characterize paste fresh properties.

- Higher aggregate contents, which correspond to a shorter average distance between aggregate particles, demand a paste with lower yield stress and lower plastic viscosity (more fluid paste), while lower aggregate contents require a paste with higher yield stress and viscosity (more viscous paste). For a given aggregate content in mortar it is possible to achieve self-compacting mortar from paste with rheological properties within a certain range, however, these properties should vary according to the established trend line.

- The defined SCZ can simplify the test protocol required to optimize a given SCC mixture, reducing the extent of laboratory work, testing time and materials used. The SCZ was defined for a specific set of materials, and therefore, variations in material characteristics are expected to change the relative size of the SCZ. Depending on the level of deviation, a limited number of mixtures can be prepared to adjust the final composition. The SCZ can also provide the basis for quality control and further behaviour assessment of new materials (addition, superplasticizer or viscosity agent).

Linking durability properties of paste, mortar and SCC

Effective Medium Theories were used to predict the influence of the aggregate (aggregate content, aggregate skeleton and aggregate shape) on some durability properties, namely, electrical resistivity and chloride diffusion coefficient. Different models derived from the D-EMT were explored and the predictions provided by the Hashin-Shtrikman bounds were also assessed. Based on the experimental study and result analyses, the following conclusions can be drawn:

- Self-compacting concrete and mortar were assumed as a composite material with two distinct phases, a cement paste phase in which insulating aggregate grains of various sizes and shapes are discontinuously embedded. Aggregate was considered as an insulating phase, given its high resistivity and low diffusivity compared to cement paste. The influence of ITZ on SCC durability properties was considered to be minor, and therefore the ITZ was assumed as part of the cement paste matrix, with the same properties.

- To predict aggregate influence on mortar/concrete properties the D-EMT seems to be the EMTs that best fits the concrete problem, once this formulation is used for materials in which one phase always percolates and is also valid for less diluted suspensions.

- For each Vs/Vm a good correlation between resistivity of paste and mortar was found, showing that aggregate increases mixture resistivity. Comparing

experimental data with D-EMT formulation, it seems that the ITZ zone has little influence on the electrical resistivity of self-compacting mortar and the main effect of aggregate is blocking and redirecting conductive flow. The D-EMT formulation for not diluted suspension of insulating spherical inclusions predicts electrical resistivity fairly accurately (average error prediction was 4.1%).

- A D-EMT formulation for ellipsoidal inclusions with an aligned orientation and electrical field aligned according to the semi-major axis of the ellipsoids was the model that best fitted the experimental results of electrical resistivity and chloride diffusion coefficient. The average prediction error was 4.3% for the electrical resistivity and 3.0% for the chloride diffusion coefficient. Concrete casting direction affects aggregate alignment in the cement paste, therefore this effect should be considered when selecting the most appropriate model to predict concrete properties.

- The lower bound established by the Hashin-Shtrikman variational analysis has also provided a very similar prediction compared to experimental results. A prediction error of 4.4% and 4.1% was achieved for the electrical resistivity and chloride diffusion coefficient, respectively.

- EMTs cannot be directly applied to predict the non-steady-state chloride diffusion coefficient, therefore, a relationship has been established to determine concrete non-steady-state chloride diffusion coefficient by EMTs, without the explicit assessment of the binding factor.

- The applied formulations may also be extended to evaluate other SCC durability properties, such as the oxygen permeability coefficient or the carbon dioxide diffusion coefficient.

Monitoring to improve service life predictions

A durability monitoring system integrating a sensorial component, a data acquisition component and a communication and data processing component was implemented. The sensorial component comprises corrosion kit-sensors that incorporate a galvanic

current sensor, a reference electrode and a temperature sensor. The CKS provides information on the galvanic current and corrosion potential of small anodes placed along the concrete cover layer and of the most external reinforcing bar. The durability monitoring system was installed in two structures, the Lezíria Bridge and a yachting harbour structure. Given the results obtained in the laboratory and in-situ, the main following conclusions can be drawn:

- The implemented durability monitoring system enables to monitor the advance of aggressive agents into the concrete cover, predict the time to corrosion initiation by extrapolation and evaluate the corrosion state of the most external reinforcing bar. Implementation of this type of durability monitoring systems can be useful to assess concrete durability, predict service life more accurately and to take in due time, the decision on adequate protection.

- The great advantage of long-term monitoring, using sensors like those presented in this research work, is to provide permanent information of the real concrete critical depth (depth of the critical chloride content). As the critical chloride contents for reinforcement corrosion depends on many factors this information is a great advantage that cannot be replaced by data from chloride profiles obtained from the structures. Furthermore, galvanic current and corrosion potential measurements are quite simple to perform and as no external current is applied, anodes potential are always in the range of natural potential of the respective metal.

- Laboratory and in-situ results highlighted the importance of continuous monitoring, given the influence of environmental conditions on the corrosion process, especially when CKS anodes are in an active corrosion process. Temperature and humidity induce variations on the nature and composition of the anode oxides layer, ions mobility through the electrolyte, kinetics of corrosion reactions and oxygen availability. Thus, variations observed in corrosion potential and galvanic current depend mainly on how environmental parameters affect these factors.

- Short-term temperature tests show that in passive state, as temperature increases, the corrosion potential and the galvanic current become more negative, decreasing on average, only, -1.6 mv/ºC and 0.0159 μA/cm²/ºC, respectively. It was also observed that corrosion potential takes longer to reach a constant value at each temperature level than galvanic current. In fact, variations observed in corrosion potential depend mainly on how temperature affects the nature, composition and distribution of the anode oxide layer. In the kinetics of electrochemical reactions of the anode oxide layer, due to temperature variation, some reactions should take place instantly while others will occur over time.

- Noteworthy that during these first years of service, the durability monitoring systems installed in two different structures, have presented a good electrical performance.

- The installation of concrete deformation transducers, e.g. vibrating wire strain gauges, with the CKSs proved to be very useful since it enables assessing cracking risk, which may indicate possible reduction of the effective capacity of the concrete cover layer and thereby a reduction of the structure service life.

- Service life predictions performed during the design phase should be updated and validated by the effective use of data obtained from field monitoring, during periodic inspections or in long-term continuous monitoring systems. Some of the input data that are commonly assumed in the design phase, even those selected from the literature, may be quite different from reality and can also vary widely in space and time. Monitoring results from yachting harbour structure seems to indicate that the predictions performed in the design stage and after the first inspection are conservative.

7.2. Future work

Possible directions in which the present research work can be extended are pointed out below.

The selection of constituent materials, the design of mix-proportion and the appropriate casting practices are essential factors to achieve specified performance-based requirements. Furthermore, sustainable design of highly durable concrete requires an adequate selection and combination of constituent materials, with exploitation of synergies between cement and additions. Thus, in order to simplify the sustainable design of a concrete mixture and ensure the required durability, it would be important to define performance ranges, in terms of durability indicators, for "new" additions or combination of additions. These performance ranges will allow selecting, at the outset, the combination of materials that ensure compliance of the defined requirements. Furthermore, within the material combinations that satisfy the established requirements, performance ranges enable the selection of the material combination that will lead to the most economical concrete composition. The link established between paste, mortar and concrete is undoubtedly a great advantage given the possibility of carrying out studies at paste level.

Concerning the prediction of transport properties of concrete from cement paste behaviour using the effective medium theories, studies conducted in the present research work show the great potential of these theories in this field. However, more parametric studies should be performed with a wide range of aggregate shape and aggregate orientation.

There are many aspects in which further research is needed to improve prediction of service life. Some of the main issues are pointed out below:

- A deeper and more exhaustive characterization of environmental actions that induce damage, with data collection and respective probabilistic analysis.

- An extensive study of materials performance, with a probabilistic analysis, to better quantify the related parameters on degradation models. Considering the results of the sensitivity analysis performed in the present research work

and the lack of available data, concrete´s ageing factor seems to be the parameter in the chloride diffusion model that most urgently needs thorough characterization. Furthermore, until now data collected in real structures enabling a better characterization of the models parameters has been lacking.

- Construction quality and variability must be considered in service life prediction. In this sense, establishing effective plans for collecting field data, adapted to each structure and exposure environment, seems to be essential to ensure accuracy of the service life prediction of concrete structures.

- Data collected by the durability monitoring systems in real structures provide important information. However interpretation of this data and incorporation into degradation models and structure management programs need further development. In this regard, more pilot structures, in actual environments, must be deployed, allowing to compare monitoring data with data collected in detail and thorough inspection campaigns.

References

@Risk (2013). Risk analysis and simulation software - Add-in for Microsoft Excel. Palisade Corporation. USA.

AFGC (2007). Concrete design for a given structure service life: durability management with regard to reinforcement corrosion and alkali-silica reaction: state of the art and guide for the implementation of a predictive performance approach based upon durability indicators. Paris, France: Association Française de Génie Civil (AFGC): Working group on concrete design for a given structure service life.

Alonso, C.; Andrade, C.; Nóvoa, X. R.; Izquierdo, M. and Pérez, M. C. (1998). Effect of protective oxide scales in the macrogalvanic behaviour of concrete reinforcements. Corrosion Science, 40(8): pp. 1379-1389.

Alonso, C.; Castellote, M. and Andrade, C. (2000). Dependence of chloride threshold with the electrical potential of reinforcements. In: Proceedings of the Second International RILEM Workshop on Testing and Modelling the Chloride Ingress into Concrete, pp. 415-425. C. Andrade and J. Kropp (Eds.), RILEM Publications SARL.

Andrade, C. (1993). Calculation of chloride diffusion coefficients in concrete from ionic migration measurements. Cement and Concrete Research, 23(3): pp. 724-742.

Andrade, C. (2004). Calculation of initiation and propagation periods of service life of reinforcements by using the electrical resistivity. In: Proceedings of the First International RILEM Symposium on Advances in Concrete Through Science and Engineering: A Tribute to Arnon. J. Weiss, K. Kovler, J. Marchand and S. Mindess (Eds.), RILEM Publications SARL. Evanston.

Andrade, C.; Alonso, C.; Artega, A. and Tanner, P. (2000). Methodology based on the electrical resistivity for the calculation of reinforcement service life. In: Proceedings of the 5th CANMET/ACI - International Conference on Durability of Concrete, pp. 899-915. V. M. Malhotra (Ed.), American Concrete Institute (ACI). Barcelona, Spain.

Andrade, C.; Alonso, C. and Molina, F. J. (1993). Cover cracking as a function of bar corrosion: Part I - experimental test. Materials and Structures, 26: pp. 453-464.

Andrade, C.; Alonso, C. and Sarría, J. (2002). Corrosion rate evolution in concrete structures exposed to the atmosphere. Cement and Concrete Composites, 24(1): pp. 55-64.

Andrade, C. and Buják, R. (2013). Effects of some mineral additions to Portland cement on reinforcement corrosion. Cement and Concrete Research, 53: pp. 59-67.

Andrade, C.; Castellote, M. and d'Andrea, R. (2011). Measurement of ageing effect on chloride diffusion coefficients in cementitious matrices. Journal of Nuclear Materials, 412(1): pp. 209-216.

Andrade, C. and d'Andréa, R. (2010). Concrete mixture design on electrical resistivity. In: Proceedings of the Second International Conference on Sustainable Construction Materials and Technologies, pp. 109-119. T. Naík, F. Canpolat, P. Claísse and E. Ganjían (Eds.), Ancona; Italy.

Andrade, C. and González, J. A. (1978). Quantitative measurements of corrosion rate of reinforcing steels embedded in concrete using polarization resistance measurements. Materials and Corrosion, 29(8): pp. 515-519.

Andrade, C.; Maribona, I. R.; Feliu, S.; González, J. A. and Feliu Jr, S. (1992). The effect of macrocells between active and passive areas of steel reinforcements. Corrosion Science, 33(2): pp. 237-249.

Andrade, C.; Merino, P.; Nóvoa, X. R.; Pérez, M. C. and Soler, L. (1995). Passivation of reinforcing steel in concrete. Materials Science Forum, 192-194: pp. 891-898.

Andrade, C.; Prieto, M.; Tanner, P.; Tavares, F. and d'Andrea, R. (2013). Testing and modelling chloride penetration into concrete. Construction and Building Materials, 39: pp. 9-18.

Andrade, C.; Rio, O.; Castillo, A.; Castellote, M. and Andrea, R. (2007). A NDT performance method based on electrical resistivity for the specification of concrete durability. In: Proceedings of the Thematic Conference on Computational Methods in Tunneling. J. Eberhardsteiner (Ed.), Vienna, Austria.

APDL. (2012). Administração dos Portos do Douro e Leixões SA. Available from: https://www.apdl.pt/gca/?id=1271859702 (Accessed in 2012-09-20).

Arup, H.; Klinghoffer, O. and Mietz, J. (1997). Long-term performance of MnO_2 - reference electrodes in concrete. In: Proceedings of the CORROSION/97, pp. 1-11. New Orleans, Louisiana.

ASTM (1997). C1202 - Standart test method for electrical indication of concrete's ability to resist chloride ion penetration. American Society for Testing and Materials. USA.

ASTM (2009). C876 - Standard test method for corrosion potentials of uncoated reinforcing steel in concrete. American Society for Testing and Materials. USA.

Bakhoum, M. M.; Sobrino, J. A. and *et al.* (2010). Structural Engineering Documents 12 - Case Studies of Rehabilitation, Repair, Retrofitting, and Strengthening of Structures. Switzerland: IABSE, AIPC, IVBH.

Banfill, P. (2006). Rheology of fresh cement and concrete. In: Rheology Reviews 2006, pp. 61-130: The British Society of Rheology.

Baroghel-Bouny, V. (2002). Which toolkit for durability evaluation as regards chloride ingress into concrete? Part II: Development of a performance approach based on durability indicators and monitoring parameters. In: Proceedings of the Third International RILEM Workshop on Testing and Modelling Chloride Ingress into Concrete, pp. 137-163. C. Andrade and J. Kropp (Eds.), RILEM Publications SARL. Madrid, Spain.

Basheer, L.; Basheer, P. A. M. and Long, A. E. (2005). Influence of coarse aggregate on the permeation, durability and the microstructure characteristics of ordinary Portland cement concrete. Construction and Building Materials, 19(9): pp. 682-690.

Basheer, P. A. M.; Srinivasan, S.; Nanukuttan, S. and Cleland, D. (2009). Smart structural materials with permanent monitoring system for concrete: Novel sensors for monitoring the durability of concrete structures. Atlantic Area, Lisbon. 26 pp. DURATINET - Working Group WG-A6 - Smart and green structural and repair materials (TR 6.4) (Ed.)

Baumell, A. (1959). The effect of additives on the corrosion behavior of steel in concrete. Zement-Kalk-Gips.

Bertolini, L.; Elsener, B.; Pedeferri, P. and Polder, R. (2005). Corrosion of steel in concrete. Prevention, diagnosis, repair. Weinheim, Germany: Wiley-Vch Verlag GmbH&Co. KGaA.

Bohlin Instruments Ltd. (1994). A basic introduction to rheology. Bohlin Instruments Ltd.

Bouvet, A.; Ghorbel, E. and Bennacer, R. (2010). The mini-conical slump flow test: analysis and numerical study. Cement and Concrete Research, 40(10): pp. 1517-1523.

Breugel, K. (2006). Key factors for producing durable concrete structures. In: Proceedings of the ConcreteLife'06 - International RILEM-JCI Seminar on Concrete durability and service life planning: curing, crack control, performance in harsh environments, pp. 302-309. K. Kovler (Ed.), RILEM Publications SARL. France.

Broomfield, J. P.; Davies, K. and Hladky, K. (2002). The use of permanent corrosion monitoring in new and existing reinforced concrete structures. Cement and Concrete Composites, 24(1): pp. 27-34.

Bui, V.; Akkaya, Y. and Shah, S. (2002). Rheological model for self-consolidating concrete. ACI Materials Journal, 99(6): pp. 549-559.

Cao, C.; Cheung, M. and Chan, B. (2013). Modelling of interaction between corrosion-induced concrete cover crack and steel corrosion rate. Corrosion Science, 69(0): pp. 97-109.

Castro, P.; Sagüés, A. A.; Moreno, E. I.; Maldonado, L. and Genescá, L. (1996). Characterization of activated titanium solid reference electrodes for corrosion testing of steel in concrete. Corrosion, 52(8): pp. 609-617.

CEB-FIP (2012). *fib* Bulletin: Model Code 2010, Final draft - Volume 1. *fib*-International Federation for Structural Concrete. Lausanne, Switzerland.

CEMBUREAU (2012). The cement sector: a strategic contributor to Europe's future. The European Cement Association (Ed.)

Chhabra, R. and Richardson, J. (1999). Non-Newtonian flow in the process industries. Fundamentals and engineering applications. Oxford: Butterworth-Heinemann, ISBN: 0 7506 3770 6.

Choy, T. C. (1999). Effective Medium Theory. Principles and applications. New York, United States: Oxford University Press.

Chrisp, T. M.; Starrs, G.; McCarter, W. J.; Owens, E. H.; Nanukuttan, S. V.; Holmes, N. and Basheer, L. (2010). Developments in intelligent monitoring of concrete structures. In: Proceedings of the Structural Faults & Repairs Conference. Edinburgh, Scotland.

Climent-Llorca, M. A.; Viqueira-Pérez, E. and López-Atalaya, M. M. (1996). Embeddable Ag/AgCl sensors for in-situ monitoring chloride contents in concrete. Cement and Concrete Research, 26(8): pp. 1157-1161.

COBA-PC&A-CIVILSER-ARCAIS (2005). Projecto de execução da ponte sobre o Rio Tejo e dos viadutos de acesso. Empreitada de concepção, projecto e construção da travessia do Tejo no Carregado, no sublanço A1/Benavente, da A10 auto-estrada Bucelas/Carregado/IC3. Portugal.

Coenza, P.; Ghorbani, A.; Camerlynck, C.; Rejiba, F.; Guérín, R. and Tabbagh, A. (2009). Effective medium theories for modelling the relationships between electromagnetic properties and hydrological variables in geomaterials: a review. Near Surface Geophysics, 7: pp. 563-578.

Comisu, C.-C. (2005). Integrated monitoring system for durability assessment of concrete bridges. The Bulletin of the Polytechnic Institute of Jassy. Construction. Architecture Section, LI: pp. 97-110.

Correia, M. J.; Pereira, E. V.; Salta, M. M. and Fonseca, I. T. E. (2006). Sensor for oxygen evaluation in concrete. Cement and Concrete Composites, 28(3): pp. 226-232.

Cost Action 521 (2003). Corrosion of steel in reinforced concrete structures. Luxembourg. R. Cigna, C. Andrade, U. Nürnberger, R. Polder, R. Weydert and E. Seitz (Eds.).

Costa, A. and Appleton, J. (1999). Chloride penetration into concrete in marine environment—Part I: Main parameters affecting chloride penetration. Materials and Structures, 32(4): pp. 252-259.

Cusson, D.; Lounis, Z. and Daigle, L. (2011). Durability monitoring for improved service life predictions of concrete bridge decks in corrosive environments. Computer-Aided Civil and Infrastructure Engineering, 26(7): pp. 524-541.

Design-Expert-Software (2007). Version 7 User's Guide. State-Ease Corporation.

Duan, H. L.; Karihaloo, B. L.; Wang, J. and Yi, X. (2006). Effective conductivities of heterogeneous media containing multiple inclusions with various spatial distributions. Physical Review B, 73(17): pp. 1-13.

DuraCrete (1999). Probabilistic methods for durability design. Probabilistic performance based durability design of concrete structures. The European Union - Brite EuRam III - Project BE96-3942.

DuraCrete (2000). General Guidelines for durability design and redesign. Probabilistic performance based durability design of concrete structures. The European Union - Brite EuRam III - Project BE96-3942.

EFNARC (2005). The European guidelines for self-compacting concrete - Specification, production and use. 63 pp. BIBM, CEMBUREAU, ERMCO, EFCA and EFNARC (Eds.).

Elsener, B.; Flückiger, D. and Böhni, H. (2005). A Percolation model for water sorption in porous cementitious materials. In: Materials for Buildings and Structures, pp. 163-169: Wiley-VCH Verlag GmbH & Co. KGaA.

Erdem, T. K.; Khayat, K. H. and Yahia, A. (2009). Correlating rheology of self-consolidating concrete to corresponding concrete-equivalent mortar. ACI Materials Journal, 106(2): pp. 154-160.

Esping, O. (2007). Early age properties of self-compacting concrete. Effects of fine aggregate and limestone filler. Ph.D., Department of Civil and Environmental Engineering, Chalmers University of Technology, Sweden.

Feldman, R.; Prudencio Jr, L. R. and Chan, G. (1999). Rapid chloride permeability test on blended cement and other concretes: correlations between charge, initial current and conductivity. Construction and Building Materials, 13(3): pp. 149-154.

Fennis, S. (2011). Measuring water demand or packing density of micro powders - comparison of methods. Delft University of Technology.

Ferrara, L.; Park, Y. and Shah, S. (2007). A method for mix-design of fiber-reinforced self-compacting concrete. Cement and Concrete Research, 37(6): pp. 957-971.

Ferraris, C. (2005). Concrete rheology: What is it and why do we need it? In: Proceedings of the 1st International Symposium on Design, Performance and Use of Self-Consolidating Concrete. Z. Yu, C. Shi, K. Khayat and Y. Xie (Eds.), RILEM Publications SARL. China.

Ferreira, R. M. (2007). Sensitivity analysis of model parameters for corrosion initiation and implications on design. In: Proceedings of the International RILEM Workshop on Integral Service Life Modelling of Concrete Structures, pp. 205-213. R. M. Ferreira, J. Gulikers and C. Andrade (Eds.), RILEM Publications SARL. Guimarães, Portugal.

Figueiras, H. (2006). Estudo e desenvolvimento experimental de composições de betão auto-compactável. Aferição das suas características mecânicas e durabilidade. Master Thesis, Faculdade de Engenharia da Universidade do Porto, Portugal.

Figueiras, H.; Maia, L.; Nunes, S.; Sousa Coutinho, J. and Andrade, C. (2013a). Durability performance-based design of a SCC exposed to severe marine environment using a statistical design approach. *(submitted for publication)*.

Figueiras, H. and Nunes, S. (2010). Sistema de medição dos parâmetros de durabilidade em estruturas de betão armado e pré-esforçado. T1.1 - Especificações do sistema de medição dos parâmetros de durabilidade. NewMENSUS, Lda / FEUP-LABEST. 84 pp. Projecto NaÓpticaDaNewMENSUS (Ed.)

Figueiras, H.; Nunes, S.; Sousa Coutinho, J. and Andrade, C. (2013b). Effective medium theories to assess the influence of aggregate skeleton on electrical resistivity and chloride diffusion coefficient. *(submitted for publication)*.

Figueiras, H.; Nunes, S.; Sousa Coutinho, J. and Andrade, C. (2014). Linking fresh and durability properties of paste to SCC mortar. Cement and Concrete Composites, 45: pp. 209-226.

Figueiras, H.; Nunes, S.; Sousa Coutinho, J. and Figueiras, J. (2009). Combined effect of two sustainable technologies: Self-compacting concrete (SCC) and controlled permeability formwork (CPF). Construction and Building Materials, 23(7): pp. 2518-2526.

Figueiras, H.; Nunes, S.; Sousa Coutinho, J. and Figueiras, J. (2011). Durability performance of SCC mortars including different types of metakaolin. In: Proceedings of the 12th International Conference on Durability of Building materials and Components, pp. 1387-1394. V. P. Freitas, H. Corvacho and M. Lacasse (Eds.), FEUP edições. Porto, Portugal.

Figueiras, J.; Félix, C.; Sousa, H. and Figueiras, H. (2007). Construção da travessia do Tejo no Carregado sublanço A1/Benavente, da A10 Auto-Estrada Bucelas/Carregado/IC3: Plano de monitorização estrutural e de durabilidade. Porto: FEUP-LABEST and NewMENSUS,Lda.

Figueiras, J.; Félix, C.; Sousa, H.; Figueiras, H. and Rodrigues, C. (2008). Construção da travessia do Tejo no Carregado sublanço A1/Benavente, da A10 Auto-Estrada

Bucelas/Carregado/IC3: Plano de monitorização estrutural e de durabilidade - Manual de utilização. Porto: FEUP-LABEST and NewMENSUS,Lda. 141 pp.

Flatt, R. J.; Larosa, D. and Roussel, N. (2006). Linking yield stress measurements: spread test versus Viskomat. Cement and Concrete Research, 36(1): pp. 99-109.

Force Technology Brøndby - Park Allé 345, 2605 Brøndby. Denmark.

Frías, M. and Cabrera, J. (2000). Pore size distribution and degree of hydration of metakaolin–cement pastes. Cement and Concrete Research, 30(4): pp. 561-569.

Garboczi, E.; Bentz, D.; Shane, J.; Mason, T. and Jennings, H. (2000). Effect of the interfacial transition zone on the conductivity of Portland cement mortars. Journal American Ceramic, 83(5): pp. 1137-1144.

Garboczi, E. and Berryman, J. (2000). New effective medium theory for the diffusivity or conductivity of a multi-scale concrete microstructure model. Concrete Science and Engineering, 2: pp. 88-96.

Giordano, S. (2003a). Differential schemes for the elastic characterisation of dispersions of randomly oriented ellipsoids. European Journal of Mechanics - A/Solids, 22(6): pp. 885-902.

Giordano, S. (2003b). Effective medium theory for dispersions of dielectric ellipsoids. Journal of Electrostatics, 58(1): pp. 59-76.

Gjørv, O. E. (2003). Durability design and construction quality of concrete structures. In: Proceedings of the International Conference in Advances in Concrete and Structures, pp. 309-319. Y. Yuan, P. Shah and H. Lu (Eds.), RILEM publications SARL.

Gjørv, O. E. (2009). Durability design of concrete structures in severe environments. London: Taylor & Francis.

Gjørv, O. E. (2010). Service life and sustainability of important concrete infrastructures. In: Proceedings of the Second International Conference on Sustainable Construction Materials and Technologies, pp. 259-269. T. Naik, F. Canpolat, P. Claisse and E. Ganjian (Eds.), Ancona, Italy.

Gjørv, O. E. and Zhang, T. (1998). Migration testing of chloride diffusivity in concrete. In: Proceedings of the 2sd International Conference on concrete under sever conditions – Environment and loading. O. E. Gjørv, K. Sakai and N. Banthia (Eds.), Tromso, Norway.

Gomes, P. (2002). Optimization and characterization of high-strength self-compacting concrete. PhD, Escola Técnica Superior D'Enginyers de Camins, Canals i Ports, Universitat Politécnica de Catalunya,

Gouda, V. K. (1970). Corrosion and corrosion inhibition of reinforcing steel: I. Immersed in alkaline solutions. British Corrosion Journal, 5(5): pp. 198-203.

Grünewald, S. (2004). Performance-based design of self-compacting fibre reinforced concrete. Ph.D., Delft University of Technology, Netherlands.

Grünewald, S. and Walraven, J. (2007). Characteristics and influence of paste on the behaviour of self-compacting concrete in the fresh state. In: Proceedings of the 5th International RILEM Symposium on Self-Compacting Concrete, pp. 137-142. G. De Schutter and V. Boel (Eds.), RILEM Publications SARL. Ghent, Belgium.

Gulikers, J. (1996). Experimental investigations on macrocell corrosion in chloride-contaminated concrete. Heron, 41(2): pp. 107-123.

Gulikers, J. (2007). Critical issues in the interpretation of results of probabilistic service life calculations. In: Proceedings of the International RILEM Workshop on Integral Service Life Modelling of Concrete Structures, pp. 195-203. R. M. Ferreira, J. Gulikers and C. Andrade (Eds.), RILEM Publications SARL. Guimarães, Portugal.

Hashin, Z. (1983). Analysis of composite materials - A survey. Journal of Applied Mechanics, 50: pp. 481-505.

Hashin, Z. and Shtrikman, S. (1962). A variational approach to the Theory of the Effective Magnetic Permeability of multiphase materials. Journal of Applied Physics, 33(10): pp. 3125-3131.

Hidalgo, J.; Chen, C. and Struble, L. (2008). Correlation between paste and concrete flow behavior. ACI Materials Journal, 105(3): pp. 281-288.

IPQ (2003a). NP EN 1097-6 - Tests for mechanical and physical properties of aggregates. Parte 6: Determination of particle density and water absorption. Instituto Português da Qualidade. Portugal.

IPQ (2003b). NP EN 12504-2 - Testing concrete in structures. Part 2: Non-destructive testing. Determination of rebound number. Instituto Português da Qualidade. Portugal.

IPQ (2006). EN 196-1 - Methods of testing cement. Part 1: Determination of strength. Instituto Português da Qualidade. Portugal.

IPQ (2007). NP EN 206-1 Concrete. Part 1: Specification, performance, production and conformity. Instituto Português da Qualidade. Portugal.

IPQ (2009). NP EN 1990 Eurocode 0: Basis of structural design. Instituto Português da Qualidade. Portugal.

IPQ (2010a). NP EN 206-9 - Concrete. Part 9: Additional Rules for Self-Compacting Concrete (SCC). Instituto Português da Qualidade. Portugal.

IPQ (2010b). NP EN 1992-1-1 Eurocode 2: Design of concrete structures. Part 1-1: General rules and rules for buildings. Instituto Português da Qualidade. Portugal.

IPQ (2010c). NP EN 12350-8 Testing fresh concrete. Part 8: Self-compacting concrete - Slump-flow test. Instituto Português da Qualidade. Portugal.

IPQ (2010d). NP EN 12350-9 Testing fresh concrete. Part 9: Self-compacting concrete - V-funnel test. Instituto Português da Qualidade. Portugal.

IPQ (2010e). NP EN 12350-10 Testing fresh concrete. Part 10: Self-compacting concrete - L box test. Instituto Português da Qualidade. Portugal.

IPQ (2010f). NP EN 12350-11 Testing fresh concrete. Part 11: Self-compacting concrete - Sieve segregation test. Instituto Português da Qualidade. Portugal.

IPQ (2011). NP EN 12390-3 Testing hardened concrete. Part 3: Compressive strength of test specimens. Instituto Português da Qualidade. Portugal.

IPQ (2012). EN 197-1 Cement. Part 1: Composition, specifications and conformity criteria for common cements. Instituto Português da Qualidade. Portugal.

Juvas, K. (2003). Experiences with SCC in the production of prefabricated elements. In: Proceedings of the 3rd International Symposium on Self-compacting Concrete, pp. 955 - 957. O. Wallevik and I. Nielsson (Eds.), RILEM Publications SARL. Reykjavik, Iceland.

Kaesche, H. (1973). Testing of the corrosion danger to steel reinforcement due to admixtures in concrete. Zement-Kalk-Gips.

Khayat, K.; Ghezal, A. and Hadriche, M. (2000). Utility of statistical models in proportioning self-consolidating concrete. Materials and Structures, 33(5): pp. 338-344.

Khayat, K.; Hu, C. and Monty, H. (1999). Stability of self-consolidating concrete, advantages, and potential applications. In: Proceedings of the 1st International RILEM Symposium on Self-Compacting Concrete. RILEM Publications SARL. Stockholm, Sweden.

Klug, Y. and Holschemacher, K. (2003). Comparison of the hardened properties of self-compacting and normal vibrated concrete. In: Proceedings of the 3rd International Rilem Symposium on Self-Compacting Concrete, pp. 596-605. O. Wallevik and I. Nielsson (Eds.), RILEM Publications SARL. Reykjavik, Iceland.

Koehler, E. and Fowler, D. (2007). Aggregates in self-compacting concrete. Aggregates Foundation for Technology, Research, and Education (AFTRE), International Center for Aggregates Research (ICAR) and The University of Texas at Austin. 353 pp.

Liu, P. C. (1991). Damage to concrete structures in a marine environment. Materials and Structures, 24: pp. 302-307.

LNEC (1993). E 391 Determinação da resistência à carbonatação. Laboratório Nacional de Engenharia Civil. Portugal.

LNEC (2004). E 463 Determination of diffusion coefficient of chlorides from non-steady-state migration test. Laboratório Nacional de Engenharia Civil. Portugal.

LNEC (2007). E 465 Methodology for estimating the concrete performance properties allowing to comply with the design working life of reinforced or prestressed concrete structures under the environmental exposures XC and XS. Laboratório Nacional de Engenharia Civil. Portugal.

Long, A. E.; Henderson, G. D. and Montgomery, F. R. (2001). Why assess the properties of near-surface concrete? Construction and Building Materials, 15(2–3): pp. 65-79.

López, A.; Tobes, J. M.; Giaccio, G. and Zerbino, R. (2009). Advantages of mortar-based design for coloured self-compacting concrete. Cement and Concrete Composites, 31(10): pp. 754-761.

Lu, X. (1997). Application of the Nernst-Einstein equation to concrete. Cement and Concrete Research, 27(2): pp. 293-302.

Luping, T. and Gulikers, J. (2007). On the mathematics of time-dependent apparent chloride diffusion coefficient in concrete. Cement and Concrete Research, 37(4): pp. 589-595.

Mansur, M. A.; Asce, M. and Islam, M. M. (2002). Interpretation of concrete strength for nonstandard specimens. Journal of Materials in Civil Engineering, 14(2): pp. 151-155.

Marques, P. F.; Costa, A. and Lanata, F. (2012). Service life of RC structures: chloride induced corrosion: prescriptive versus performance-based methodologies. Materials and Structures, 45(1-2): pp. 277-296.

MATLAB 2011b, Ed. (2011). Optimization Toolbox - User's Guide, MathWorks.

McCarter, W. J.; Emerson, M. and Ezirim, H. (1995). Properties of concrete in the cover zone: developments in monitoring techniques. Magazine of Concrete Research, 47(172): pp. 243-251.

McCarter, W. J.; Ezirim, H. and Emerson, M. (1992). Absorption of water and chloride into concrete. Magazine of Concrete Research, 44(158): pp. 31-37.

McCarter, W. J. and Vennesland, Ø. (2004). Sensor systems for use in reinforced concrete structures. Construction and Building Materials, 18(6): pp. 351-358.

Mehta, P. K. (2003). Concrete in the marine environment. Taylor & Francis Books.

Monfore, G. E. (1968). The electrical resistivity of concrete. Journal of PCA: pp. 35-48.

Montemor, M.; Alves, J.; Simões, A.; Fernandes, J.; Lourenço, Z.; Costa, A.; Appleton, A. and Ferreira, M. (2006). Multiprobe chloride sensor for in situ monitoring of reinforced concrete structures. Cement and Concrete Composites, 28(3): pp. 233-236.

Montgomery, D. (2001). Design and Analysis of Experiments. fifth ed. New York: Wiley.

Myrdal, R. (2007). The electrochemistry and characteristics of embeddable reference electrodes for concrete. USA: Woodhead.

Myrdal, R.; Videm, K.; Vennesland, Ø. and Sellevold, E. (1997). Sensor technology and electrochemical measurements. What has been learnt on the Gimsoystraumen project. In: Proceedings of the Repair of concrete structures - From theory to the practice in a marine environment, pp. 419-424. A. Blankvoll (Ed.), Svolvaer, Norway.

Nehdi, M. and Summer, J. (2002). Optimization of ternary cementitious mortar blends using factorial experimental plans. Materials and Structures, 35(8): pp. 495-503.

Neville, A. M. (1998). Properties of concrete. Fourth ed. England: Longman.

Nielsen, E. (2004). The durability of white Portland cement to chemical attack. Ph.D., DTU-Danmarks Tekniske Universitet, Denmark.

Nokken, M.; Boddy, A.; Hooton, R. D. and Thomas, M. (2006). Time dependent diffusion in concrete—three laboratory studies. Cement and Concrete Research, 36(1): pp. 200-207.

NORDTEST (1999). NT BUILD 492 - Concrete, mortar and cement-based repair materials: Chloride migration coefficient from non-steady-state migration experiments. Finland.

Norris, A. N.; Sheng, P. and Callegari, A. J. (1984). Effective-medium theories for two-phase dielectric media. Journal of Applied Physics, 57(6): pp. 1990-1996.

Nunes, S. (2008). Performance-based design of self-compacting concrete (SCC): a contribution to enhance SCC mixtures robustness. Ph.D., Faculdade de Engenharia da Universidade do Porto, Portugal.

Nunes, S.; Figueiras, H.; Coutinho, J. and Figueiras, J. (2005a). Método para definição da composição de betão auto-compactável. e-Mat- Revista de Ciência e Tecnologia de Materiais de construção 2: pp. 1-11.

Nunes, S.; Figueiras, H.; Milheiro, P.; Coutinho, J. and Figueiras, J. (2006a). A methodology to assess the robustness of SCC mixtures. Cement and Concrete Research, 36: pp. 2115-2122.

Nunes, S.; Figueiras, H.; Oliveira, P. M.; Coutinho, J. S. and Figueiras, J. (2006b). A methodology to assess robustness of SCC mixtures. Cement and Concrete Research, 36(12): pp. 2115-2122.

Nunes, S.; Figueiras, H.; Proença, A. M.; Magalhães, R.; Leite, A.; Santos, R.; Sousa Coutinho, J. and Figueiras, J. (2005b). Desenvolvimento de uma tecnologia robusta para o fabrico transporte e aplicação do betão auto-compactável. Relatório final do projecto de invertigação BACPOR. LABEST/FEUP.

Nunes, S.; Figueiras, H.; Sousa Coutinho, J. and Figueiras, J. (2005c). SCC implementation in the Portuguese industry. In: Proceedings of the The 2nd North American Conference on the Design and use of Self-Consolidating Concrete (SCC) and the 4th International RILEM Symposium on Self-Compacting Concrete, pp. 1165-1171. S. P. Shah (Ed.), Hanley Wood. Chicago.

Nunes, S.; Figueiras, H.; Sousa Coutinho, J. and Figueiras, J. (2009a). SCC and conventional concrete on site: property assessment. IBRACON Structures and Materials Journal, 2(1): pp. 25-36.

Nunes, S.; Oliveira, P. M.; Sousa Coutinho, J. and Figueiras, J. (2009b). Interaction diagrams to assess SCC mortars for different cement types. Construction and Building Materials, 23(3): pp. 1401-1412.

Nunes, S.; Oliveira, P. M.; Sousa Coutinho, J. and Figueiras, J. (2011). Rheological characterization of SCC mortars and pastes with changes induced by cement delivery. Cement and Concrete Composites, 33(1): pp. 103-115.

Oh, S.; Noguchi, T. and Tomosawa, F. (1999). Toward mix design for rheology of self-compacting concrete. In: Proceedings of the First International RILEM Symposium on Self-Compacting Concrete, pp. 361-372. Å. Skarendahl and Ö. Petersson (Eds.), RILEM Publications SARL. Stockholm, Sweden

Okamura, H. and Ouchi, M. (2003). Self-compacting concrete. Journal of Advanced Concrete Technology, 1(1): pp. 5-15.

Okamura, H.; Ozawa, K. and Ouchi, M. (2000). Self-compacting concrete. Structural Concrete: Journal of fib, 1(1): pp. 3-17.

Parande, A. K.; Chitradevi, R. H.; Thangavel, K.; Karthikeyan, M. S.; Ganesh, B. and Palaniswamy, N. (2009). Metakaolin: a versatile material to enhance the durability of concrete – an overview. Structural Concrete: Journal of fib, 10(3): pp. 125-138.

Pereira, E. (2004). Monitorização da corrosão no betão armado. Ph.D., Departamento de Engenharia Química, Faculdade de Ciências da Universidade de Lisboa, Portugal.

Petrou, M. F.; Wan, B.; Gadala-Maria, F.; Kolli, V. G. and Harries, K. A. (2000). Influence of mortar rheology on aggregate settlement. ACI Materials Journal, 97(4): pp. 479-485.

Polder, R. B.; Peelen, W. H. A. and Leegwater, G. (2008a). Corrosion monitoring for underground and submerged concrete structures - examples and interpretation issues. In: Proceedings of the International *FIB* Symposium - Tailor made concrete structures: new solutions for our society pp. 187-192. J. C. Walraven and D. Stoelhorst (Eds.), Tailor & Francis Group. Amsterdam, Netherlands.

Polder, R. B.; Peelen, W. H. A. and Leegwater, G. (2008b). Corrosion monitoring for underground and submerged concrete structures - examples and interpretation issues. In: Tailor Made Concrete Structures: new solutions for our society, pp. 187-192. J. C. Walraven and D. Stoelhorst (Eds.), London: Taylor & Francis Group.

Portugal, A.; A. Perry da Câmara; Virtuoso, F. and Rebelo, V. (2006). Nova travessia do rio Tejo no Carregado. In: Proceedings of the JPEE 2006 - 4as Jornadas Portuguesas de Engenharia de Estruturas. A. M. Baptista and P. Silveira (Eds.), LNEC. Lisboa, Portugal.

Price, W. F. (2000). Report C511 Controlled Permeability Formwork. London, UK: Construction Industry Research & Information Association (CIRIA)

Qian, S.; Cusson, D. and Chagnon, N. (2003). Evaluation of reinforcement corrosion in repaired concrete bridge slabs - a case study. Corrosion, 59(5): pp. 457-468.

Qin, Y.; Lai, S.; Jiang, Y.; Yang, T. and Wang, J. (2005). Transmembrane voltage induced on a cell membrane in suspensions exposed to an alternating field: A theoretical analysis. Bioelectrochemistry, 67(1): pp. 57-65.

Rajabipour, F. and Weiss, J. (2007). Electrical conductivity of drying cement paste. Materials and Structures, 40(10): pp. 1143-1160.

Raupach, M. (1996). Chloride-induced macrocell corrosion of steel in concrete—theoretical background and practical consequences. Construction and Building Materials, 10(5): pp. 329-338.

Raupach, M. and Schießl, P. (2001). Macrocell sensor systems for monitoring of the corrosion risk of the reinforcement in concrete structures. NDT & E International, 34(6): pp. 435-442.

Raupach, M. and Schiessl, P. (1997). Monitoring system for the penetration of chlorides, carbonation and the corrosion risk for the reinforcement. Construction and Building Materials, 11(4): pp. 207-214.

Raupach, M. and Schiessl, P. (2000). Monitoring Corrosion risk in concrete structures-Review of 10 years experience and new developments. Special Publication, 192: pp. 19-24.

RILEM-Report 38 (2007). Durability of Self-Compacting Concrete - State-of-the-Art Report of RILEM Technical Committee 205-DSC. RILEM Publications SARL. 208 pp. G. Schutter and K. Audenaert (Eds.).

RILEM TC 116-PCD (1999). Permeability of concrete as a criterion of its durability: Determination of the absorption of water of hardened concrete. Materials and Structures, 32(217): pp. 163-173.

RILEM TC 154-EMC (2003). Electrochemical techniques for measuring metallic corrosion. Half-cell potential measurements – Potential mapping reinforced concrete structures. Materials and Structures, 36: pp. 461-471.

Roussel, N. (2005). Steady and transient flow behaviour of fresh cement pastes. Cement and Concrete Research, 35(9): pp. 1656-1664.

Roussel, N.; Lemaître, A.; Flatt, R. J. and Coussot, P. (2010). Steady state flow of cement suspensions: A micromechanical state of the art. Cement and Concrete Research, 40(1): pp. 77-84.

Roussel, N.; Ovarlez, G.; Garrault, S. and Brumaud, C. (2012). The origins of thixotropy of fresh cement pastes. Cement and Concrete Research, 42(1): pp. 148-157.

Roussel, N. and Roy, R. L. (2005). The Marsh cone: a test or a rheological apparatus? Cement and Concrete Research, 35(5): pp. 823-830.

Saak, A. (2000). Characterization and modeling of the rheology of cement paste: with applications toward self-flowing materials. Ph.D., Materials Science and Engineering, Northwestern University, Evanston, Illinois.

Saak, A.; Jennings, H. and Shah, S. (2004). A generalized approach for the determination of yield stress by slump and slump flow. Cement and Concrete Research, 34(3): pp. 363-371.

Saak, A. W.; Jennings, H. M. and Shah, S. P. (2001). New methodology for designing self-compacting concrete. ACI Materials Journal, 98(6): pp. 429-439.

Saassouh, B. and Zoubir Lounis (2012). Probabilistic modeling of chloride-induced corrosion in concrete structures using first- and second-order reliability methods. Cement and Concrete Composites, 34(9): pp. 1082-1093.

Sakai, K.; Shimonura, T. and Sugiyama, T. (1999). Design of concrete structures in the 21st century. In: Proceedings of the Controlling concrete degradation, pp. 27-44. R. Dhir and M. D. Newlands (Eds.), Thomas Telford. Scotland, UK.

Schiessl, P. and Raupach, M. (1992). Monitoring system for the corrosion risk of steel in concrete structures. Concrete International, 14(7): pp. 52-55.

Schutter, G. (2011). Effect of limestone filler as mineral addition in self-compacting concrete. In: Proceedings of the 36th Conference on our world in concrete & structures. Singapore Concrete Institute. Singapore.

Shah, S. P.; Akkaya, Y. and Bui, V. K. (1999). Innovations in microstructure, processing and properties. In: Proceedings of the Innovations and Developments in concrete Materials and Construction, pp. 1-15. R. Dhir, P. C. Hewlett and L. J. Csetenyi (Eds.), Thomas Telford. Scotland, UK.

Sheskin, D. J. (2003). Handbook of parametric and nonparametric statistical procedures. Chapman and Hall/CRC, ISBN: 978-1-58488-440-8.

Shi, C.; Stegemann, J. A. and Caldwell, R. J. (1998). Effect of supplementary cementing materials on the specific conductivity of pore solution and its implications on the rapid chloride permeability test (AASHTO T277 and ASTM C1202) results. ACI Materials Journal, 94(4): pp. 389-393.

Short, N. R.; Page, C. L. and Glass, G. K. (1991). A galvanic sensor for monitoring corrosion of steel in carbonated concrete. Magazine of Concrete Research, 43(156): pp. 149-154.

Siddique, R. and Khan, M. I. (2012). Supplementary Cementing Materials. Springer.

Siddique, R. and Klaus, J. (2009). Influence of metakaolin on the properties of mortar and concrete: A review. Applied Clay Science, 43(3–4): pp. 392-400.

Skarendahl, A. and Petersson, O. (2001). Self-Compacting Concrete. State-of-art report of RILEM Committee 174-SCC. RILEM Publications.

Sonebi, M. (2001). Factorial design modelling of mix proportion parameters of underwater composite cement grouts. Cement and Concrete Research, 31(11): pp. 1553-1560.

Sonebi, M. (2004). Medium strength self-compacting concrete containing fly ash: modelling using factorial experimental plans. Cement and Concrete Research, 34(7): pp. 1199-1208.

Sonebi, M.; Bartos, P.; Zhu, W.; Gibbs, J. and Tamimi, A. (2000). Final Report of Task 4: Properties of Hardened Concrete. Rational production and improved working environment through using self-compacting concrete. Brite EuRam project BRPR-CT96-0366. 72 pp.

Song, H.-W. and Saraswathy, V. (2007). Corrosion monitoring of reinforced concrete structures - a review. Electrochemical science, 2: pp. 1-28.

Sousa Coutinho, J. (2003). The combined benefits of CPF and RHA in improving the durability of concrete structures. Cement and Concrete Composites, 25(1): pp. 51-59.

Sousa Coutinho, J. (2005). Melhoria da durabilidade dos betões por tratamento em cofragem. Faculdade de Engenharia da Universidade do Porto: FEUP edições, ISBN: 223433/05.

Stanish, K. D.; Hooton, R. D. and Thomas, M. D. A. (1997). Testing the chloride penetration resistance of concrete: a literature review. University of Toronto, Federal Highway Administration. 33 pp.

Struble, L.; Szecsy, R. and Salinas, G. (1996). Rheology of fresh concrete. In: Proceedings of the 4th ASCE Materials Engineering Conference Proceedings, Materials for the New Millennium, pp. 1121-1128. K. P. Chong (Ed.), American Society of Civil Engineers. New York.

Struble, L. J. and Lei, W. (1995). Rheological changes associated with setting of cement paste. Advanced Cement Based Materials, 2(6): pp. 224-230.

Swamy, R. N. (2007). Sustainable concrete for the 21st. century. Concept of strength through durability. Indian Concrete Journal, 81: pp. 7-15.

Tennis, P. D.; Thomas, M. D. A. and Weiss, W. J. (2011). State-of-art-report on the use of limestone in cements at levels up to 15%. Skokie, Illinois, USA: Portland Cement Association. 78 pp.

Torquato, S. and Rubinstein, J. (1991). Improved bounds on the effective conductivity of high-contrast suspensions. Journal of Applied Physics, 69(10): pp. 7118-7125.

Tuutti, K. (1982). Corrosion of steel in concrete. Stockholm, Sweden: Swedish Cement and Concrete Research Institute.

Uller, L.; Ricón, O.; Alanis, I.; Helene, P.; Gutiérrez, R.; O´Reilly, V.; Andrade, C.; Carpio, J.; Díaz, I.; Salta, M.; Rodríguez, G. and Carruyo, A. (2000). DURAR - Red temática XV.B - Durabilidade de la armadura. Manual de inspección, evaluación y diagnóstico de corrosión en estructuras de hormigón armado.

Utsi, S.; Emborg, M. and Calswärd, J. (2003). Relation between workability and rheological parameters. In: Proceedings of the 3rd International Symposium on Self-compacting Concrete, pp. 154-164. O. Wallevik and I. Nielsson (Eds.), RILEM publications SARL. Reykjavik, Iceland.

Veiga, J.; Carvalho, A. and Figueiras, H. (2011). Sistema de medição dos parâmetros de durabilidade em estruturas de betão armado e pré-esforçado. T3.4 - Desenvolvimento de um sistema de base eléctrica para a medição da corrosão em armaduras. Parte 2. NewMENSUS, Lda / FEUP-LABEST. 18 pp.

Vennesland, Ø.; Raupach, M. and Andrade, C. (2007). Recommendation of Rilem TC 154-EMC: "Electrochemical techniques for measuring corrosion in concrete"-measurements with embedded probes. Materials and Structures, 40(8): pp. 745-758.

Videm, K. and Myrdal, R. (1997). Electrochemical behavior of steel in concrete and evaluation of the concrete rate. Corrosion, 53(9): pp. 734-742.

Wallevik, J. E. (2009). Rheological properties of cement paste: thixotropic behavior and structural breakdown. Cement and Concrete Research, 39(1): pp. 14-29.

Wallevik, O. H. and Wallevik, J. E. (2011). Rheology as a tool in concrete science: The use of rheographs and workability boxes. Cement and Concrete Research, 41(12): pp. 1279-1288.

Walraven, J. (2005). Self-compacting concrete: Challenge for designer and researcher. In: Proceedings of the The Second North American Conference on the Design and use of Self-Consolidating Concrete and the Fourth International RILEM Symposium on Self-compacting Concrete. S. P. Shah (Ed.), RILEM publications SARL. Chicago, United States of America.

Walraven, J. C. (2009). Design for service life: How should it be implemented in future codes. In: Concrete Repair, Rehabilitation and Retrofitting II, pp. 3-11. M. G. Alexander (Ed.): Taylor & Francis Group.

Walraven, J. C. and Bigaj-van Vliet, A. J. (2008). A new future-oriented Model Code for concrete structures. In: Proceedings of the *fib* Symposium. Tailor Made Concrete Structures: New Solutions for our Society, pp. 611-618. J. C. Walraven and D. Stoelhorst (Eds.), Tailor&Francis Group. Amsterdam, Netherlands.

Yahia, A. and Khayat, K. H. (2001a). Analytical models for estimating yield stress of high-performance pseudoplastic grout. Cement and Concrete Research, 31(5): pp. 731-738.

Yahia, A. and Khayat, K. H. (2001b). Experiment design to evaluate interaction of high-range water-reducer and antiwashout admixture in high-performance cement grout. Cement and Concrete Research, 31: pp. 749-757.

Zerbino, R.; Barragán, B.; Garcia, T.; Agulló, L. and Gettu, R. (2009). Workability tests and rheological parameters in self-compacting concrete. Materials and Structures, 42(7): pp. 947-960.

Zhu, W.; Quinn, J. and Bartos, P. (2001). Transport properties and durability of self-compacting concrete. In: Proceedings of the Proceedings of the 2nd International

RILEM Symposium Self-Compacting Concrete, pp. 451-458. K. Ozawa and M. Ouchi (Eds.), RILEM publications SARL. Tokyo, Japan.

Zimmermann, L.; Schiegg, Y.; Elsener, B. and Boehni, H. (1997). Electrochemical techniques for monitoring the conditions of concrete bridge structures. In: Proceedings of the Repair of concrete structures - from theory to the practice in a marine environment, pp. 213-222. A. Blankvoll (Ed.), Svolvaer, Norway.

Appendix: Mixtures formulation

Mix proportions of paste, mortar and concrete prepared in this research work were obtained using the following universal formulation. The volumetric composition of concrete, by cubic meter, is given by:

$$Vs + Vgd + Vp + Vw + Va = 1m^3 \quad \text{(A.1)}$$

where Vs is the sand volume, Vgd the coarse aggregate volume, Vp the powder volume, Vw the water volume and Va the air content. For a given solid volume Vap ($Vap = Vg/Vg, lim$) and a defined Va, the coarse aggregate volume can be obtained from:

$$Vgd = {}^{Vg}/_{Vg,\,lim} \times Vg, lim \times (1 - Va) \quad \text{(A.2)}$$

For a given value of (Vs/Vm), volume of mortar (Vm) and sand volume (Vs), can be defined as:

$$Vm = 1 - Va - Vgd \quad \text{(A.3)}$$

$$Vs = {}^{Vs}/_{Vm} \times Vm \quad \text{(A.4)}$$

And for a given value of (Vw/Vp), the powder volume (Vp) and the water volume (Vw) can be defined as:

$$V_p = \frac{Vm - Vs}{1 + {}^{Vw}/_{Vp}} \quad \text{(A.5)}$$

$$Vw = {}^{Vw}/_{Vp} \times Vp \tag{A.6}$$

Finally, from the Vp and Vw values the weight values of water (w_w), cement (w_c), metakaolin (w_{mtk}) and limestone filler (w_f) can be determined as follows:

$$w_w = Vw \times \rho_w \tag{A.7}$$

$$w_c = \frac{w_w}{{}^{w}/_{c}} \tag{A.8}$$

$$w_{mtk} = {}^{mtk}/_{c} \times w_c \tag{A.9}$$

$$w_f = \left(Vp - \frac{w_c}{\rho_c} - \frac{w_{mtk}}{\rho_{mtk}}\right) \times \rho_f \tag{A.10}$$

where ρ_w, ρ_c, ρ_{mtk} and ρ_f represent the specific gravity of water, cement, metakaolin and limestone filler, respectively, w/c is the water to cement weight ratio and mtk/c is the metakaolin to cement weight ratio. From the superplasticizer to powder weight ratio (Sp/p) and the weight values of cement, metakaolin and limestone filler the liquid weight of superplasticizer (w_{sp}) is given by:

$$w_{sp} = {}^{Sp}/_{p} \times \left(w_c + w_{mtk} + w_f\right) \tag{A.11}$$

Since aggregates used in this work were made of a mixture of two sands and gravel, the dry aggregate contents (w_{gd}, w_{sd1}, w_{sd2}) can be obtained as follows:

$$w_{gd} = Vgd \times \rho_{gd} \tag{A.12}$$

$$w_{sd} = \frac{Vs}{\frac{{}^{s_1}/_{s}}{\rho_{sd1}} + \frac{\left(1 - {}^{s_1}/_{s}\right)}{\rho_{sd2}}} \tag{A.13}$$

$$w_{sd1} = {}^{s_1}/_{s} \times w_{sd} \tag{A.14}$$

$$w_{sd2} = \left(1 - {}^{S_1}/_{S}\right) \times w_{sd} \tag{A.15}$$

where ρ_{gd}, ρ_{sd1}, ρ_{sd2} represent the specific gravity of coarse aggregate, sand 1 and sand 2, respectively. The water added to the mixture has to be corrected (w_{wc}) by subtracting the water content of the superplasticizer and adding the water needed for saturating the aggregate, from a dry state, as follows:

$$w_{wc} = w_w - w_{Sp} \times \left(1 - \gamma_{Sp}\right) + \sum_{i=1}^{2} (w_{sdi} \times A_{sdi}) + w_{gd} \times A_{gd} \tag{A.16}$$

where γ_{sp}, A_{sdi} and A_{gd} represent the solid content of superplasticizer (%), the absorption coefficient of sand (%) and the absorption coefficient of coarse aggregate (%), respectively.